0015252

Rockwell Hanford Operations

BWIP SUPPORTING DOCUMENT

End Function Activity: Licensing	Project No.: N/A
Document Title: The State of In Situ Stresses as Determined by Hydraulic Fracturing at the Hanford Site	

Borehole No.:	Stratigraphic Formations:	Doc. Type	Subj. Code
DC-12, RRL-2, RRL-6 and DC-4	Cohassett, Grande Ronde 7, Umtanum, and McCoy Canyon	2003	H260

Number: SD- BWI-TD-014	Rev./Chg. No.: 0	Page 1 Of 157	Total Pages 157
CIN No.: N/A Date: N/A			
Baseline Doc.: Yes ☐ No ☒	Class: N/A		
WBS No. or Work Package No.: L5D2	CEI No.: 005		
Prepared by (type & sign name): [signature] See reverse side for additional approvals	Date: 1-10-85		

THIS DOCUMENT IS FOR USE IN PERFORMANCE OF WORK UNDER CONTRACTS WITH THE U.S. DEPARTMENT OF ENERGY BY PERSONS OR FOR PURPOSES WITHIN THE SCOPE OF THESE CONTRACTS. DISSEMINATION OF ITS CONTENTS IS HANDLED IN ACCORDANCE WITH THE FREEDOM OF INFORMATION ACT.

Abstract This report summarizes the hydraulic fracturing stress determinations that have been conducted during the period 1981 through 1983 by the Basalt Waste Isolation Project. These tests have been conducted in boreholes DC-12, RRL-2, RRL-6, and DC-4 to estimate the state of stress in and about the candidate repository horizons within the Hanford Site.

Test procedures, test data, analysis methodology, and calculated in situ stresses in the Cohassett, Grande Ronde 7, Umtanum, and McCoy Canyon basalt flows are presented, along with a brief discussion of seismic activity in the Pasco Basin, core disking, and borehole spalling observed in Hanford site boreholes.

Hydraulic fracturing test results obtained at depths of 921 to 1,195 m (3,022 to 3,921 ft) indicate that the maximum principal stress is oriented generally north-south, the intermediate principal stress is east-west, and the minimum principal stress is vertical. This result is consistent with focal mechanism solutions of earthquakes in the Pasco Basin area, east-west borehole spalling, and tectonic models that explain the evolution of geologic structure. In situ stresses at candidate repository horizons do not vary significantly with depth from the surface, test hole location, or basalt flow. Based on fracture reopening and shut-in pressures, and assuming that pore pressure acts in the fracture interval prior to reopening, the mean maximum and minimum horizontal stresses from all tests are 61.1 MPa (8,860 lbf/in^2) and 33.8 MPa (4,910 lbf/in^2), with standard deviations of 5.4 MPa (780 lbf/in^2) and 2.7 MPa (390 lbf/in^2), respectively. Within the reference repository location, the mean maximum and minimum horizontal stresses are 61.1 MPa (8,860 lbf/in^2) and 33.4 MPa

(continued on reverse side)

*	Distribution Name	Mail Address
*	E. B. Ash	PBB/110
*	R. J. Gimera	PBB/1100
	L. R. Fitch	PBB/1100
	G. S. Hunt	PBB/1100
	S. M. Price	PBB/1100
*	A. M. Tallman	PBB/1100
	P. E. Long	PBB/1100
	W. H. Price	MO-029/600
	D. J. Moak	MO-029/600
	S. R. Strait	MO-029/600
	S. M. Baker	PBB/1100
	M. J. Smith	PBB/1100
	R. C. Edwards	2101-M/200E
*	L. C. Hulstrom	2101-M/200E
	T. B. McCall	MO-407/200E
	R. T. Wilde	1135 Jad/1100
*	G. C. Evans	PBB/1100
*	J. F. Marron	PBB/1100
*	L. Connell	CDC #1/3000
*	D. J. Dodds	CDC #1/3000
*	T. A. Curran	GM/600
	N. A. Steger	GM/600
*	R. J. Bielefeld	GM/600
*	W. M. McCabe	CDC #1/3000
*	A. D. Krug	CDC #1/3000
*	S. A. Dischler	GM/600
	J. L. Ash	CDC #1/3000
	R. M. Ybarra	MO-410/600
	D. A. Turner	CDC #1/3000
	H. B. Dietz	MO-346/600
*	T. M. Wintczak	MO-346/600
	H. W. Brandt	MO-410/600
	M. F. Nicol	PBB/1100

(Continued on reverse side)

* COMPLETE DOCUMENT (No asterisk, title page/summary of revision page only)

BASALT

Release Stamp/Date:

10

OFFICIALLY RELEASED

1985 JAN 10 PM 4:17

Prepared By: Rockwell (Company & Contract No.) Date: 12-16-84

Used By: Rockwell (Company)

AUG 1991 RECEIVED EDMC

Number	Rev./Chg. No.
SD- BWI-TD-014	0

BWIP SUPPORTING DOCUMENT

Approvals	Date
☒ Author's Manager	1-9-85
☒ Peer Review	1/10/85
☒ Patentability/Sensitive Material	1/10/85
☐ Research/Licensing Manager	
☐ Engineering & Construction Manager	1-9-85
☒ Project Integ./Perf. Assessment Manager	1/10/85
☐ Exploratory Shaft Prog. Manager	
☐ Repository Program Manager	
☐ Associate Director	
☐ Director	
☐ Health, Safety & Environment	
☒ Quality Assurance	1/10/85
☒ Configuration Management	1-10-85
☒ Project Integration	1/10/85
☐ Licensing	1/10/85
☐	
☐	
☐	
☐	
☐	
☐	
☐	

Peer Review Identification No(s): 11200, 10546, 10700, 10153.

*	Distribution Name	Mail Address
	J. V. Mohatt	MO-410/600
*	W. J. Karwoski	CDC #1/3000
*	M. T. Black	CDC#1/3000
	D. J. Brown	PBB/1100
	D. J. Carrell	PBB/1100
	R. G. Baca	1135 Jad/1100
	A. E. Cottam	CDC #1/3000
*	W. F. Todish (Orig. + 2)	1135 Jad/1100
	Rec. Retn.	1135 Jad/1100
	P. J. Reder	1135 Jad/1100
	PRS	Fed/700
	U.S. Department of Energy	
	R. E. Constant	Fed/700
	J. H. Anttonen	Fed/700
*	O. L. Olson (2)	Fed/700
*	R. Stein (2)	DOE-HQ
*	R. P. Saget	Fed/700

Abstract (continued)

(4,840 lbf/in^2), with standard deviations of 4.9 MPa (710 lbf/in^2) and 2.7 MPa (390 lbf/in^2), respectively. Within the Cohassett flow, which is the preferred repository horizon, mean maximum and minimum horizontal stresses are 61.5 MPa (8,920 lbf/in^2) and 32.8 MPa (4,760 lbf/in^2), with standard deviations of 5.7 MPa (830 lbf/in^2) and 2.2 MPa (320 lbf/in^2), respectively. The relative consistency of the data exhibited from the test results implies that they may represent the true state of in situ stress at the candidate horizons in the Hanford site. It should be noted, however, that the hydraulic fracturing method is the only developed method for determining stress at depth from surface boreholes and that the absolute accuracy of the data can be validated only when the tests planned at the Exploratory Shaft are conducted. The method is widely accepted in the engineering community for providing engineering estimates of in situ stresses.

All test data are presented in the appendices.

SD-BWI-TD-014
REV 0

THE STATE OF IN SITU STRESSES DETERMINED BY HYDRAULIC FRACTURING AT THE HANFORD SITE

K. Kim
S. A. Dischler

J. R. Aggson
M. P. Hardy

J. F. T. Agapito and Associates, Inc.

August 1984

Prepared for the United States
Department of Energy
Under Contract DE-AC06-77RL01030

ROCKWELL INTERNATIONAL
Rockwell Hanford Operations
Energy Systems Group
P.O. Box 800
Richland, Washington 99352

ACKNOWLEDGEMENT

This report is a compilation of hydraulic fracturing test results that have been obtained through the efforts and cooperation of the following individuals. Dr. B. C. Haimson conducted the hydraulic fracturing tests and performed the data analysis for borehole DC-12. Mr. T. A. Rundle developed the test plans and was involved in the field program for boreholes RRL-2, RRL-6, and DC-4. Mr. T. M. Wintczak and Mr. D. J. Moak were involved in various stages of the test program and have provided logistic support on arranging drilling and packer equipment.

The contribution of these individuals is greatly appreciated.

CONTENTS

Acknowledgement 4

1.0 Introduction 8

2.0 Site Description 11
2.1 Geologic Setting 11
2.2 Stress Indicators 14
2.2.1 Seismic Activity 14
2.2.2 Core Disking 16
2.2.3 Borehole Spalling 20

3.0 Test Description 24
3.1 Determination of Principal Stress Magnitudes 24
3.1.1 Minimum Horizontal Principal Stress 24
3.1.2 Maximum Horizontal Principal Stress 26
3.1.3 Vertical Stress 27
3.2 Determination of Principal Stress Orientations 28
3.2.1 Impression Tests 28
3.2.2 Acoustic Borehole Televiewer 28
3.3 Equipment and Instrumentation 29
3.3.1 Downhole Equipment 29
3.3.2 Surface Equipment 31
3.4 Basalt Wast Isolation Project Hydraulic Fracturing Procedures 33
3.4.1 Hydraulic Fracturing Procedures 33
3.4.2 Impression Test Procedures 34

4.0 Test Results 35
4.1 Data Interpretation 35
4.1.1 Data Classification 35
4.1.2 Interpretation of Pressure-Time Curves 37
4.2 Data Analysis Rationale 38
4.3 Test Data and In Situ Stresses 41

5.0 Discussion of Results 47
5.1 Uncertainties Associated with Hydraulic Fracturing 47
5.2 Vertical and Lateral Variation of Horizontal Stresses 49
5.3 Comparison of Test Results with Stress Indicators 56
5.4 Stress Field in Relation to Regional Tectonics 56
5.5 Stress State for Repository Design 63

6.0 Summary and Conclusions 64

7.0 References 65

FIGURES:

1 Location of the Columbia Plateau, Pasco Basin, and Hanford Site 9
2 Location of the Reference Repository Location and Boreholes Used for Hydraulic Fracturing Tests at the Basalt Waste Isolation Project 10
3 Stratigraphic Nomenclature--Pasco Basin Cold Creek Syncline . 13
4 Instrumental Seismicity of the Central Columbia Plateau 15
5 Basalt Core Recovered from Borehole DC-12 at a Test Depth Between 1,011 and 1,014 m (3,317 and 3,325 ft) 17
6 Saddle or Potato Chip Disk 18
7 Examples of Continuous and Discontinuous Borehole Wall Breakouts Observed in Dense Interior by an Acoustic Televiewer in Borehole RRL-6 21
8 Plan View Representation of Borehole Spalling 22
9 Correlation of Core Disking with Borehole Spalling in Boreholes DC-4, RRL-6, and DC-12 23
10 Typical Flow Rate and Borehole Pressure Versus Time, Borehole RRL-2--Test Depth of 928 meters (3,044 ft) 25
11 Typical Fracture Impression Obtained from a Borehole RRL-2 Test 29
12 (a) Schematic Representation of the Hydrofracturing Tool 30
(b) Schematic Representation of the Impression Packer 30
13 Schematic of Surface Equipment 32
14 Typical Repressurization Cycle, Borehole RRL-6--Depth of 1,008 meters (3,306 ft) 39
15 Hanford Site Maximum and Minimum Horizontal Stress Versus Depth 50
16 Hanford Site Ratios of Maximum Horizontal Stress to Minimum Horizontal Stress and Maximum Horizontal Stress to Vertical Stress Versus Depth 51
17 Stress Direction and Mean Stress Magnitudes in Each Test Borehole 55
18 (a) Maximum Horizontal Stress Orientations--Individual Boreholes 57
(b) Stress Orientation Frequency Diagram 57
19 Compression and Tension Axes Derived From all Available Focal Mechanisms in the Central Plateau of Eastern Washington Through 1982 58
20 Variation in Ratio of Average Horizontal to Vertical Stress with Depth 60
21 In Situ Effective Stresses Compared to Joint Strength Envelopes 61

TABLES:

1 Core Disking Percentages for the Dense Interiors of Candidate Repository Horizons in Boreholes RRL-2, RRL-6, and RRL-14 ... 19
2 Number of Hydraulic Fracturing Tests Yielding Information on Stress Magnitudes and/or Orientations 37
3 Hydraulic Fracturing Test Results, (McCoy Canyon flow), 1,005 m (3,624 ft), Borehole RRL-6..... 40

4 Hanford Hydraulic Fracturing Test Data 43
5 Orientation of Induced Hydraulic Fractures 44
6 In Situ Stresses Obtained from Hydraulic Fracturing Tests ... 45
7 Summary of Mean Stress Values (±1 Standard Deviation) Obtained in Tested Basalt Flows 52
8 Summary of Mean Stress Values (±1 Standard Deviation) Obtained in Each Test Borehole 53
9 Summary of Mean Stress Values Obtained in the Umtanum Flow: RRL and Non-RRL 54
10 Preliminary Recommended Design Stresses for the Cohassett Flow 62

1.0 INTRODUCTION

The Basalt Waste Isolation Project (BWIP) has been investigating the feasibility of long-term disposal of civilian high-level nuclear waste in basalt flows beneath the Hanford Site in southeastern Washington State (Fig. 1). The proposed method of waste disposal is the construction of mined openings at depth within a basalt flow and the placement of waste canisters in bored holes in the walls of the storage rooms. After emplacement, the waste will be stored in a retrievable storage mode before decommissioning the underground facility by backfilling and sealing the storage rooms, underground accesses, and shafts.

Because the repository will be a licensed facility, certain regulatory requirements must be met before a license to construct a repository will be issued by the U.S. Nuclear Regulatory Commission (NRC). One of these requirements is that in situ stress should be measured before and after repository construction (NRC 1983 §60.21, p. 60-65). In situ rock stresses are an important parameter in establishing the feasibility of long-term disposal of civilian high-level nuclear waste in basaltic flows because rock stress affects mine design, mine safety, and waste isolation. Microseismic events, core disking, and borehole spalling have indicated that the stresses at the depths proposed for waste emplacement and storage could be sufficiently high to cause problems with construction and impact the waste emplacement density.

The proposed repository location, known as the reference repository location (RRL), shown in Figure 2, was located in 1981 from structural geology and then-existing siting guidelines (WCC 1981) but with limited subsurface site-specific data. Later, the Horizon Identification report (Long 1983) evaluated subsurface data and repository performance assessment analyses to select a dense flow interior as the preferred repository horizon below the RRL. From preliminary selection guidelines based primarily on dense flow interior thickness, uniform lateral continuity, and depth four candidate horizons were evaluated more fully in the selection process. The four horizons in descending stratigraphic order were the Rocky Coulee, Cohassett, McCoy Canyon, and Umtanum flows, of which the Cohassett flow was selected as the preferred horizon.

At the present time, access to the preferred horizon is limited to holes drilled from the surface so methods of stress measurement at depth are restricted to the hydraulic fracturing technique. When the Exploratory Shaft is completed and access is available to the dense interior of the Cohassett flow, additional stress determinations using alternate techniques are to be performed to confirm the hydraulic fracturing test results.

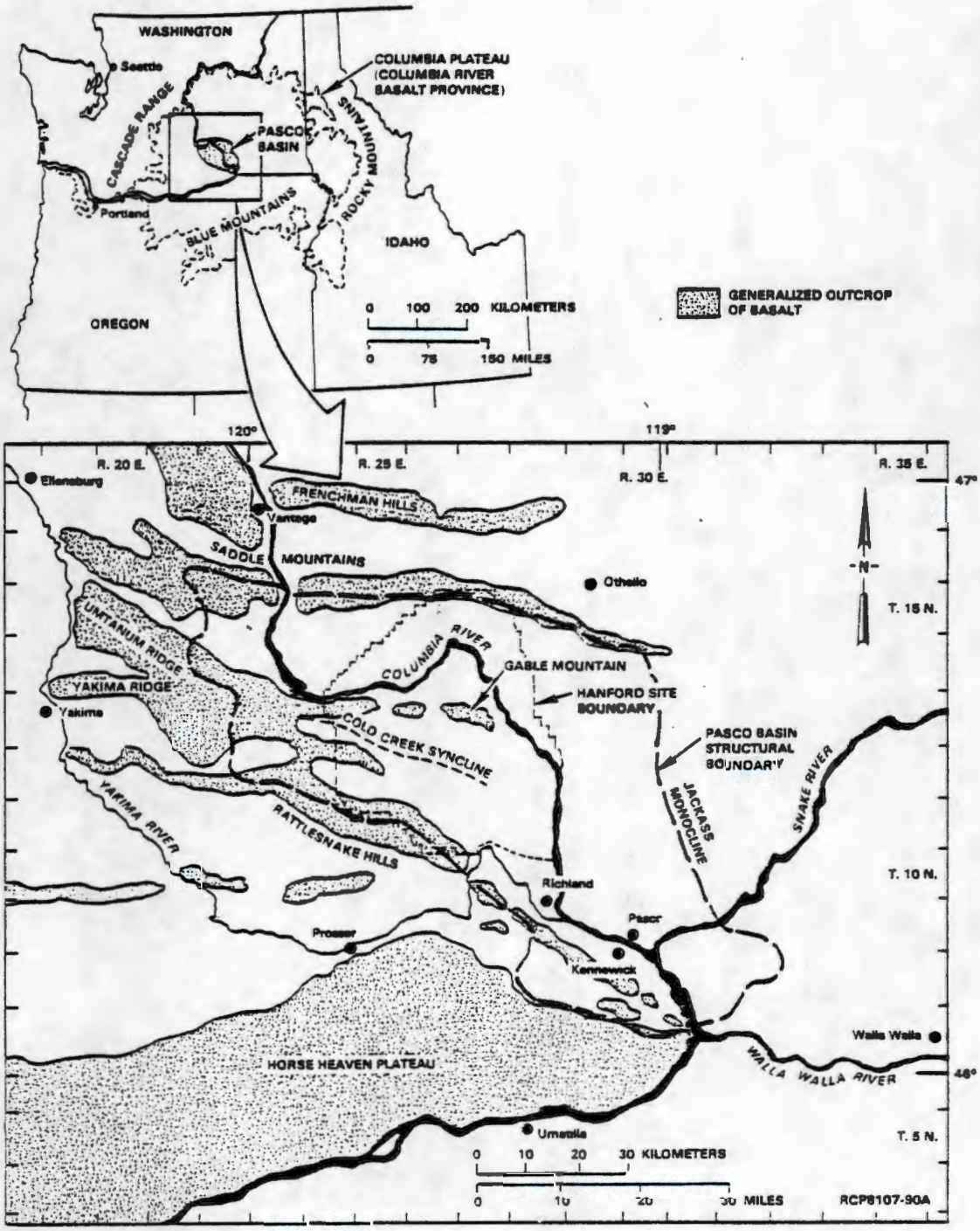

FIGURE 1. Location of the Columbia Plateau, Pasco Basin, and Hanford Site.

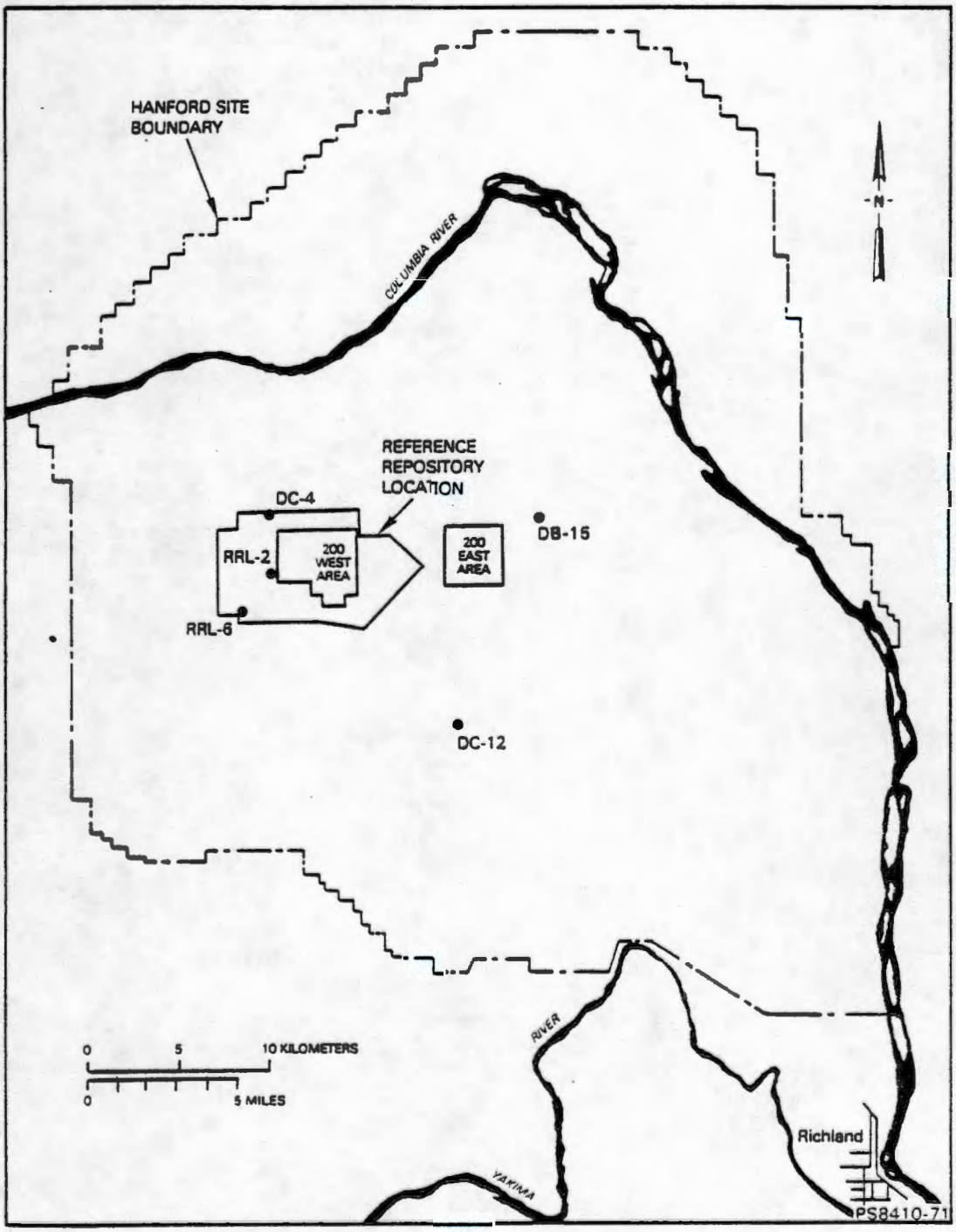

FIGURE 2. Location of the Reference Repository Location and Boreholes Used for Hydraulic Fracturing Tests at the Basalt Waste Isolation Project.

The first hydraulic fracturing tests at the Hanford Site were conducted in 1978 as part of the Near Surface Test Facility program at Gable Mountain. These tests, conducted in the Pomona flow, were 16.8 to 69.2 m (55.1 to 227.0 ft) from the surface (Haimson 1979) and did not provide a basis for estimating the in situ stresses at depth. Deep hole equipment and procedure development tests were then conducted in the Roza flow at a depth of 343 m (1,128 ft) in borehole DB-15 (Kim 1981). This testing demonstrated that the hydraulic fracturing technique could be applied to the jointed basalt beneath the Hanford Site and that test results could be interpreted so as to quantify the in situ stresses.

Following the equipment and procedure development tests conducted in borehole DB-15, hydraulic fracturing tests were conducted in boreholes DC-12, RRL-2, RRL-6, and DC-4 (see Fig. 2). This series of tests was designed to quantify the in situ stresses at candidate repository horizons with particular emphasis on the RRL. The data obtained from these tests indicate that the horizontal stresses are higher than the vertical stress and that the maximum principal stress is acting in a general north-south direction. This north-south orientation is in general agreement with focal mechanism solutions of earthquakes, geologic structures (Rohay and Davis 1983), and stress orientations inferred from borehole spalling.

The prime purpose of the stress measurement program described in this report is to obtain quantitative data on the in situ stress near the candidate repository horizon. This report summarizes the BWIP hydraulic fracturing stress measurement program and the results obtained to date. All data are presented in the appendixes with a full description of the data screening and data interpretation methods given in the report. A brief discussion of the interrelationship between the observed stress state and the regional tectonism and the suggested in situ stress values for use in repository design are presented.

2.0 SITE DESCRIPTION

The geographic locations of the Columbia Plateau, Pasco Basin, and Hanford Site are shown in Figure 1. The location of the RRL and the boreholes used for the hydraulic fracturing tests are shown in Figure 2.

2.1 GEOLOGIC SETTING

The Columbia Plateau, a flood basalt province, is underlain by Miocene tholeiitic basalts that were erupted from north-northwest trending linear vent systems exposed mostly in southeastern Washington, northeastern Oregon, and west-central Idaho (Waters 1961, Taubeneck 1970, Swanson et al. 1977). These highly fluid lavas spread over great distances from their source vents and flowed generally westward along a gentle slope before consolidating in a basin between the ancestral Cascade and Rocky Mountain ranges in the

interval 16.5 to 6 m.y. ago. Some voluminous flows extended down an ancestral Columbia River gorge and are now found along the Oregon coast (Beeson and Moran 1979). The total areal extent of the Columbia River basalts is ≅200,000 km^2 (77,000 mi^2). Basalts reach a maximum known thickness of >3 km (>1.9 mi) in the Pasco Basin (Reidel et al. 1982).

The Pasco Basin is one of several Tertiary synclinal basins in the central Columbia Plateau that contains Neogene and Quaternary sediments and is bordered mostly by anticlinal ridges. The oldest formation of the Columbia River Basalt Group known in the Pasco Basin is the Grand Ronde Basalt Group, which is overlain by Wanapum and Saddle Mountains Basalts. The generalized stratigraphy below the RRL is shown in Figure 3. Intercalated with the basalts are fluvial, tuffaceous sediments of the Ellensburg Formation, which are common in the Wanapum and Saddle Mountains Basalts. The basalts are, in turn, overlain by mostly fluvial sediments of Ringold and Quaternary Hanford Formations. Narrow, asymmetrical anticlines of the Yakima Fold Belt border the basin to the north (Saddle Mountains), west (Umtanum and Yakima Ridges), and the southwest (Rattlesnake Hills) (see Fig. 1). Structural relief on these folds decreases eastward from the western margin of the basin where the axes of the Umtanum and Yakima Ridges plunge beneath sediments in the basin. Basalt crops out in the Pasco Basin on Gable Butte and Gable Mountain, which are eastward continuations of the Umtanum Ridge. The Yakima Ridge extends eastward where its extension is recognized beneath the surface from drilling and geophysical data. The eastern margin of the Pasco Basin is essentially the north-trending Jackass monocline, east of where the basalt thins and rises gently eastward onto the Palouse slope. Details of the Pasco Basin geology, along with geologic maps, can be found in Myers/Price et al. (1979).

The RRL is in the axial region of the western part of the southeast-trending Cold Creek syncline, one of several synclines in the Pasco Basin. The Cold Creek syncline is asymmetrical with strata rising more gently to the north on the south limb of the Umtanum Ridge/Gable Mountain structure and more steeply onto the buried extension of Yakima Ridge to the south.

Individual basalt flows generally consist of a porous and often brecciated flow top material above the dense interior. The dense interior materials can consist of two layers differentiated on the basis of intraflow structures, texture, and percentage of mesostasis into the entablature and colonnade. However, the dense interior of some flows consists of multiple layers of entablature and colonnade zones. The colonnade and entablature zones differ primarily in the frequency and orientation of cooling joints, with the colonnade made up of hexagonal columns with some horizontal intercolumn joints; whereas, the entablature joints are more closely spaced and form an irregular blocky pattern.

Assessment of structural and hydrologic basalt flow characteristics lead to the conclusion that the repository should be located within the dense interior of a flow and be isolated from the porous and permeable flow top. Four flows in the RRL were identified as having sufficient thickness for repository construction, and one of these (the Cohassett flow) appears to provide the thickest section of dense interior material for repository construction (Long 1983, p. I-230).

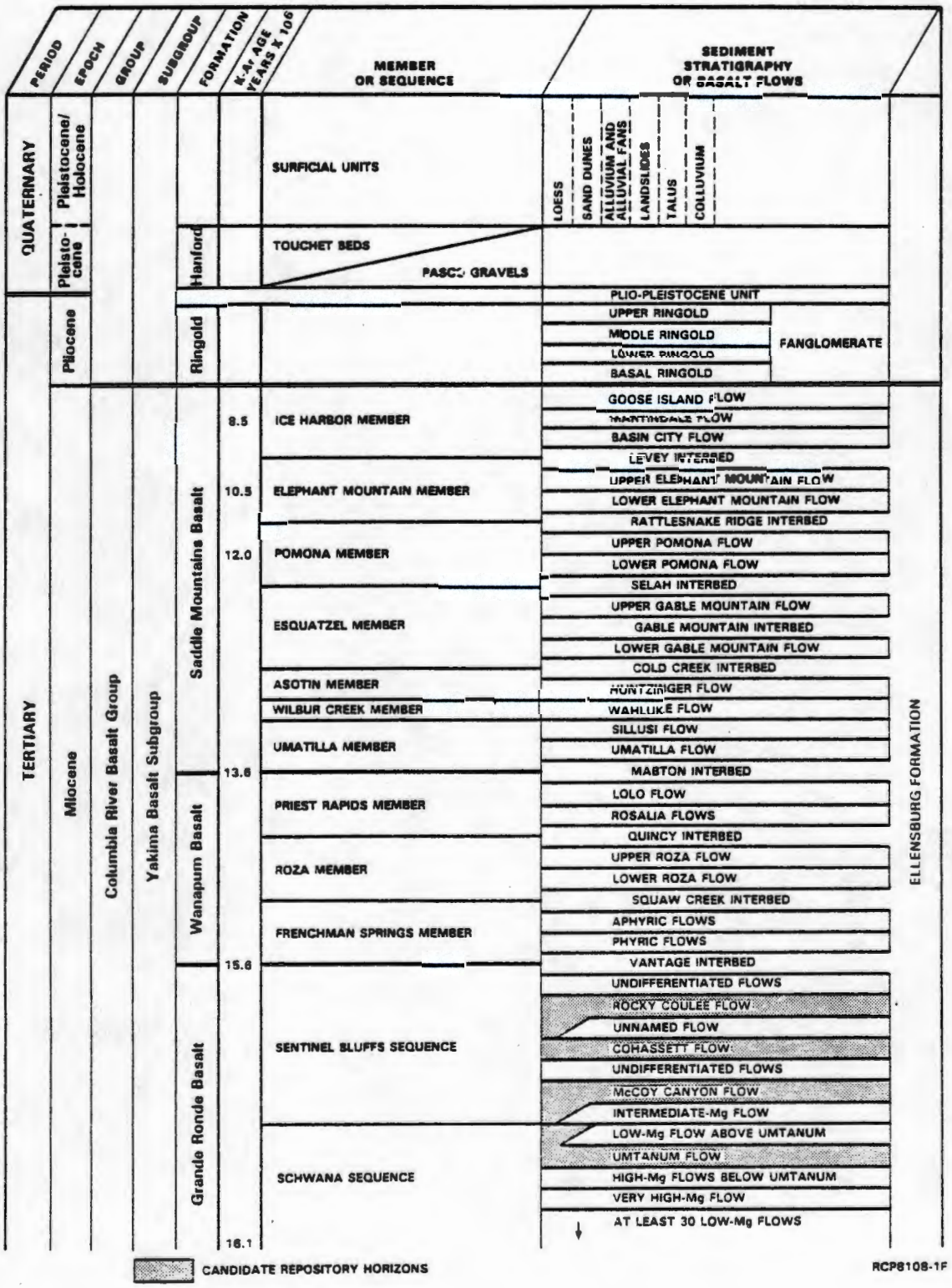

NOTE: The position of the Grande Ronde 7 in RRL 2 is right above the McCoy Canyon flow.

FIGURE 3. Stratigraphic Nomenclature--Pasco Basin, Cold Creek Syncline.

The dense interior of the Cohasset flow consists of multiple layers of entablature and colonnade intraflow structures with one laterally extensive vesicular zone located approximately one third of the distance down from the top of the dense interior. The repository could be located in the 30- to 50-m-thick interval immediately below the vesicular zone.

In an assessment of the tectonic evolution of the RRL, Caggiano and Duncan (1983) have concluded that the stress regime suggested by nearly east-west folds and subparallel thrust and reverse faults, and steeply dipping northwest- and northeast-trending faults in the Yakima Fold Belt is one of nearly north-south, nearly horizontal compression, with a nearly vertical axis of least compression.

2.2 STRESS INDICATORS

Contemporary seismic activity beneath the Columbia Plateau, along with core disking and borehole wall spalling experienced in exploratory boreholes, indicates the in situ stress at depth is not lithostatic. These stress indicators have been used to gain qualitative insights into the nature of the in situ stress distribution beneath the Hanford Site.

2.2.1 Seismic Activity

Contemporary deformation of the Columbia Plateau is indicated by the observed pattern of seismicity. Earthquake swarms are the predominant characteristic of the Columbia Plateau seismicity (Rohay and Davis 1983). These earthquake sequences typically last a few days to several months and occur in a volume of rock with typical dimensions of ≅5 km (3.1 mi). Earthquake swarms (as detected and located by the regional seismic network) may contain several to ≅100 locatable earthquakes of magnitude 1.0 to 3.5, but most are smaller than magnitude 2.0. During a swarm, there is no distinctively large event that is followed by a generally decreasing level of seismicity, as is typical of a mainshock-aftershock sequence. Swarm earthquakes tend to gradually increase and decay in frequency, but not in magnitude. The distribution of seismicity of the central Columbia Plateau is shown in Figure 4 (Rohay and Davis 1983).

Shallow earthquakes occur at a significantly greater rate than deep earthquakes. Approximately 75% of the earthquakes are located shallower than 4 km (2.5 mi) deep, and 80% of these shallow events occur during earthquake swarms (Rohay and Davis 1983, pp. 6-7). A distinction between shallow and deep seismicity also is reflected in the recurrence relations or size distribution of the earthquakes.

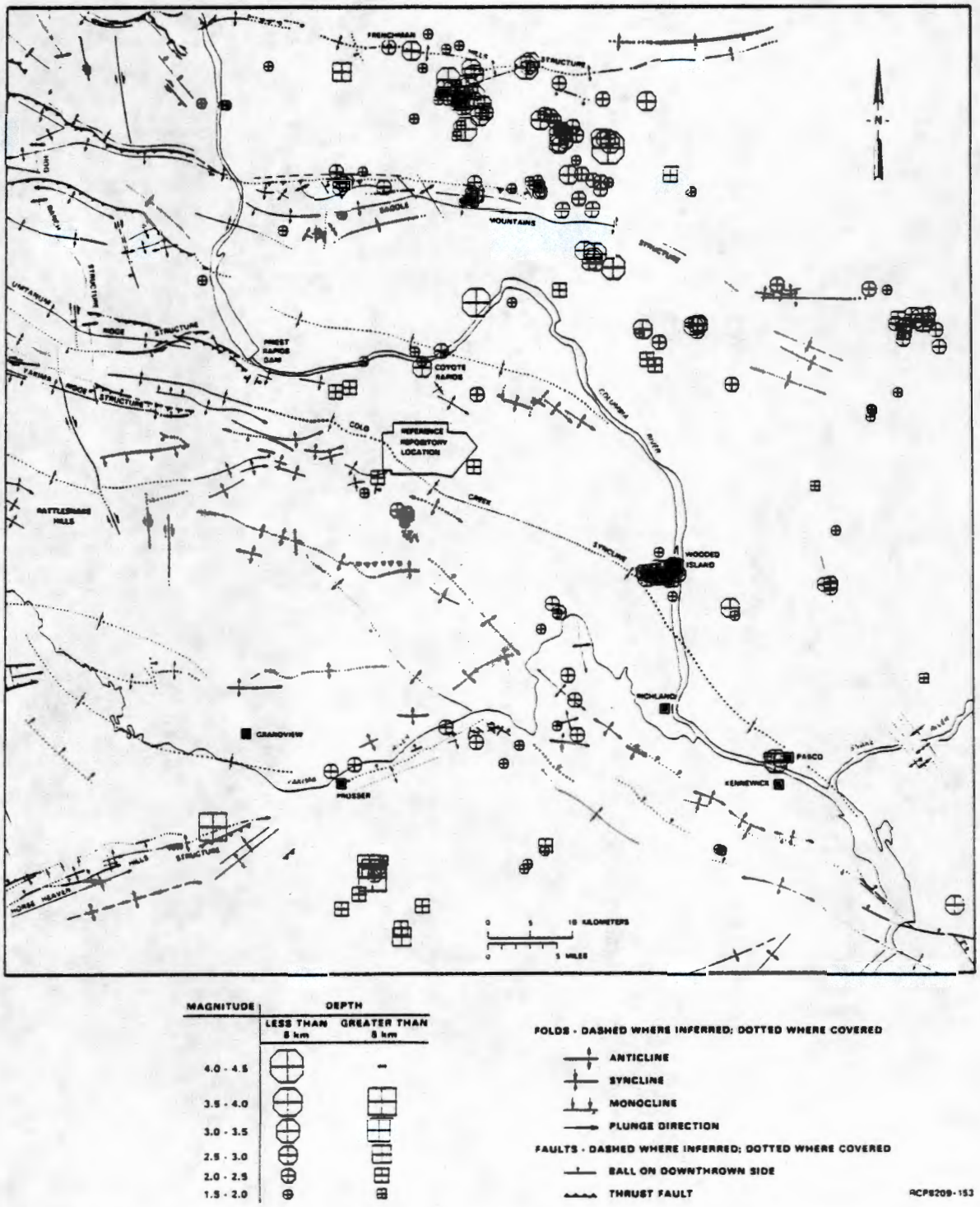

FIGURE 4. Instrumental Seismicity of the Central Columbia Plateau.

Earthquake swarm activity is concentrated in the central portion of the Columbia Plateau, principally north and east of the Hanford Site between the Saddle Mountains and Frenchman Hills structures (see Fig. 4). It is within this region that most events (in swarms and as individual events) larger than magnitude 3.0 occur including the largest magnitude swarm earthquake instrumentally recorded, the December 20, 1973, magnitude 4.4 Royal Slope earthquake.

Focal mechanism solutions of earthquakes in central Columbia Plateau indicate a response to a nearly horizontal principal compression oriented north-south (Malone et al. 1975, Rohay and Davis 1983). Focal mechanism solutions also indicate that the minimum compression is generally vertical. Thus, thrust or reverse faulting on east-west striking planes is indicated. These principal stress directions are in agreement with mapped east-west orientations of fold axes and associated thrust or reverse faults mentioned in Section 2.1.

2.2.2 Core Disking

The possibility of relatively high in situ stress in the rocks beneath the Hanford Site was first indicated by the occurrence of core disking. Core disking is the phenomenon by which drill core fractures into thin disks during the drilling process. Examples of core disking are shown in Figures 5 and 6.

Core disking at the Hanford Site has been described by Moak (1981) and Long (1983, p. I-230). Table 1 is presented to demonstrate the occurrence of core disking in typical RRL boreholes. In Table 1, core disking in boreholes RR1-2, RRL-6, and RRL-14 (see Fig. 2) is given as a percentage of the dense interior thickness for each horizon (Long 1983, p. I-230).

Core disking has long been known to be an indicator of high stress (Obert and Stephenson 1965; Jaeger and Cook 1965). Lehnhoff et al. (1982) have reviewed the published literature associated with the core disking phenomenon, conducted finite element analyses of the borehole/bit geometry, and interpreted the results of their investigations in terms of the Hanford Site. Their conclusions can be summarized as follows:

- The saddle-shaped disking, as shown in Figure 6, is the result of nonaxisymmetric horizontal stresses
- Oriented core from holes producing saddle-shaped disks indicate the maximum horizontal stress is generally north-south
- The ratio of average horizontal stress to vertical stress is predicted to be in the range of 1.6:1 to 2.0:1 at the 1,130 m (3,700 ft) depth
- The ratio of maximum horizontal stress to minimum horizontal stress is predicted to be in the range of 1.2:1 to 1.5:1 at the 1,130 m (3,700 ft) depth.

8100468-187cn

FIGURE 5. Basalt Core Recovered from Borehole DC-12 at Test Depth Between 1,011 and 1,014 Meters (3,317 and 3,325 ft). This core is from the Umtanum flow (see Figure 9 for correlation).

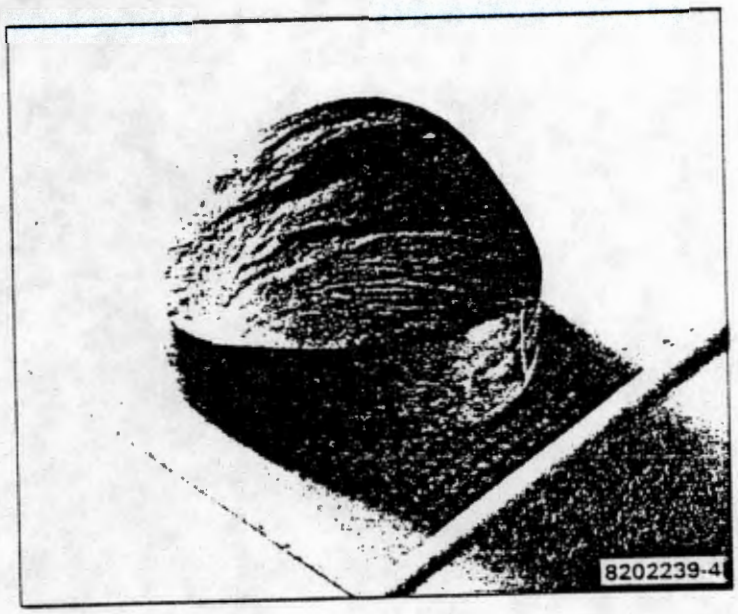

FIGURE 6. Saddle or Potato Chip Disk
(Lehnhoff et al. 1982).

TABLE 1. Core Disking Percentages for the Dense Interiors of Candidate Repository Horizons in Boreholes RRL-2, RRl-6, and RRL-14 (Long 1983 p. I-230).

Borehole	Rocky Coulee flow			Cohassett flow			McCoy Canyon flow			Umtanum flow		
	Dense interior, m (ft)	Disked (m)	Disked (%)	Dense interior, m (ft)	Disked, m (ft)	Disked (%)	Dense interior, m (ft)	Disked, m (ft)	Disked (%)	Dense interior, m (ft)	Disked, m (ft)	Disked (%)
RRL-2	46.6 (152.9)	9.1 (29.9)	19.5	45.1 (148.0)	10.3 (33.8)	22.8	31.4 (103.0)	14.7 (48.2)	46.8	25.3 (83.0)	17.4 (57.1)	68.9
RRL-6	46.2 (151.6)	38.5 (126.3)	83.3	43.3 (142.1)	3.8 (12.5)	8.8	30.5 (100.1)	8.1 (26.6)	26.6	41.8 (137.1)	23.1 (75.8)	55.3
RRL-14	30.5 (100.1)	20.8 (68.2)	68.2	35.7 (117.1)	22.8 (74.8)	63.9	33.2 (108.9)	17.7 (58.1)	53.3	39.0 (128.0)	36.9 (121.1)	94.6
Total	123.3 (404.5)	68.4 (224.4)		124.1 (407.2)	36.9 (121.1)		95.1 (312.0)	40.5 (132.9)		106.1 (348.1)	77.4 (253.9)	
Average percent disked			55.5			29.7			42.6			73.0

A discussion regarding the relationships between the findings of the foregoing study and the stress state determined by hydraulic fracturing at the Hanford Site is found in Section 5.3 of this report.

2.2.3 Borehole Spalling

Azimuthally aligned east-west borehole spalling in deep boreholes on the Hanford Site has been observed by downhole television surveys, impression test results, and acoustic televiewer techniques. The televiewer is an ultrasonic device that produces a photographic image of the pattern of acoustic reflectivity off the borehole wall. Detailed descriptions of the televiewer logging system and a discussion of imaging techniques employed in the processing of televiewer logs are given by Zemanek et al. (1969). Paillet (1984) has obtained acoustic televiewer logs for 400-m (1,312 ft) intervals in boreholes DC-4, RRL-6, and DC-12 and concludes that borehole spalling or borehole wall breakouts have a consistent east-west orientation at the Hanford Site. Examples of acoustic televiewer intervals and borehole spalling in borehole RRL-6 are shown in Figure 7.

Gough and Bell (1981) first suggested that borehole spalling or breakouts occur in the direction of least horizontal compression because they are caused by shear failure of the rock in the region where the concentration of compressive stress near the borehole is greatest. Zoback et al. (1984) have extended the theoretical analysis of the mechanism in order to better explain the observed breakout shapes. The consistent east-west orientation of borehole spalling at the Hanford Site indicates that the maximum horizontal stress is generally north-south, as indicated by the plan view representation of borehole spalling shown in Figure 8.

Paillet (1984) has compared the extent of borehole-wall breakouts or spalling to the extent of core disking in boreholes RRL-6, DC-4, and DC-12. This comparison is represented graphically in Figure 9, showing a relatively good correlation between core disking and borehole spalling, and that core disking and borehole spalling are confined to the interiors of individual flows.

The frequency of core disking and borehole spalling and the correlation between these phenomena support the premise that the in situ stress distribution at the Hanford Site is not lithostatic.

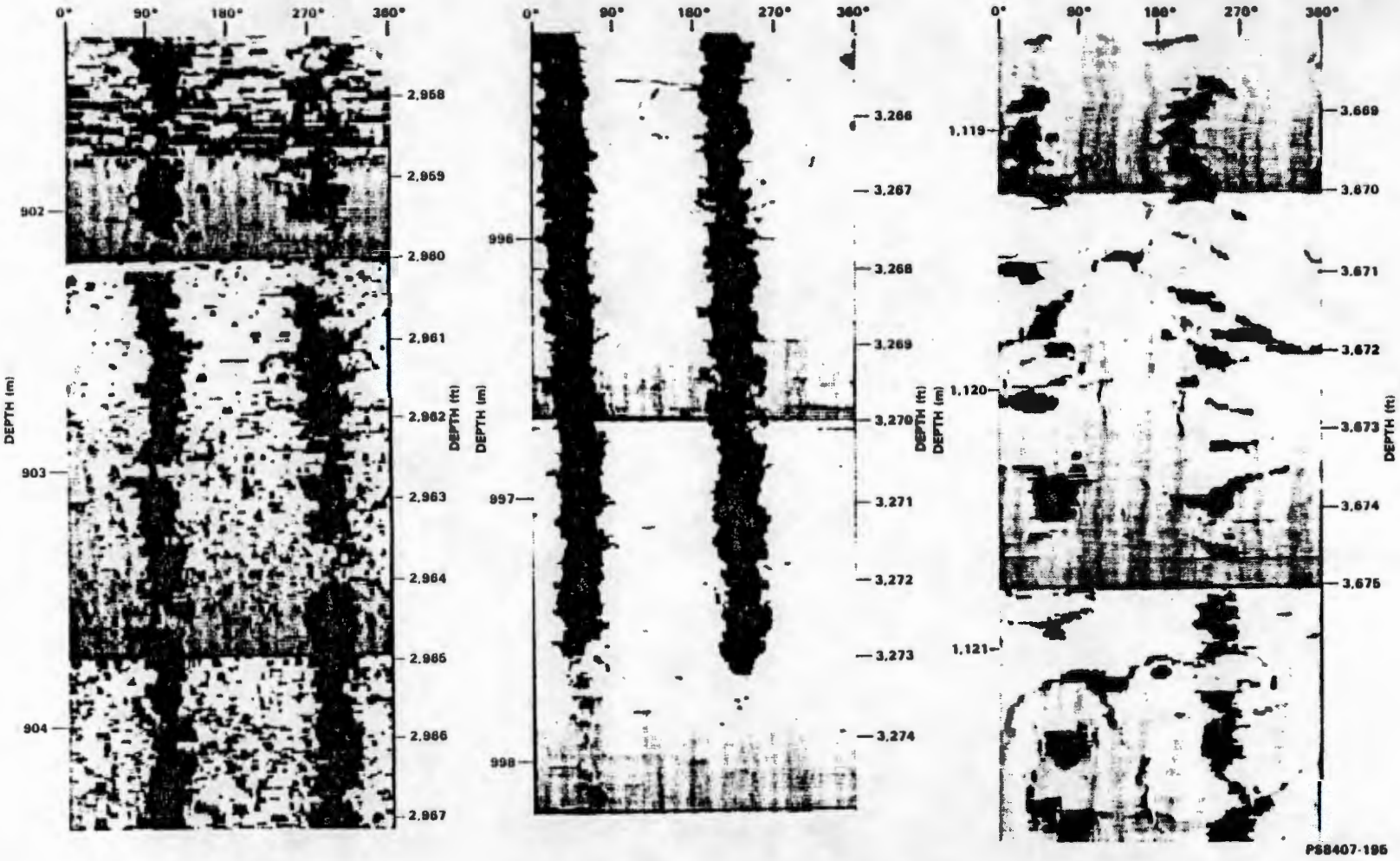

FIGURE 7. Examples of Continuous and Discontinuous Borehole Wall Breakouts Observed in Dense Interior by an Acoustic Televiewer in Borehole RRL-6 (Paillet 1984).

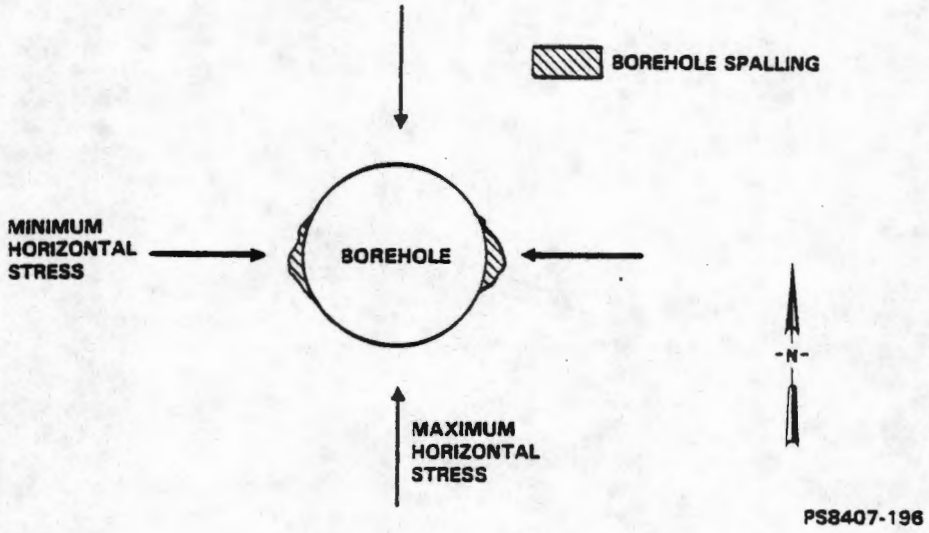

FIGURE 8. Plan View Representation of Borehole Spalling.

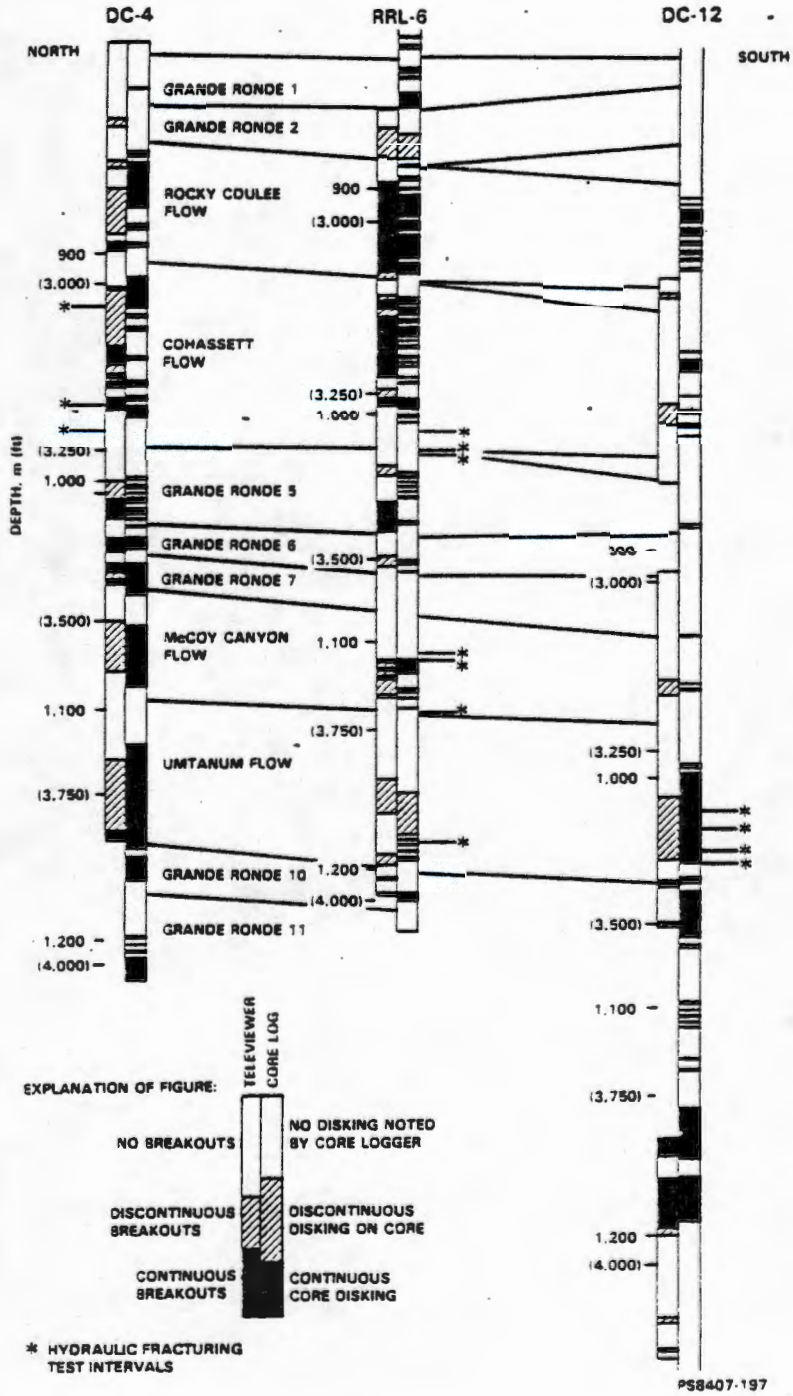

FIGURE 9. Correlation of Core Disking with Borehole Spalling in Boreholes DC-4, RRL-6, and DC-12 (Paillet 1984).

3.0 TEST DESCRIPTION

The hydraulic fracturing stress determination method has gained a wide acceptance in the geotechnical community in recent years (Zoback and Haimson 1982a). The method consists of isolating a segment of a small diameter borehole, 76 mm (3 in.) in this case, using a straddle packer system and pressurizing the sealed-off borehole segment using hydraulic fluid (e.g., water). As fluid pressure is increased in the test interval, the initial compressive tangential stress around the borehole wall is decreased to tensile stress. When this tensile stress reaches the strength of the rock, borehole rupture occurs. This rupture is also called "borehole breakdown." The pressure at this moment is defined as the breakdown pressure.

Although the test operation is relatively simple, the actual physical phenomenon occurring at the test interval is not clearly understood, and therefore, judgments need to be made during test operation as well as during data analysis. It should be noted that the measurement techniques are still improving, and new methods of data interpretation are evolving.

Equipment and hydraulic fracturing test procedures are described in the hydraulic fracturing test plans (Rundle 1982, 1983). A general description of the hydraulic fracturing stress determination method is presented in this section to assist readers with a minimal background in understanding the test procedure and data analysis methods.

3.1 DETERMINATION OF PRINCIPAL STRESS MAGNITUDES

3.1.1 Minimum Horizontal Principal Stress

The principal stress magnitudes are interpreted from the pressure history; a typical set of flow rate and interval pressure versus time curves is shown in Figure 10. The minimum horizontal stress, σ_h, is measured directly as the instantaneous shut-in pressure (P_{isi}), based on the assumption that the induced fracture is perpendicular to σ_h.

$$\sigma_h = P_{isi} \tag{1}$$

The shut-in pressure is defined as the equilibrium pressure in the fracture immediately after pumping stops. The methods used to determine shut-in pressures are discussed in detail in Section 4.1.2, which describes interpretation procedures.

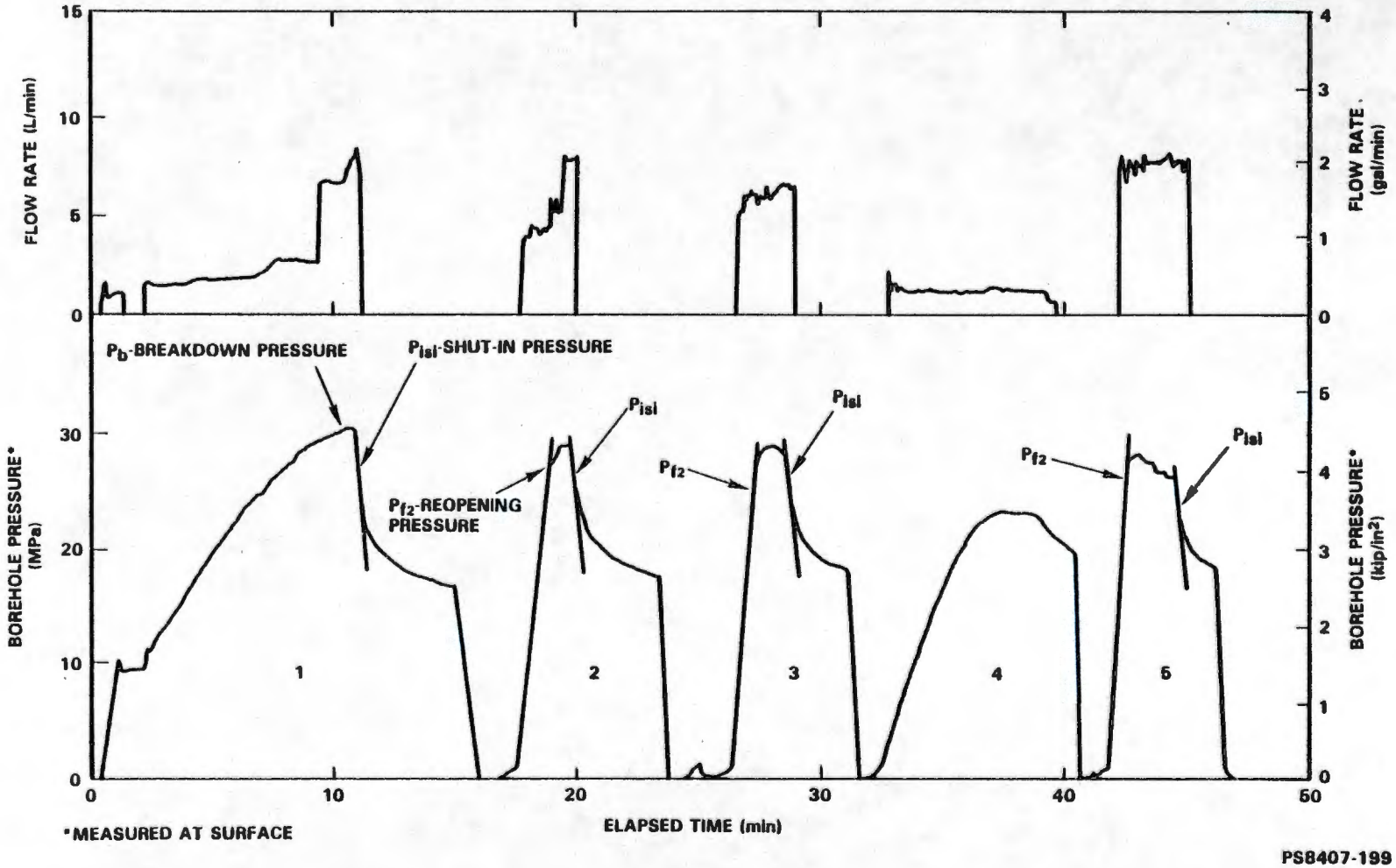

FIGURE 10. Typical Flow Rate and Interval Pressure Versus Time, Borehole RRL-2--Test Depth of 928 Meters (3,044 ft).

3.1.2 Maximum Horizontal Principal Stress

Determination of the maximum horizontal stress, σ_H, requires definition of the elastic stress concentrations around a circular hole as determined by Kirsch (1898). Currently, two methods of determining σ_H are used: (1) the initial breakdown and (2) fracture reopening methods.

3.1.2.1 Initial Breakdown Method. As the test interval is pressurized, a tensile crack is initiated (breakdown) when the tangential stress (σ_{tan}) around the borehole equals the in situ tensile strength of the rock or borehole rupture strength, T_o.

$$\sigma_{tan} = P_b - 3\sigma_h + \sigma_H = T_o \tag{2}$$

The pressure in the borehole at fracture initiation is termed the breakdown pressure, P_b, and is equal to the following:

$$P_b = (3\sigma_h - \sigma_H) + T_o \tag{3}$$

The maximum horizontal stress can be expressed as follows:

$$\sigma_H = 3\sigma_h - P_b + T_o \tag{4}$$

The breakdown pressure, P_b, is defined as the peak pressure attained during the first cycle as shown in Figure 10. The borehole rupture strength, T_o, is difficult to obtain. The tensile strength of the core from the test interval can be determined experimentally in the lab; however, tensile strengths vary depending upon geometry, specimen size, and test method (Zoback and Haimson 1982b), and uncertainty is involved in extrapolation of laboratory-determined tensile strengths to in situ conditions, although several techniques have been proposed and are often used (Ratigan 1982; Doe et al. 1983). If a pore pressure, P_o, is present in the rock, Equation 2 is modified according to the principle of effective stress (Haimson 1968) as in Equation 5.

$$\sigma_H = 3\sigma_h - P_b + T_o - P_o \tag{5}$$

3.1.2.2 Fracture Reopening Method. The fracture reopening method, as described by Bredehoeft et al. (1976), uses the pressure necessary to reopen a hydraulic fracture without the resistance due to T_o. This assumes that the difference between breakdown (P_b) and reopening (P_{f2}) pressures is equal to T_o. In terms of Equation 5, P_b is replaced by P_{f2} and T_o becomes zero, or:

$$\sigma_H = 3\sigma_h - P_{f2} - P_o \tag{6}$$

The fracture reopening method of interpreting hydraulic fracturing tests is widely used (Zoback and Haimson 1982a), seems to yield consistent results (Zoback and Haimson 1982b), and has been selected as the preferred method of analyzing the tests presented in this report.

Critical pressures were measured by a pressure transducer at the surface, thus, the hydrostatic pressure (P_h) at the test interval must be added to Equations 1 through 6. The resulting equations used to calculate horizontal principal stresses are as follows:

$$\sigma_h = P_{isi} + P_h \tag{7}$$

$$\sigma_H = 3\sigma_h - (P_{f2} + P_h) - P_o \tag{8}$$

3.1.3 Vertical Stress

The vertical stresses, σ_v, are calculated from the density and thickness of the overlying strata according to Equation 9.

$$\sigma_v = (D-\tau)\frac{\delta_b}{1{,}000} + \tau\frac{\delta_s}{1{,}000} \tag{9}$$

where

D = test depth (m)

τ = depth of sediments overlying basalt (m)

δ_b = density of basalt (kN/m^3)

δ_s = average density of overlyling sediments (kN/m^3)

It is assumed that the vertical stress is a principal stress.

3.2 DETERMINATION OF PRINCIPAL STRESS ORIENTATIONS

The fracture induced by hydraulic pressurization occur, theoretically, in the direction normal to the highest induced tensile stress around the borehole. Fractures are induced either vertically or horizontally. Horizontal hydraulic fractures have been reported at depths of <300 m (800 ft) (Haimson et al. 1976, Haimson 1982, Rummel 1982, Roegiers and McLennan 1982), but in most deep hydraulic fracturing tests, the fractures initiate vertically at the borehole wall even though the vertical stress may be the least principal stress (Zoback and Haimson 1982b, Zoback and Pollard 1978). This initial fracture orientation is because of the complex interaction of the straddle packers and pressurization fluid that combine to produce the stress distribution in the pressurized section of the borehole wall. Ensuing pressurizations may allow the fracture rotate to the direction normal to the minimal principal stress.

In the case of vertical fractures, the principal stress directions can be determined by measuring the orientation of the induced fractures. In the BWIP tests, impression tests were used to determine fracture orientation in all test intervals, and in selected boreholes, the acoustic televiewer method was used to confirm the impression tests. The theory and the operating principles of the acoustic televiewer method can be found elsewhere (Paillet 1984).

3.2.1 Impression Tests

Impression tests involve the use of an inflatable packer long enough to cover the test interval. The packer, with a thin layer of semicured rubber epoxied on the outer surface, is lowered to the previously fractured test interval. This rubber liner conforms easily to the borehole wall when the packer is pressurized and retains the impression upon the depressurization of the packer. Orientation of the impression packer with respect to true north is obtained by a gyroscopic compass (to eliminate magnetic effects), which is photographed with an internal camera. The orienting device is lowered by wireline to attach to a key on the top of the impression packer. A typical impression tracing is shown in Figure 11.

3.2.2 Acoustic Borehole Televiewer

The acoustic borehole televiewer has some advantages as well as disadvantages over the impression method. Advantages include the relatively simple operation and the ease in fracture image data processing. The most significant advantage is that this method provides a view of the entire borehole condition. The major disadvantage is that magnetic influence on the image processing is difficult to eliminate. This method was used primarily to delineate areas of borehole wall spalling. Relative orientations of borehole spalling and hydraulic fractures can be used to verify spalling direction. Resolution of hydraulic fractures from the televiewer image is not always good due to vertical scale compression and very tight fractures due to the relatively high stresses.

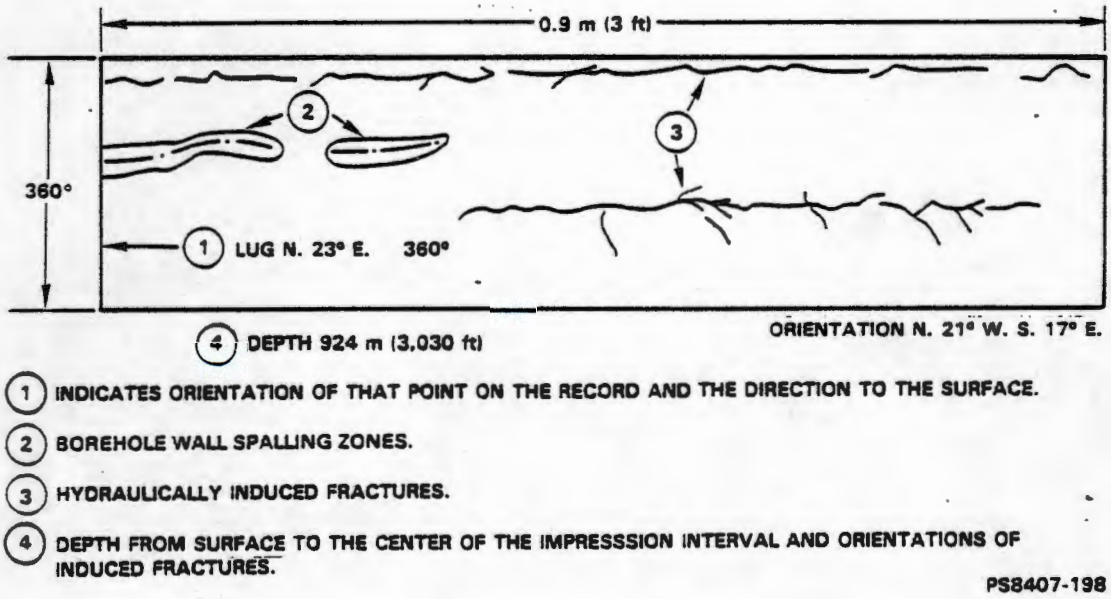

FIGURE 11. Typical Fracture Impression Obtained from a Borehole RRL-2 Test.

3.3 EQUIPMENT AND INSTRUMENTATION

Hydraulic fracturing tests conducted in borehole DC-12 were conducted by Haimson using equipment similar to that described here (Haimson and Kim 1982). The remaining tests in boreholes RRL-2, RRL-6, and DC-4 were conducted using the equipment described here. All equipment and instrumentation were calibrated (traceable to the National Bureau of Standards) with calibration records kept on file at the BWIP Records Retention Center.

3.3.1 Downhole Equipment

Downhole equipment consisted of the hydraulic fracturing straddle packer system and the impression packer. A schematic representation of these downhole components is presented in Figure 12.

The hydraulic fracturing tool consists of two 1.2-m- (4 ft) long, 6.7-cm- (2-5/8 in.) dia. inflatable rubber packers connected by an inner mandrel to isolate a 0.6-m (2.0 ft) interval of the borehole. The tool has two independent hydraulic circuits, one for inflation of the packers and the other for pressurization of the test interval. The packer assembly (see Fig. 12) is suspended in the borehole by 2.5-cm (1.0 in.) tubing from a standard oil field workover rig. This high pressure pipe also serves as the conduit through which the test interval is pressurized. Two 9.5-mm- (3/8 in.) OD high pressure hoses are strapped to the tubing and provide a means of inflating and venting the packers.

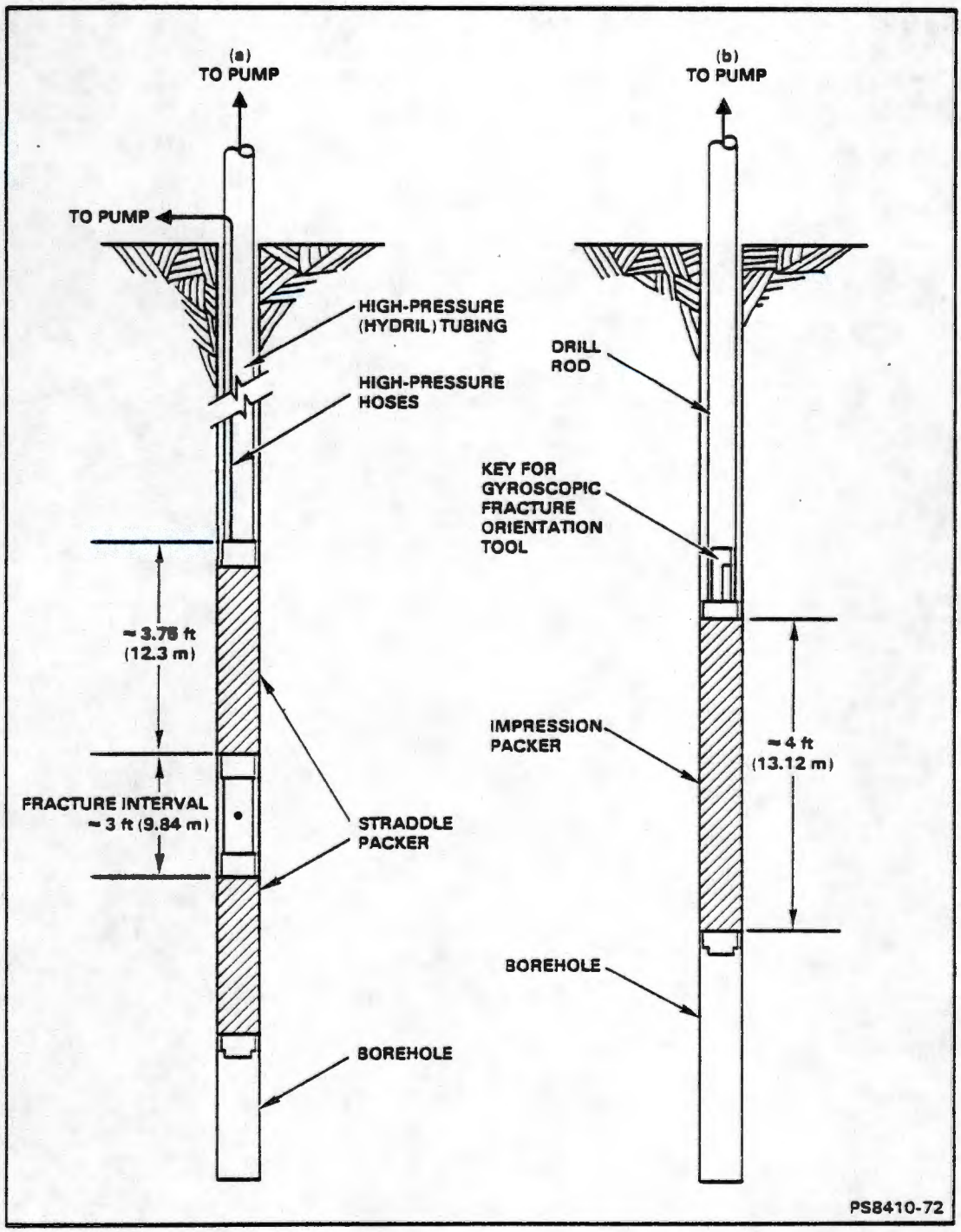

FIGURE 12. (a) Schematic Representation of Hydrofracturing Tool.
(b) Schematic Representation of Impression Packer.

In all tests, borehole pressure in the test interval, packer pressure, and flow rate were measured at the surface. Tests in borehole DC-4 incorporated a downhole instrumentation assembly and a surface readout/control unit, which allowed the comparison of pressures measured downhole and at the surface. The downhole instrument assembly was located immediately above the straddle packers and contained a surface-activated packer fill/release valve, packer pressure transducer, and a test interval pressure transducer. Downhole valves reduced the time required to set and release the interval packers, and the use of downhole pressure transducers provided a true measure of test pressure, thus, eliminating the correction for the hydrostatic head, P_h, in Equations 7 and 8.

Orientations of induced hydraulic fractures at the borehole wall were determined by an impression packer. The impression packer, shown in Figure 12, consists of a 0.91-m- (3.0 ft) long, 5.4-cm- (2 1/8 in.) dia. inflatable packer covered with a sleeve of semicured rubber. The rubber sleeve conforms to the borehole wall when the packer is pressurized and retains an impression of features on the borehole wall upon depressurization.

Orientation of the impression packer with respect to true north was obtained by the addition of a special fitting that was attached between the packer and the drill stem. This fitting contained a lug designed to mate with a downhole survey tool that used an internal camera to photograph a gyroscopic compass.

3.3.2 Surface Equipment

Surface equipment included a workover drill rig, three high-pressure air-driven pumps, hydraulic accumulator, valve manifold, and instrumentation to measure and record packer pressure, interval pressure, and flow rate. A schematic of the surface equipment is shown in Figure 13.

The compressed air-activated pumps could develop pressure in the range of 0 to 45 MPa (0 to 6,500 lbf/in^2). Two pumps were used to pressurize the test interval, while the third pump supplied pressure to the packers. An accumulator was incoporated to reduce pressure pulses produced by the pumps.

Pressures in the packers and test interval were measured by strain gage-type pressure transducers calibrated by the manufacturer in the range of 0 to 70 MPa (0 to 10,000 lbf/in^2) ±0.25% full scale. Pressures were monitored on a digital readout device, which also supplied an analog signal to a strip chart recorder.

Flow into the test interval was measured by a turbine flowmeter, which was also monitored by a digital readout device with analog output recorded on the strip chart recorder. The flowmeter, calibrated by the manufacturer, had a linear range of 0.3 to 15.1 L/min (0.08 to 4.0 gal/min) ±0.05% full scale.

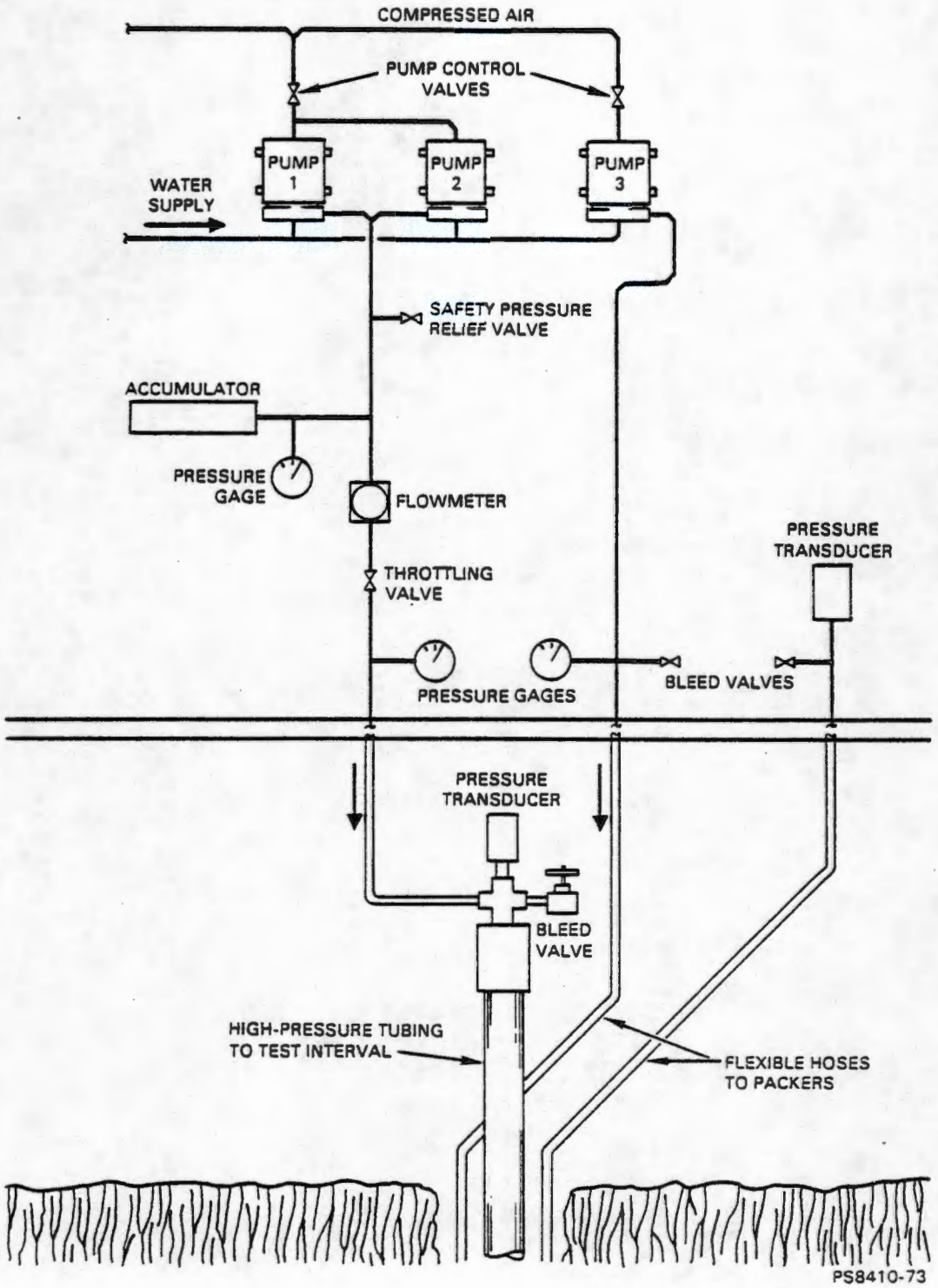

FIGURE 13. Schematic of Surface Equipment.

A pressure transducer used to monitor borehole pressure was located at the wellhead. With the transducer at the wellhead, pressures measured at the surface must be corrected for hydrostatic pressure. The pressure drop due to friction in the tubing was neglected due to the low flow rates used.

3.4 BASALT WASTE ISOLATION PROJECT HYDRAULIC FRACTURING PROCEDURES

The early feasibility tests conducted in borehole DB-15 at a depth of 343 m (1,128 ft) demonstrated the applicability of the hydraulic fracturing tests in closely jointed basalt. These tests in the borehole DB-15 lead to the development of a test plan used in four boreholes at the candidate horizons. The procedures employed for these tests are summarized below. Test procedures are documented in detail in the test plans describing hydraulic fracturing stress measurements in boreholes RRL-2 (Rundle 1982) and RRL-6 and DC-4 (Rundle 1983).

3.4.1 Hydraulic Fracturing Procedures

The following are the test procedures used for the hydraulic fracturing tests.

- Test intervals for all boreholes were determined from examination of core and core photographs. In boreholes RRL-6 and DC-4, acoustic televiewer logs were also used to select zones free of borehole wall spalling. An ideal test interval was one that was totally free of discontinuities. It was not possible to identify any interval as being free from discontinuities. In many intervals, intense core disking was present. Test depths were measured at the center of the test interval.

- The hydrofracturing tool was assembled on the surface and tested for leaks.

- The tool was lowered to the predetermined depth for each test using ~9.2 m (30 ft) lengths of Hydril tubing. Two flexible high-pressure hoses were strapped to the tubing at 3-m (10-ft) intervals. The tool was lowered by an oil field workover rig.

- Upon reaching the depth of the test interval, the inflatable straddle packers were set by pumping water through one of the flexible hoses using an air-activated pump. The other hose was used to vent any air in the packer and then closed. Pressure was increased to ~5.5 MPa (800 lbf/in^2) and held at this level. Pressure readings were made at the ends of both flexible hoses to assure that equilibrium had been achieved. At this point, the test interval was ready for pressurization.

- The top of the Hydril rod was connected by means of a valve manifold to two air-operated pumps in parallel with a 48-MPa (7,000 lbf/in^2), 19-L (5 gal) accumulator. The accumulator was

used to minimize pressure pulses from the pump strokes. Once the packers were inflated and the hydraulic line to the test interval completed, pressurization began. A positive differential pressure of ~2 MPa (300 lbf/in^2) was maintained between the packers and the test interval to prevent leakage past the packers. Pressurization continued until a peak was reached and the pressure started dropping. At this point, it was assumed that fracturing had occurred (breakdown). Shortly after breakdown, the throttling valve was closed (shut-in).

- After allowing a few minutes for recording the pressure response following shut-in, pressure in the test interval was vented to the atmosphere while maintaining pressure in the packers at a constant value. After backflow of excess water ceased, pressurization cycles were repeated. These repressurization cycles were conducted to obtain fracture reopening and shut-in pressures. Four or more cycles were attempted in most of the test intervals. One of these cycles usually utilized lower flow rates during pressurization. This cycle would not yield a measurement of fracture reopening pressure but would stabilize at a lower pressure, which is interpreted as a lower bound on the shut-in pressure (Zoback and Haimson 1982b). Flow rates in the last one or two cycles were increased to assure complete breakdown of the test interval.

- After completing the number of cycles necessary to obtain the hydrofracturing pressure data, the test interval and packers were vented to the atmosphere. The downhole tool was then moved to the next testing depth, and the above steps were repeated for the next test interval.

3.4.2 Impression Test Procedures

Analysis of pressure-time curves provides the information necessary to evaluate in situ stresses. The following procedures were used for conducting fracture impression tests.

- The impression packer was prepared on the surface with the orientation fitting mounted on top of the packer and marked to record the relative positions of the fitting lug and the packer.

- A 76-mm-OD heavy wall drill rod was attached to the impression packer and lowered to the previously hydrofractured test interval.

- The impression packer was pressurized to 17 MPa (2,500 lbf/in^2) for 10 min and then reduced to 7 MPa (kip/in^2) for 10 min.

- A gyroscopic downhole survey tool was used to determine the absolute orientation of the impression packer. This instrument is capable of taking a picture of an internal gyrocompass at a preselected time delay. Fresh film was loaded, the time clock set,

and the instrument inserted in a waterproof housing. The housing was then lowered by wireline inside the drill rod until the bottom of the housing engaged the lug on top of the impression packer. Once a picture of the gyrocompass was taken, the survey camera was retrieved to the surface. The film was developed immediately after retrieval to assure that an acceptable negative was obtained.

- The impression packer was then retrieved to the surface and immediately inspected for hydraulic fracture traces. Observed features were recorded by tracing to a clear plastic film, which was wrapped around the packer. Another prepared packer was attached to the drill stem for the next step, and the above procedures repeated.

4.0 TEST RESULTS

The application of the hydraulic fracturing technique to the jointed basalt beneath the Hanford Site has presented some rather unique data interpretation problems. Data interpretation procedures are described in Section 4.1, and the data analysis rationale is discussed in Section 4.2. A summary of the test data and results of the hydraulic fracturing test data analysis are presented in Section 4.3. The results of preliminary feasibility tests in borehole DB-15 are not included in this report. Tests in boreholes DC-12, RRL-2, RRL-6, and DC-4 were in candidate repository horizons and were within or relatively near the RRL and are, thus, directly applicable to preliminary design of the repository.

4.1 DATA INTERPRETATION

This section discusses the data interpretion procedures used to analyze the results of hydraulic fracturing tests at the Hanford Site.

4.1.1 Data Classification

The hydraulic fracturing tests conducted at 40 test intervals in 4 boreholes yielded varying degrees of success. Some tests yielded a complete set of information, including magnitudes and orientations of principal stresses, whereas other tests yielded only partial information. Based on the completeness of the information each test produced, the test results were classified into two categories. The first yielded both the magnitudes and orientations of the principal stresses, and the second yielded partial information only. These are presented in Appendixes A and B, respectively. Test data (including flow rate and pressure-time curves), a representation of the fracture impression, and a photograph of the core from the test interval are included in these appendixes.

Most of the tests classified to the first category indicated well-defined vertical fractures with a minimal degree of inclined fracturing or spalling.

The impression tests used in the determination of stress direction showed varying degrees of inclined fracturing or branching. Tests with significant amounts of branching were rejected, as the nature of these fractures is uncertain.

The equations used for the determination of maximum horizontal stress rely on the assumption that the borehole is circular and behaves elastically. Thus, the presence of significant spalling within the test interval was sufficient cause to reject test results. However, several tests with a minor amount of spalling were accepted. The spalling observed in these instances covered only a small portion of the test interval and was assumed to have a negligible effect on the results. Determination of the degree of branching or spalling that is sufficient to invalidate test results requires subjective judgment.

Limited drill rig availability and other constraints prevented the successful completion of impression tests in several instances. When this occurred, the nature of the induced fractures and the degree of spalling were not known. However, if the interval pressure history indicated shut-in and fracture reopening pressures that were similar to other nearby tests, the test was considered successful and used to calculate stress magnitudes.

In some tests, vertical fractures were clearly generated, but the degree of spalling made the test unacceptable for the determination of stress magnitudes. These tests were used to determine stress orientations only.

The division of test data into two categories is a matter of interpretation, even with fairly well-defined criteria; there are cases that do not clearly fit into one category or the other. This appears to be the nature of hydraulic fracturing tests in jointed basalt and points out the necessity of conducting multiple tests, thereby reducing the sensitivity of calculated mean values on the data selection process. The number of hydraulic fracturing tests conducted in each hole and the number of tests that yielded stress magnitudes and stress orientation data are summarized in Table 2.

TABLE 2. Number of Hydraulic Fracturing Tests Yielding Information on Stress Magnitudes or Orientations.

Borehole	Number of tests attempted	Number of tests used to determine stress direction	Number of tests used to determine stress magnitudes
DC-12	6	4	6
RRL-2	23	11	5
RRL-6	8	7	7
DC-4	3	3	1

4.1.2 Interpretation of Pressure-Time Curves

Pressure-time curves obtained from some tests did not exhibit clear, well-defined breakdown, shut-in, or fracture reopening pressures; thus, the results required interpretation. This subsection discusses the procedure used to determine the breakdown, shut-in, and fracture reopening pressures from the pressure versus time curves.

4.1.2.1 Breakdown Pressure. The borehole breakdown pressure, which was taken as the maximum pressure attained during the initial pressurization cycle, is not critical to the calculation of stress magnitudes. The breakdown pressure, however, was recorded and is presented with the test data.

4.1.2.2 Shut-in Pressure. The determination of shut-in pressures after the cessation of pumping is not always straightforward. As a function of time, the borehole pressure decays as a result of fluid leak-off into the surrounding rock from the straddled interval and fracture, leakage past the packers, or further fracture propagation after pumping stops.

Various investigators have proposed analysis techniques to deal with indistinct shut-in pressures. Gronseth and Kry(1982) suggest using the inflection point in the pressure time record. Doe (1982) recommends plotting pressure as a function of log time. McLennan and Roegiers (1982) suggest plotting pressure as a function of log $[(t + \Delta t)/t]$, where Δt is shut-in time and t is pumping time. Aamodt and Kuriyagawa (1982) suggest using a method of plotting the log of pressure as a function of time and extrapolating back the linear curve to zero time. Haimson has found that plotting log pressure as a function of log time gives sharp shut-ins (Zoback and Haimson 1982b).

Zoback and Haimson (1982b) report that these five methods seem to help identify the change in slope associated with fracture closure in at least the few tests examined by each investigator and point out that all methods are based on different theoretical models that have not been rigorously developed or tested.

The shut-in pressures for the Hanford Site hydraulic fracturing tests have been selected by application of the inflection point method described by Gronseth and Kry (1982). The inflection point method has been evaluated under laboratory conditions (Gronseth 1982) and seems to produce acceptable results. This method consists of drawing a line tangent to the pressure-time record immediately following shut-in and selecting the shut-in pressure as the point at which the pressure-time curve diverges from this tangent. The selection of this point is scale dependent. Thus, all shut-in pressures were selected from the original pressure histories obtained during the field tests and not from replotted representations of these histories as shown in the data appendixes. Figure 14 is a scale reproduction of a typical repressurization cycle demonstrating the method of selecting the shut-in pressure value.

4.1.2.3 Fracture Reopening Pressure. Measurement of the fracture reopening pressure or secondary breakdown pressure is required to calculate the maximum horizontal stress as suggested by Bredehoeft et al. (1976) and described in Section 3.1. Hickman and Zoback (1982) discuss the method at length and state that different forms of pressure-time curve result from variation in the relative magnitudes of the horizontal principal stress.

The fracture reopening pressure is the pressure at which the already-formed fracture at the borehole opens to accept fluid. Fracture reopening pressures for the Hanford Site tests have been determined by the method suggested by Hickman and Zoback (1982), which is the point at which the repressurization curve deviates from a straight line under constant flow conditions. Again, this selection procedure is scale dependent. Thus, all pressure values were selected from the original pressure history obtained during a test. An example of this method of selecting the fracture reopening pressure is shown in Figure 14.

4.2 DATA ANALYSIS RATIONALE

The shut-in and reopening pressures are not necessarily constant during subsequent repressurization cycles, so the analysis procedure requires a decision as to which values to use in Equations 7 and 8 to calculate in situ stress magnitudes.

Various investigators (Hickman and Zoback 1982, Gronseth and Kry 1982, Enever and Wooltorton 1982, and Gronseth 1982) have observed a decrease in the instantaneous shut-in pressure after each pressurization cycle. Hickman and Zoback (1982) discuss this phenomenon in detail and recommend, as does Gronseth (1982), that the minimum value of the shut-in pressure or the stable value attained after repeated pressurization cycles be used as the measure of the minimum horizontal stress. This recommendation should be regarded with caution when the vertical stress is suspected to be the minimum stress because vertical hydraulic fractures induced in the borehole wall may tend to reorient as they propagate away from the borehole. If fractures do deviate from a vertical plane with subsequent repressurization cycles, the minimum value of the shut-in pressure may be less than the minimum horizontal stress.

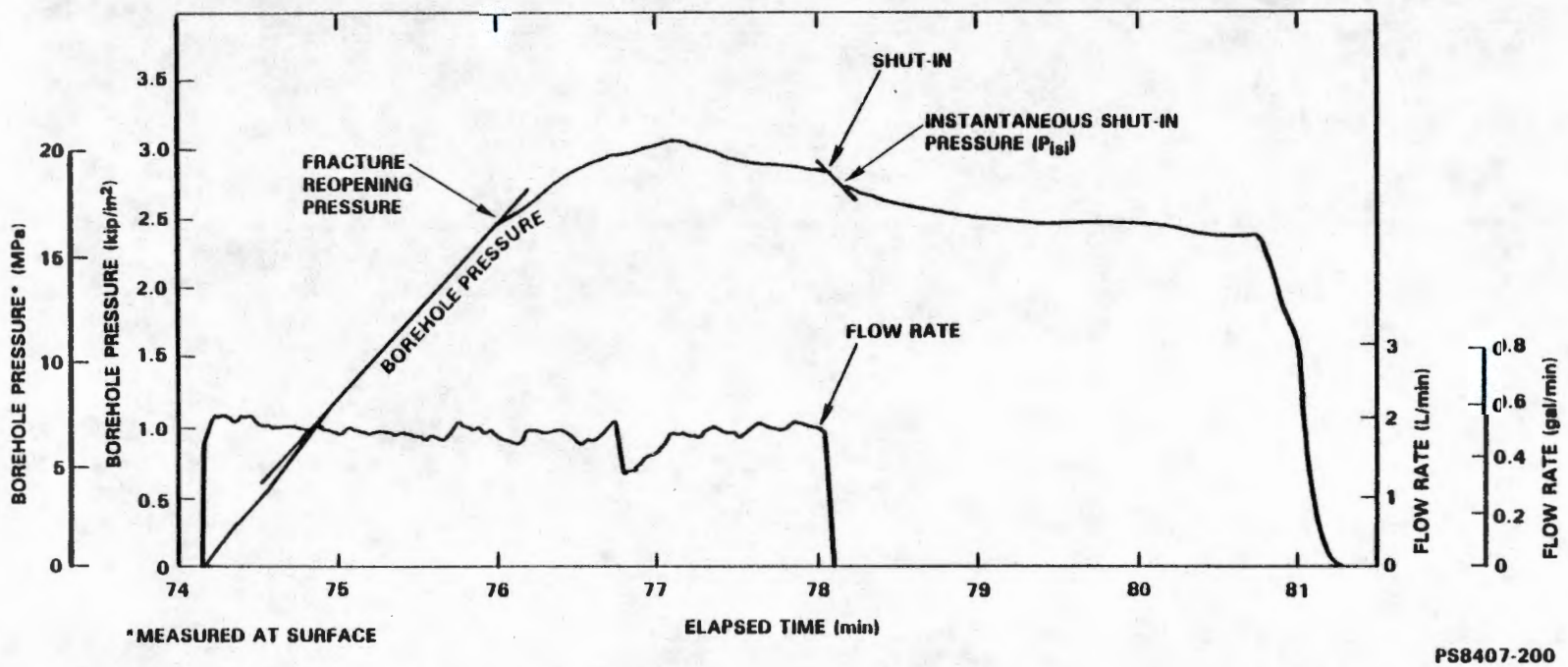

FIGURE 14. Typical Repressurization Cycle, Borehole RRL-6--Depth of 1,008 Meters (3,306 ft).

The Hanford Site hydraulic fracturing data have been analyzed by using the mean value of the instantaneous shut-in pressure as the measure of the minimum horizontal stress. This accounts for the possibilities that the initial value of the shut-in pressure may overestimate the minimum horizontal stress, and the minimum value of the shut-in pressure may underestimate the minimum horizontal stress.

Hickman and Zoback (1982) have observed that fracture reopening pressures also decrease with successive repressurization cycles. They suggest that the fracture reopening pressure observed in the third pressurization cycle be used in the determination of the maximum horizontal stress.

The impact of using mean values of the shut-in and reopening pressures, as opposed to the minimum value of the shut-in pressure recommended by Gronseth and Kry (1982), and the fracture reopening pressure of the third cycle recommended by Hickman and Zoback (1982) can be evaluated by calculating horizontal stresses by both methods for a typical test. Test results for the test at 1,005 m (3,624 ft) in borehole RRL-6 are presented in Table 3.

TABLE 3. Hydraulic Fracturing Test Results,1,005 m (3,624 ft) (McCoy Canyon flow), Borehole RRL-6 (pressures measured at surface).

Cycle	1	2	3	4	5	6
Breakdown pressure, P_b (MPa)	32.3	-	-	-	-	-
Fracture reopening pressure, P_{f2} (MPa)	-	26.9	22.1	22.8	22.1	21.4
Shut-in pressure, P_{isi} (MPa)	27.6	26.2	27.6	26.3	23.4	24.9

For this test, the hydrostatic pressure head, P_h, and the pore pressure, P_o, generated by the water level in the borehole are 10.8 MPa (1,569 lbf/in^2) and 10.1 MPa (1,465 lbf/in^2), respectively.

If mean values of shut-in and fracture reopening pressures are used with Equations 7 and 8, in situ stress magnitudes are as follows:

$$\sigma_h = 36.8 \text{ MPa } (5{,}340 \text{ lbf/in}^2) \tag{10}$$

and

$$\sigma_H = 66.6 \text{ MPa } (9{,}650 \text{ lbf/in}^2) \tag{11}$$

Using the minimum value of the shut-in pressure and the fracture reopening pressure from the third cycle, the calculated stress magnitudes are

$$\sigma_h = 34.3 \text{ MPa } (4{,}970 \text{ lbf/in}^2) \tag{12}$$

and

$$\sigma_H = 59.8 \text{ MPa } (8{,}670 \text{ lbf/in}^2) \tag{13}$$

The variation in calculated principal stress magnitudes for this example are on the order of 4% for the minimum horizontal stress and 10% for the maximum horizontal stress.

Since there is a degree of uncertainty as to which values of the shut-in pressure and fracture reopening pressure should be used to calculate in situ stress magnitudes, the method that results in the higher in situ stress magnitudes has been chosen. This should result in a more conservative repository design.

4.3 TEST DATA AND IN SITU STRESSES

The data appendixes contain all hydraulic fracturing data obtained in boreholes DC-12, RRL-2, RRL-6, and DC-4. Test data consist of pressure versus time and flow rate versus time curves, a photograph of the core recovered from the test interval, and a representation of the fracture impression, if available. Test records yielding principal stress magnitudes and orientations are presented in Appendix A. All other data are contained in Appendix B.

The pressure and flow rate curves presented in the data appendixes are condensed curves produced by digitizing the original analog strip chart plots and reproducing them by computer. (The original analog strip chart records and fracture impression traces are kept in the BWIP record retention system.) In Appendix A, the values of the breakdown pressure (P_b), fracture reopening pressure (P_{f2}), and instantaneous shut-in pressure (P_{isi}), selected using the methods described in Section 4.1.2, are listed with the pressure and flow rate versus time curves.

The orientation of induced fractures, if applicable, is given with available impression packer representations included in the data appendixes. The fracture orientation and, thus, the direction of the maximum horizontal stress have been obtained by averaging the orientations of the two vertical fractures in appropriate test intervals. Due to the sometimes inclined and undulating nature of the induced fractures, determination of fracture orientation is somewhat subjective. Fracture impressions from test intervals unacceptable for the determination of stress magnitudes were sometimes acceptable for determination of stress orientations.

A summary of all pertinent data required to calculate in situ stress magnitudes is presented in Table 4. Breakdown pressures (P_b) listed in Table 4 were not used for the determination of stress magnitudes by the fracture reopening method but are included for completeness.

Mean values and standard deviations (from repressurization cycles) of the instantaneous shut-in pressures (P_{isi}) and fracture reopening pressures (P_{f2}) for the various fracture reopening tests at a particular depth location are given in Table 4 and have been calculated from values listed in Appendix A. Values obtained from fast or slow pressurization cycles and other obvious irregularities have been excluded in calculating the mean. Pressures given in Table 4 were measured at the surface, except as noted in borehole DC-4.

The pressure head, P_h, which is required when interval pressure is measured at the surface, has been calculated by multiplying the pressure gradient of water, 9.79 kpa/mL (0.433 lbf/in^2/ft), by the test depth. The pore pressure, P_o, at the test interval has been calculated by multiplying the pressure gradient of water by the test depth minus the depth to water in the borehole (given as d in Table 4).

The thickness of sediments overlying the basalt is also presented in Table 4. This thickness is used in the calculation of the vertical stress at each test location.

The orientation of induced hydraulic fractures from impressions presented in the appendixes is given in Table 5 for each test interval that produced vertical fractures at the borehole wall.

The in situ stresses resulting from the hydraulic fracturing tests within the Hanford Site are summarized in Table 6. In situ stress magnitudes and directions contained in Table 6 are based on information contained in Tables 4 and 5 and application of the fracture reopening method in Equations 7 and 8.

In Table 6, the maximum horizontal stress, σ_H, has been calculated with the pore pressure, P_o, equal to zero and equal to the pressure generated by the static water level in the open hole. This is done to identify the range of the maximum horizontal stress and demonstrate the dependence of this stress on estimates of the pore pressure.

Values for the vertical stess (σ_v) given in Table 6 were determined by assuming that the vertical stress is due to the weight of the overburden using the following (average density values calculated from data presented by Robbins et al. 1979):

- 2.64 gm/cm^3 as the average density of basalt
- 2.17 gm/cm^3 as the average density of sediments.

TABLE 4. Hanford Hydraulic Fracturing Test Data.

Borehole	Flow	Test depth (m)	Breakdown pressure (MPa)	Shut-in pressure MPa (Std. Dev.)	Fracture reopening pressure MPa (Std. Dev.)	Hydrostatic head[a] (MPa)	Pore pressure (MPa)
DC-12 (d = 32.9) (t = 60.4)	Umtanum	1,001.9	29.7	23.4 (0.7)	25.2 (0.7)	9.8	9.5
		1,012.9	29.3	24.5 (0.3)	20.7 (0)	9.9	9.6
		1,020.8	33.6	21.4 (1.0)	20.7 (0)	10.0	9.7
		1,030.8	31.0	24.1 (0.9)	24.7 (1.0)	10.1	9.8
		1,036.0	32.8	29.3 (0.5)	26.9 (1.0)	10.2	9.8
		1,041.8	32.1	25.3 (0.7)	20.9 (1.0)	10.2	9.9
RRL-2 (d = 73.2) (t = 183.8)	Cohassett	923.5	24.8	21.3 (0.7)	21.0 (0.5)	9.1	8.3
		927.8	31.4	26.6 (0.3)	26.1 (0.5)	9.1	8.4
	Grande Ronde 7	1,058.0	26.2	23.2 (0.3)	22.6 (0.2)	10.4	9.7
	Umtanum	1,160.4	29.3	26.1 (1.1)	25.2 (0.7)	11.4	10.7
		1,166.5	27.6	24.1 (1.2)	20.5 (0.9)	11.4	10.7
RRL-6 (d = 73.2) (t = 198.4)	Cohassett	1,007.7	32.1	24.0 (5.6)	18.1 (4.2)	9.9	9.2
		1,016.8	30.3	23.5 (3.8)	13.8 (3.9)	10.0	9.3
	McCoy Canyon	1,104.6	32.3	26.0 (2.2)	23.0 (2.2)	10.8	10.1
		1,108.6	35.2	17.5 (1.6)	7.3 (1.6)	10.9	10.1
		1,130.5	26.3	22.9 (0.7)	16.2 (1.2)	11.1	10.4
	Umtanum	1,188.7	23.4	21.6 (0.2)	19.3 (1.8)	11.7	10.9
		1,194.5	21.8	19.3 (0)	16.8 (2.6)	11.7	11.0
DC-4 (d = 99.7) (t = 189.9)	Cohassett	976.0	27.9	21.2 (1.8)	14.2 (2.1)	9.6	8.6
		976.0	38.3[b]	30.5 (2.0)[b]	24.1 (1.5)[b]	N/A	8.6

NOTE: To convert MPa to lbf/in^2, multiply by 145.
To convert meters to feet, multiply by 3.28

[a]Hydrostatic head required when pressures measured at surface.
[b]Pressures measured downhole
d = Depth to water in open borehole (m).
t = Thickness of sediments overlying basalt (m).

TABLE 5. Orientation of Induced Hydraulic Fractures.

Borehole	Flow	Test depth		Borehole
		m	ft	
DC-12	Umtanum	1,012.9	3,322.3	N. 40° E.
		1,020.9	3,348.6	N. 09° E.
		1,030.8	3,381.0	N. 01° E.
		1,036.0	3,398.1	N. 42° E.
RRL-2	Cohassett	923.5	3,068.4	N. 19° W.
		927.8	3,043.2	N. 04° E.
		945.5	3,101.2	N. 17° E.
		946.7	3,105.2	N. 03° E.
		967.4	3,173.1	N. 19° W.
		969.6	3,180.3	N. 16° E.
		991.2	3,251.1	N. 23° W.
	Grande Ronde 7	1,058.0	3,470.2	N. 08° W.
	Umtanum	1,146.7	3,761.2	N. 03° E.
		1,160.4	3,806.1	N. 08° E.
		1,166.5	3,826.1	N. 10° W.
RRL-6	Cohassett	1,007.7	3,305.3	N. 28° E.
		1,016.8	3,335.1	N. 15° E.
		1,018.0	3,339.0	N. 15° E.
	McCoy Canyon	1,104.6	3,623.1	N. 08° E.
		1,108.6	3,636.2	N. 30° W.
		1,130.5	3,708.0	N. 22° E.
	Umtanum	1,188.7	3,898.9	N. 21° W.
DC-4	Cohassett	920.8	3,020.2	N. 18° E.
		966.2	3,169.1	N. 23° E.
		976.0	3,201.3	N. 06° W.

TABLE 6. In Situ Stresses Obtained from Hydraulic Fracturing Tests. (Sheet 1 of 2)

Borehole	Basalt flow	Test depth (m)	Minimum horizontal stress σ_h (MPa)	Maximum horizontal stress σ_H (MPa)		Vertical stress σ_v (MPa)	Orientation of maximum horizontal stress	Stress ratios		Stress ratios		Average horizontal stress $\frac{\sigma_H + \sigma_h}{2}$ (MPa)
				P_o from Table 4	$P_o = O$			P_o from Table 4		$P_o = O$		
								σ_H/σ_h	σ_H/σ_v	σ_H/σ_h	σ_H/σ_v	
DC-12	Umtanum	1,002	33.3	55.3	64.8	25.6	--	1.66	2.16	1.95	2.53	44.3
		1,013	34.4	63.0	72.6	25.9	N. 40° E.	1.83	2.43	2.11	2.80	48.7
		1,021	31.4	53.8	63.4	26.1	N. 09° E.	1.71	2.06	2.02	2.43	42.6
		1,031	34.2	58.2	67.9	26.4	N. 01° E.	1.70	2.20	1.99	2.57	46.2
		1,036	39.5	71.5	81.4	26.5	N. 42° E.	1.81	2.70	2.06	3.07	55.5
		1,042	35.7	65.7	75.6	26.7	--	1.84	2.46	2.12	2.83	50.7
RRL-2	Cohassett	924	30.3	52.6	60.9	23.0	N. 19° W.	1.73	2.28	2.01	2.65	41.5
		928	35.7	63.4	71.7	23.2	N. 04° E.	1.78	2.73	2.01	3.09	49.6
		945	--	--	--	--	N. 17° E.	--	--	--	--	--
		947	--	--	--	--	N. 03° E.	--	--	--	--	--
		967	--	--	--	--	N. 19° W.	--	--	--	--	--
		970	--	--	--	--	N. 16° E.	--	--	--	--	--
		991	--	--	--	--	N. 23° W.	--	--	--	--	--
	Grande Ronde 7	1,058	33.6	58.1	67.7	26.5	N. 08° W.	1.73	2.19	2.02	2.55	45.9
	Umtanum	1,147	--	--	--	--	N. 03° E.	--	--	--	--	--
		1,160	37.5	65.3	75.9	29.2	N. 08° E.	1.74	2.24	2.02	2.60	51.4
		1,166	35.5	63.9	74.6	29.4	N. 10° W.	1.80	2.17	2.10	2.54	49.7

NOTE: To convert MPa to lbf/in^2, multiply by 145.
To convert meters to feet, multiply by 3.28.

TABLE 6. In Situ Stresses Obtained from Hydraulic Fracturing Tests. (Sheet 2 of 2)

Borehole	Basalt flow	Test depth (m)	Minimum horizontal stress σ_h (MPa)	Maximum horizontal stress σ_H (MPa)		Vertical stress σ_v (MPa)	Orientation of maximum horizontal stress	Stress ratios		Stress ratios		Average horizontal stress $\frac{\sigma_H + \sigma_h}{2}$ (MPa)
				P_o from Table 4	$P_o = O$			P_o from Table 4		$P_o = O$		
								σ_H/σ_h	σ_H/σ_v	σ_H/σ_h	σ_H/σ_v	
RRL-6	Cohassett	1,008	33.9	64.4	73.6	25.2	N. 28° E.	1.90	2.56	2.17	2.92	49.2
		1,017	33.4	67.4	76.7	25.4	N. 15° E.	2.01	2.66	2.29	3.02	50.4
		1,018	--	--	--	--	N. 15° E.	--	--	--	--	--
	McCoy Canyon	1,105	36.8	66.6	76.7	27.7	N. 08° E.	1.81	2.41	2.08	2.71	51.7
		1,109	28.4	56.9	67.0	27.8	N. 30° W.	2.00	2.05	2.36	2.41	42.7
		1,131	34.0	64.3	74.7	28.3	N. 22° E.	1.89	2.27	2.20	2.64	49.2
	Umtanum	1,189	33.2	57.9	68.8	29.9	N. 21° W.	1.74	1.94	2.07	2.30	45.6
		1,195	31.0	53.6	64.6	30.0	--	1.73	1.78	2.08	2.15	42.3
DC-4	Cohassett	921	--	--	--	--	N. 18° E.	--	--	--	--	--
		966	--	--	--	--	N. 23° E.	--	--	--	--	--
		976	30.8	59.9	68.5	24.4	N. 06° W.	1.95	2.45	2.23	2.81	45.3

NOTE: To convert MPa to lbf/in^2, multiply by 145.
To convert meters to feet, multiply by 3.28.

5.0 DISCUSSION OF RESULTS

Test data and in situ stresses obtained from hydraulic fracturing tests at the Hanford Site have been presented in the previous section. This section contains a discussion of the uncertainties associated with hydraulic fracturing, an evaluation of the vertical and lateral variation of test results, a comparison of test results with stress indicators, a discussion of the relationship between in situ stresses and regional tectonics, and a summary of the stress state for repository design.

5.1 UNCERTAINTIES ASSOCIATED WITH HYDRAULIC FRACTURING

The hydraulic fracturing method of stress determination has been used for more than 20 yr to measure stress in shallow and deep boreholes and has been extensively studied under laboratory conditions; however, uncertainties regarding the accuracy of the resulting stress determination still exist. Comparisons between stress determinations from the hydraulic fracturing method and other methods have been made, but those comparisons are limited to shallow boreholes since other methods are not capable of measuring stresses in deep boreholes. Hence, the degree of confidence in hydraulic fracturing stress measurements is high for shallow boreholes but, for deep borehole determinations, uncertainties remain.

One uncertainty arises from the influence of the pore pressure in the interpretation of the test results. Results given in the previous section are based on two possible extreme pore pressure conditions. One extreme has the pore pressure at the test interval equal to zero, as recommended by Rummel et al. (1982), and the other extreme has the pore pressure equal to the pressure generated by the height of the water column in the open hole, as recommended by Haimson (1981). It is believed that during the fracturing process the pore pressure and the fracturing pressure for a tight, highly impermeable rock mass may respond in a fashion similar to that predicted for the low pore pressure case. Hence, the in situ stresses are expected to be between the two extremes. The remainder of this report and conclusions resulting from the Hanford hydraulic fracturing tests are based on the condition that the pore pressure term in Equation 8 is equal to the pressure generated by the column of water in the borehole (see Table 4).

The difficulty of determining exact shut-in, crack reopening, or breakdown pressures from the pressure-time curves results in a degree of uncertainty in the estimation of the in situ state of stress. The interpretation of the stress distribution around the borehole used in the data analysis is based on linear elasticity; this assumption may lead to some uncertainty in the stress determination. Roegiers and McLennan (1982) and McLennan and Roegiers (1982) have identified additional factors that can influence the test data, interpretation, and results of hydraulic fracturing stress determinations. These include the following:

- The effect of preexisting fractures

- Fluid viscosity
- Pumping rate
- Packer type and configuration
- Packer bypass
- Pressure loss by permeations
- Inclined fracturing
- Fracture reorientation
- Incomplete fracture closure.

The hydraulic fracturing tests presented in this report were planned and conducted to minimize, where possible as explained in previous sections, the uncertainties assqciated with these factors. However, the degree of influence these factors have is difficult to quantify. This emphasizes the fact that hydraulic fracturing stress determinations in jointed rock produce engineering estimates of the conditions at depth, not exact measurements of the in situ stresses.

The possibility of fracture rollover introduces the uncertainty that the shut-in pressure is a measure of the vertical stress and not the least horizontal stress. When the vertical stress is the minimum stress, it is conceivable that horizontal fractures may open at the borehole wall or vertical fractures that initiate at the borehole wall may reorient or roll over to the horizontal plane. Fracture rollover can sometimes be detected by a significant decrease in shut-in pressure during repressurization tests (Zoback and Pollard 1978; Zoback and Haimson 1982b). Impression tests at the Hanford Site indicate that hydraulic fracturing generated vertical fractures at the borehole wall and that various degrees of branching into inclined and near-horizontal planes did occur. In general, the shut-in pressure did decrease slightly during cyclic repressurization tests. This result has been observed in other locations (Hickman and Zoback 1982) and does not by itself demonstrate that the fractures have reoriented into the horizontal plane. Since the shut-in pressures were always greater than the calculated vertical stress, it is concluded that fractures did not reorient into the horizontal plane and that the shut-in pressure produced a measure of the minimum horizontal stress. It is possible that either the number of cycles was not sufficient to produce fracture reorientation or that reorientation was inhibited by vertical jointing in the basalt.

5.2 VERTICAL AND LATERAL VARIATION OF HORIZONTAL STRESSES

Figure 15 is a plot of maximum and minimum horizontal stress as a function of depth from surface for all test results given in Table 6. The ± 1 standard deviation given with each measurement have been calculated from the standard deviations of the mean shut-in pressure and mean fracture reopening pressure obtained during repressurization tests and given in Table 4. Figure 15 does not reveal a correlation between the horizontal principal stress magnitudes and depth. This result indicates that the gravitational horizontal stress gradient (which is relatively small) is lost in the scatter of the measured values. The ratio of maximum horizontal stress to minimum horizontal stress and the ratio of maximum horizontal stress to vertical stress from Table 6 are plotted as a function of depth in Figure 16.

Another method of evaluating the variation of horizontal stress with depth is to compare the results of hydraulic fracturing tests within each basalt flow. The mean values and standard deviations (from Table 6) for each basalt flow are presented in Table 7 and indicate that test results do not vary greatly within the various basalt flows tested.

The lateral variation of horizontal stress can be evaluated by comparing the results from each hole and the results obtained in the Umtanum flow from inside the RRL and outside the RRL. The results from each borehole are summarized in Table 8, and the results obtained in the Umtanum flow outside the RRL (borehole DC-12) and inside the RRL (boreholes RRL-2 and RRL-6) are summarized in Table 9. For the limited number of tests conducted, these tables indicate results do not vary greatly with lateral changes in test location. A summary of all results obtained within the RRL is included in Table 8. A representation of mean value in situ stresses determined in each test borehole is presented in Figure 17 demonstrating the consistency of results within the RRL.

A statistical comparison of mean values and standard deviations given in Tables 7, 8, and 9 indicates that the horizontal principal stress magnitudes in the various holes, flows, and locations are not significantly different at the 95% confidence level. Also, stress orientations within the RRL are not significantly different at the 95% confidence level. However, statistical analysis of stress orientations obtained in boreholes DC-12 and RRL-2 [$\sim$12 km (7.5 mi) apart] are significantly different at the 95% confidence level. This rotation appears to conform to the change in the trend of the Cold Creek Syncline axis.

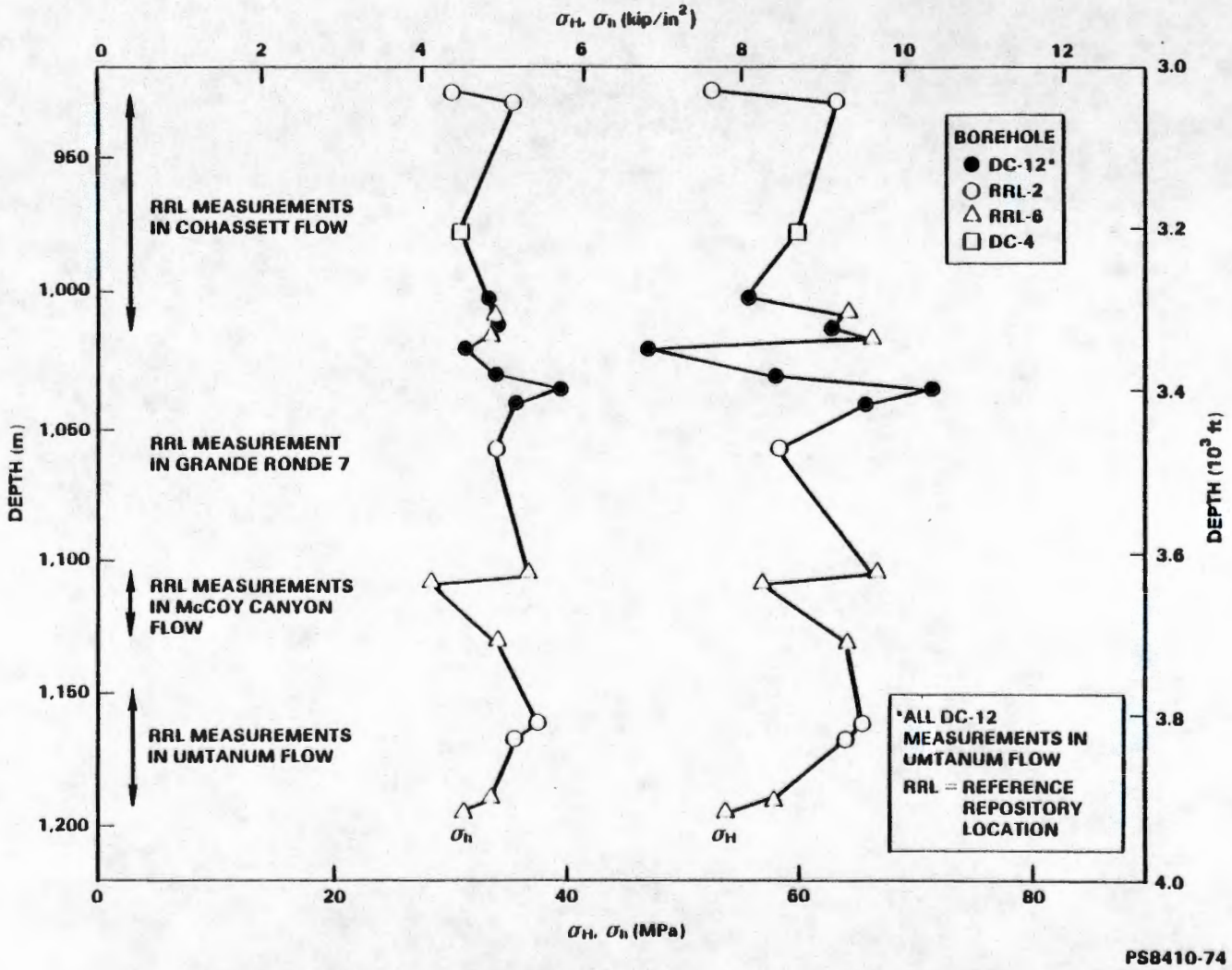

FIGURE 15. Hanford Site Maximum and Minimum Horizontal Stress Versus Depth.

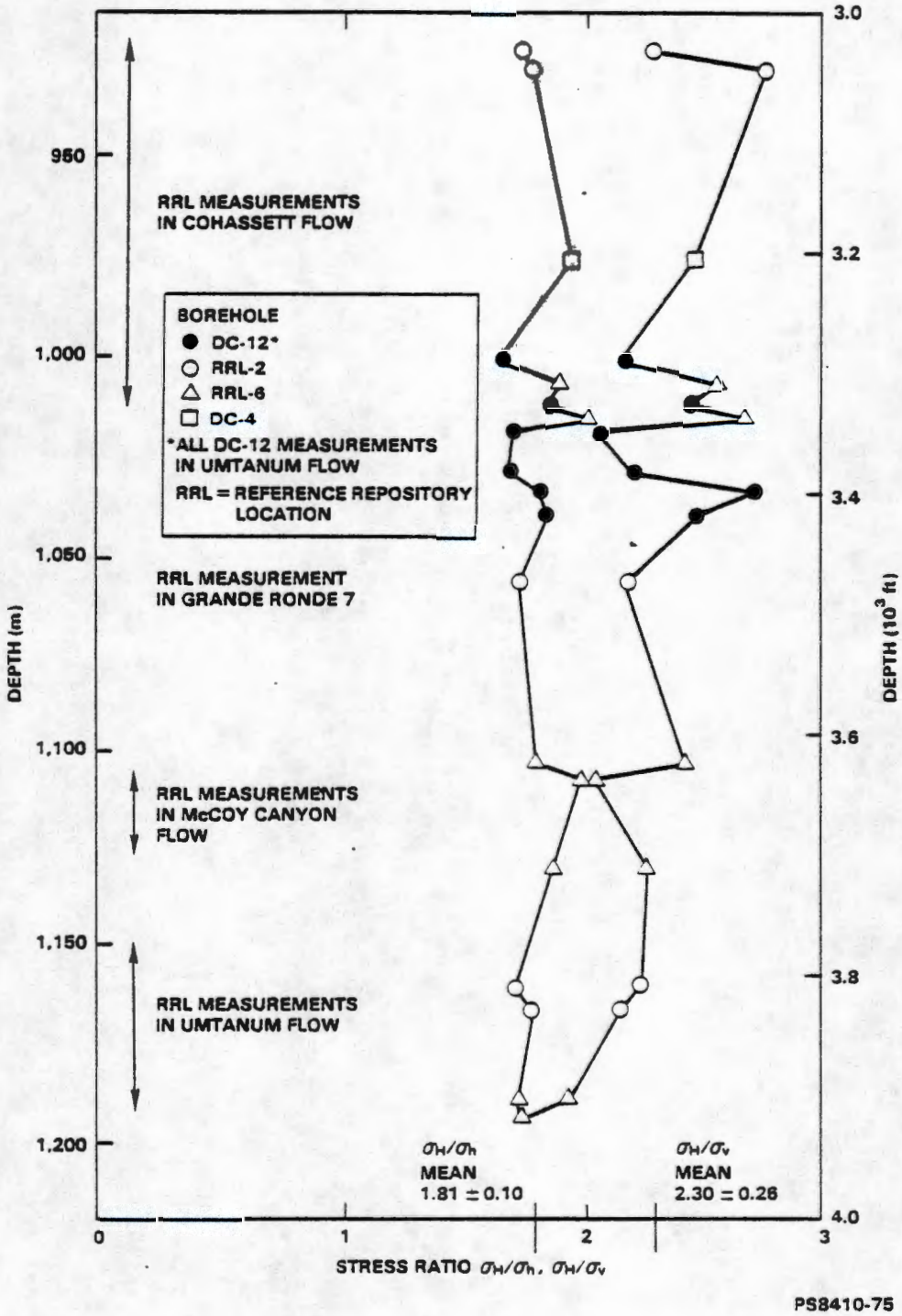

FIGURE 16. Hanford Site Ratios of Maximum Horizontal Stress to Minimum Horizontal Stress and Maximum Horizontal Stress to Vertical Stress Versus Depth.

TABLE 7. Summary of Mean Stress Values ±1 Standard Deviation Obtained in Tested Basalt Flows.

Borehole	Number of tests	Mean depth, m (ft)	Mean, σ_h, MPa (lbf/in²)	Mean, σ_H, MPa (lbf/in²)	Mean, σ_v, MPa (lbf/in²)	Mean fracture orientation	Mean stress ratios	
							σ_H/σ_h	σ_H/σ_v
Cohassett flow RRL-2 RRL-6 DC-4	5	970 ± 44 (3,181.6 ± 144.3)	32.8 ± 2.2 (4,756 ± 319)	61.5 ± 5.7 (8,917.5 ± 826.5)	24.2 ± 1.1 (3,509 ± 159.5)	N. 06° E.[a] ± 17°	1.87 ± .12	2.54 ± .18
Grande Ronde 7 RRL-2	1	1,058 (3,470.2)	33.6 (4,872)	58.1 (8,424.5)	26.6 (3,857)	N. 08° W.	1.73	2.19
Umtanum flow RRL-12 RRL-2 RRL-6	10	1,085 ± 81 (3,558.8 ± 265.7)	34.6 ± 2.6 (5,017 ± 377)	60.8 ± 6.0 (8,816 ± 870)	27.6 ± 1.8 (4,002 ± 261)	N. 09° E.[b] ± 22°	1.76 ± 0.6	2.21 ± .27
McCoy Canyon RRL-6	3	1,115 ± 14 (3,657.2 ± 45.9)	33.1 ± 4.3 (4,799.5 ± 623.5)	62.6 ± 5.1 (9,077 ± 739.5)	27.9 ± 0.3 (4,045.5 ± 43.5)	N. 00° E. ± 27°	1.90 ± .10	2.24 ± .18

[a]Mean orientation based on 13 impression tests.

[b]Mean orientation based on eight impression tests.

TABLE 8. Summary of Mean Stress Values ±1 Standard Deviation Obtained in Each Test Borehole.

Borehole	Number of tests	Mean depth, m (ft)	Mean, σ_h, MPa (lbf/in²)	Mean, σ_H, MPa (lbf/in²)	Mean, σ_v, MPa (lbf/in²)	Mean fracture orientation	Mean stress ratios	
							σ_H/σ_h	σ_H/σ_v
DC-4	1	976 (3,201.3)	30.8 (4,466)	59.9 (8,685.5)	24.4 (3,538)	N. 12° E.[a] ±16°	1.95	2.45
DC-12	6	1,024 ± 15 (3,350.7 ± 49.2)	34.8 ± 2.7 (5,046 ± 391.5)	61.2 ± 6.8 (8,874 ± 986)	26.2 ± 0.4 (3,799 ± 58)	N. 23° E.[b] ±21°	1.76 ± .08	2.33 ± .24
RRL-2	5	1,047 ± 119 (3,434.2 ± 390.3)	34.5 ± 2.7 (5,002.5 ± 391.5)	60.6 ± 5.3 (8,787 ± 768.5)	26.3 ± 3.1 (3,813.5 ± 449.5)	N. 03° W.[c] ±14°	1.76 ± .03	2.32 ± .23
RRL-6	7	1,174 ± 74 (3,850.7 ± 242.7)	33.0 ± 2.4 (4,785 ± 348)	61.6 ± 5.4 (8,932 ± 783)	27.8 ± 1.9 (4,031 ± 275.5)	N. 05° E. ±22°	1.87 ± .11	2.24 ± .33
All RRL holes Combined-DC-4 RRL-2, RRL-6	13	1,074 ± 96 (3,522.7 ± 314.9)	33.4 ± 2.7 (4,843 ± 362.5)	61.1 ± 4.9 (8,859.5 ± 710.5)	26.9 ± 2.5 (3,900.5 ± 362.5)	N. 02° E.[d] ±17°	1.83 ± .11	2.29 ± .28

[a]Mean orientation based on three impression tests.
[b]Mean orientation based on four impression tests.
[c]Mean orientation based on 11 impression tests.
[d]Mean orientation based on 21 impression tests.

TABLE 9. Summary of Mean Stress Values (±1 Standard Deviation) Obtained in the Umtanum Flow: RRL and Non-RRL.

Borehole	Number of tests	Mean depth, m (ft)	Mean, σ_h, MPa (lbf/in^2)	Mean, σ_H, MPa (lbf/in^2)	Mean, σ_v, MPa (lbf/in^2)	Mean fracture orientation	Mean stress ratios	
							σ_H/σ_h	σ_H/σ_v
Umtanum flow outside RRL DC-12	6	1,024 ± 15 (3,358.7 ± 49.2)	34.8 ± 2.7 (5,046 ± 391.5)	61.2 ± 6.8 (8,874 ± 986)	26.2 ± 0.4 (3,799 ± 58)	N. 23° E. ± 21°	1.76 ± .08	2.33 ± .24
Umtanum flow within RRL RRL-2 RRL-6	4	1,177 ± 16 (3,860.6 ± 52.5)	34.3 ± 2.8 (4,973.5 ± 406)	60.2 ± 5.4 (8,729 ± 783)	29.6 ± 0.4 (4,292 ± 58)	N. 05° E.[b] ± 13°	1.75 ± .03	2.03 ± .21

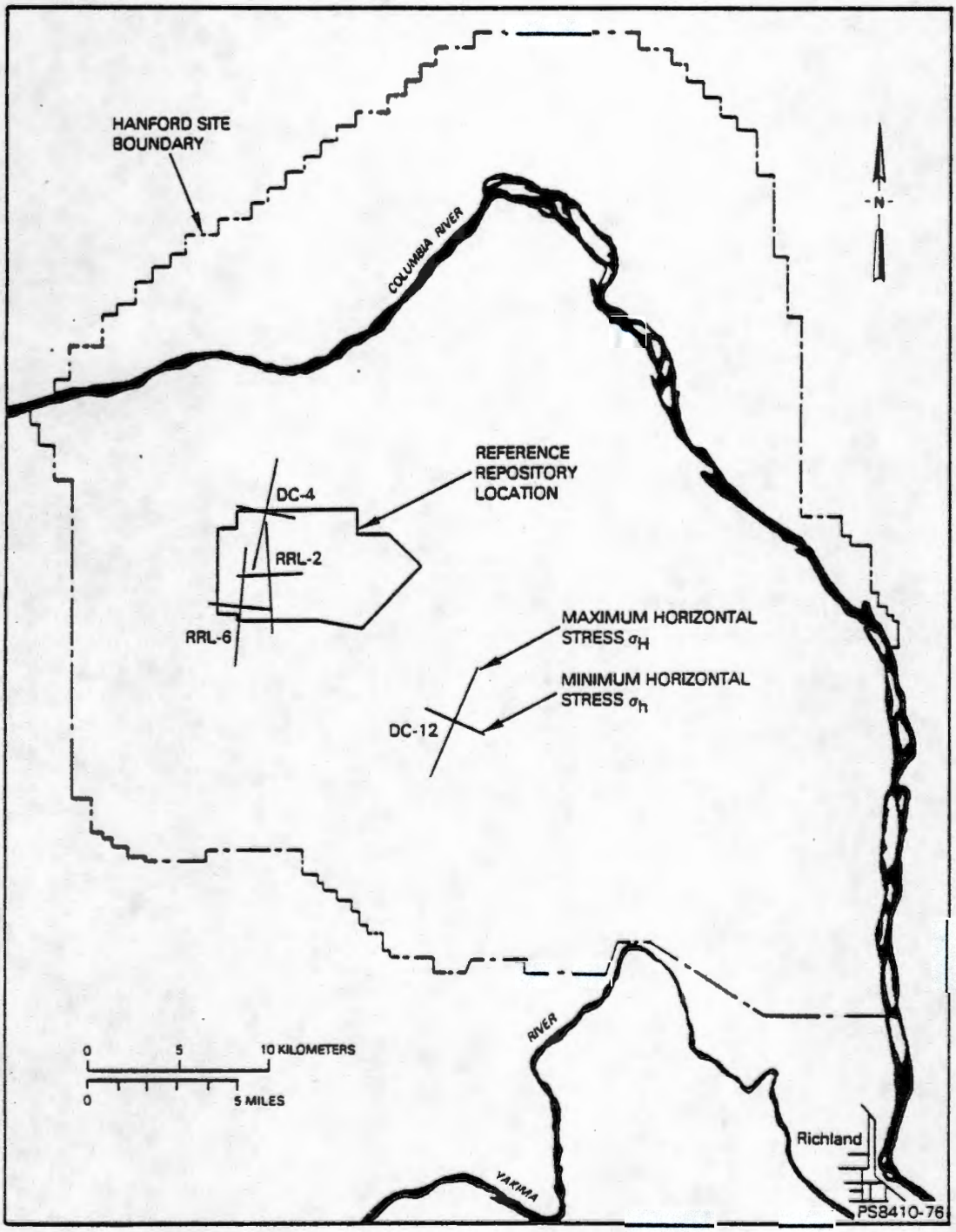

FIGURE 17. Stress Direction and Mean Stress Magnitudes in Each Test Borehole.

5.3 COMPARISON OF TEST RESULTS WITH STRESS INDICATORS

The orientation of induced hydraulic fractures and, thus, the orientation of the maximum horizontal stress, is shown in Figure 18. The fracture orientations obtained in each test hole are shown in Figure 18(a). Fracture orientation frequency plots for results within the RRL and all test results combined are shown in Figure 18(b). The average orientation of hydraulic fractures from tests within the RRL is N. 02° E., with a standard deviation of 17°; the average fracture orientation for all deep hole hydraulic fracture tests at the Hanford Site is N. 5° E. with a standard deviation of 19°. This north-south orientation of maximum horizontal stress is consistent with geologic indications of stress direction and observed east-west borehole spalling, which are discussed in Section 2.0.

The maximum and minimum principal stress directions determined from focal mechanisms for eastern Washington are summarized in Figure 19 (Rohay and Davis 1983) and indicate general north-south maximum compression and near-vertical minimum compression. Hydraulic fracturing test results are in general agreement with these focal mechanism solutions of seismic data.

Analysis of the core disking phenomenon by Lehnoff et al. (1982) indicated, from the assumed basalt core strength and applied drill fluid pressures, that disking would occur when the ratio of average horizontal stress to average vertical stress is in the range of 1.6 to 2.0. The ratio of average horizontal stress to average vertical stress from the hydraulic fracturing tests (see Table 6) is 1.78 for the Hanford Site. The correspondence between the predicted mean horizontal stress to vertical stress ratio by Lehnhoff et al. (1982) and that measured from all hydraulic fracturing tests at the Hanford Site may be misleading. Aggson (1978) indicates the initiation of disking to be dependent on the maximum stress perpendicular to the core axis. Lehnhoff et al. (1982) attribute the saddle-shape disks observed in the Hanford Site drill core to horizontal stress anisotropy with the ratio of maximum to minimum horizontal stress estimated to be in the range of 1.2 to 1.5. Hydraulic fracturing results indicate the ratio of maximum to minimum horizontal stress is 1.81 $\pm$ .10 (see Fig. 16). The analysis by Lehnhoff et al. (1982) was directed toward determining the stress ratio at which disking could occur but does not limit the upper bound of the stress ratio.

5.4 STRESS FIELD IN RELATION TO REGIONAL TECTONICS

Caggiano and Duncan (1983) state that the nearly east-west folds and subparallel thrust and the reverse faults and steeply dipping northwest- and northeast-trending faults in the Yakima fold belt suggest a stress regime of nearly north-south, nearly horizontal compression with a nearly vertical axis of least compression. Focal mechanism solutions of earthquakes in the central Columbia Plateau indicate this stress regime exists today and suggests this regime has been relatively unchanged for more than 14 m.y. (Caggiano and Duncan 1983).

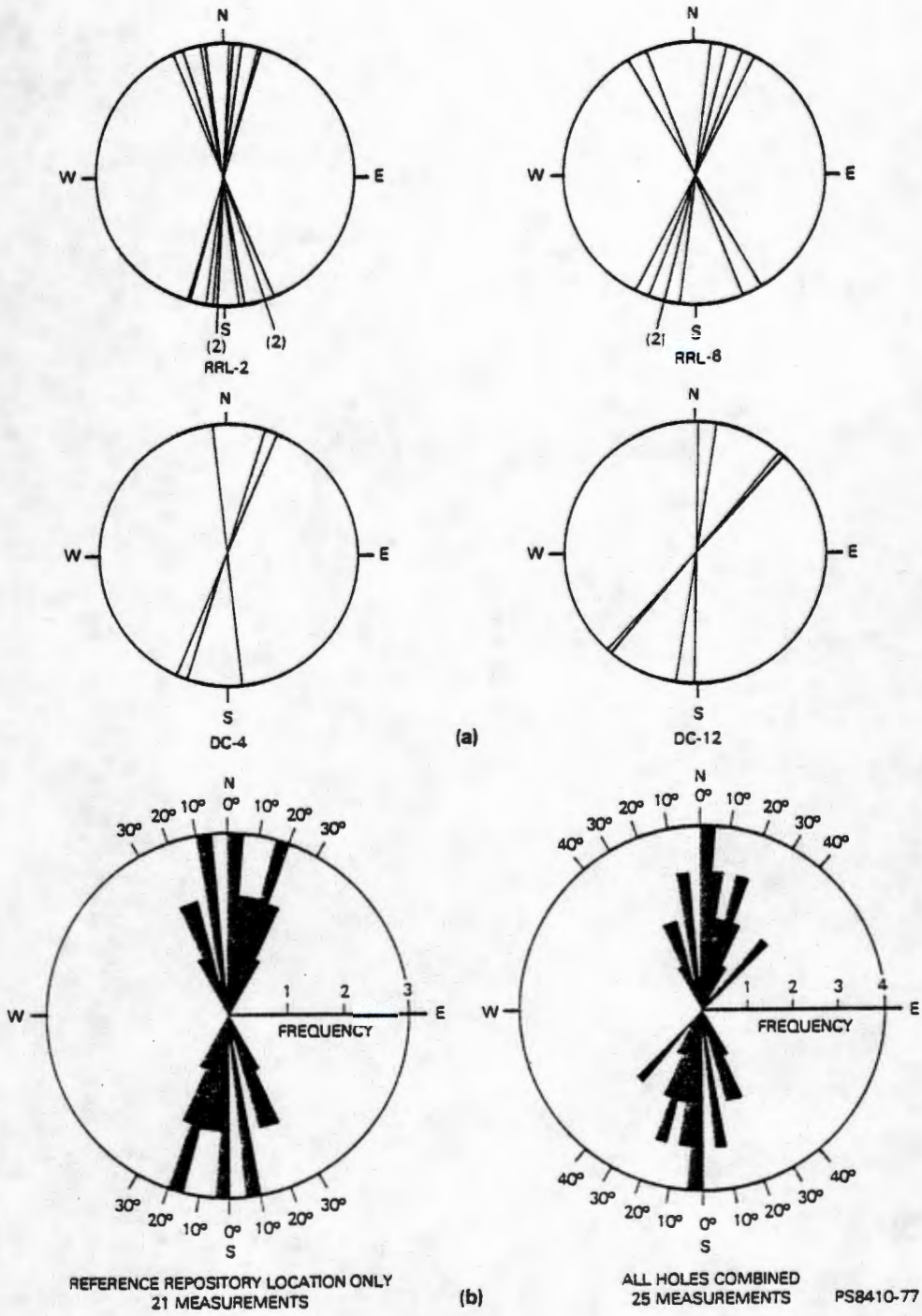

FIGURE 18. (a) Maximum Horizontal Stress Orientations--Individual Boreholes.
(b) Stress Orientation Frequency Diagram.

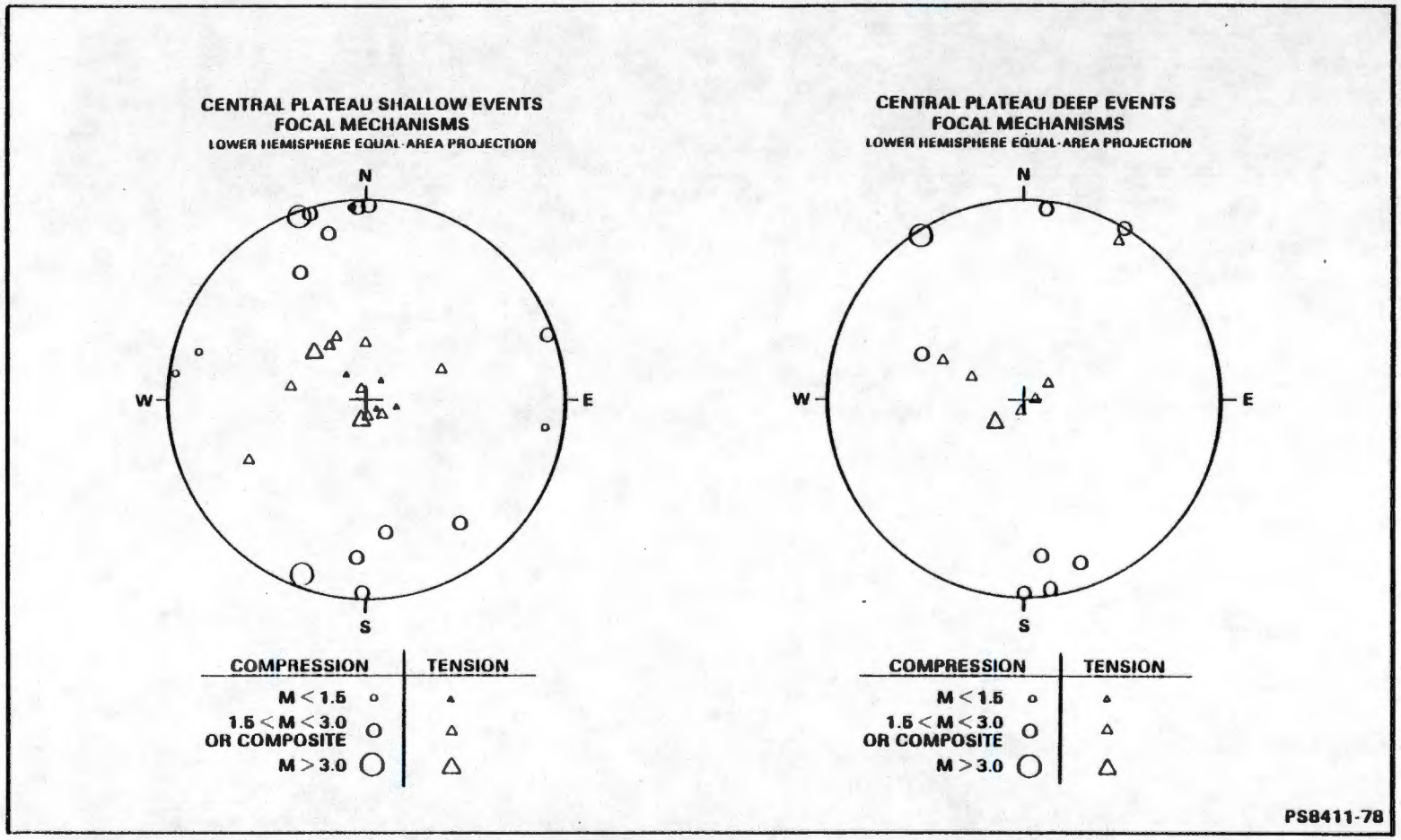

FIGURE 19. Focal Mechanisms of Eastern Washington. (Lower hemisphere, equal area projection of compression and tension axes derived from focal mechanism solutions.)

Regional and local tectonic models are being developed and evaluated in order to assess the tectonic stability of the Hanford Site. A tectonic model is a theory or hypothesis that satisfactorily explains the evolution of geologic formations and their structural development during the geologic past. The various tectonic models of the Columbia Plateau are similar in that the major structural features were formed as a result of north-south compression (Caggiano and Duncan 1983). Rates of north-south contraction and vertical uplift have been calculated from both seismic activity and geologic data. It has been concluded that the Columbia River basalt in the central Columbia Plateau has been deforming under nearly horizontal, nearly north-south compression over the past 14.5 m.y. (Caggiano and Duncan 1983). This tectonically induced contraction is responsible for the formation of structural features, observed seismicity, and elastic horizontal strain energy. This elastic strain and the gravitational load of the overlying rock combine to form the in situ stresses beneath the Hanford Site.

Core disking, borehole spalling, seismic activity, and hydraulic fracturing test results all indicate that horizontal stresses beneath the Hanford Site are significantly greater than would be expected from lithostatic load. Similar observations at numerous other locations have been summarized by Aggson (1978), Lindner and Halpern (1978), Hoek and Brown (1980), and Zoback and Zoback (1980); and the existence of horizontal stresses that exceed the gravitational horizontal stress is generally attributed to regional and/or global tectonics. The horizontal stress magnitudes at the Hanford Site can be compared to stresses determined at other locations by plotting the ratio of average horizontal stress to average vertical stress at the Hanford Site, with similar ratios reported by Hoek and Brown (1980). The average horizontal stress at the Hanford Site (see Table 6) is 47.5 MPa (6,890 lbf/in^2) with a standard deviation of 3.8 MPa (560 lbf/in^2). The average calculated vertical stress and the average hydraulic fracturing test depth are 26.7 MPa (3,870 lbf/in^2) and 1,058 m (3,472 ft), respectively. Thus, the ratio of average horizontal stress to average vertical stress at the Hanford Site is 1.78. As seen in Figure 20, this value is at the high end of the range of values determined at numerous other locations at similar depths, indicating that the basalt at the Hanford Site is within a zone of relatively high regional tectonic forces.

The stress magnitudes at the Hanford Site can be related to the potential for slip along favorably orientated joints or faults by comparison of the stress state with expected joint strength characteristics. The Mohr's circles for the stress state in the Cohassett flow and the joint strength data extracted from the triaxial test on jointed samples of basalt core (Mitchell 1984) are shown in Figure 21. Also shown is the joint strength envelope suggested by Byerlee (1978). The stresses plotted are the mean value effective stresses from Tables 4 and 10 ($\sigma_H - P_o$), ($\sigma_h - P_o$), and ($\sigma_v - P_o$) and indicate that the failure along favorably oriented joints is possible for joints with an effective friction angle of 33°. However, the triaxial compressive strength data on basalt joints show an effective friction angle of 43° plus a small effective cohesion, which indicates that the maximum horizontal stress in the Cohassett flow could be increased to 99.7 MPa (14,460 lbf/in^2), a 62% increase, before joint slip or thrust faulting would occur. With the Byerlee (1978) envelope, the horizontal stress could be increased to 80.9 MPa (11,730 lbf/in^2), a 32% increase.

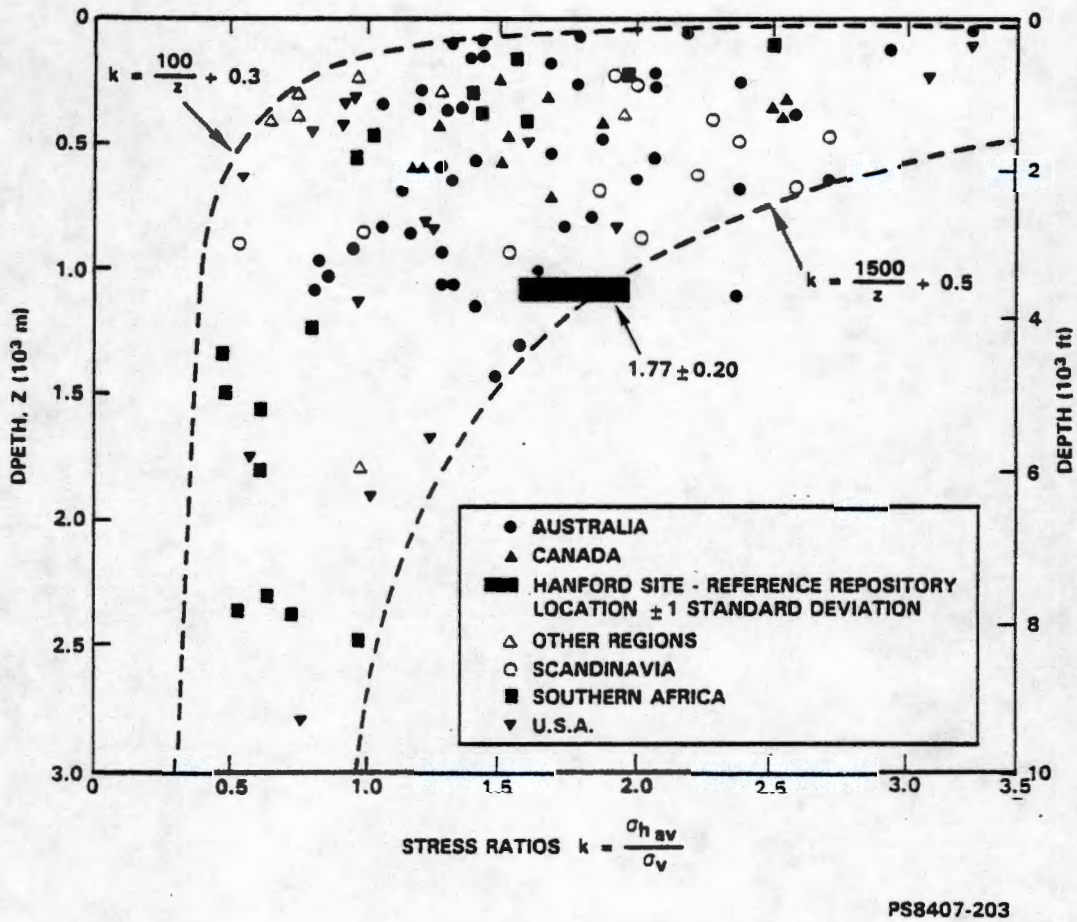

FIGURE 20. Variation in Ratio of Average Horizontal to Vertical Stress with Depth (from Hoek and Brown 1980).

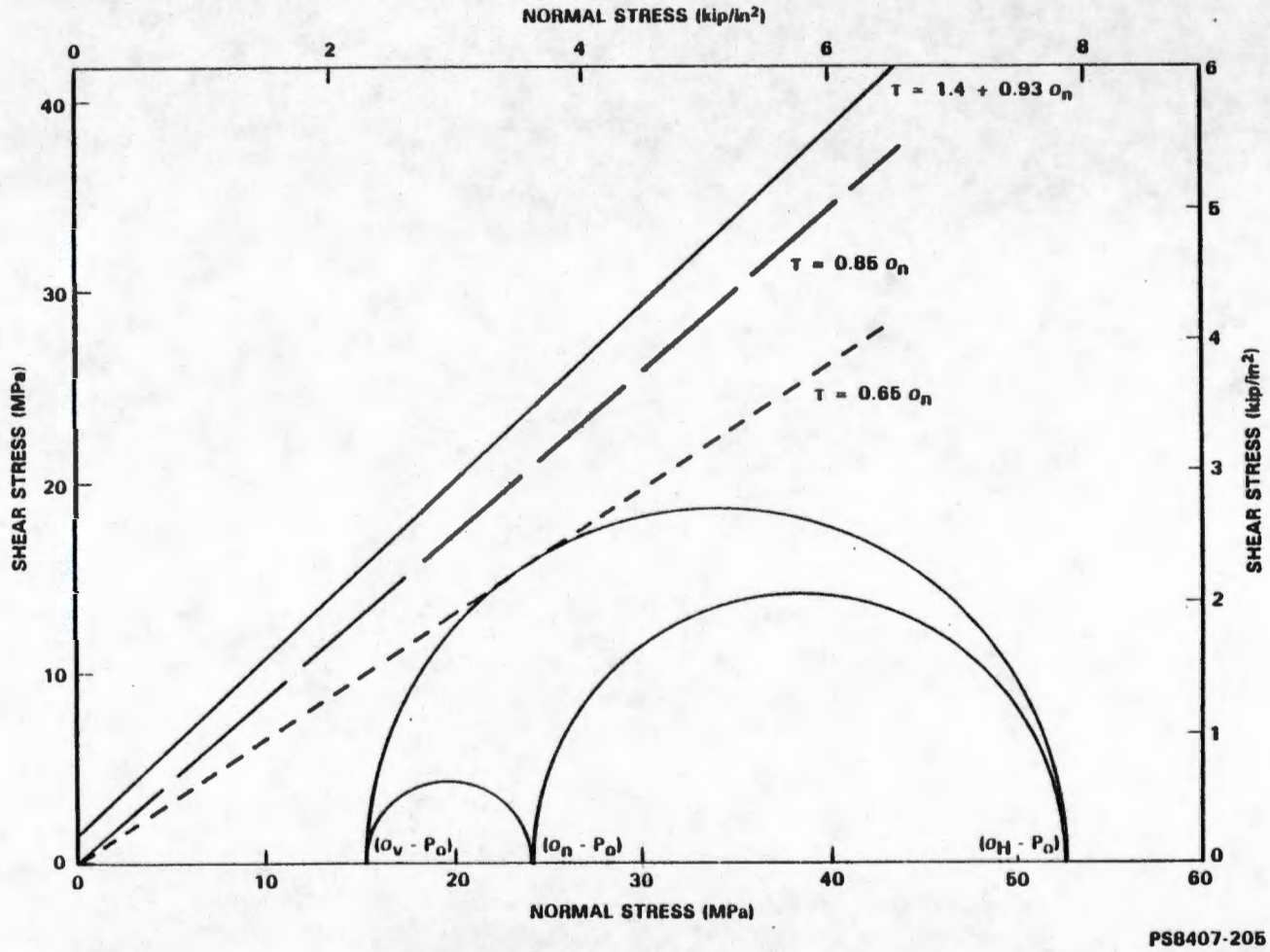

FIGURE 21. In Situ Effective Stresses Compared to Joint Strength Envelopes.

TABLE 10. Preliminary Recommended Design Stresses for the Cohassett Flow.

Stress component	Mean value MPa (lbf/in^2)	Extreme max. value MPa (lbf/in^2)	Extreme min. value MPa (lbf/in^2)
Maximum horizontal			
Magnitudes	61.5 (8,920)	72.9 (10,570)	50.1 (7,260)
Orientations	N. 06° E.	--	--
Minimum horizontal			
Magnitudes	32.8 (4,160)	37.2 (5,390)	28.4 (4,120)
Orientations	N. 84° W.	--	--
Vertical stress*	24.2 (3,510)	24.2 (3,510)	24.2 (3,510)

*Vertical stress dependent on depth and density of overlying rock.

The upper limit in horizontal stress is important in assessing the allowable stress change induced following emplacement of heat generating waste material and is clearly highly dependent on the estimated rock mass strength properties. A large-scale shear failure would involve failure of intact rock and slip/rotation of existing joint surfaces. This implies the joint or rock mass strength envelope should involve a considerable component to represent cohesion. The existing microseismic events can be interpreted to represent local slip along preexisting joint surfaces (Rothe 1978) or along several small sections of preexisting joint surfaces, some of which may have joint friction angles of 33° or less.

The correlation between changes in stress and changes in seismic activity have been documented at a number of sites and have even been used to interpret the in situ strength of joints and faults. The change in siesmic activity following fluid injection, which caused a change in pore fluid pressure and hence a change in effective stress, has been used to evaluate in situ joint strengths by Haimson (1972) and Raleigh et al. (1972). Haimson found that when the stress state exceeded a strength envelope represented by a friction angle of 40° (coefficient of internal friction of 0.85 as suggested by Byerlee (1978) as being representative of all rock types), microseismic activity increased in the Weber sandstones at the Rangely oil field.

Subsequent evaluations of stress state with relation to seismic activity by Zoback and Hickman (1982) and Haimson and Lee (1984) at the Monticello Reservoir reference a coefficient of internal friction of 0.6 (friction angle of 31°) as being critical for the initiation of microseismic activity; this 0.6 friction coefficient was suggested by Byerlee (1978) to represent joint friction with a cohesion of 50 MPa (7,250 lbf/in^2) for joints with stresses perpendicular to the joint surface in excess of 100 MPa (14,500 lbf/in^2). This is well beyond the range of interest for a repository in basalt as described elsewhere (DOE 1982, p. 4.1-2; Section 4.3 of this report).

5.5 STRESS STATE FOR REPOSITORY DESIGN

The preferred repository horizon is the Cohassett flow, where sufficient thickness of dense interior material is projected to meet both operational and long-term isolation objectives (Long 1983). The stress measurements to date in the Cohassett flow have been from 3 holes, with a total of 5 successful measurements of stress magnitude and 13 measurements of stress direction. For repository design purposes, a number of assumptions as to the stress state at depth can be made to provide an acceptable design of room shapes and rock support/reinforcement requirements. It is beyond the scope of this document to comment on design procedures for the various aspects of subsequent repository layout. However, it is appropriate to comment on the level of uncertainty in the stress measurements and the possible range of horizontal stress to be encountered at the repository depth.

Five measurements in the Cohasset flow do not constitute a statistically valid sample. However, several questions can be asked that directly relate to the applicability of the hydraulic fracturing results to repository design. Some questions are listed below.

- Are unspalled borehole wall locations, where tests were completed, in intervals of lower stress or are they unspalled because of locally higher rock strength or some other characteristic?

- Are unjointed test locations in areas of high stress thereby biasing the test results to the high side? Haimson and Lee (1984) recently concluded that, in areas of high-joint frequency at the Monticello dam site, lower stresses were measured; in areas of low-joint frequency, high stresses were measured.

- Is the stress in the colonnade the same as in the entablature? To date, all measurements in the Cohassett flow were in the colonnade.

- Do horizontal stresses vary laterally (i.e., is the number of tests conducted sufficient to evaluate the lateral variation of stresses)?

- What is the fluid pressure in the dense interior material of the Cohassett flow, and how does the fluid pressure interact with the fracturing fluid during the hydraulic fracturing tests?

- How significantly could the method of interpretation of the hydraulic fracture test data impact the estimated in situ stress?

In selecting the value of in situ stress used in design, some engineering judgment must be used. Given the following, some confidence must be placed in the numbers generated:

- The level of confidence in the hydraulic fracturing method expressed at the conference on hydraulic fracturing (Zoback and Haimson 1982a)

- The correspondence shown in the few existing comparisons of hydraulic fracturing stress measurements and overcoring results at specific sites (Haimson 1981)

- The general agreement between the hydraulic fracturing results and the geologic indicators

- The level of consistency between the hydraulic fracturing results from four holes in four flows.

The numbers calculated for the Cohassett flow are suggested, therefore, to be used as the current best estimate of the stress in the flow for repository design purposes. The mean value of 61.5 MPa (8,920 lbf/in^2) for σ_H, 32.8 MPa (4,760 lbf/in^2) for σ_h, and the vertical stress dependent on the actual repository depth should be used until additional data become available. For sensitivity studies used to evaluate the influence of in situ stresses on subsurface repository layout or room shapes, stresses equal to the mean ± 2 standard deviations are expected to encompass all reasonably likely in situ stress conditions. The suggested in situ stress design ranges for the Cohassett flow are listed in Table 10. Should another horizon be of interest, corresponding mean values and extremes would be applicable.

6.0 SUMMARY AND CONCLUSIONS

This report describes the test procedures, test data, analysis methodology, and calculated in situ stresses that have resulted from the BWIP hydraulic fracturing program. A total of 40 hydraulic fracturing tests were attempted in boreholes DC-12, RRL-2, RRL-6, and DC-4 at depths ranging from 921 to 1,195 m (3,022 to 3,921 ft). Of these tests, which were in the Cohassett, Grande Ronde 7, McCoy Canyon, and Umtanum basalt flows, 25 tests were used to determine stress direction and 19 tests were used to calculate in situ stress magnitudes. The majority of this testing (85%) was conducted within the RRL.

The following conclusions have resulted from the hydraulic fracturing test program.

- The maximum principal stress is generally north-south, the intermediate stress is east-west, and the minimum principal stress is vertical. This result is consistent with focal mechanism solutions of seismic activity, east-west borehole spalling, and the style and orientation of geologic structures.

- Stress ratios calculated from the results of hydraulic fracturing tests are in general agreement with an analysis of core disking at the Hanford Site.

- Hydraulic fracturing stress determinations conducted to date indicate that in situ stresses at candidate repository horizons within the RRL do not vary significantly with depth from surface, test hole location, or basalt flow.

- Engineering estimates on the stress magnitudes have been obtained from the tests.

  - The average maximum and minimum horizontal stresses from all tests at candidate repository horizons are 61.1 MPa (8,860 lbf/in^2) and 33.8 MPa (4,900 lbf/in^2), with standard deviations of 5.4 MPa (780 lbf/in^2) and 2.7 MPa (390 lbf/in^2), respectively.

  - Within the RRL, the average maximum and minimum horizontal stresses are 61.1 MPa (8,860 lbf/in^2) and 33.4 MPa (4,840 lbf/in^2) with standard deviations of 4.9 MPa (710 lbf/in^2) and 2.7 MPa (390 lbf/in^2), respectively.

- It is recommended that preliminary repository design in the Cohassett flow be based on maximum and minimum horizontal stresses of 61.5 MPa (8,920 lbf/in^2) and 32.8 MPa (4,760 lbf/in^2).

7.0 REFERENCES

Aamodt, A. and M. Kuriyagawa (1982), "Measurement of Instantaneous Shut-In Pressure in Crystalline Rock," Proceedings of the Workshop on Hydraulic Fracturing Stress Measurements, Open-File Report 82-1075, U.S. Geological Survey, Washington, D.C., pp. 394-403.

Aggson, J. R. (1978), "Coal Mine Floor Heave in the Beckley Coalbed," U.S. Bureau of Mines Report of Investigations, No. 8274, U.S. Bureau of Mines, Washington, D.C.

Beeson, M. H. and M. R. Moran (1979), Stratigraphy and Structure of the Columbia River Basalt Group in the Cascade Range, Oregon, RLO-040-T1, U.S. Department of Energy, Richland, Washington, pp. 5-77.

Bredehoeft, J. D, R. G. Wolff, W. S. Keys, and E. Shutter (1976), "Hydraulic Fracturing to Determine the Regional In-Situ Stress Field in the Piceance Basin, Colorado," Geological Society of America Bulletin, 87, pp. 250-258.

Byerlee, J. D. (1978), "Friction of Rocks," Pure and Applied Geophysics, Vol. 116, No. 4-5, reprinted in CCRG No. 6, "Rock Friction and Earthquake Prediction," Ed. by J. D. Byerlee and M. Wiss, Berkhauser Verlag, Basel, Switzerland, pp. 615-626.

Caggiano, J. A. and D. W. Duncan, eds. (1983), Preliminary Interpretation of the Tectonic Stability of the Reference Repository Location, RHO-BW-ST-19 P, Rockwell Hanford Operations, Richland, Washington.

DOE (1982), Site Characterization Report for the Basalt Waste Isolation Project, DOE/RL 82-3, 3 Volumes, Rockwell Hanford Operations for the U.S. Department of Energy, Washington, D.C.

Doe, T. W. (1982), "Determination of the State of Stress at the Stripa Mine, Sweden," Proceedings of the Workshop on Hydraulic Fracturing Stress Measurements, Open-File Report 82-1075, U.S. Geological Survey, Washington, D.C., pp. 305-332.

Doe, T. W., K. Ingevald, L. Strindell, B. Leijon, W. Hustrulid, E. Majer, and H. Carlsson (1983), In Situ Stress Measurements at the Stripa Mine, Sweden, Lawrence Berkeley Laboratory, University of California, Berkeley, California.

Enever, J. R. and B. A. Wooltorton (1982), "Experience with Hydraulic Fracturing as a Means of Estimating In Situ Stress in Australian Coal Basin Sediments," Proceedings of the Workshop on Hydraulic Fracturing Stress Measurements, Open-File Report 82-1075, U.S. Geological Survey, Washington, D.C., pp. 62-103.

Gough, D. I. and J. S. Bell (1981), "Stress Orientations from Oil Well Fractures in Alberta and Texas," Canadian Journal of Earth Science, 18, pp. 638-645.

Gronseth, J. M. (1982), "Determination of the Instantaneous Shut-in Pressure from Hydraulic Fracturing Data and Its Reliability as a Measure of the Minimum Principal Stress," Proceedings of the 23rd U.S. Symposium on Rock Mechanics, Berkeley, California, pp. 183-189.

Gronseth, J. M. and P. R. Kry (1982), "Instantaneous Shut-in Pressure and Its Relationship to the Minimum In Situ Stress," Proceedings of the Workshop on Hydraulic Fracturing Stress Measurements, Open-File Report 82-1075, U.S. Geological Survey, Washington, D.C., pp. 147-167.

Haimson, B. C. (1968), Hydraulic Fracturing in Porous and Nonporous Rock and Its Potential for Determining In Situ Stresses at Great Depth, Ph.D. thesis, University of Minnesota, Minneapolis, Minnesota, p. 235.

Haimson, B. C. (1972), "Earthquake Related Stresses at Rangely, Colorado," Proceedings of the 14th Symposium on Rock Mechanics, Pennsylvania State University, University Park, Pennsylvania, p. 689.

Haimson, B. C., T. W. Doe, S. R. Erbstoesser, and G. T. Fuh (1976), "Site Characterization for Tunnels Housing Energy Storage Units," Proceedings of the 17th Symposium on Rock Mechanics, Snowbird, Utah, pp. 4B-41, 4B-49.

Haimson, B. C. (1979), Heater Test Planning for the Near Surface Test Facility at the Hanford Reservation, "Hydrofracturing Tests for In Situ Stress Measurement - Near Surface Test Facility, Hole DC-11, Hanford Reservation," LBL-8730, Vol. II, Appendix, Lawrence Berkeley Laboratory, Berkeley, California, pp. 10-1 through 10-19.

Haimson, B. C. (1979), Hydraulic Fracturing Results at Gable Mountain, LBL-7061, Lawrence Berkeley Laboratory, Berkeley, California.

Haimson, B. C. (1981), "Confirmation of Hydraulic Fracturing Results through Comparisons with Other Stress Measurements," Proceedings of the 22nd U.S. Symposium on Rock Mechanics, Massachusetts Institute of Technology, Cambridge, Massachusetts, pp. 379-385.

Haimson, B. C. (1982), "Deep Stress Measurements in 3 Ohio Quarries and Their Comparison to Near Surface Tests," Proceeding of the 23rd U.S. Symposium on Rock Mechanics, Berkeley, California, pp. 190-202.

Haimson, B. C. and K. Kim (1982), "Deep Hole Hydrofracturing Stress Measurement in the Columbia Basin at the Hanford Site," EOS Transactions, 63, American Geophysical Union, p. 1120.

Haimson, B. C. and M. Y. Lee, (1984), "Development of a Wire Line Hydrofracturing Technique and Its Use at a Site of Induced Seismicity," Proceedings of the 25th U.S. Symposium on Rock Mechanics, Northwestern University, pp. 194-203.

Hickman, S. H. and M. D. Zoback (1982), "Interpretation of Hydraulic Fracturing Pressure-Time Data for In Situ Stress Determination," Proceedings of the Workshop on Hydraulic Fracturing Stress Measurements, Open-File Report 82-1075, U.S. Geological Survey, Washington, D.C., pp. 103-146.

Hoek, E. and E. T. Brown (1980), "Underground Excavations in Rock," The Institution of Mining and Metallurgy, London, England, p. 100.

Jaeger, J. C. and N. G. W. Cook (1965), "Pinching-Off and Disking of Rocks," Journal of Geophysical Research, 68:6, pp. 1659-1765.

Kim, K. (1981), "Determination of the In Situ Stress for Nuclear Waste Repository Design in Hanford Site," RHO-BWI-SA-183 P, Rockwell Hanford Operations, Richland, Washington.

Kim, K. and B. C. Haimson (1982), In-Situ Stress Measurement at a Candidate Repository Horizon, RHO-BW-SA-257 P, Rockwell Hanford Operations, Richland, Washington.

Kirsch, G. (1898), "Die Theorie der Elastizitat und die Bedurforisse der Festigkeitslehre," Zeitschrift des Vereines Duetscner Ingenieure, 42, p. 707.

Lehnhoff, T. F., B. Stefansson, K. Thirumalae, and T. M. Wintczak (1982), The Core Disking Phenomenon and Its Relation to In-Situ Stress at Hanford, SD-BWI-TI-085, Rockwell Hanford Operations, Richland, Washington.

Lindner, E. and J. Halpern (1978), "In Situ Stress in North America: A Compilation," International Journal of Rock Mechanics and Mining Science, 15:4, pp. 183-204.

Long, P. E., ed. (1983), Repository Horizon Identification Report, SD-BWI-TY-001, Rockwell Hanford Operations, Richland, Washington.

McLennan, J. D. and J. C. Roegiers (1982), "DOE Instantaneous Shut-in Pressures Accurately Represent the Minimum Principal Stress," Proceedings of the Workshop on Hydraulic Fracturing Stress Measurements, Open-File Report 82-1075, U.S. Geological Survey, Washington, D.C., pp. 181-208.

Malone, S. D., G. H. Rothe, and S. W. Smith (1975), "Details of Microearthquake Swarms in the Columbia Basin, Washington," Bulletin of the Seismological Society of America, 65:4, pp. 855-864.

Mitchell, S. J. (1984), "Direct Shear Testing Data Reduction," Data Analysis of the Colorado School of Mines Jointed Triaxial Tests, RHO-BWI Computational Brief No. CB-00066.

Moak (1981), "Borehole Geologic Studies," Subsurface Geology of the Cold Creek Syncline, RHO-BWI-ST-14, C. W. Myers and S. M. Price (eds.), Rockwell Hanford Operations, Richland, Washington.

Myers, C. W./Price, S. M., J. A. Caggiano, M. P. Cochran, N. J. Czimer, N. J. Davidson, R. C. Edwards, K. R. Fecht, G. E. Holmes, M. G. Jones, J. R. Kunk, R. D. Landon, R. K. Legerwood, J. T. Lillie, P. E. Long, T. H. Mitchell, E. H. Price, S. P. Reidel, and A. M. Tallman (1979), Geologic Studies of the Columbia Plateau: A Status Report, RHO-BWI-ST-4, Rockwell Hanford Operations, Richland, Washington.

NRC (1983), Disposal of High-Level Radioactive Wastes in Geologic Repositories: Licensing Procedures, Title 10, Chapter 1, Code of Federal Regulations - Energy, Part 60, U.S. Nuclear Regulatory Commission, Washington, D.C.

Obert, L. and D. E. Stephenson (1965), "Stress Conditions under Which Core Disking Occurs," SME Transactions, 232, pp. 227-225.

Paillet, F. L. (1984), Acoustic Well Log and Hydraulic Fracture Application in the Characaterization of Deeply Buried Basalt Flows (in print).

Raleigh, C. B., J. H. Healy, and J. D. Bredehoeft (1972), "Faulting and Crustal Stress at Rangely, Colorado: Geophysical Monograph 16," American Geophysical Union, pp. 257-284.

Ratigan, J. L. (1982), "A Statistical Fracture Mechanics Determination of the Apparent Tensile Strength in Hydraulic Fracture," Proceedings of the workshop on Hydraulic Fracturing Stress Measurements, Open-File Report 82-1075, U.S. Geological Survey, Washington, D.C., pp. 444-463.

Reidel, S. P., K. R. Fecht, and R. W. Cross (1982), "Constraints on Tectonic Models for the Columbia Plateau from the Age and Growth Rates of Yakima Folds," Proceedings of the 33rd Alaska Science Conference, Artic Division: American Association for Advancement of Science, p. 131.

Robbins, S. L., R. J. Martinez, and D. L. Smith (1979), Principal Facts for Borehole Gravity Stations in Wells DC-3, DC-5, and DC-7 on the Hanford Site, Washington, and in Well RSH-1 on Rattlesnake Hills, Washington, Open-File Report 79-849, U.S. Geological Survey, Washington, D.C.

Rockwell (1984), Basalt Operating Procedure C-3.16, "Field Test: Impression Packers" and C-3.17, "Field Test: Hydrofracture Testing," Rockwell Hanford Operations, Richland, Washington.

Roegiers, J. C. and J. D. McLennan (1982), "Factors Influencing the Initiation Orientation of Hydraulically Induced Fractures," Proceedings of the workshop on Hydraulic Fracturing Stress Measurements, Open-File Report 82-1075, U.S. Geological Survey, Washington, D.C., pp. 489-502.

Rohay, A. C. and J. D. Davis (1983), "Contemporary Deformation in the Pasco Basin Area of the Central Columbia Plateau," Preliminary Interpretation of the Tectonic Stability of the Reference Repository Location, RHO-BW-ST-19 P, J. A. Caggiano and D. W. Duncan (eds.), Rockwell Hanford Operations, Richland, Washington, pp. 6-1 through 6-11.

Rothe, G. H. (1978), "Earthquake Swarms in the Columbia River Basalts," in Addendum, University of Washington annual technical report, Earthquake Monitoring of the Hanford Region, Ph.D. thesis, University of Washington, Seattle, Washington, pp. 152-154.

Rummel, F., J. Baumgartner, and H. J. Alheid (1982), "Hydraulic Fracturing Stress Measurements along the Eastern Boundary of the SW-German Block," Proceedings of the workshop on Hydraulic Fracturing Stress Measurements, Open-File Report 82-1075, U.S. Geological Survey, Washington, D.C., pp. 1-35.

Rundle, T. A. (1982), Test Plan for In Situ Stress Measurement by Hydraulic Fracturing Method in Borehole RRL-2, SD-BWI-TP-018, Rockwell Hanford Operations, Richland, Washington.

Rundle, T. A. (1983), Test Plan for In Situ Stress Measurement by the Hydraulic Fracturing Method in Boreholes RRL-6 and DC-4, SD-BWI-TP-030, Rockwell Hanford Operations, Richland, Washington.

Swanson, D. A., T. L. Wright, V. E. Camp, J. N. Gardner, R. T. Helz, S. M. Price, and M. E. Ross (1977), Reconnaissance Geologic Map of the Columbia River Basalt Group, Pullman and Walla Walla Quadrangles, Southeast Washington and Adjacent Idaho, Open-File Map 77-100, U.S. Geological Survey, Washington, D.C.

Taubeneck, W. H. (1970), "Dikes of Columbia River Basalt in Northeastern Oregon, Western Idaho, and Southeastern Washington," Proceedings of the Second Columbia River Basalt Symposium, E. H. Gilmour and D. Stradling (eds.), Eastern Washington State College Press, Cheney, Washington, pp. 73-96.

WCC (1981), Study to Identify a Reference Repository Location for a Nuclear Waste Repository on the Hanford Site, RHO-BWI-C-107, Woodward-Clyde Consultants for Rockwell Hanford Operations, Richland, Washington.

Waters, A. C. (1961), "Stratigraphic and Lithologic Variations in the Columbia River Basalt," American Journal of Science, 259, pp. 581-611.

Zemanek, J. et al. (1969), "The Borehole Televiewer - A New Logging Concept for Fracture Location and Other Types of Borehole Inspection," Journal of Petroleum Technology, 21, pp. 762-774.

Zoback, M. D. and B. C. Haimson, eds. (1982a), Proceedings of workshop on Hydraulic Fracturing Stress Measurements, Open-File Report 82-1075, U.S. Geological Survey, Washington, D.C.

Zoback, M. D. and B. C. Haimson (1982b), "Status of the Hydraulic Fracturing Method for In-Situ Stress Measurements," Proceedings, U.S. 23rd Symposium on Rock Mechanics, University of California, Berkeley, California, pp. 143-156.

Zoback, M. D. and S. Hickman (1982), "In-Situ Study of the Physical Mechanisms Controlling Induced Seismicity at Monticello Reservoir, South Carolina," Journal of Geophysical Research, 87, pp. 6959-6974.

Zoback, M. D., D. Moos, L. Mastin, and R. N. Anderson (1984), "Wellbore Breakouts and In-Situ Stress," Journal of Geophysical Research, (in press).

Zoback, M. D. and D. D. Pollard (1978), "Hydraulic Fracture Propagation and Interpretation of Pressure-Time Records for In-Situ Stress Determinations," Proceedings of the 19th U.S. Symposium on Rock Mechanics, State Line, Nevada, pp. 14-23.

Zoback, M. L. and M. D. Zoback (1980), "State of Stress in the Coterminous United States," Journal of Geophysical Research, 85, pp. 6113-6156.

APPENDIX A

Pressure Versus Time Curves, Flow Versus Time Curves,
Fracture Impression Traces, and Core Photographs
Obtained from Test Intervals Which Yielded
Magnitudes and Orientations of the
Principal Stresses

Note: All pressures and flow rates were measured on the surface.

DC-12 TEST 1A 1041.5 METERS

FLOW RATE DATA NOT AVAILABLE

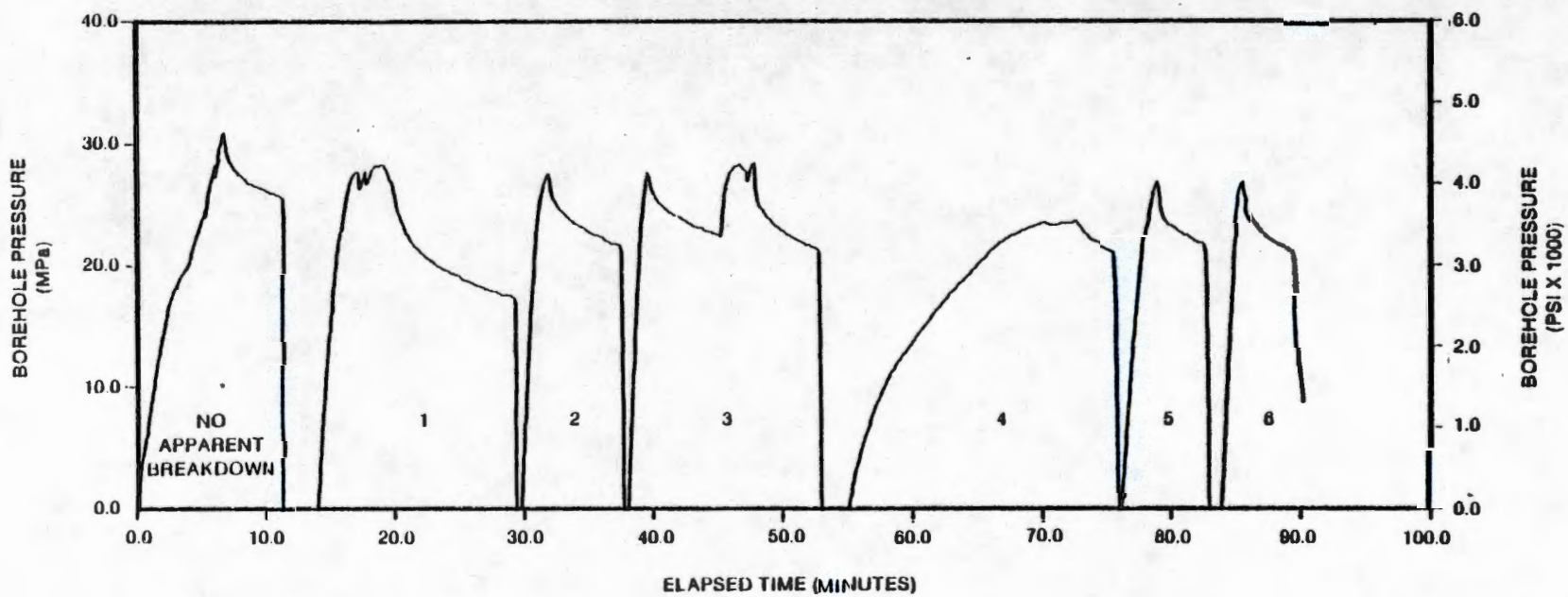

CYCLE	1	2	3	4	5	6	AVERAGE (STD DEV)
P_b	32.1	-	-	-	-	-	
P_{isi}	25.2	26.2	25.9	24.1	24.8	24.8	SEE PART B
P_{I_2}	-	20.7	20.7	-	20.7	20.7	

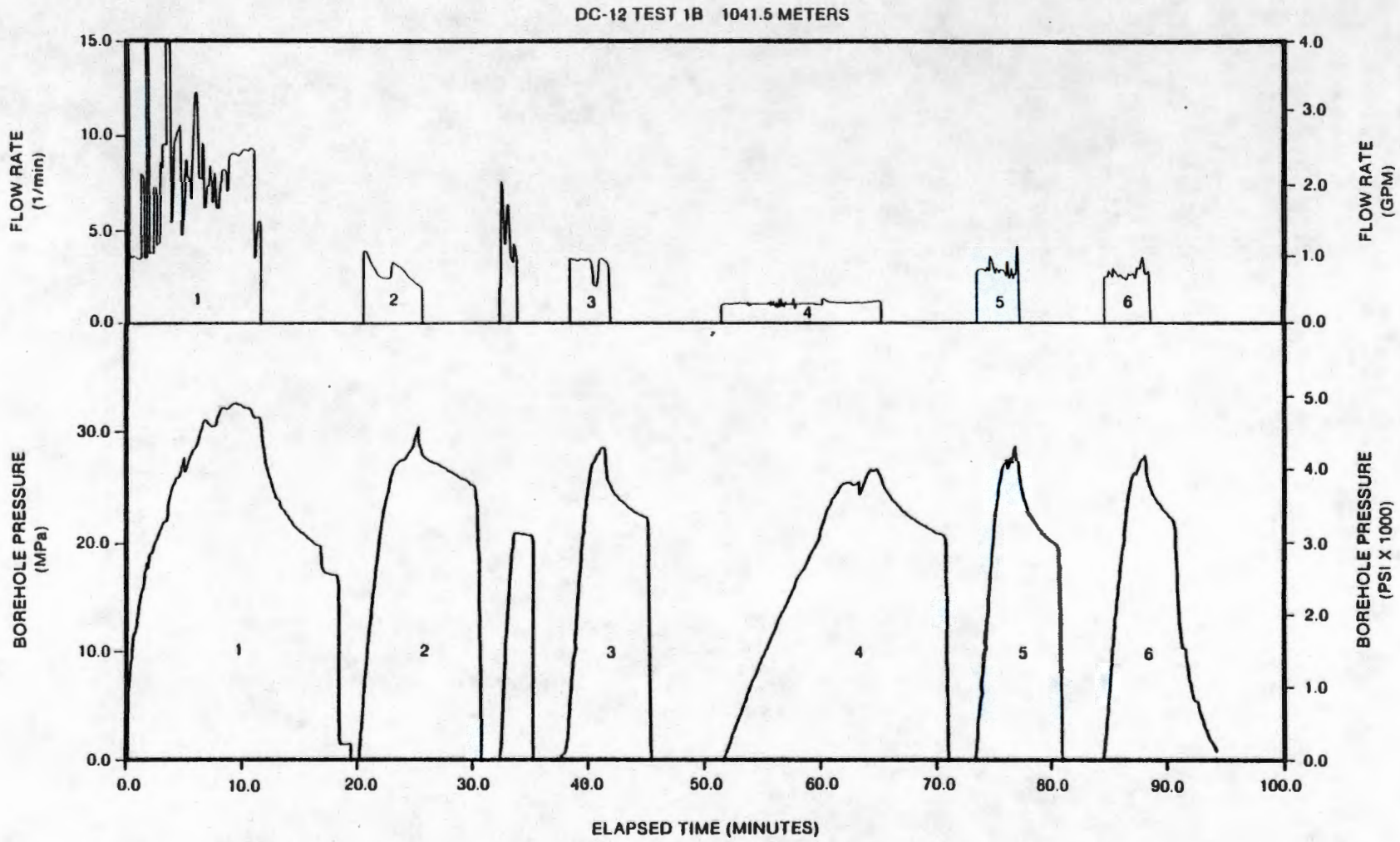

CYCLE	1	2	3	4	5	6	AVERAGE (DSTD DEV)
P_b	-	-	-	-	-	-	1A AND 1B COMBINED
P_{isi}	-	-	26.2	26.2	24.8	25.5	25.3 (0.7)
P_{f_2}	-	20.7	22.4	-	22.4	19.0	20.9 (1.0)

DEPTH 1041.5 M NO FRACTURE IMPRESSION TAKEN

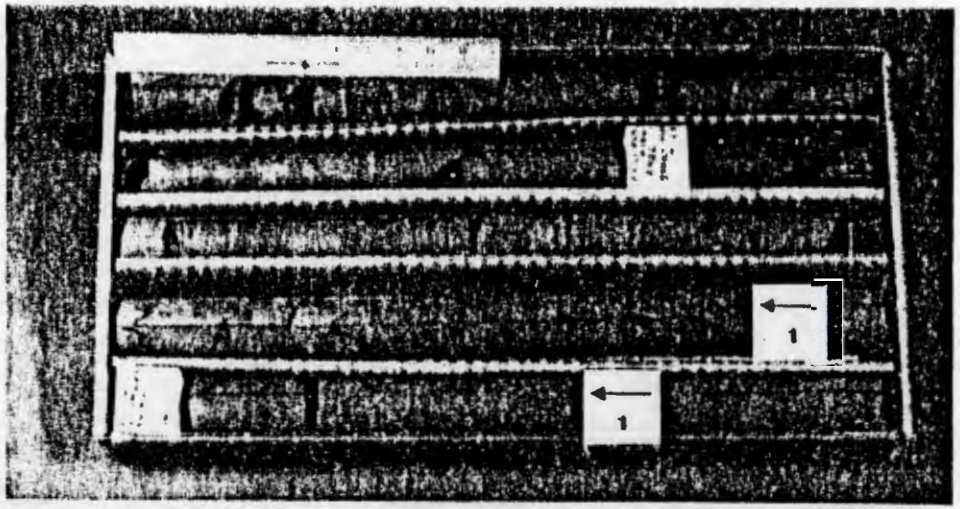

CORE PHOTOGRAPH, DC-12 TEST 1

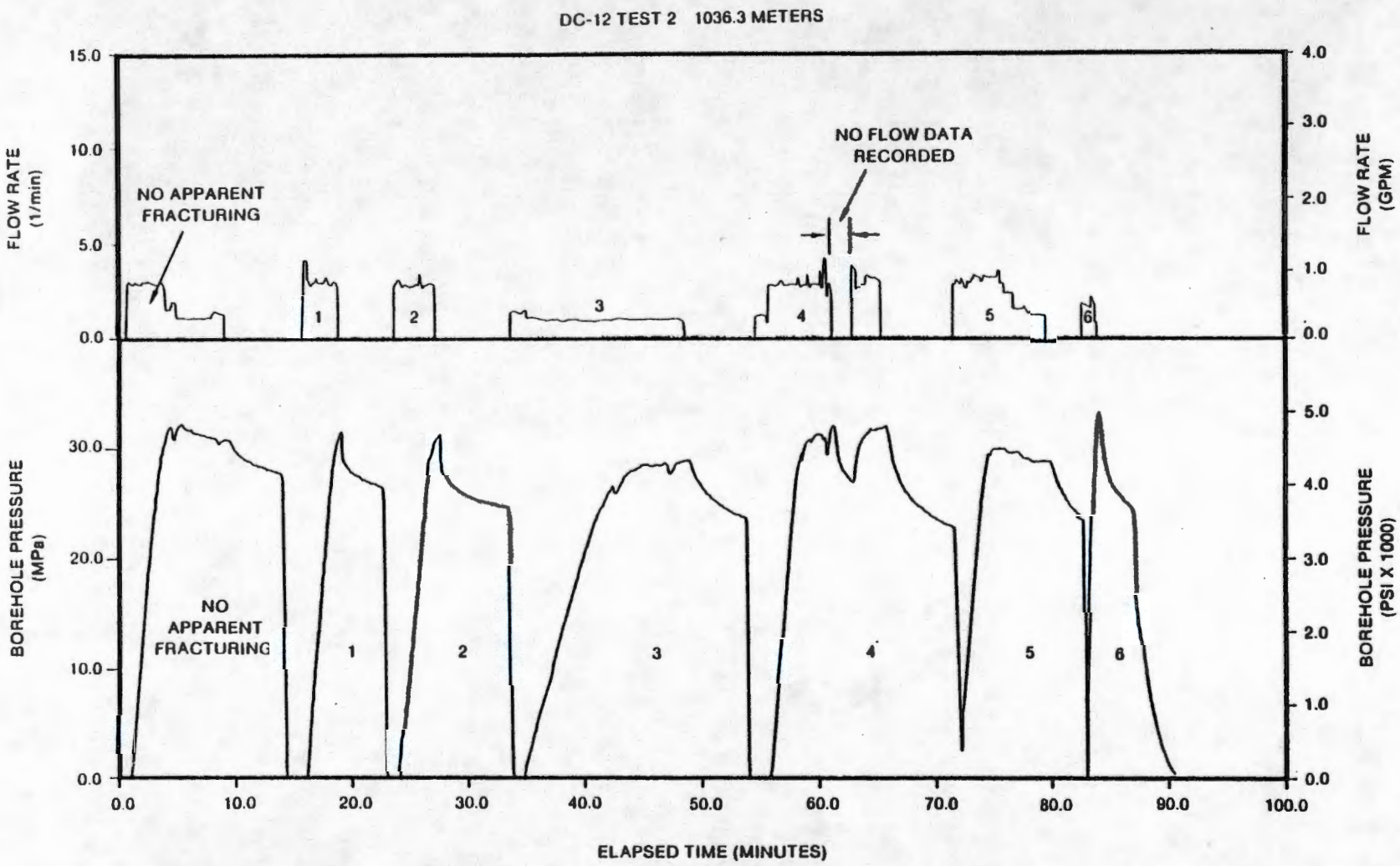

CYCLE	1	2	3	4	5	6	AVERAGE (STD DEV)
P_b	32.8	-	-	-	-	-	-
P_{isi}	30.0	29.0	29.3	29.0	29.7	-	29.3 (0.5)
P_{f_2}	-	27.6	-	25.9	27.6	-	26.9 (1.0)

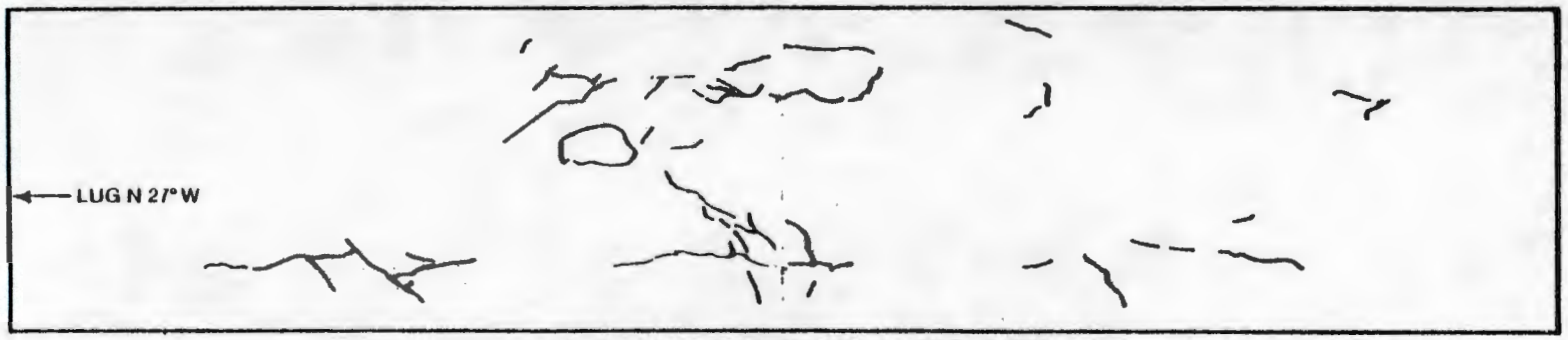

DEPTH 1036.3 M ORIENTATION N 38° E S 47° W

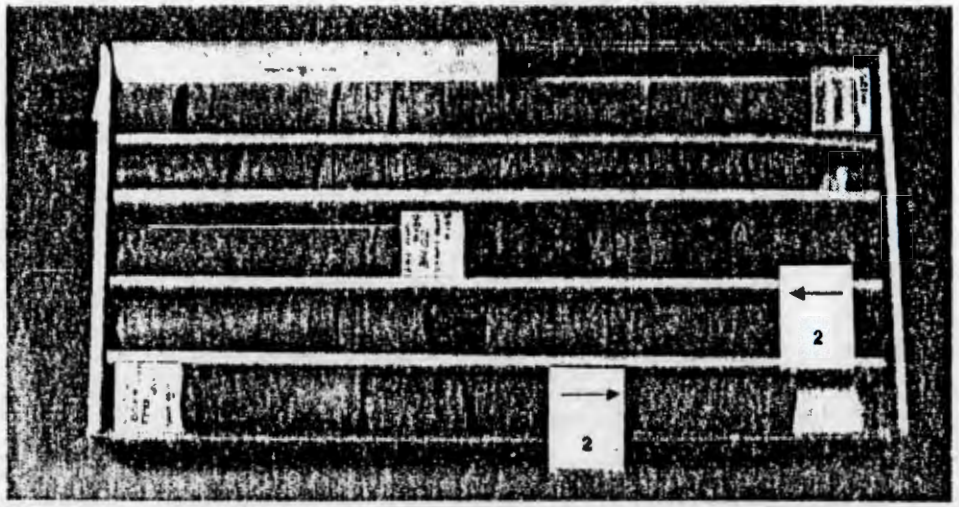

FRACTURE IMPRESSION AND CORE PHOTOGRAPH, DC-12 TEST 2

DC-12 TEST 3 1030.8 METERS

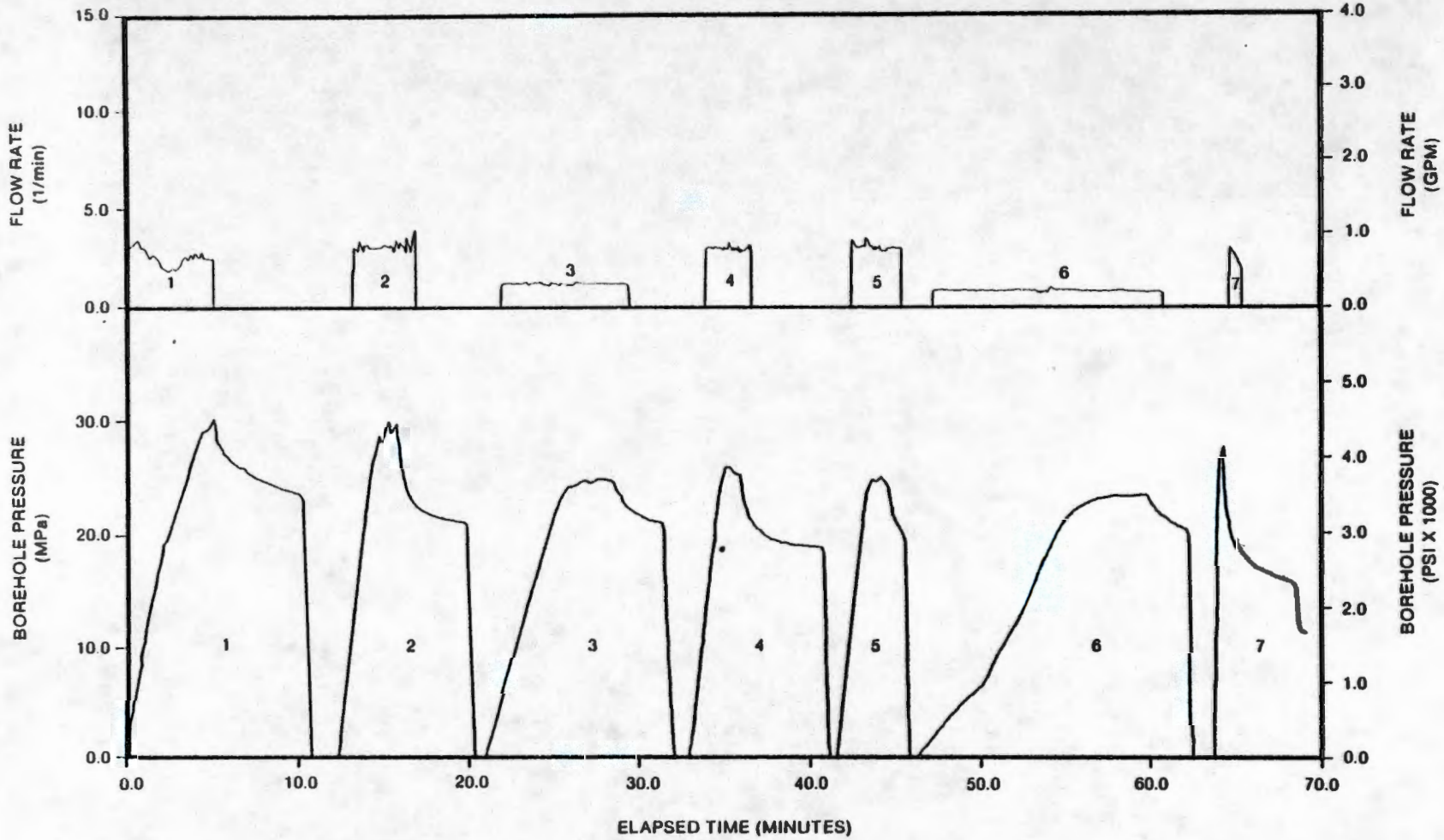

CYCLE	1	2	3	4	5	6	7	AVERAGE (STD DEV)
P_b	31.0	-	-	-	-	-	-	-
P_{isi}	-	24.1	25.2	23.1	-	24.1	-	24.1 (0.9)
P_{l_2}	-	25.9	-	24.1	24.1	-	-	24.7 (1.0)

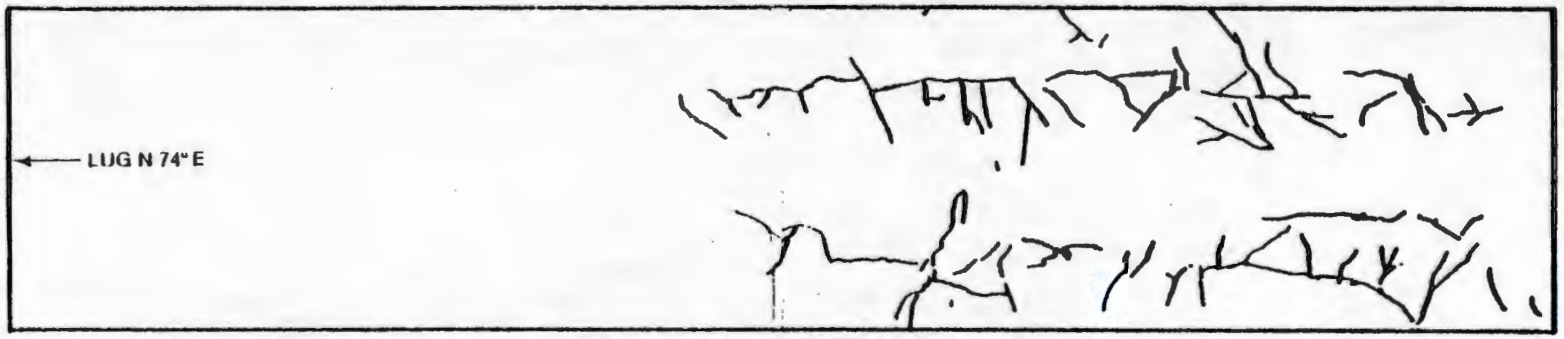

DEPTH 1030.8 M ORIENTATION S 00° E N 02° E

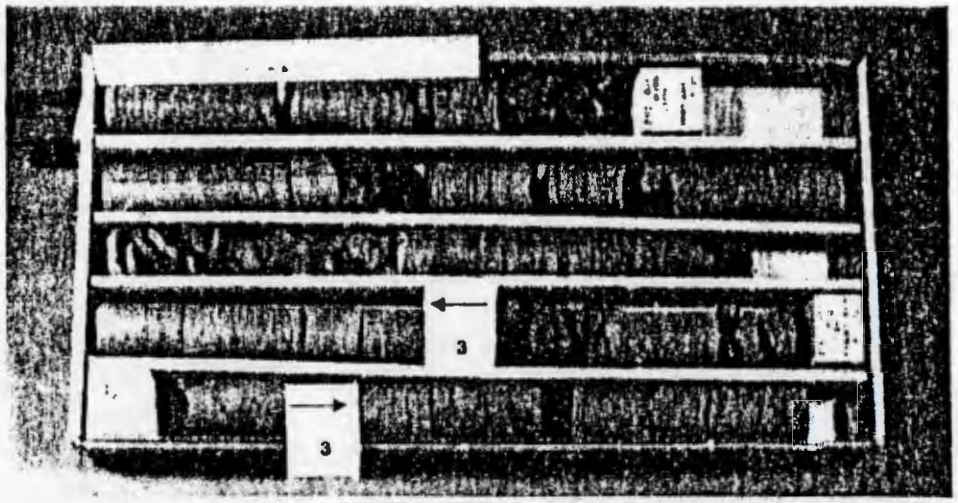

FRACTURE IMPRESSION AND CORE PHOTOGRAPH, DC-12 TEST 3

DC-4 TEST 4 1021.1 METERS

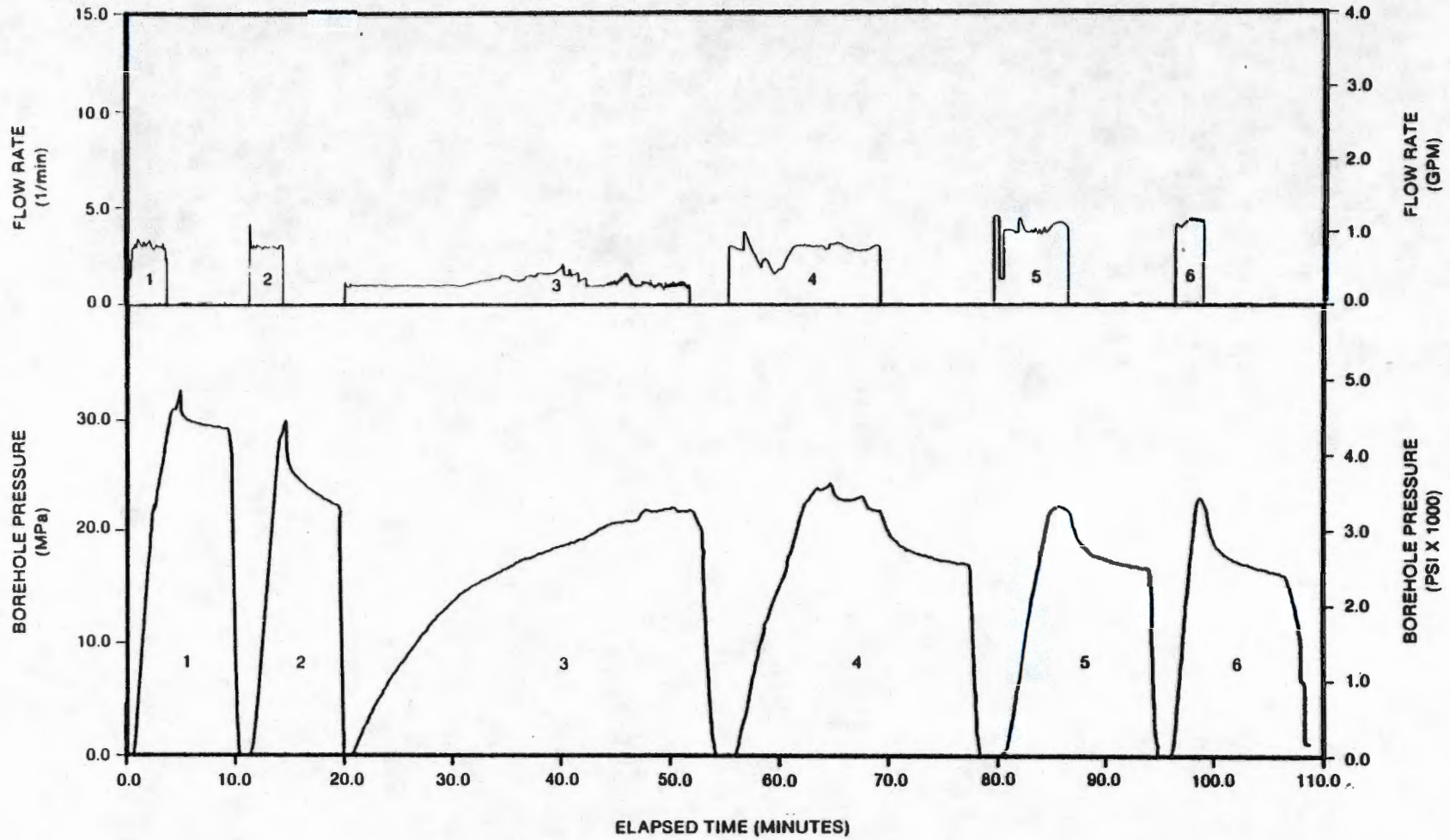

CYCLE	1	2	3	4	5	6	AVERAGE (STD DEV)
P_b	33.6	-	-	-	-	-	-
P_{isi}	-	-	22.4	-	20.7	20.7	21.4 (1.0)
P_{f_2}	-	-	-	-	20.7	20.7	20.7 (0.0)

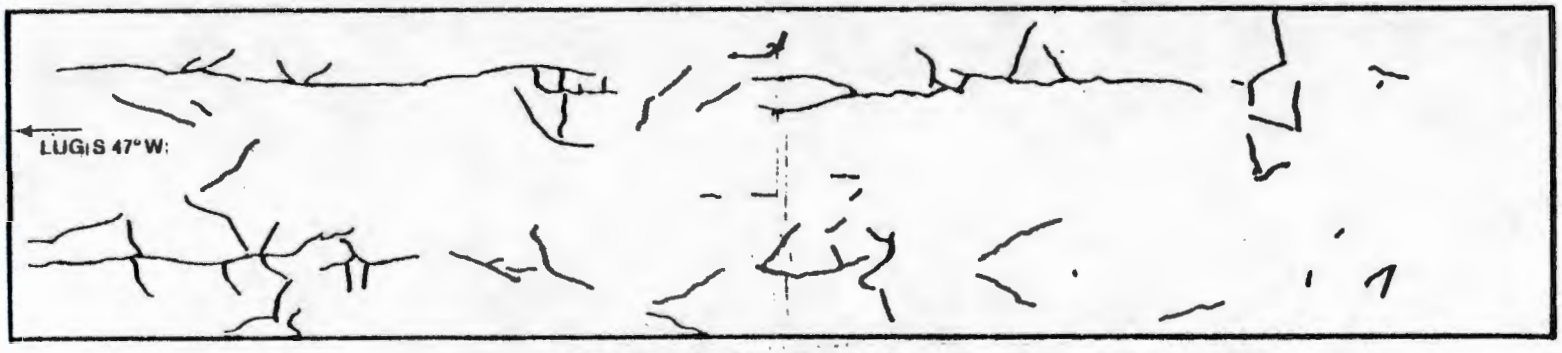

DEPTH 1021.1 M ORIENTATION N 12°E S07°W

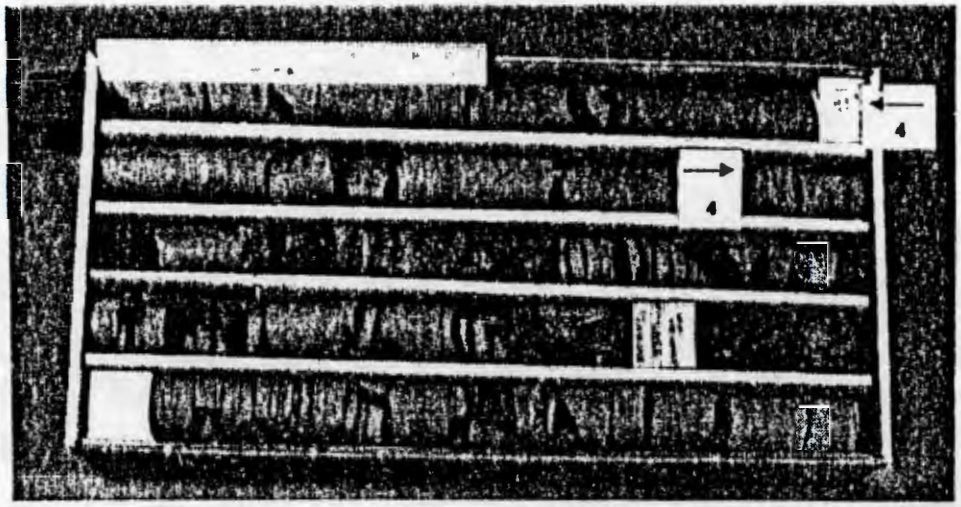

FRACTURE IMPRESSION AND CORE PHOTOGRAPH, DC-12 TEST 4

DC-12 TEST 5 1012.9 METERS

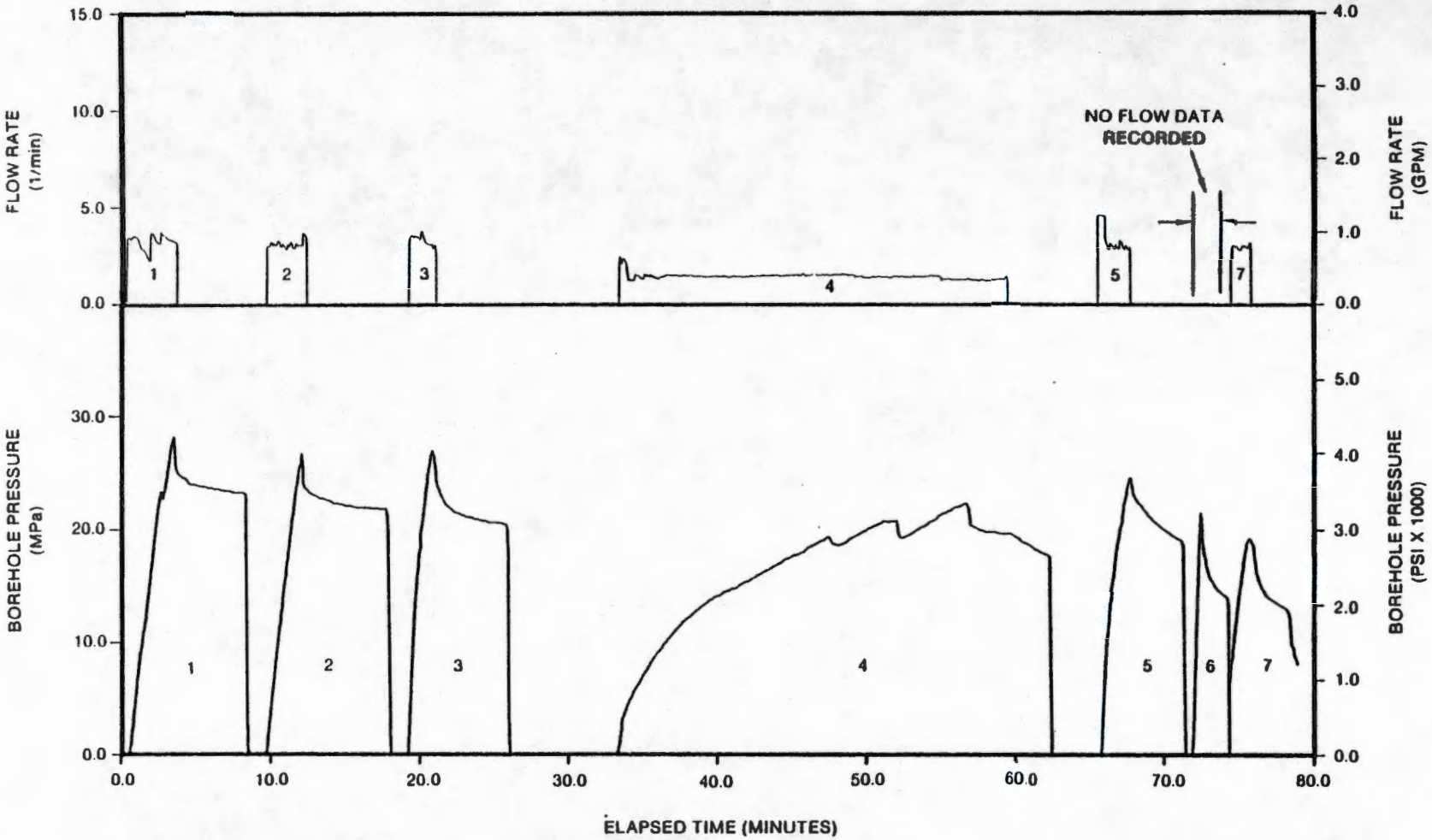

CYCLE	1	2	3	4	5	6	7	AVERAGE (STD DEV)
P_b	29.0	-	-	-	-	-	-	-
P_{isi}	-	24.8	24.8	-	24.1	-	-	355.0 (0.3)
P_{f_2}	-	20.7	-	-	20.7	-	-	20.7 (0.0)

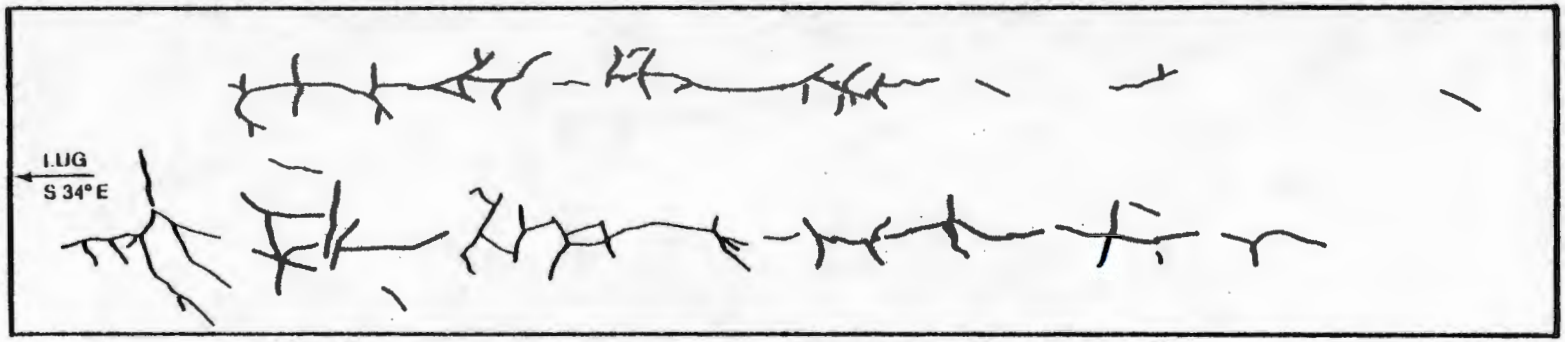

DEPTH 1012.9 M ORIENTATION S 38° W N 42° E

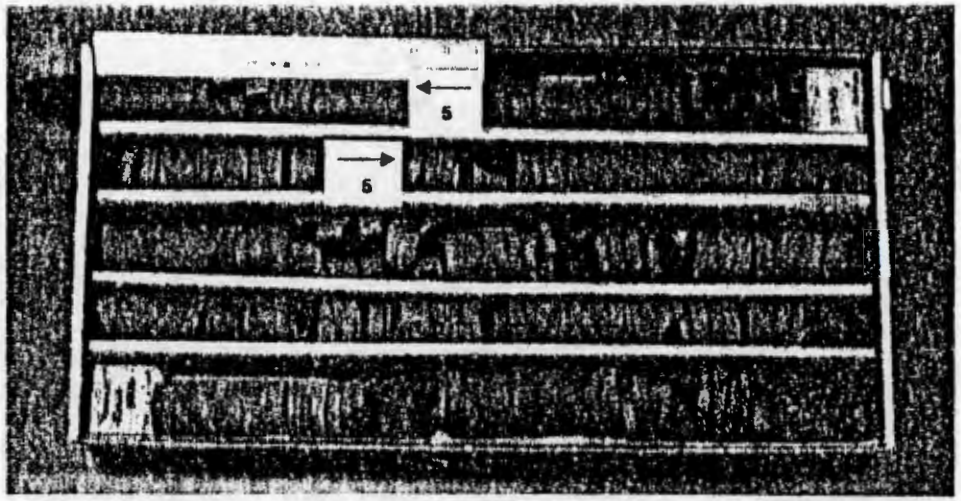

FRACTURE IMPRESSION AND CORE PHOTOGRAPH, DC-12 TEST 5

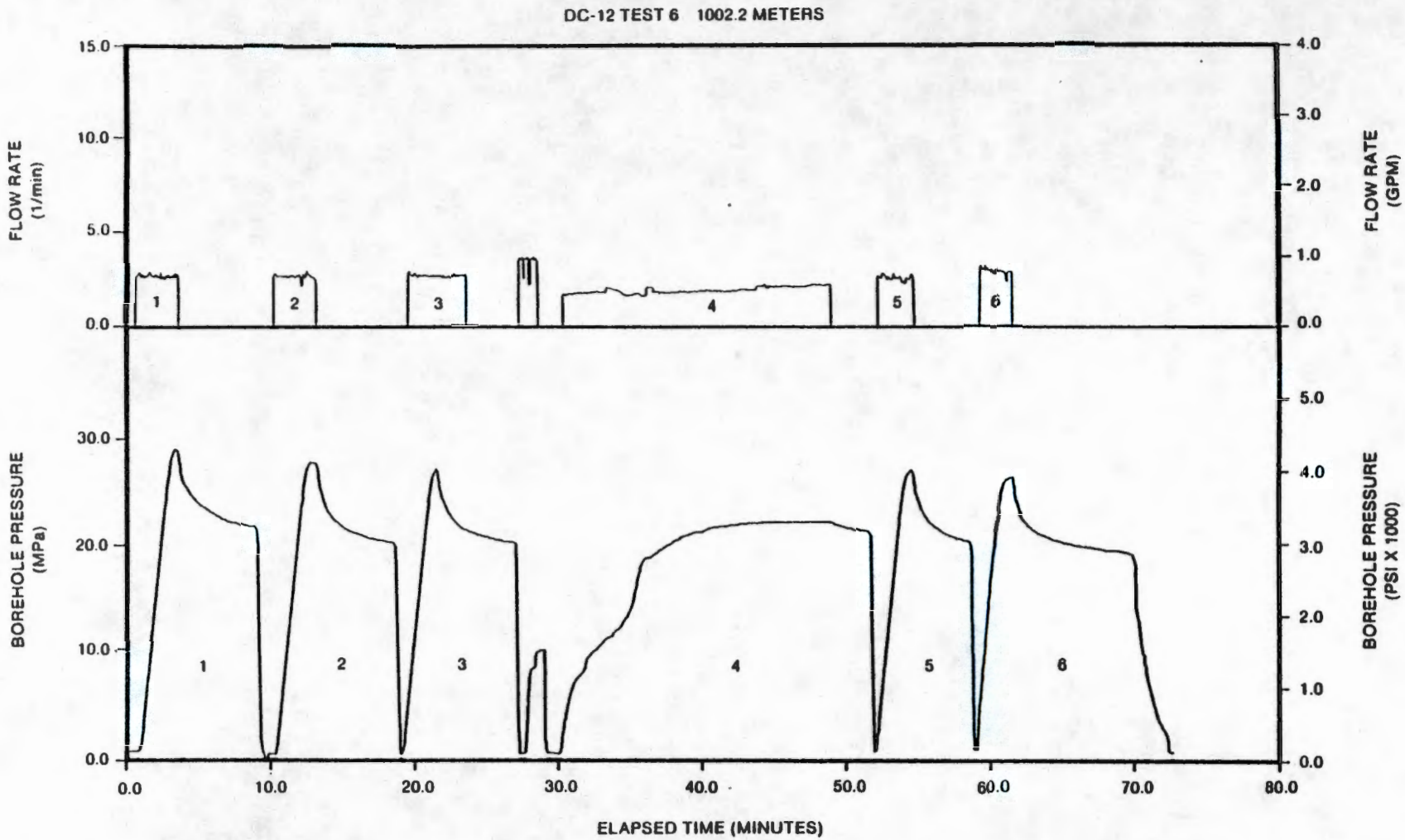

CYCLE	1	2	3	4	5	6	AVERAGE (STD DEV)
P_b	29.6	-	-	-	-	-	-
P_{Isi}	-	24.1	24.1	22.8	23.4	23.1	23.4 (0.7)
P_{I_2}	-	25.9	25.5	-	24.5	24.8	25.2 (0.7)

DEPTH 1002.2 M NO FRACTURE IMPRESSION TAKEN

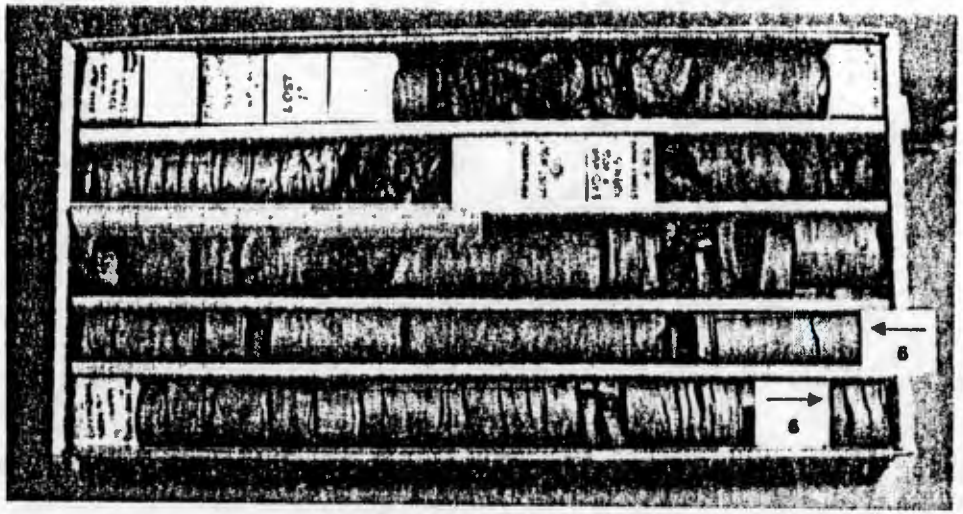

CORE PHOTOGRAPH, DC-12 TEST 6

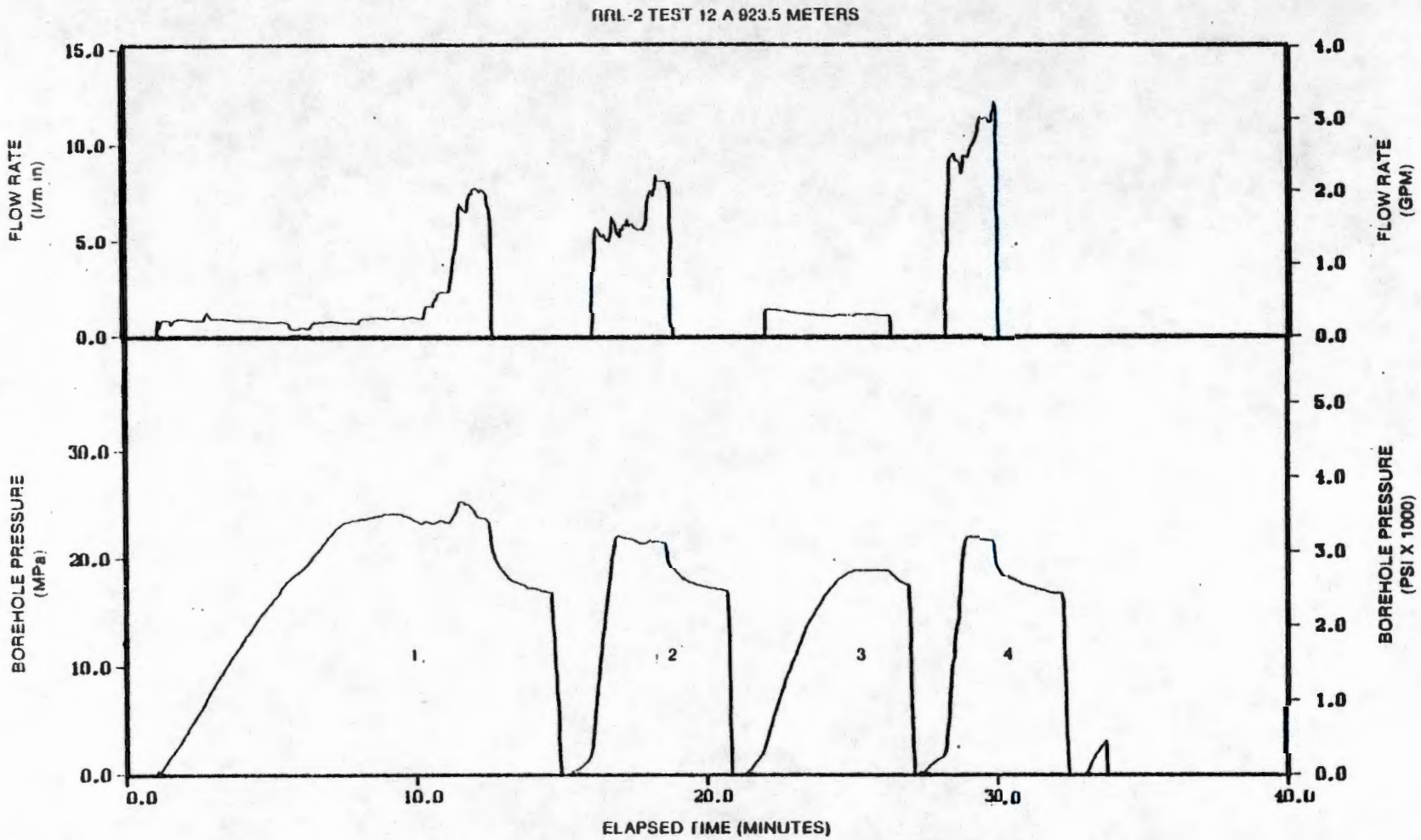

CYCLE	1	2	3	4	AVERAGE (STD DEV)	
P_b	24.8	-	-	-	-	-
P_{isi}	22.1	20.7	-	21.0	21.2	(0.7)
P_{f_2}	-	21.4	-	20.7	21.0	(0.5)

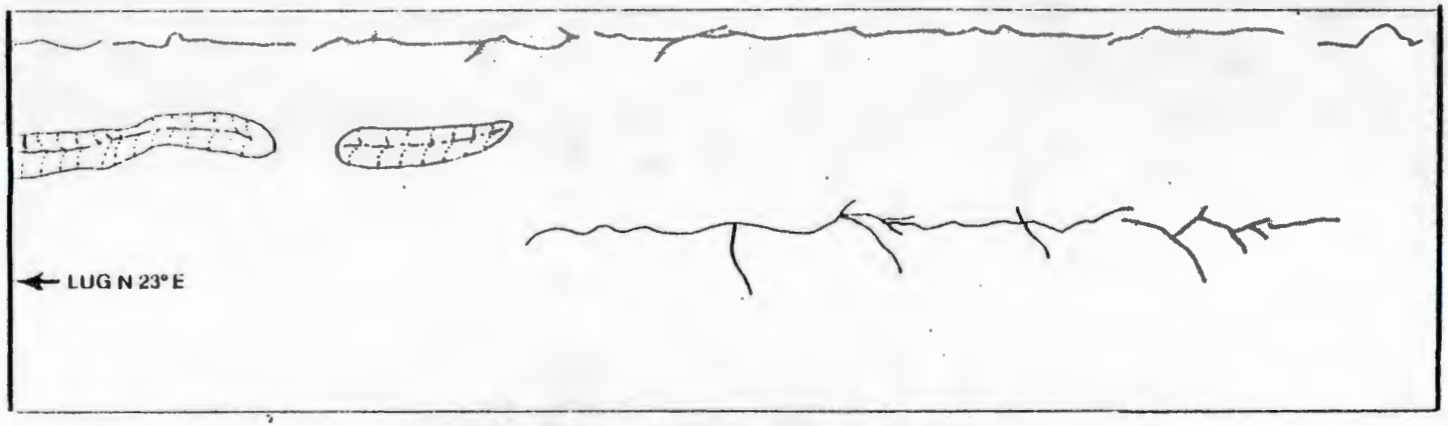

DEPTH 923.5 M ORIENTATION N 21° W S17° E

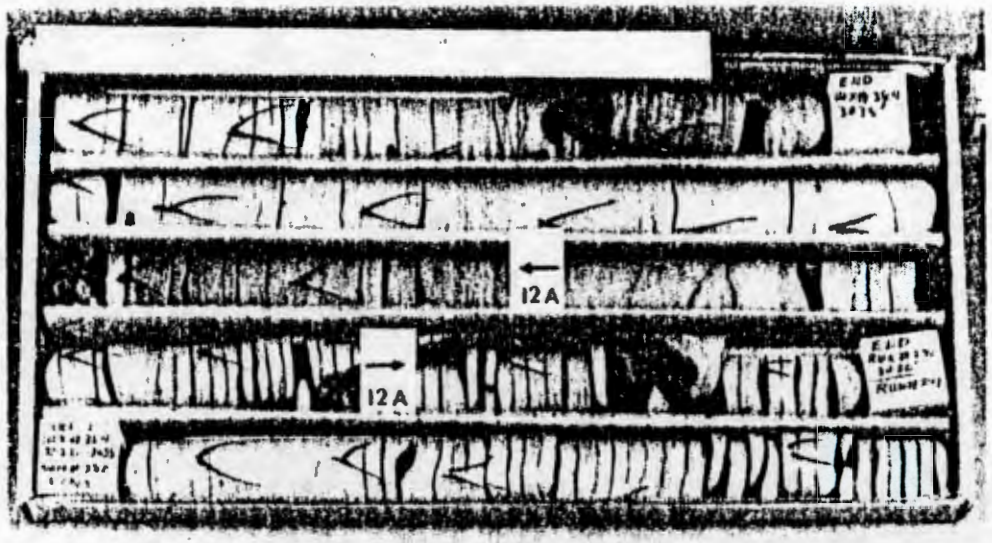

FRACTURE IMPRESSION AND CORE PHOTOGRAPH, RRL-2 TEST 12A

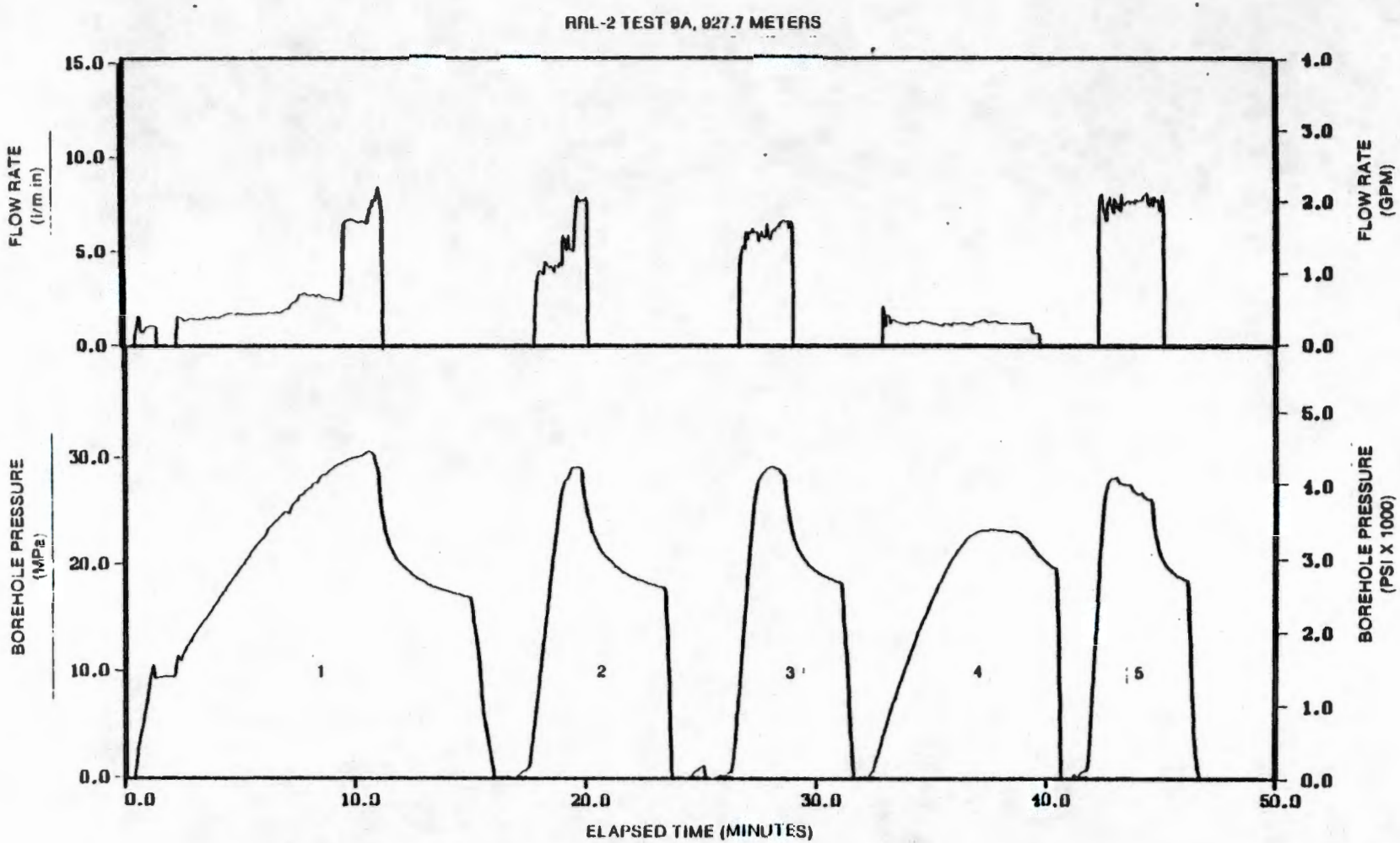

CYCLE	1	2	3	4	5	AVERAGE (STD DEV)	
P_b	31.4	-	-	-	-	-	-
P_{isi}	26.6	26.9	26 2	-	23.4	26.6	(0.3)OMIT CYCLE 5
P_{f_2}	-	26.6	25.5	-	26.2	26.1	(0.5)

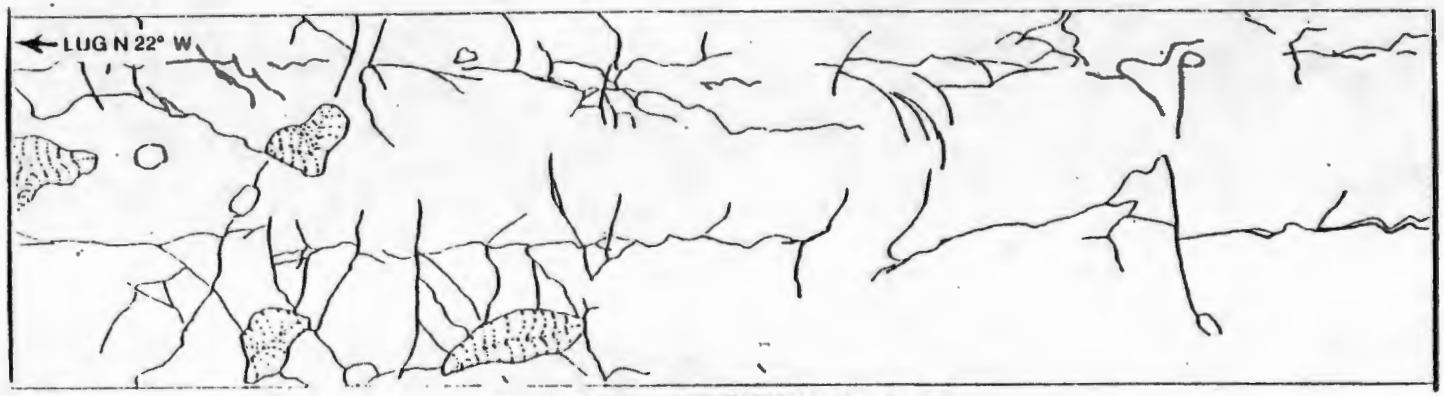

DEPTH 927.7M ORIENTATION N 05° S 02° W

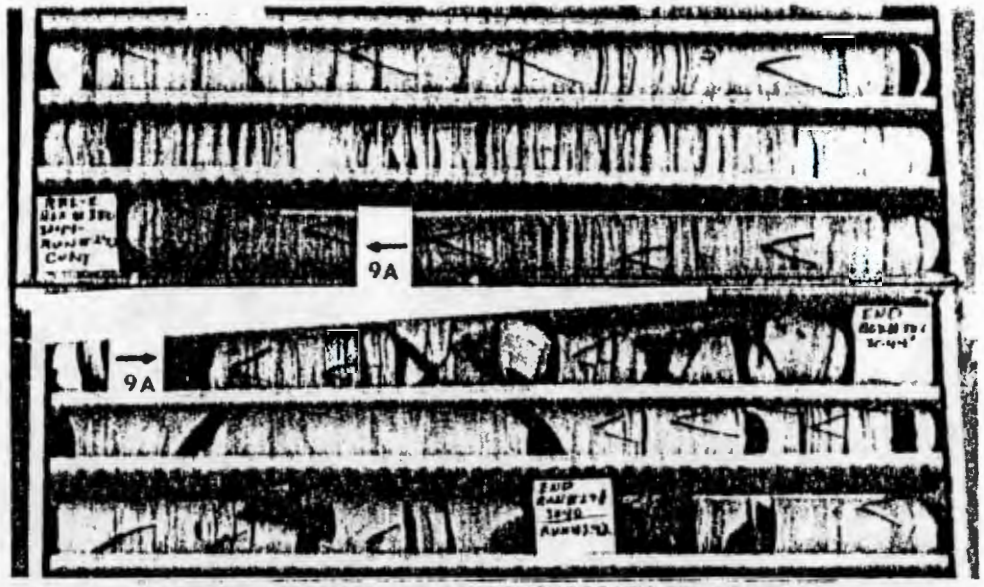

FRACTURE IMPRESSION AND CORE PHOTOGRAPH, RRL-2 TEST 9A

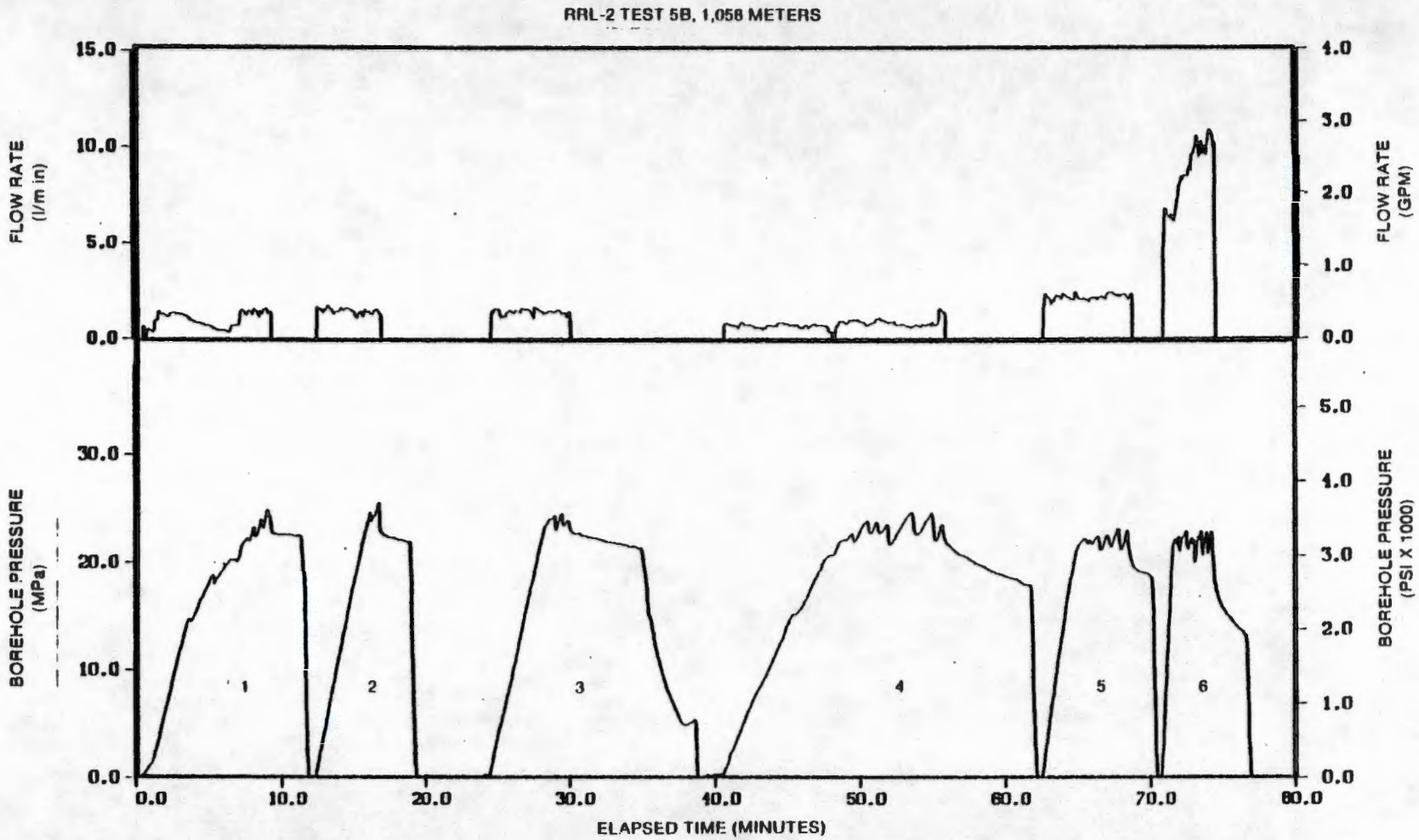

CYCLE	1	2	3	4	5	6	AVERAGE (STD DEV)	
P_b	25.5	-	-	-	-	-	-	-
P_{isi}	23.4	23.1	23.4	22.8	20.7	18.6	23.2	(0.3) - OMIT 5 & 6
P_{i_2}	-	-	22.8	22.4	-	20.3	22.6	22.6 (0.2) - OMIT 6

DEPTH 1,058.0 M ORIENTATION N 09° W S 08° E

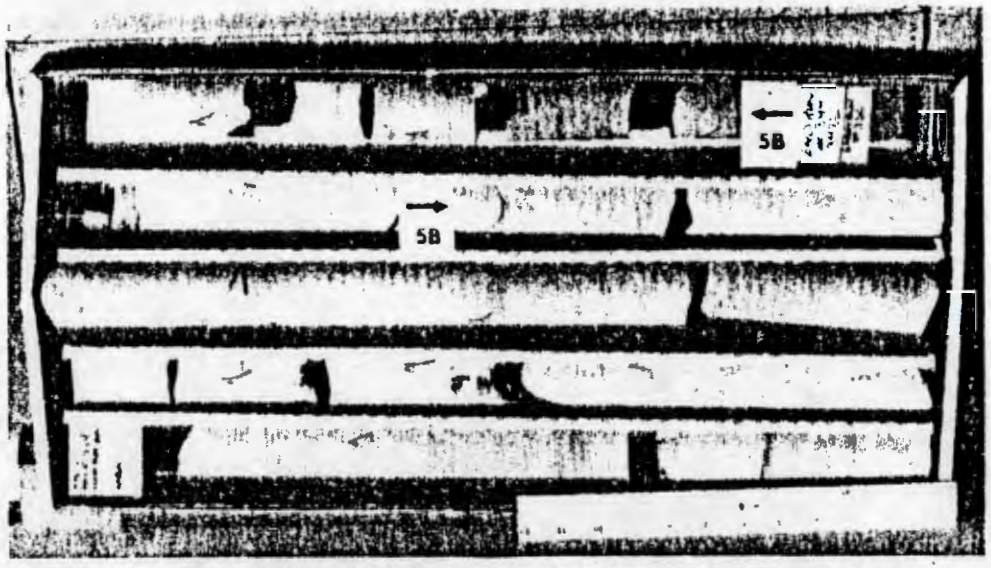

FRACTURE IMPRESSION AND CORE PHOTOGRAPH, RRL-2 TEST 5B

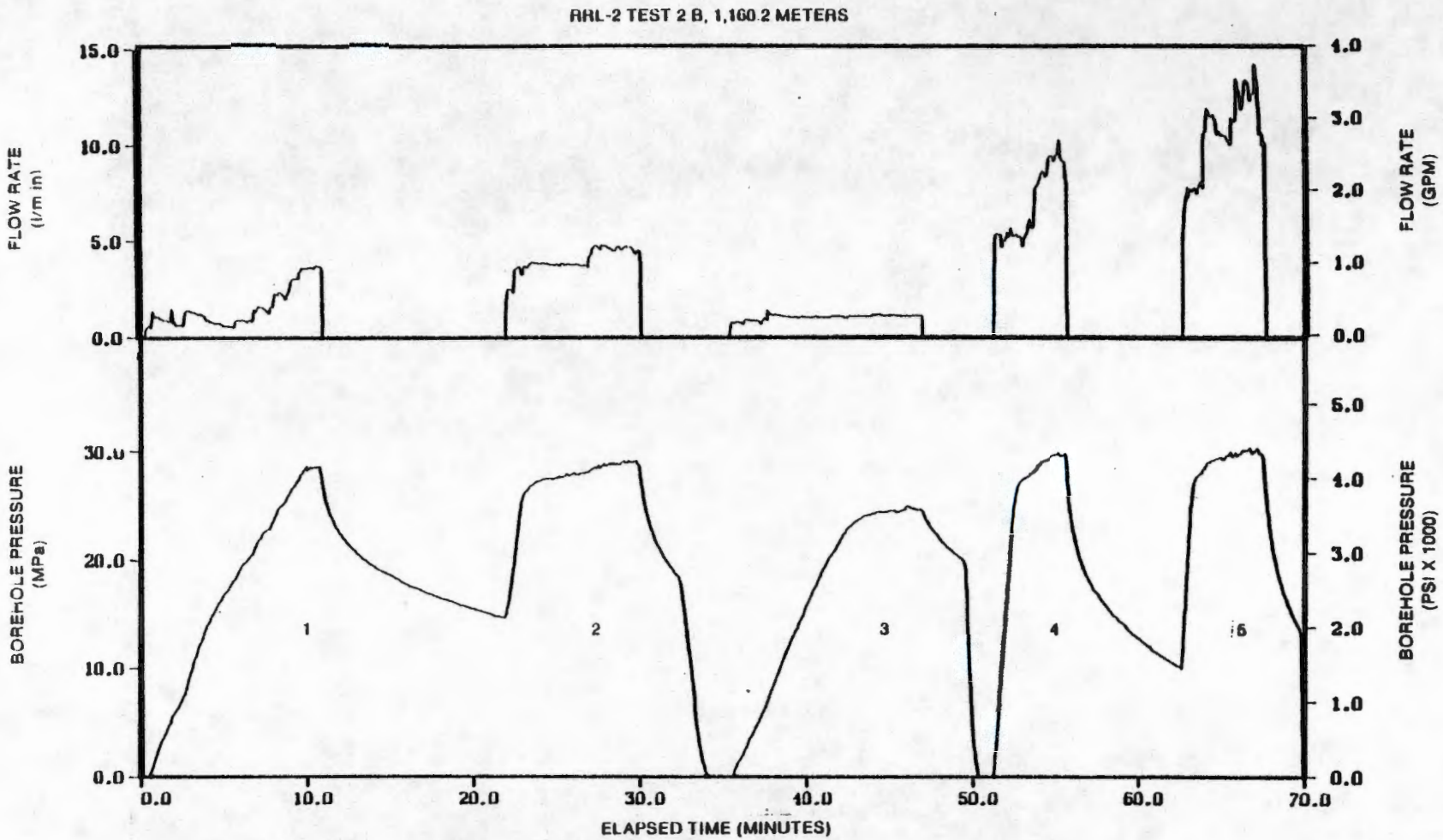

CYCLE	1	2	3	4	5	AVERAGE	(STD DEV)
P_b	29.3	-	-	-	-	-	-
P_{isi}	26.9	27.2	-	25.5	24.8	26.1	(1.1)
P_{I_2}	-	25.9	-	24.5	25.2	25.2	(0.7)

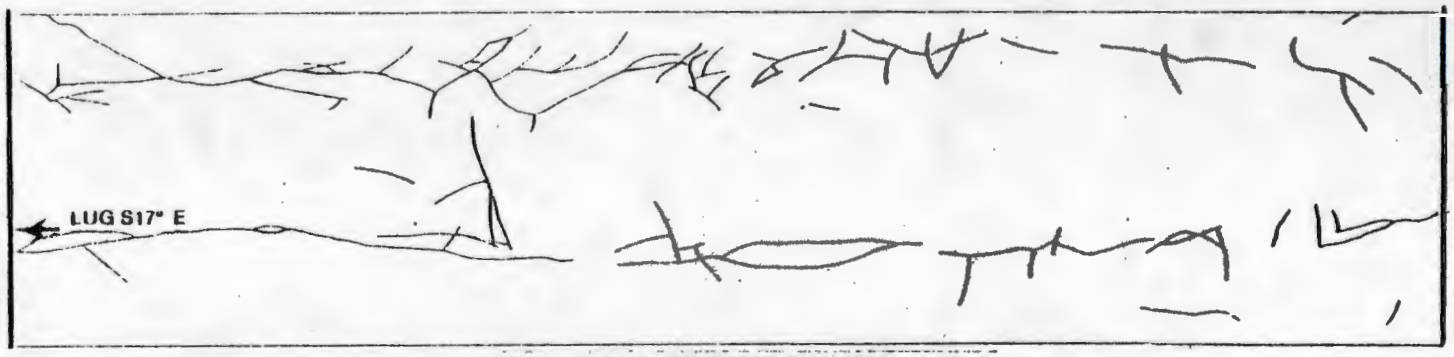

DEPTH 1,160.2 M ORIENTATION N 05° E S 10° W

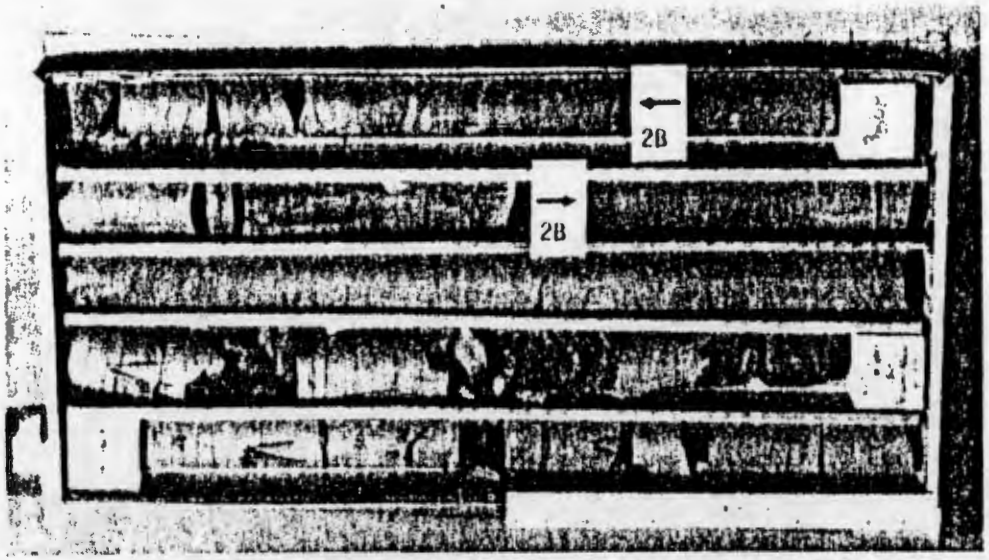

FRACTURE IMPRESSION AND CORE PHOTOGRAPH, RRL-2 TEST 2B

RHL-2 TESTS 1A, 1,168.5 METERS

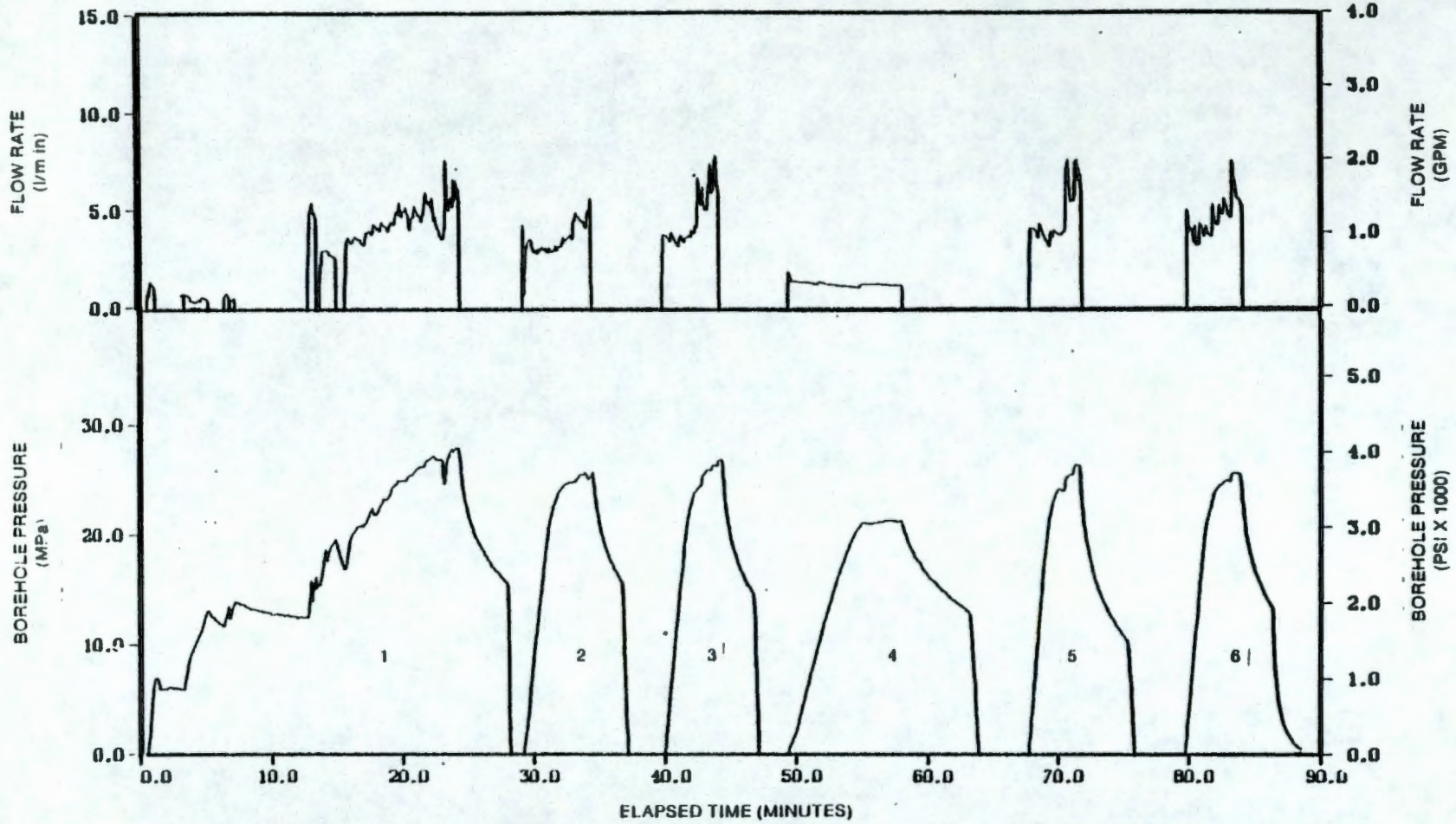

CYCLE	1	2	3	4	5	6	AVERAGE (STD DEV)	
P_b	27.6	-	-	-	-	-	-	-
P_{isi}	25.9	24.1	24.1	-	23.4	22.8	24.1	(1.2)
P_{l_2}	-	20.7	20.7	-	19.3	21.4	20.5	(0.9)

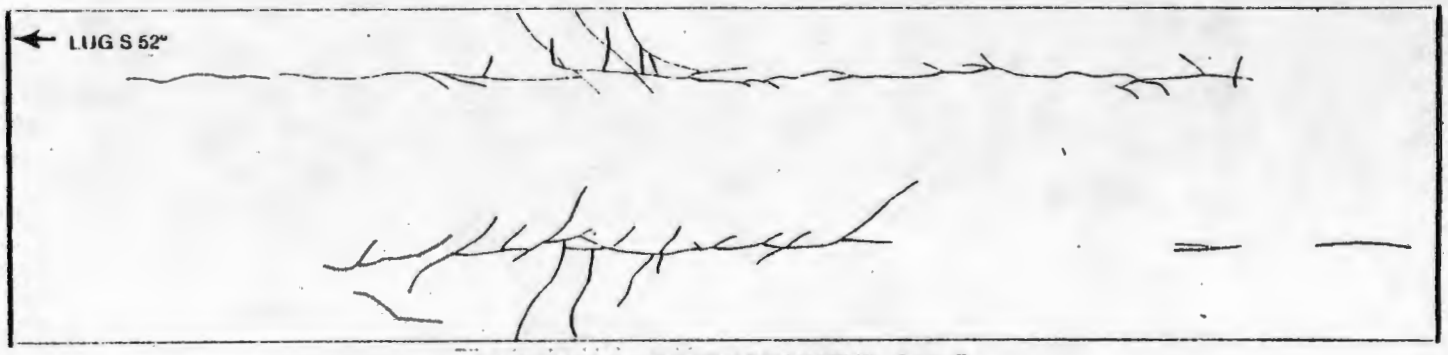

DEPTH 1,166.5 M ORIENTATION N 08° W S 11° E

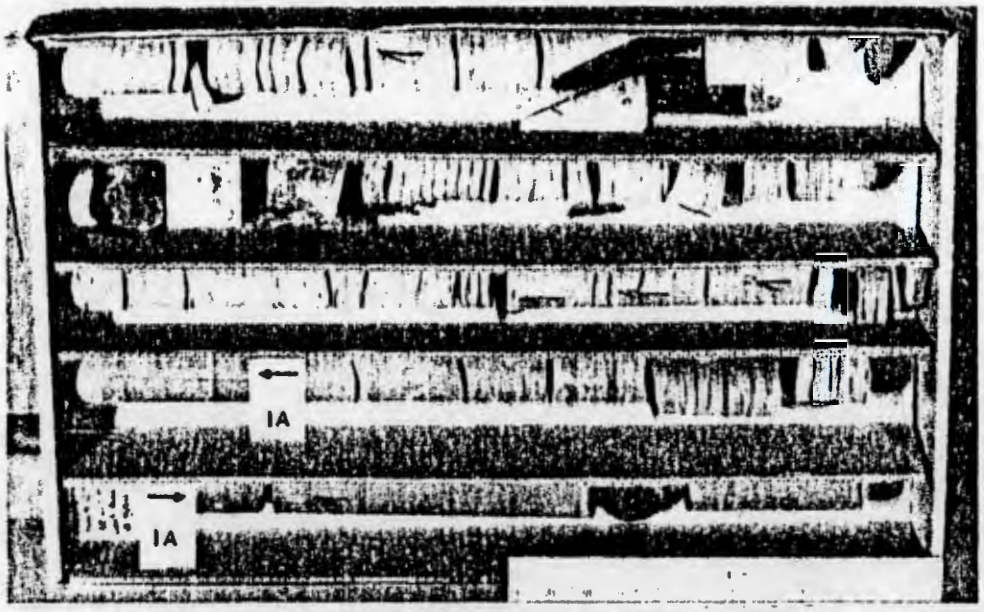

FRACTURE IMPRESSION AND CORE PHOTOGRAPH, RRL-2 TEST 1A

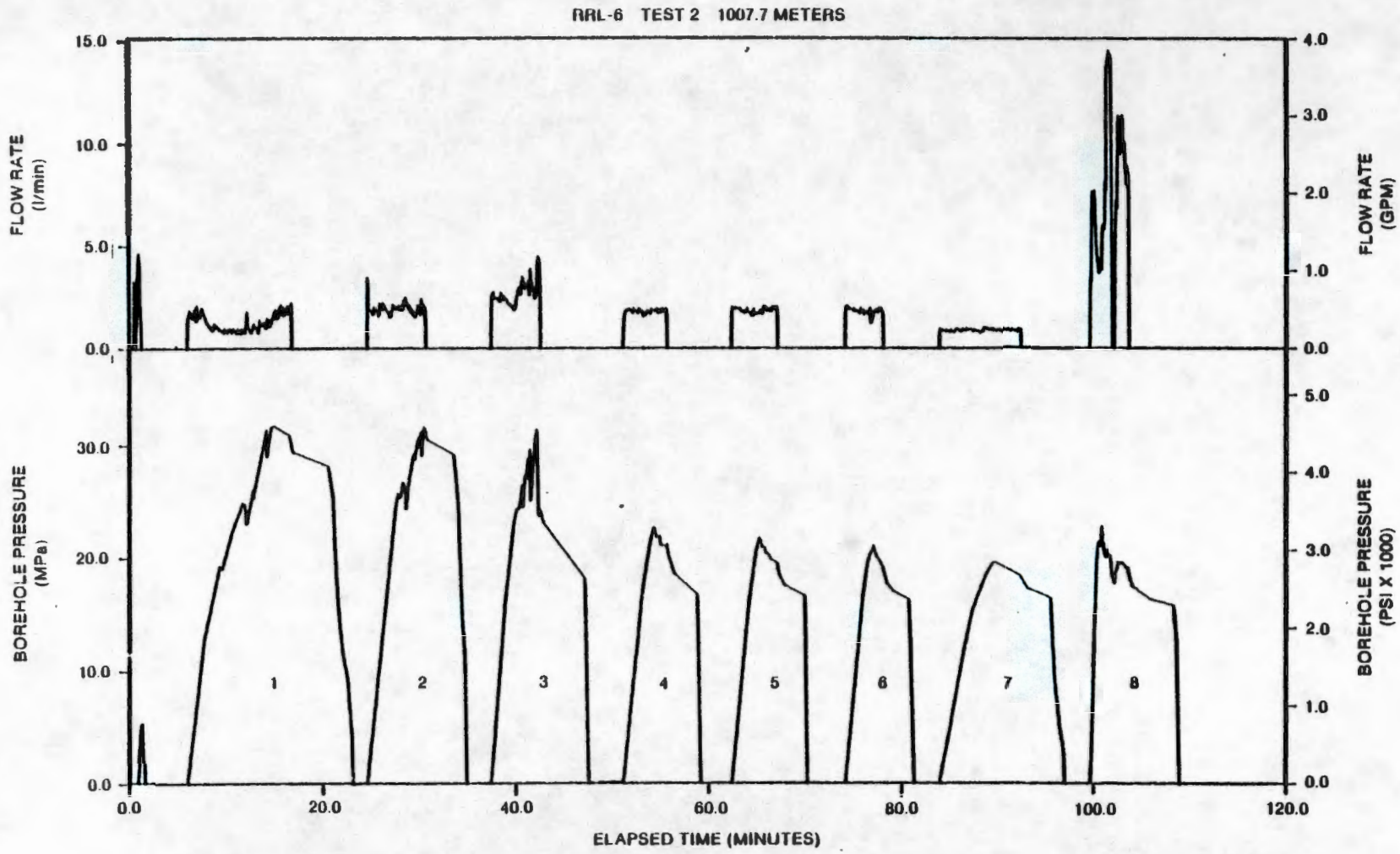

CYCLE	1	2	3	4	5	6	7	8	AVERAGE (STD DEV)	
P_b	32.1	-	-	-	-	-	-	-	-	
P_{isi}	30.0	31.3	24.1	20.7	19.0	18.6	-	-	24.0	(5.6)
P_{f_2}	-	24.8	18.6	15.9	13.8	17.2	-	-	18.1	(4.2)

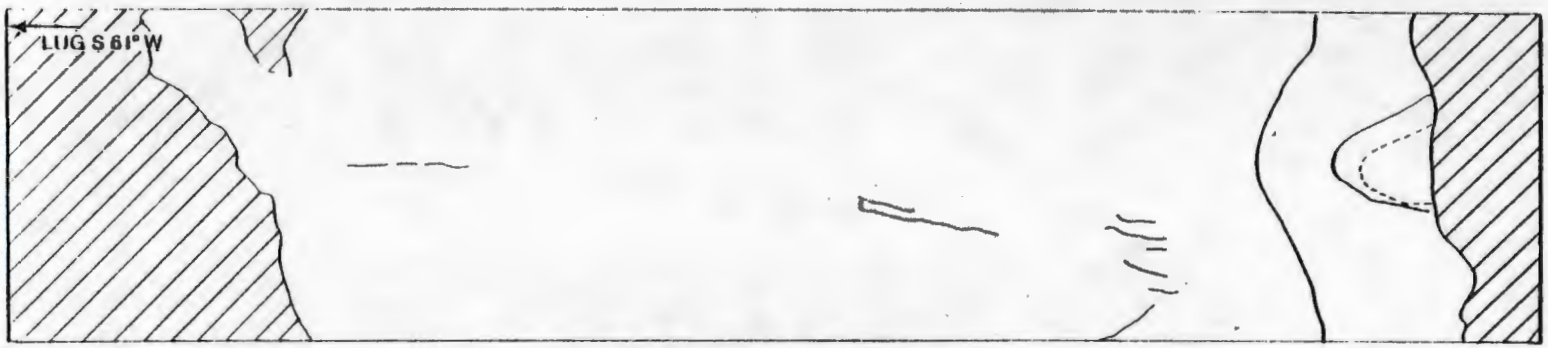

DEPTH 1007.7M ORIENTATION N 28° E

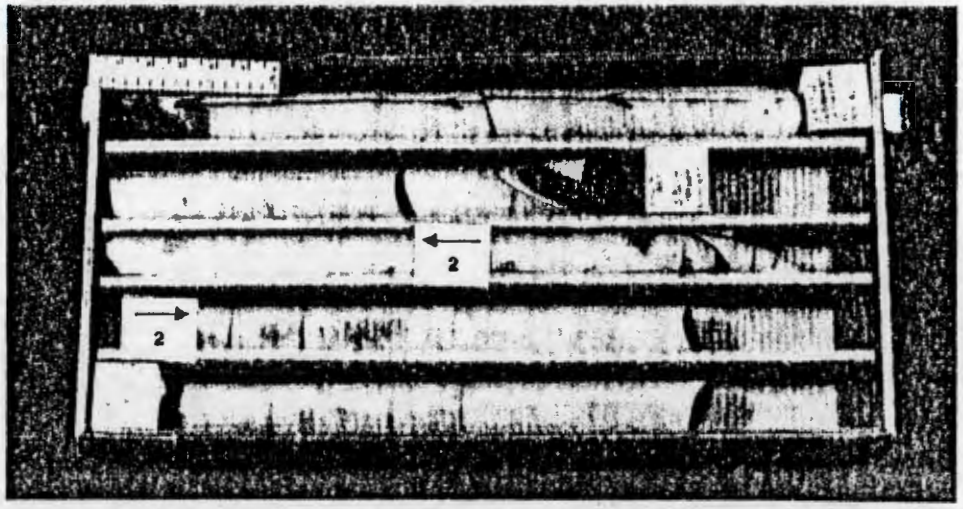

FRACTURE IMPRESSION AND CORE PHOTOGRAPH, RRL-6 TEST 2

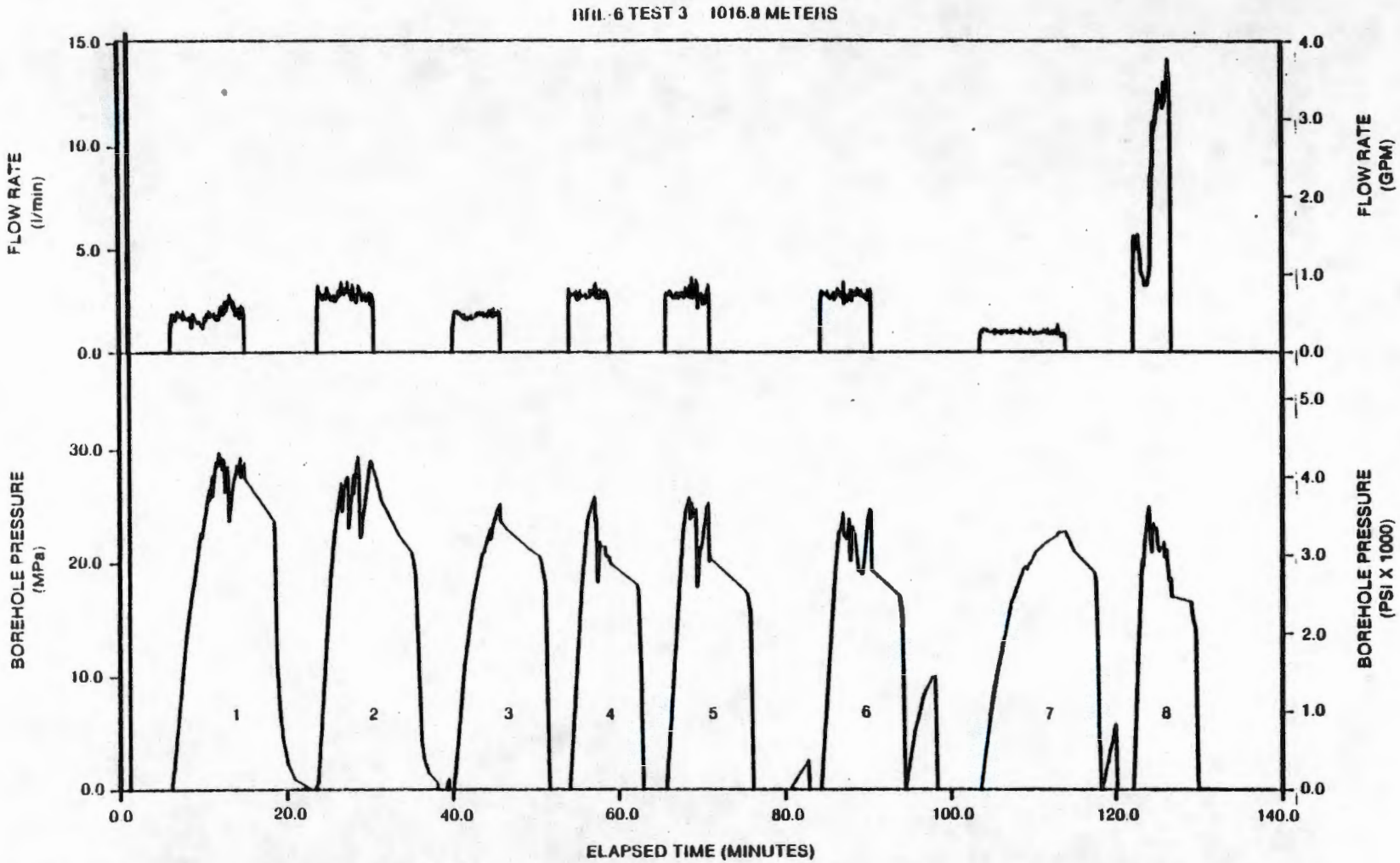

CYCLE	1	2	3	4	5	6	7	8	AVERAGE (STD DEV)
P_b	30.3	-	-	-	-	-	-	-	-
P_{isi}	27.9	27.9	24.1	20.3	21.0	19.7	-	-	23.6 (3.8)
P_{f_2}	-	19.3	8.3	13.8	13.8	13.8	-	-	13.8 (3.9)

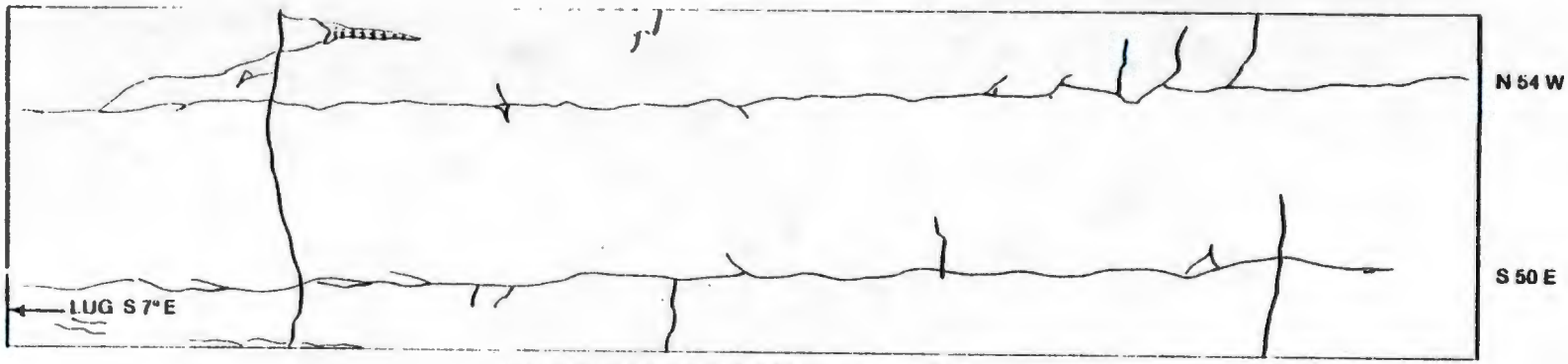

DEPTH 1016.8 M ORIENTATION N54° W, 550° E

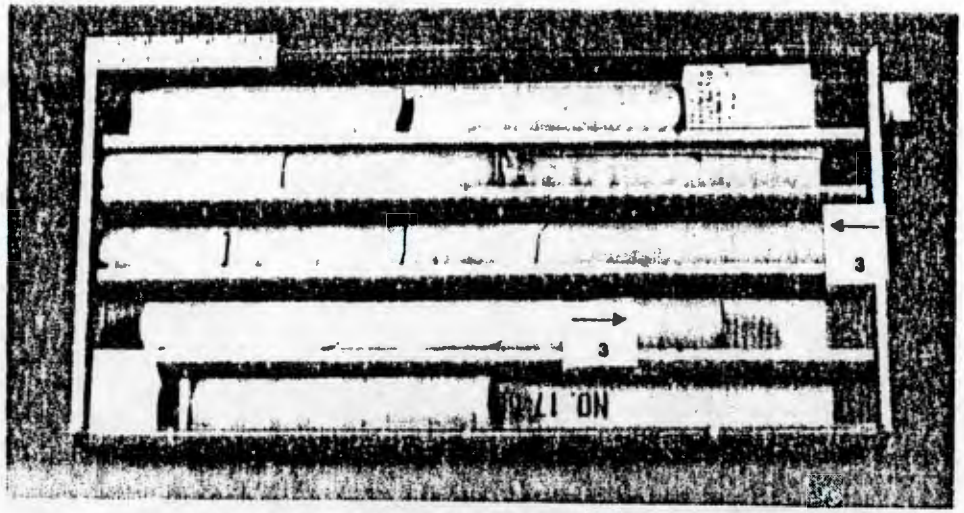

FRACTURE IMPRESSION AND CORE PHOTOGRAPH, RRL-6 TEST 3

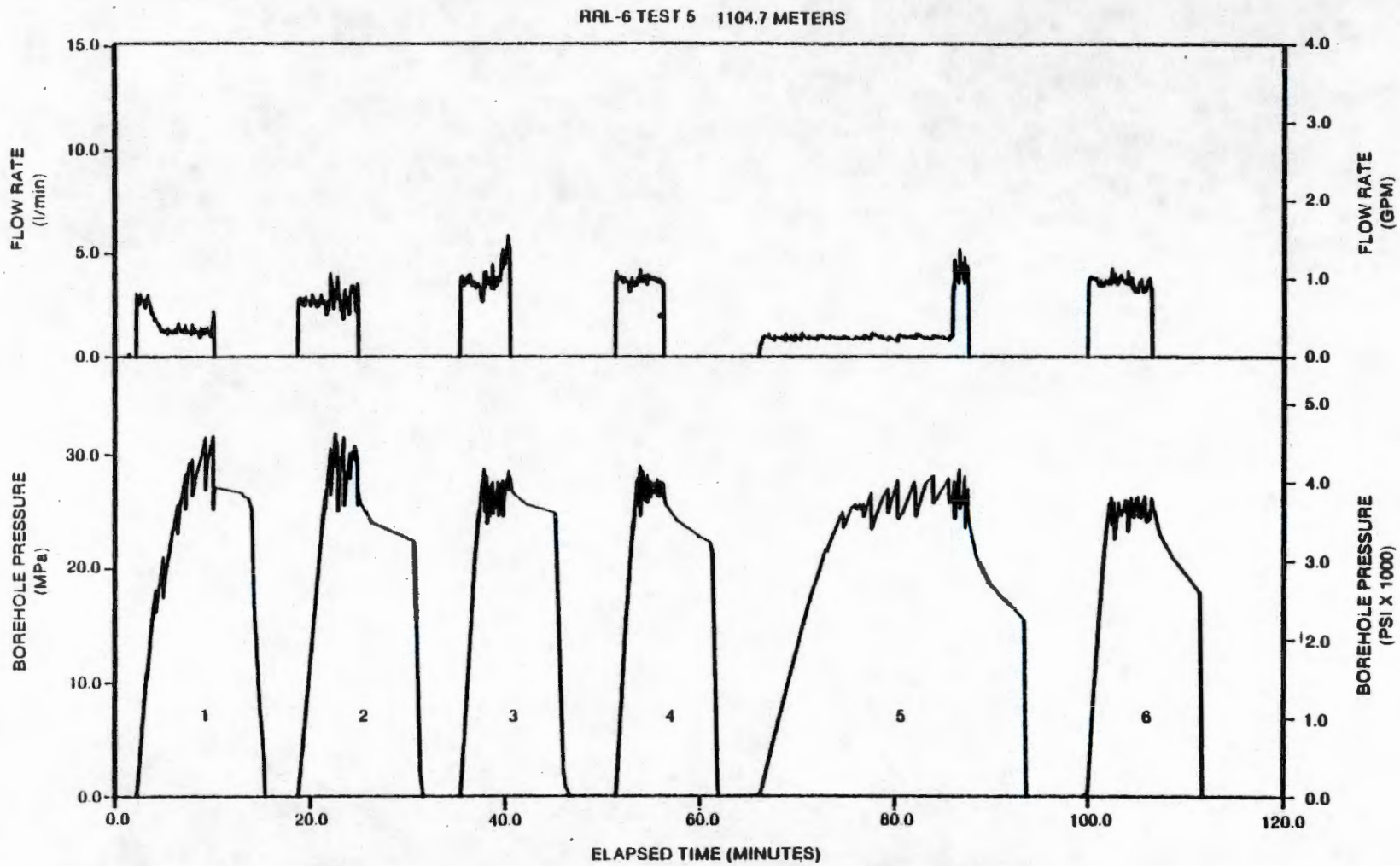

CYCLE	1	2	3	4	5	6	AVERAGE (STD DEV)
P_b	32.3	-	-	-	-	-	-
P_{isi}	27.6	26.2	27.6	26.3	23.4	24.9	26.0 (1.6)
P_{I_2}	-	26.9	22.1	22.8	22.1	21.4	23.0 (2.2)

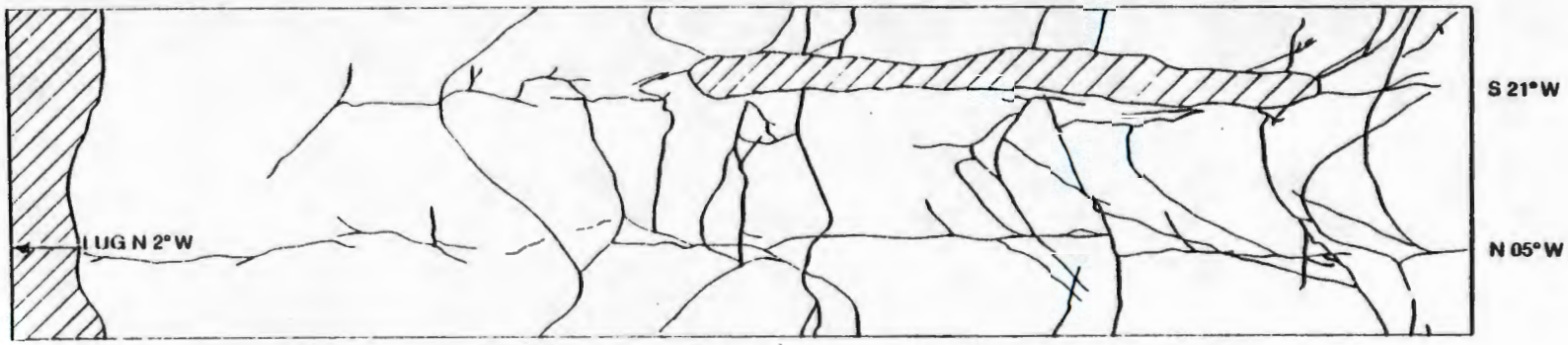

DEPTH 1104.6M ORIENTATION S 21° W, N 05°W

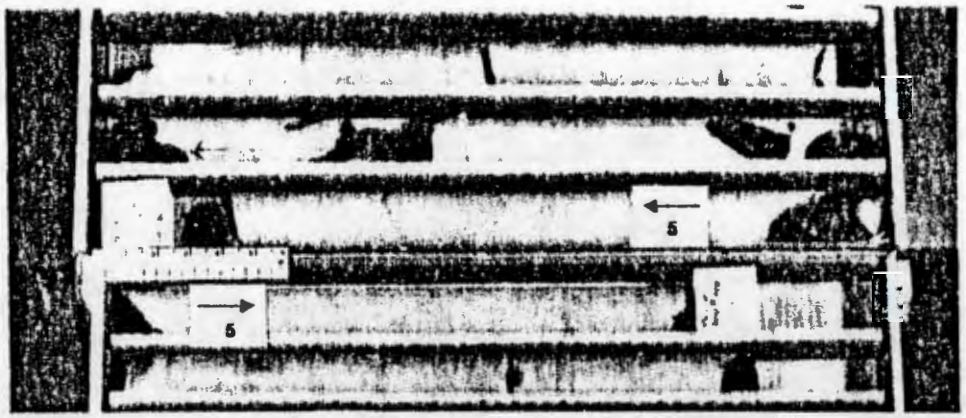

FRACTURE IMPRESSION AND CORE PHOTOGRAPH, RRL-6 TEST 5

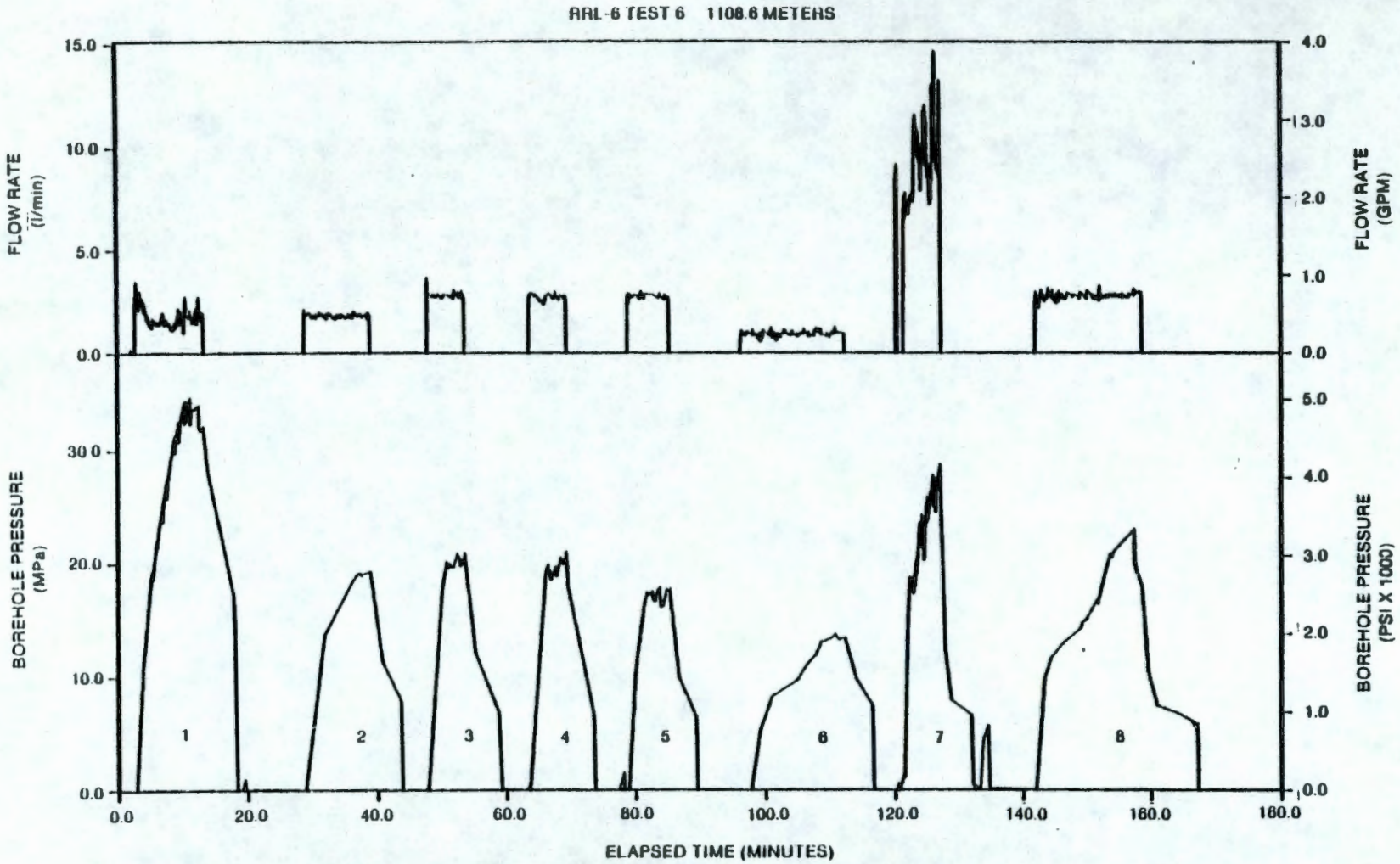

CYCLE	1	2	3	4	5	6	7	8	AVERAGE (STD DEV)
P_b	-	-	-	-	-	-	-	-	-
P_{isi}	31.7	17.9	19.3	18.6	16.2	-	-	15.6	17.5 (1.6)(OMIT CYCLE 1)
P_{f_2}	-	18.3	8.3	8.3	7.2	-	-	4.5	7.3 (1.6)

DEPTH 1108.6 M ORIENTATION N 11° E, S 49° W

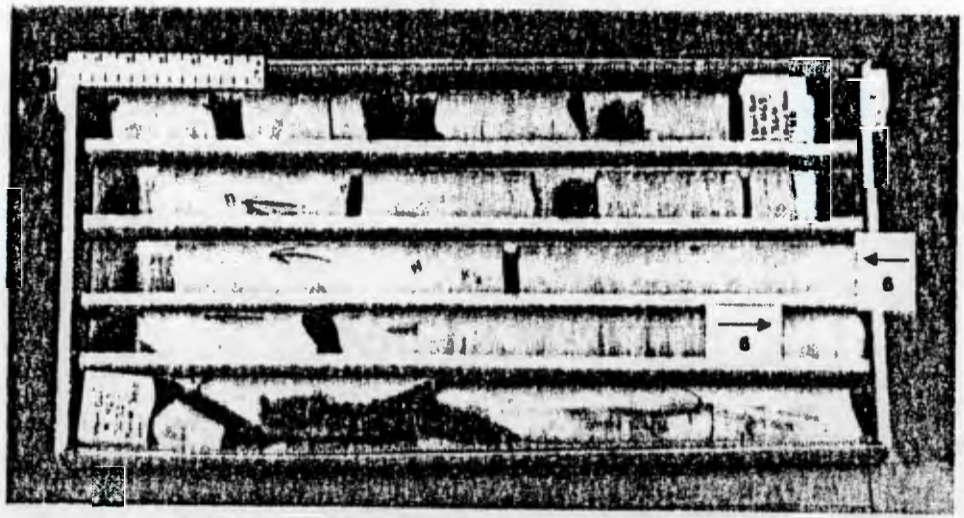

FRACTURE IMPRESSION AND CORE PHOTOGRAPH, RRL-6 TEST 6

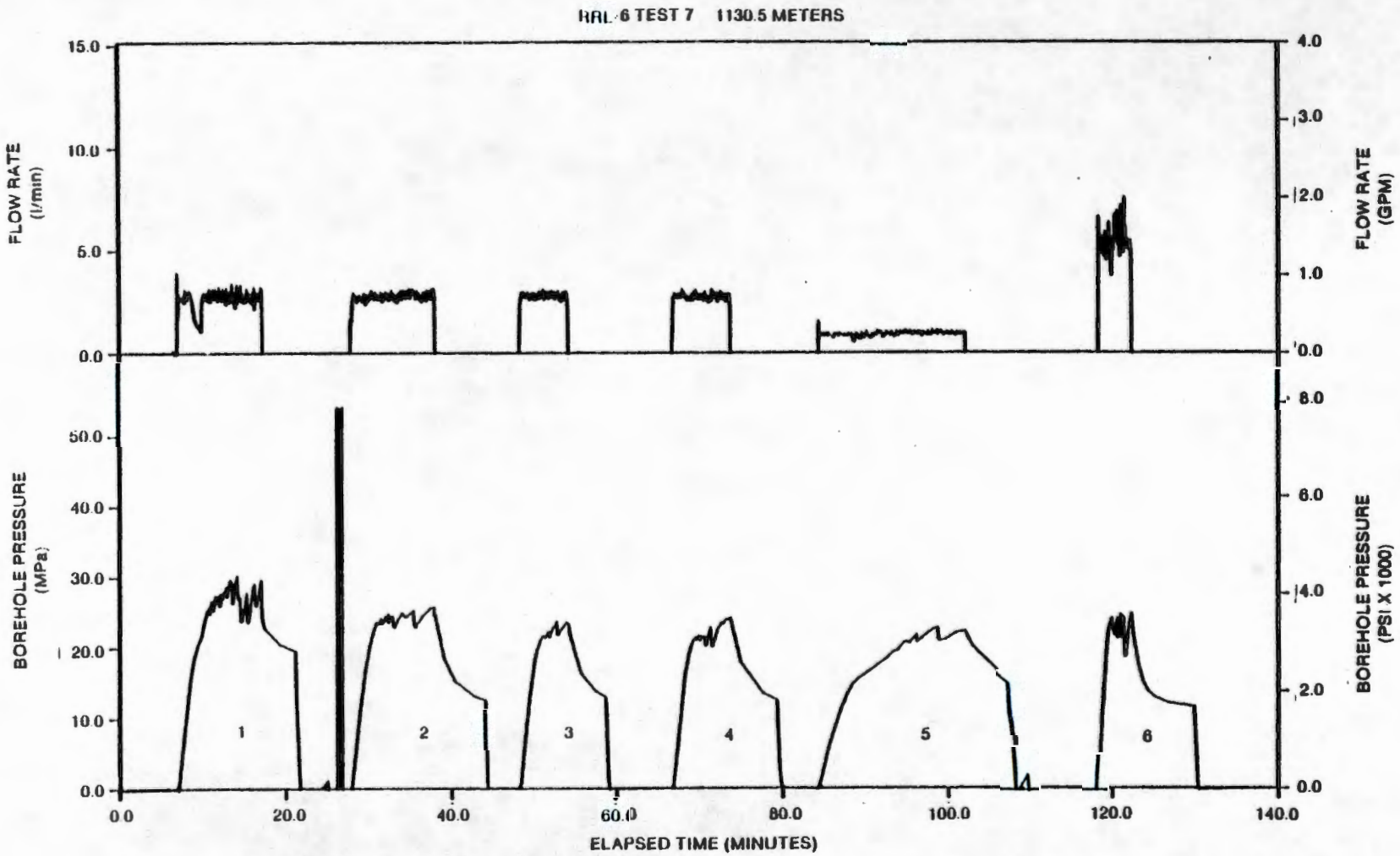

CYCLE	1	2	3	4	5	6	AVERAGE (STD DEV)
P_b	26.3	-	-	-	-	-	-
P_{isi}	23.6	22.6	22.1	23.1	-	-	22.9 (0.7)
P_{f_2}	-	17.2	14.8	16.4	-	-	16.2 (1.2)

DEPTH 1130.5 M ORIENTATION S 21W, N 22° E

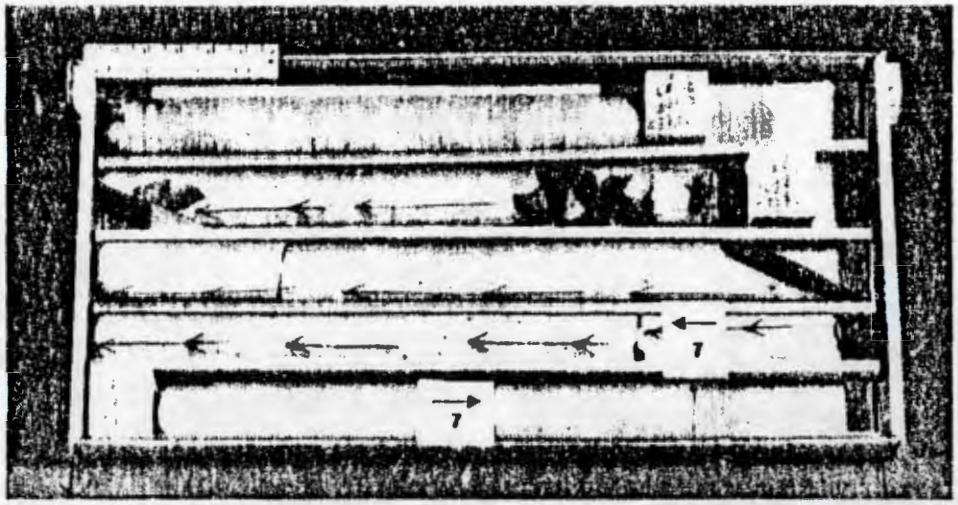

FRACTURE IMPRESSION AND CORE PHOTOGRAPH, RRL-6, TEST 7

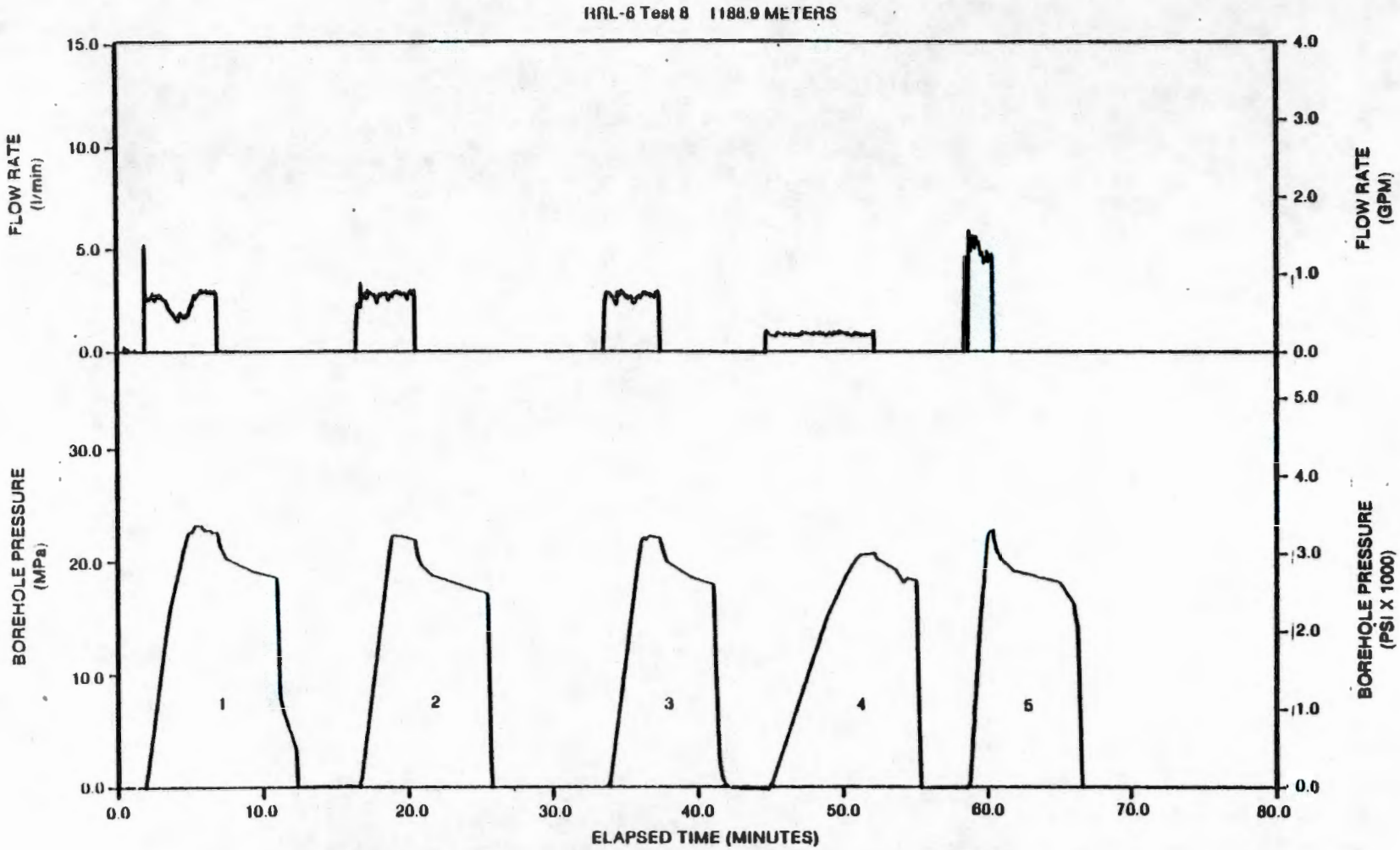

CYCLE	1	2	3	4	5	AVERAGE (STD DEV)
P_b	23.4	-	-	-	-	-
P_{isi}	21.7	21.7	21.4	-	-	21.6 (0.2)
P_{l_2}	-	20.6	18.1	-	-	19.3 (1.8)

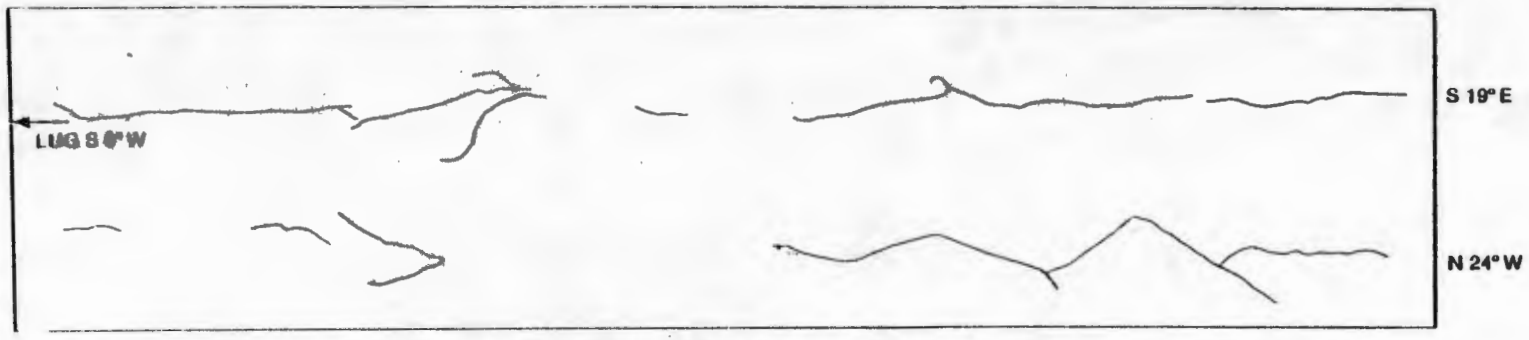

DEPTH 1188.9 M ORIENTATION S 19° E, N 24° W

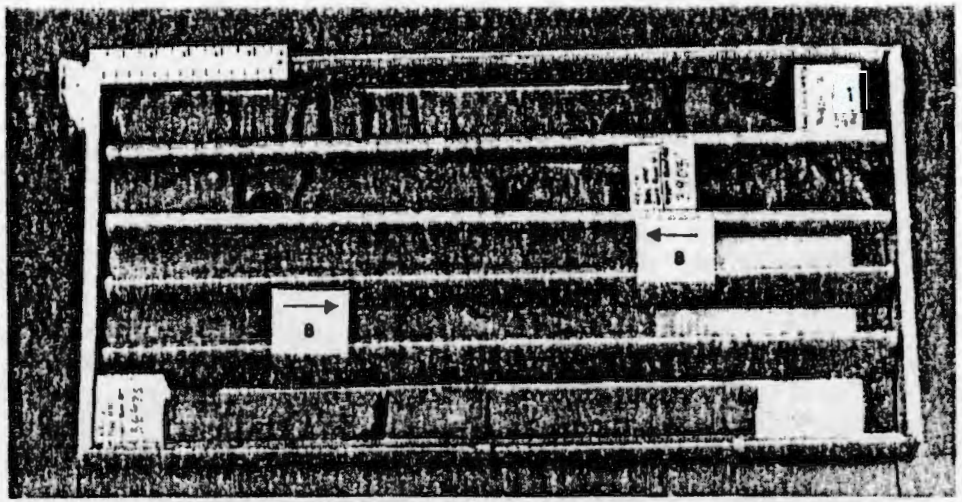

FRACTURE IMPRESSION AND CORE PHOTOGRAPH, RRL-6 TEST 8

DC-4 TEST 2 976.0 METERS (DOWNHOLE PRESSURE)

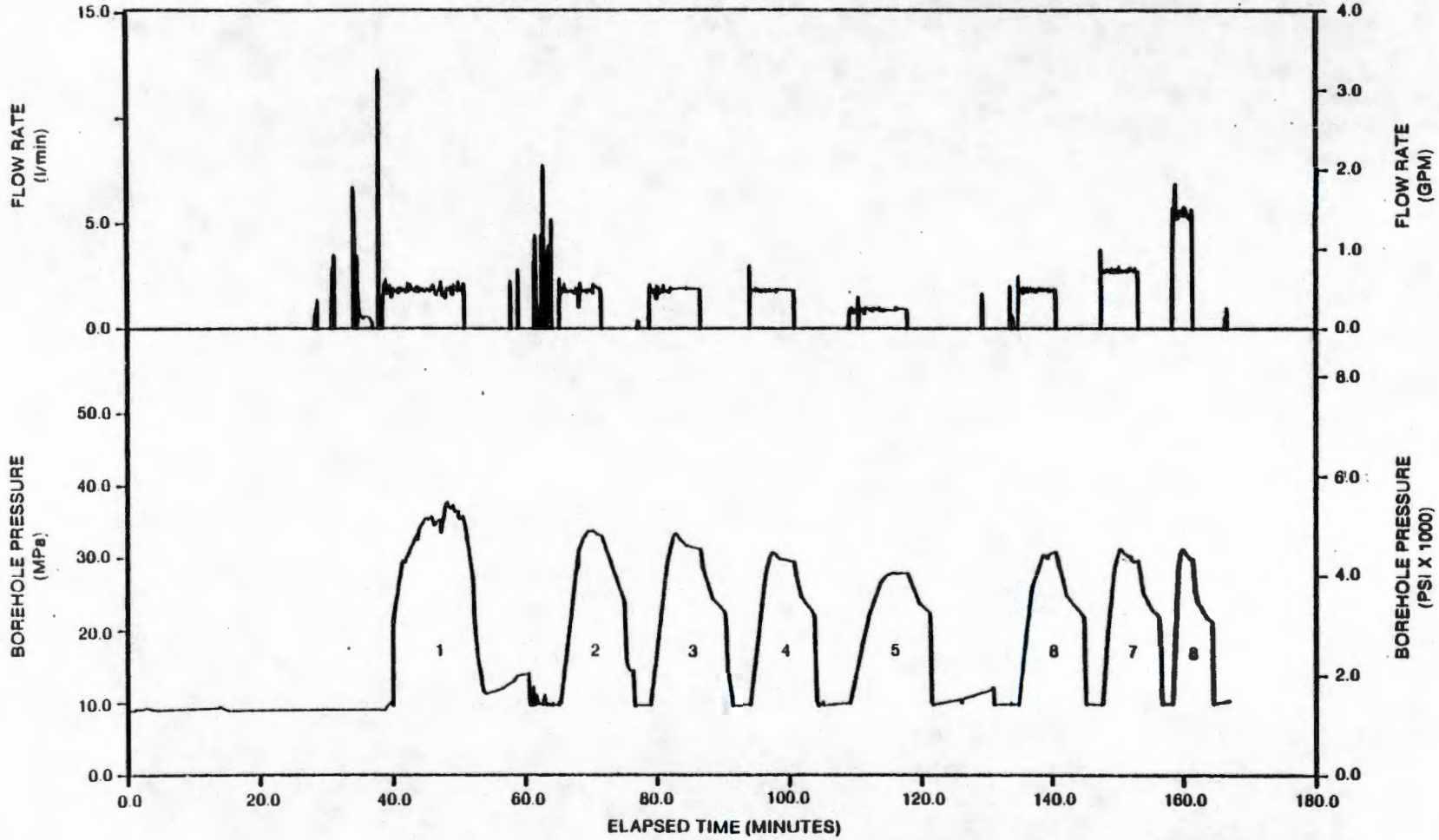

CYCLE	1	2	3	4	5	6	7	8	AVERAGE (STD DEV)
P_b*	38.3	-	-	-	-	-	-	-	-
P_{isi}*	34.1	31.4	29.3	29.0	-	30.0	29.0	-	30.5 (2.0)
P_{f_2}*	-	25.5	25.7	23.4	-	22.1	23.8	-	24.1 (1.5)

*NOTE: PRESSURE MEASURED DOWNHOLE

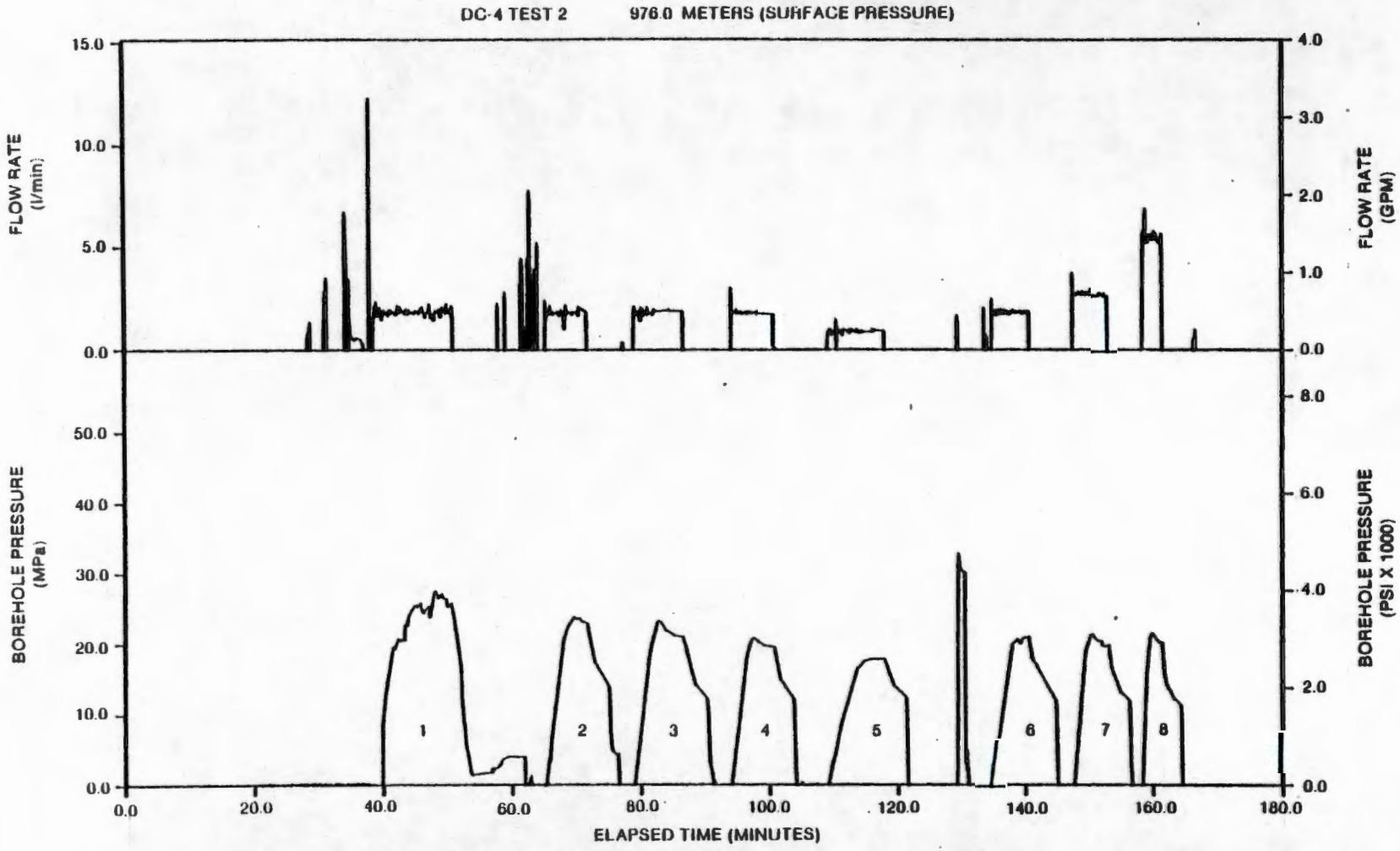

CYCLE	1	2	3	4	5	6	7	8	AVERAGE (STD DEV)
P_b*	27.9	-	-	-	-	-	-	-	-
P_{isi}*	23.8	22.1	20.0	22.1	-	20.6	18.6	-	21.2 (1.8)
P_{l_2}*	-	16.7	15.5	14.5	-	11.4	13.1	-	14.2 (2.1)

*NOTE: PRESSURE MEASURED AT SURFACE

DEPTH 975.0 M ORIENTATION N 06° W

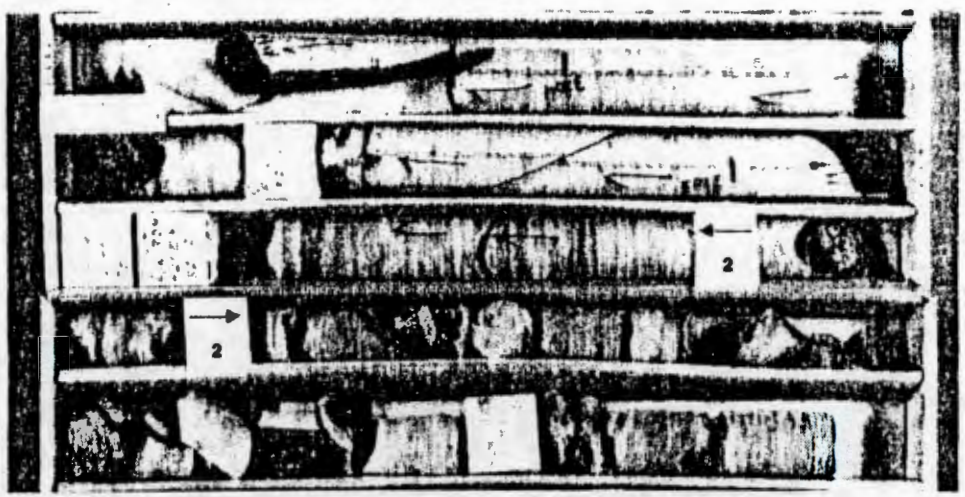

FRACTURE IMPRESSION AND CORE PHOTOGRAPH, DC-4 TEST 2

APPENDIX B

Pressure Versus Time Curves, Flow Versus Time Curves,
Fracture Impression Traces, and Core Photographs
Obtained from Test Intervals Which Yielded
Partial Informations

Note: All pressures are in psi measured on the surface. No fracture impressions were obtained for tests 2A, 5A, 6A, 10A, and 3B.

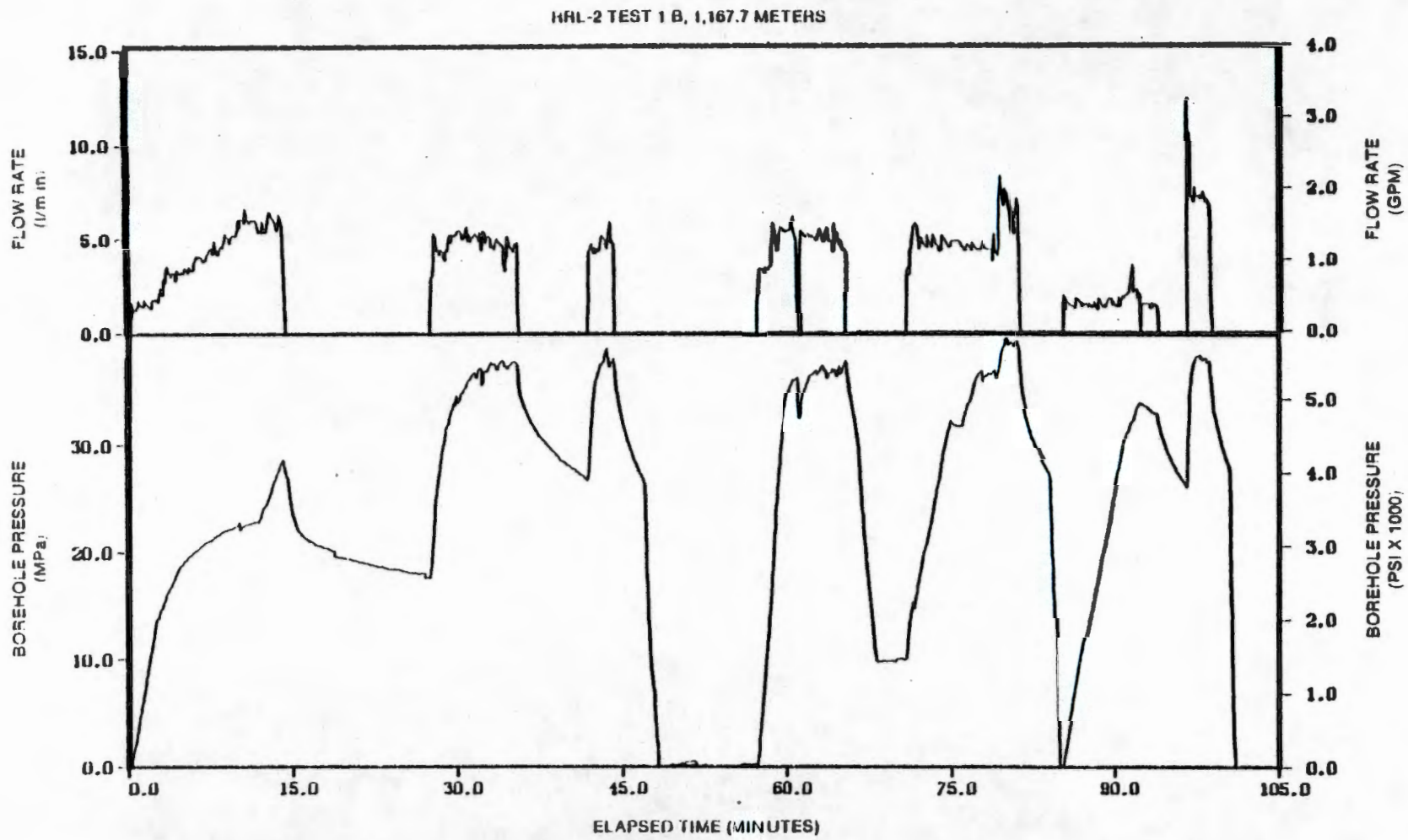
HRL-2 TEST 1 B, 1,167.7 METERS
FLOW RATE (l/min)
FLOW RATE (GPM)
BOREHOLE PRESSURE (MPa)
BOREHOLE PRESSURE (PSI X 1000)
ELAPSED TIME (MINUTES)
15.0
10.0
5.0
0.0
4.0
3.0
2.0
1.0
0.0
30.0
20.0
10.0
0.0
5.0
4.0
3.0
2.0
1.0
0.0
0.0
15.0
30.0
45.0
60.0
75.0
90.0
105.0

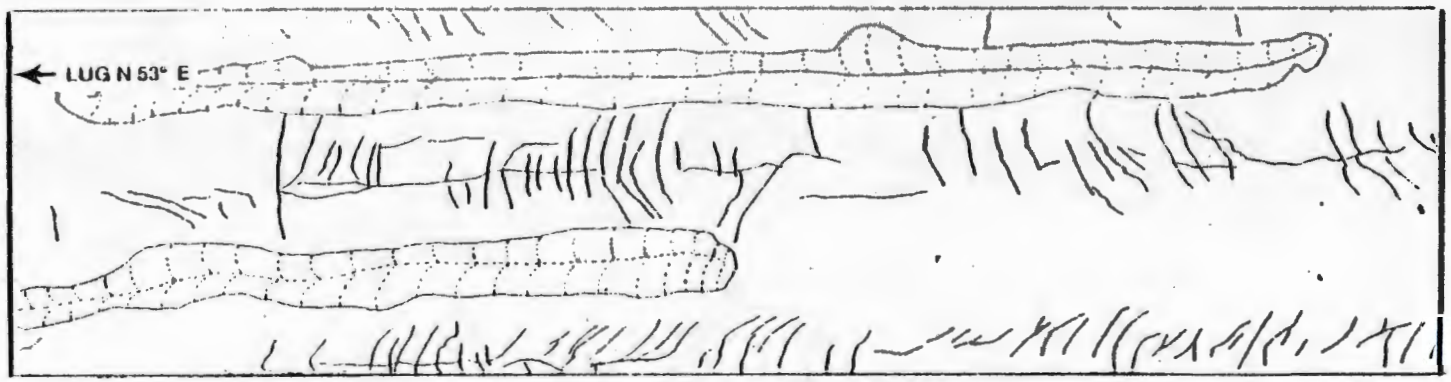

DEPTH 1,167.7 M ORIENTATION S31° E N 23° W

FRACTURE IMPRESSION AND CORE PHOTOGRAPH, RRL-2 TEST 1B

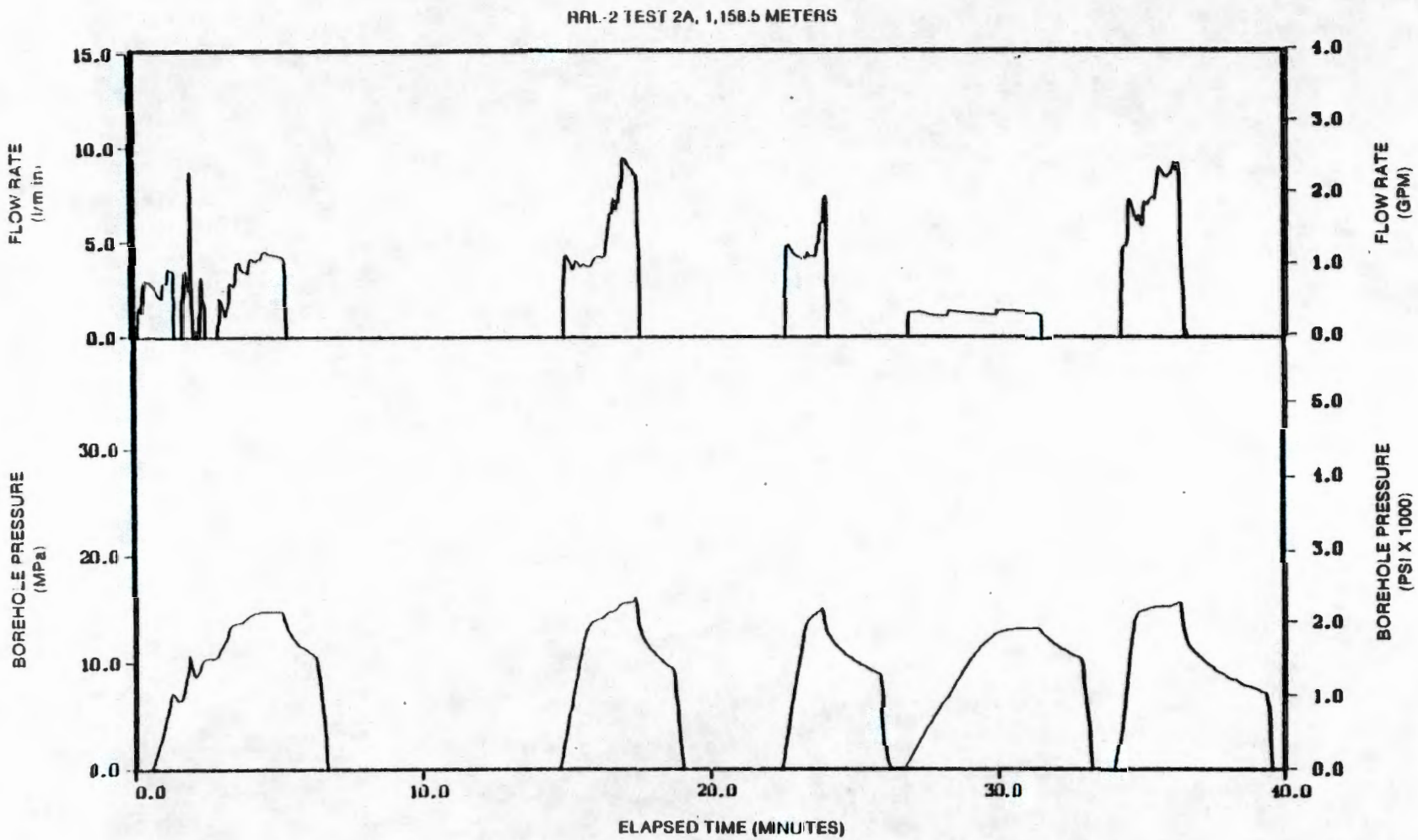
RRL-2 TEST 2A, 1,158.5 METERS
FLOW RATE (l/m in)
FLOW RATE (GPM)
BOREHOLE PRESSURE (MPa)
BOREHOLE PRESSURE (PSI X 1000)
ELAPSED TIME (MINUTES)
15.0
10.0
5.0
0.0
4.0
3.0
2.0
1.0
0.0
30.0
20.0
10.0
0.0
5.0
4.0
3.0
2.0
1.0
0.0
0.0
10.0
20.0
30.0
40.0

No fracture impression taken for test interval 2A

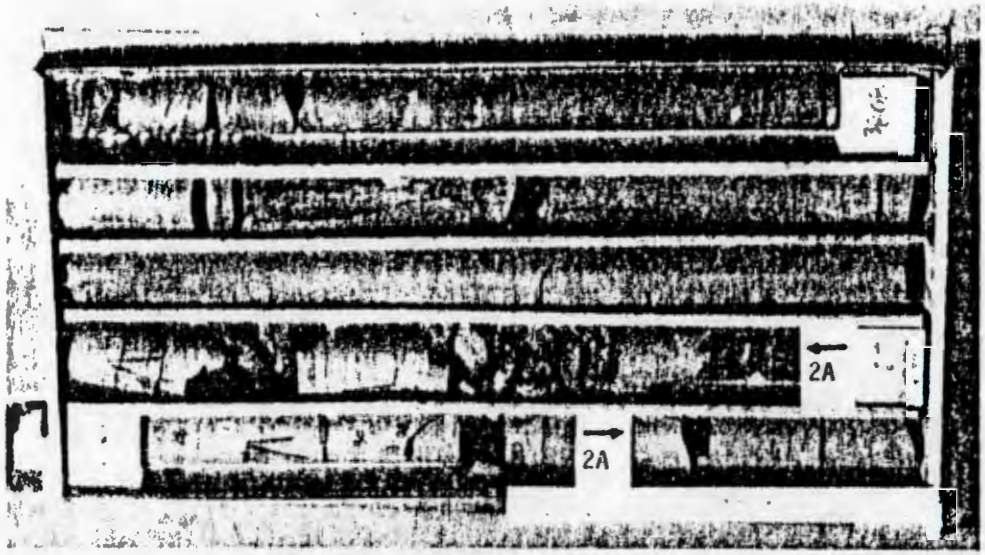

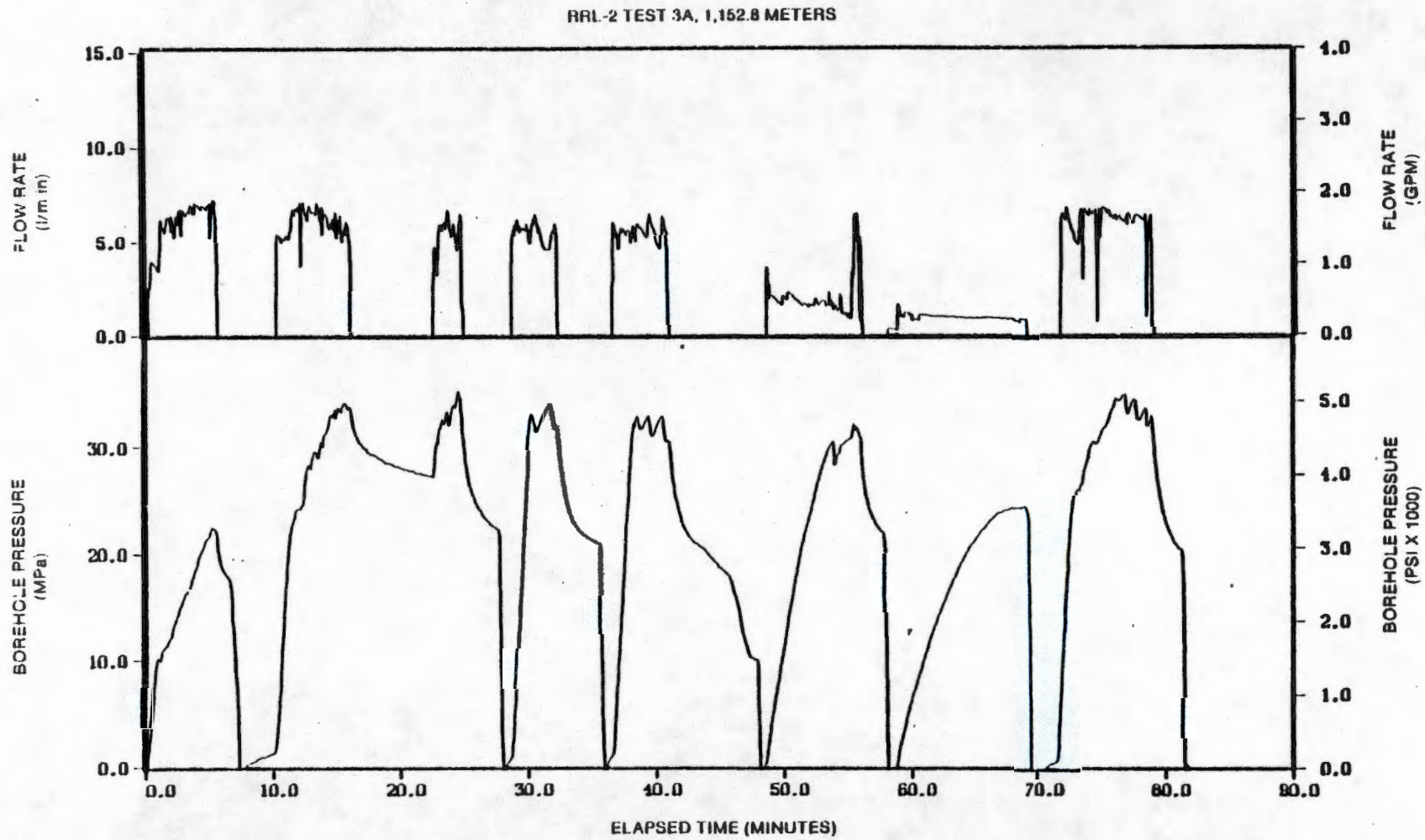
RRL-2 TEST 3A, 1,152.8 METERS
FLOW RATE (l/m in)
FLOW RATE (GPM)
BOREHOLE PRESSURE (MPa)
BOREHOLE PRESSURE (PSI X 1000)
ELAPSED TIME (MINUTES)
15.0
10.0
5.0
0.0
4.0
3.0
2.0
1.0
0.0
30.0
20.0
10.0
0.0
5.0
4.0
3.0
2.0
1.0
0.0
0.0
10.0
20.0
30.0
40.0
50.0
60.0
70.0
80.0
90.0

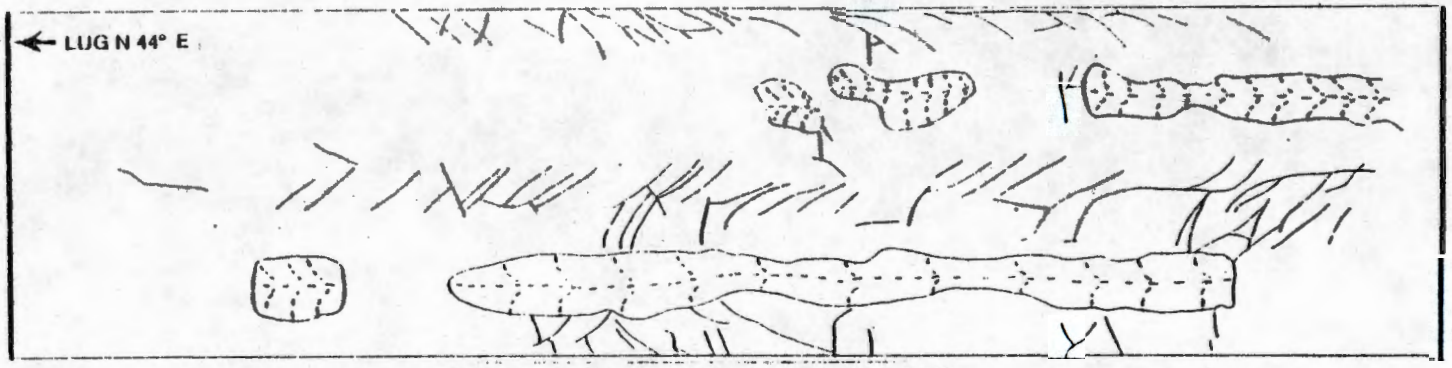

DEPTH 1,152.8M ORIENTATION N 16° E S 52° W

No core recovered for test interval 3A

FRACTURE IMPRESSION AND CORE PHOTOGRAPH, RRL-2 TEST 3A

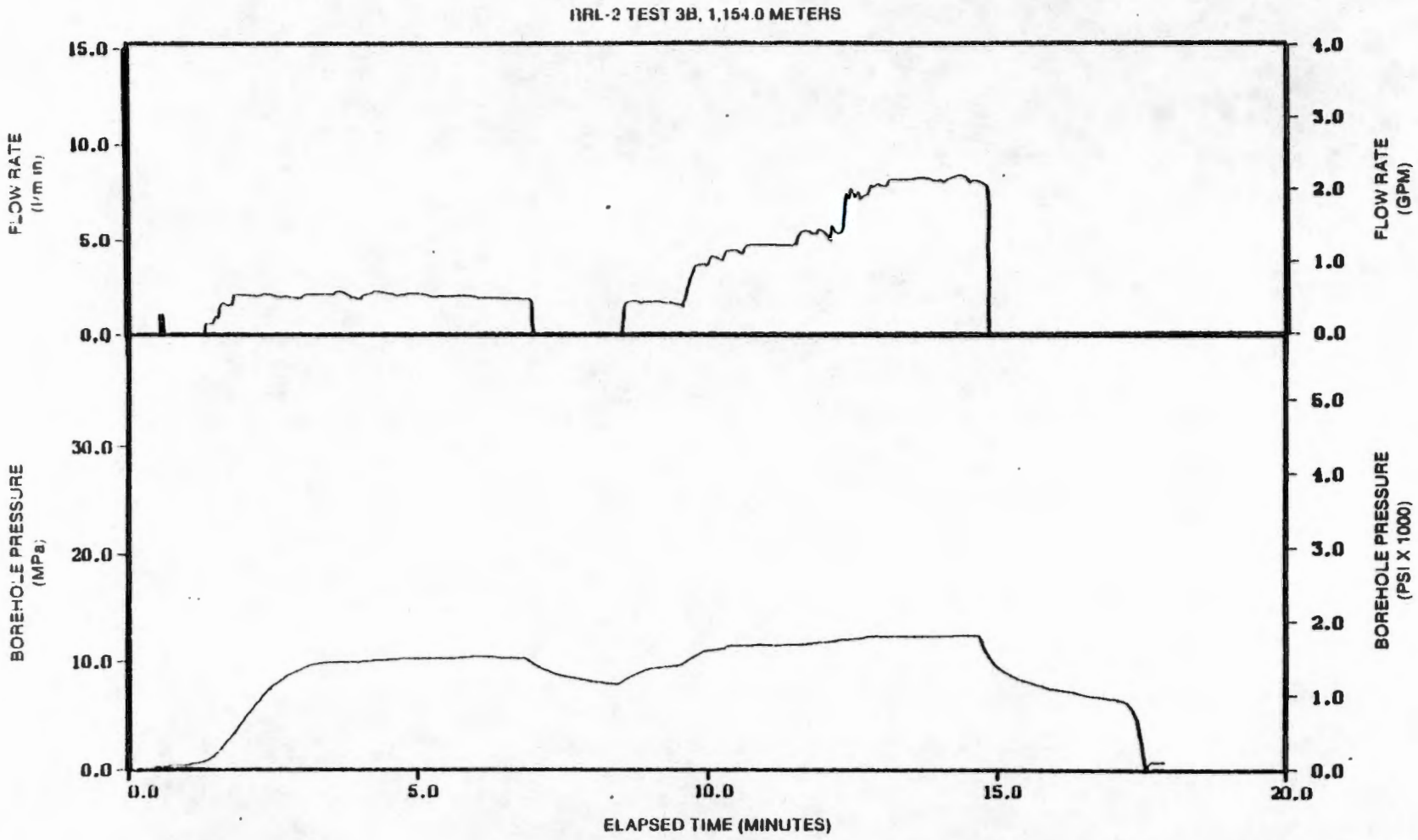
HRL-2 TEST 3B, 1,154.0 METERS
FLOW RATE (l/min)
FLOW RATE (GPM)
BOREHOLE PRESSURE (MPa)
BOREHOLE PRESSURE (PSI X 1000)
ELAPSED TIME (MINUTES)
15.0
10.0
5.0
0.0
4.0
3.0
2.0
1.0
0.0
30.0
20.0
10.0
0.0
5.0
4.0
3.0
2.0
1.0
0.0
0.0
5.0
10.0
15.0
20.0

No fracture impression taken for test interval 3B

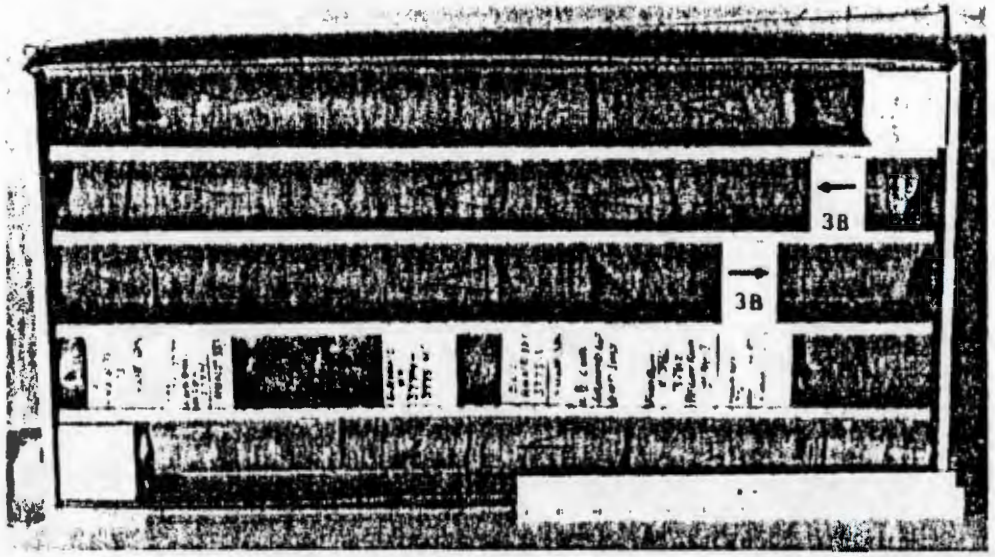

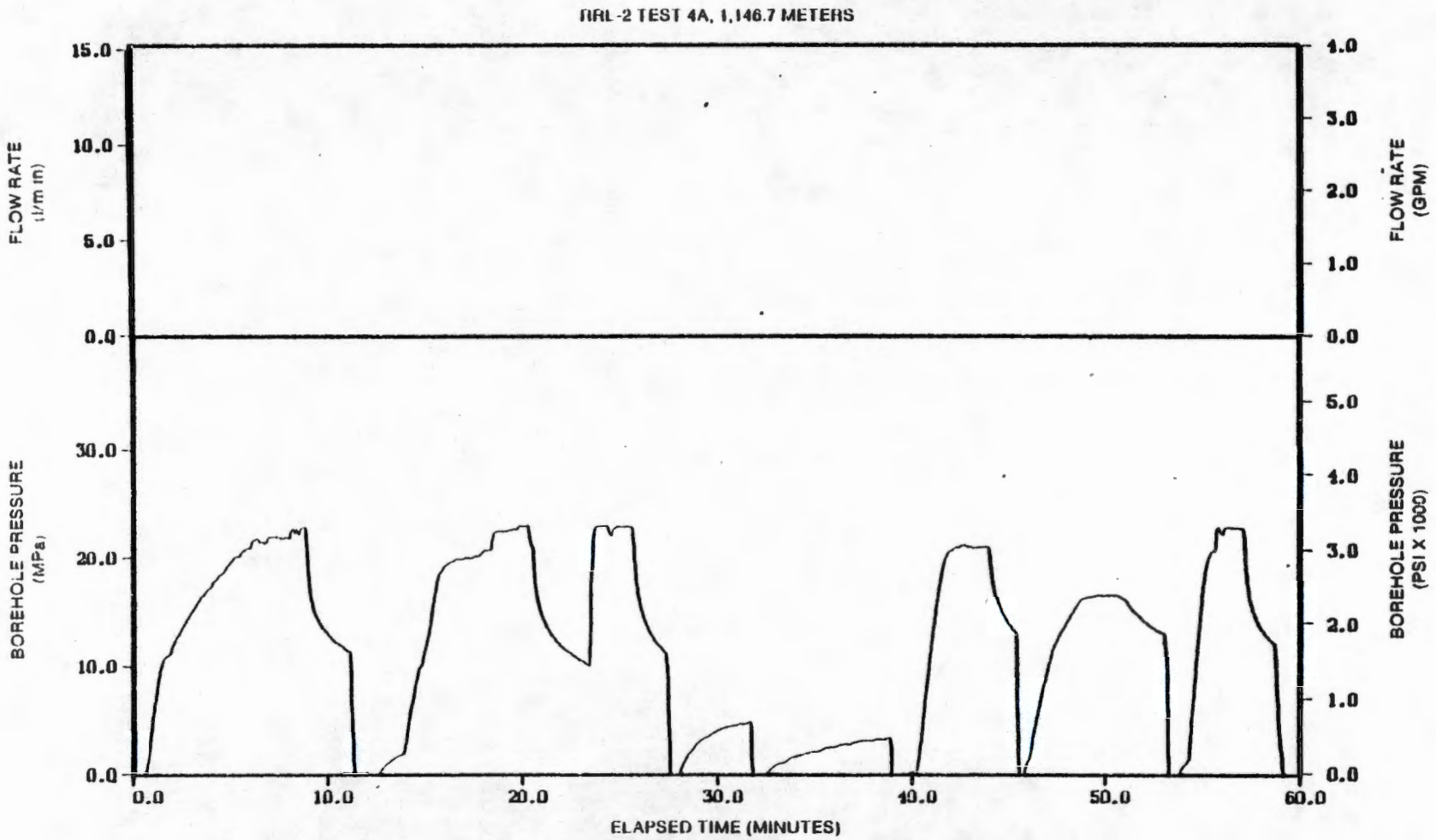
RRL-2 TEST 4A, 1,146.7 METERS
FLOW RATE (l/min)
15.0
10.0
5.0
0.0
FLOW RATE (GPM)
4.0
3.0
2.0
1.0
0.0
BOREHOLE PRESSURE (MPa)
30.0
20.0
10.0
0.0
BOREHOLE PRESSURE (PSI X 1000)
5.0
4.0
3.0
2.0
1.0
0.0
0.0
10.0
20.0
30.0
40.0
50.0
60.0
ELAPSED TIME (MINUTES)

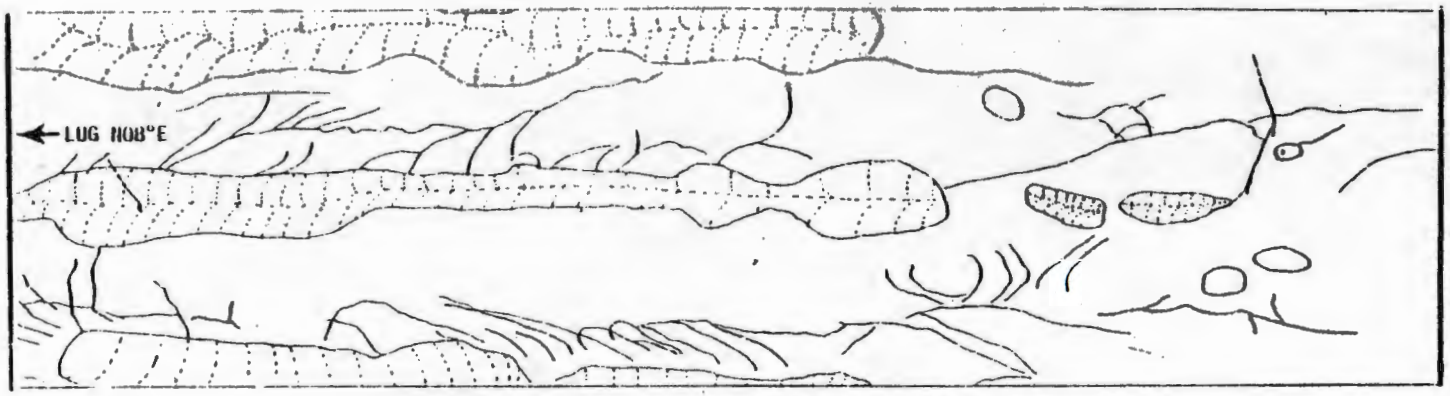

DEPTH 1,146.7 M ORIENTATION N 04° E S 02° E

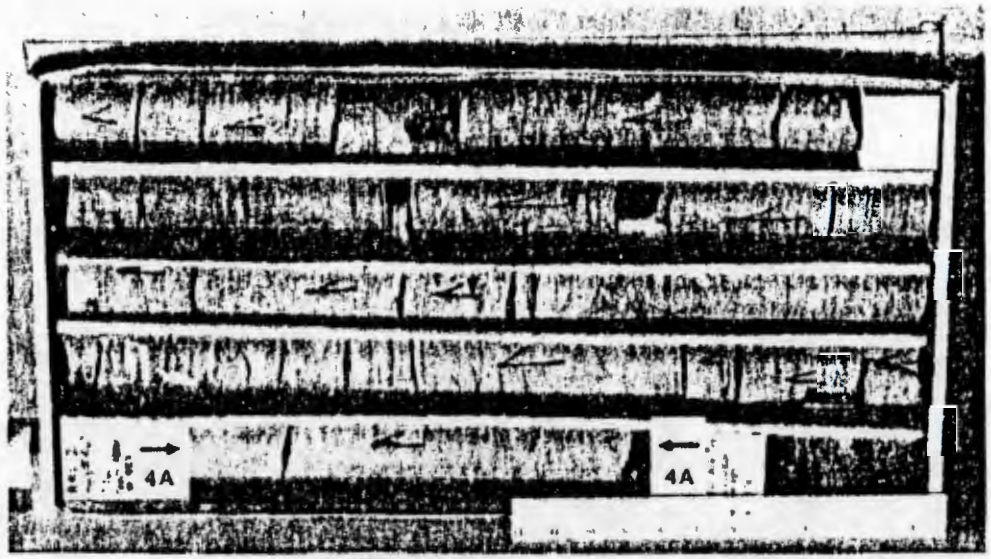

FRACTURE IMPRESSION AND CORE PHOTOGRAPH, RRL-2 TEST 4A

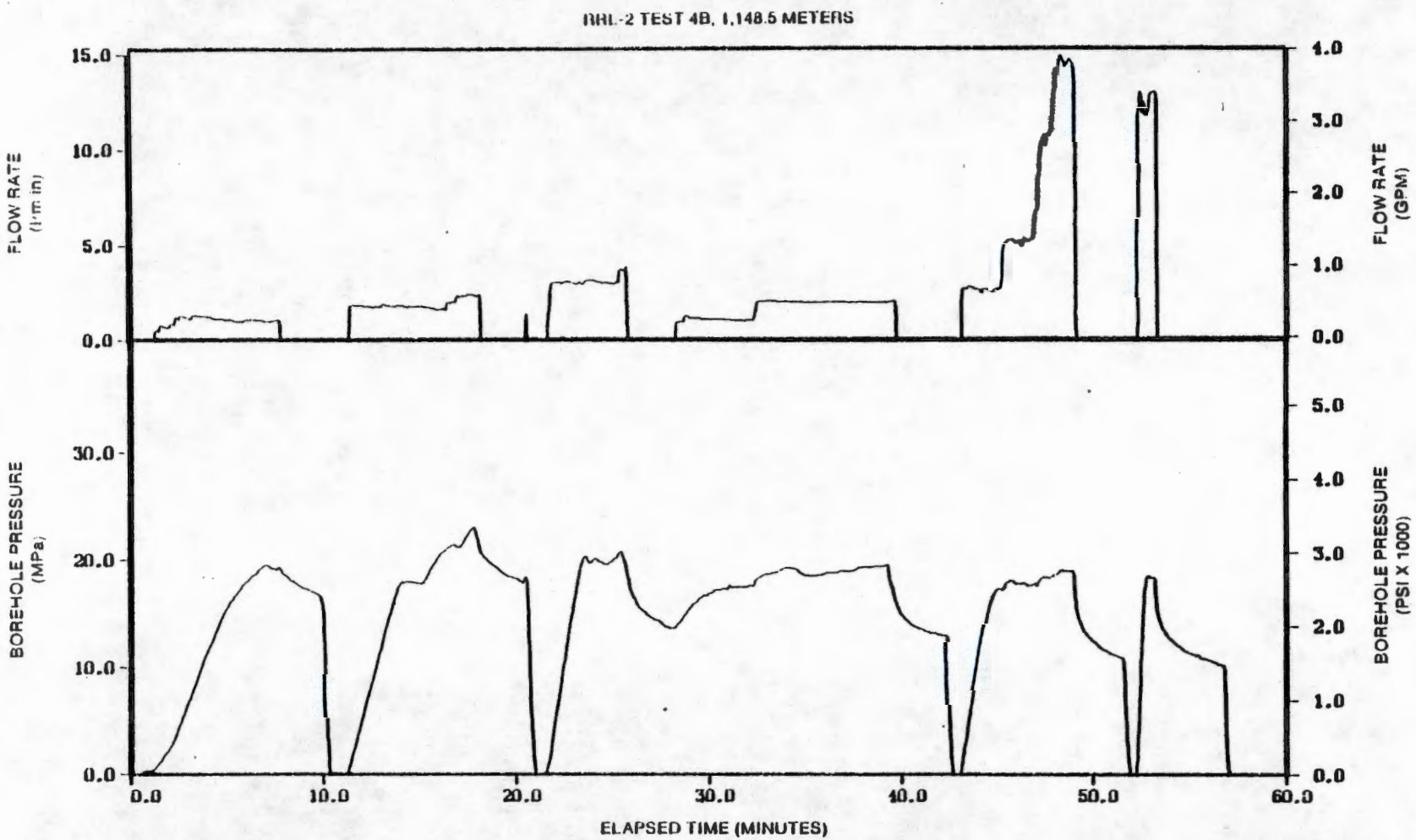
RRL-2 TEST 4B, 1,148.5 METERS
FLOW RATE (l/m in)
FLOW RATE (GPM)
BOREHOLE PRESSURE (MPa)
BOREHOLE PRESSURE (PSI X 1000)
ELAPSED TIME (MINUTES)
15.0
10.0
5.0
0.0
4.0
3.0
2.0
1.0
0.0
30.0
20.0
10.0
0.0
5.0
4.0
3.0
2.0
1.0
0.0
0.0
10.0
20.0
30.0
40.0
50.0
60.0

DEPTH 1,148.5 M ORIENTATION N 23° E

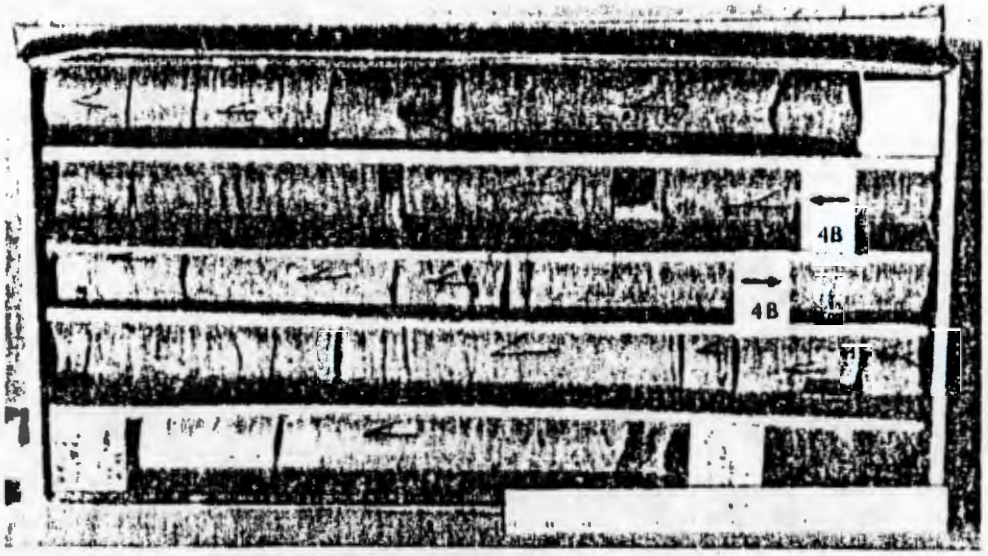

FRACTURE IMPRESSION AND CORE PHOTOGRAPH, RRL-2 TEST 4B

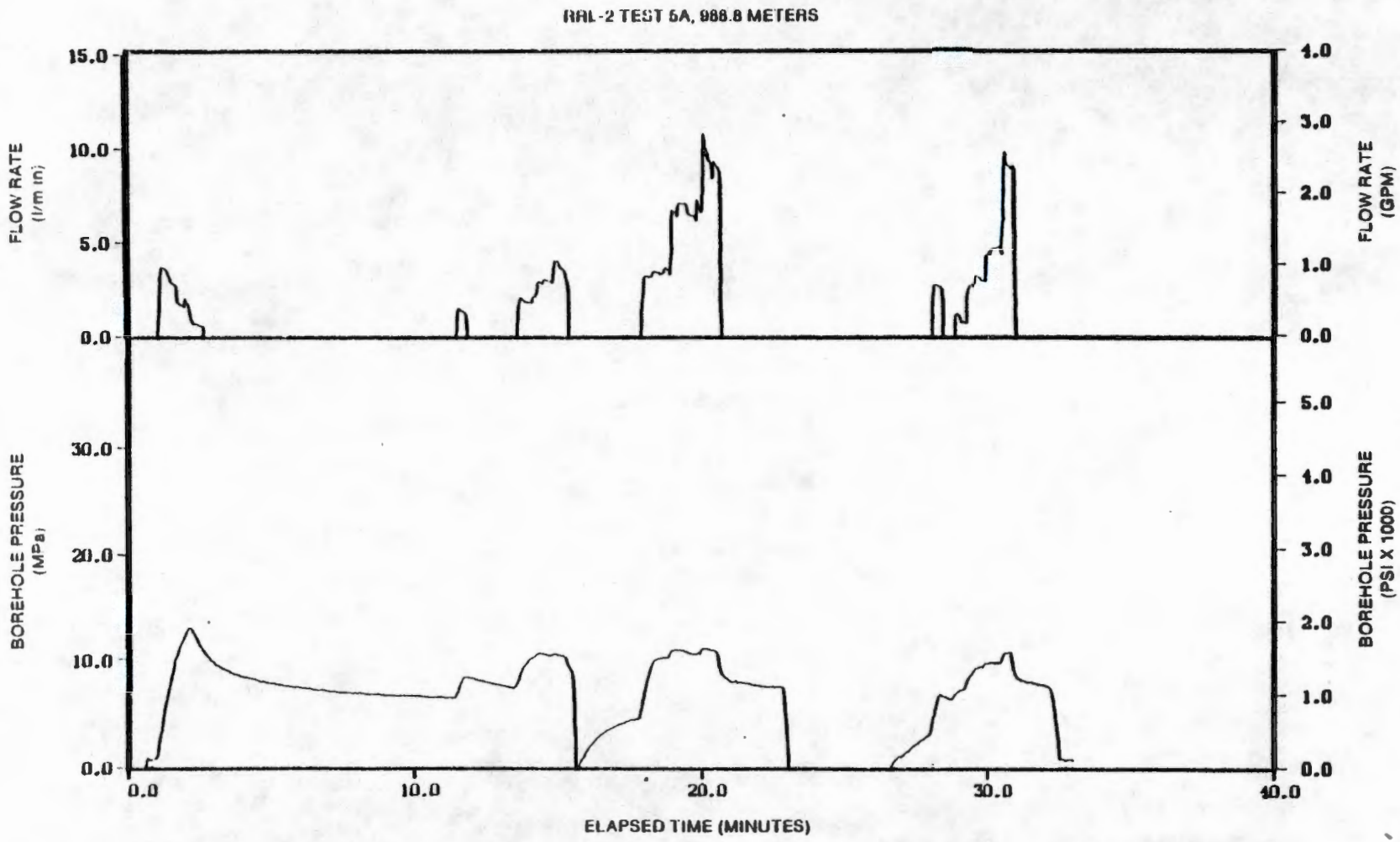
RRL-2 TEST 5A, 988.8 METERS
FLOW RATE (l/m in)
FLOW RATE (GPM)
BOREHOLE PRESSURE (MPa)
BOREHOLE PRESSURE (PSI X 1000)
ELAPSED TIME (MINUTES)
15.0
10.0
5.0
0.0
4.0
3.0
2.0
1.0
0.0
30.0
20.0
10.0
0.0
5.0
4.0
3.0
2.0
1.0
0.0
0.0
10.0
20.0
30.0
40.0

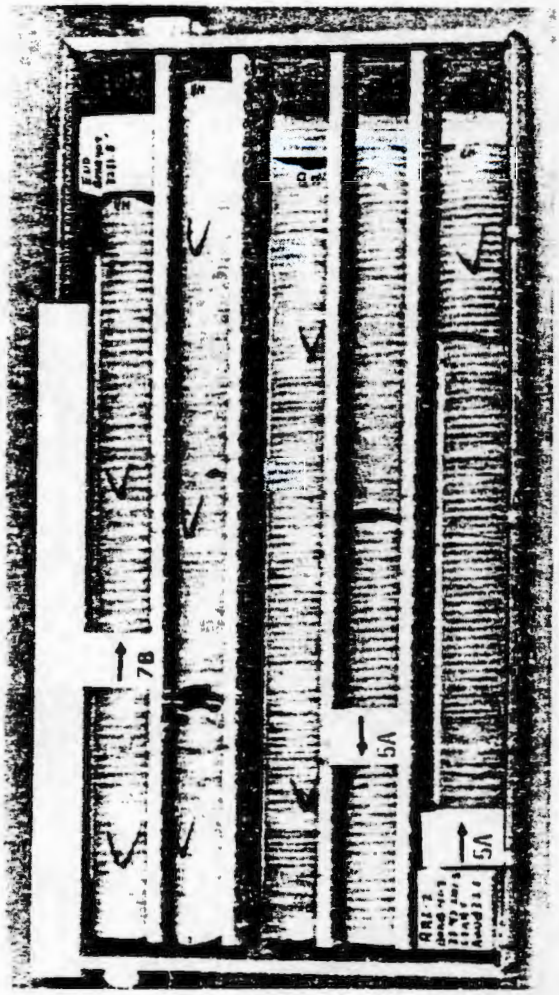

No fracture impression taken for test interval 5A

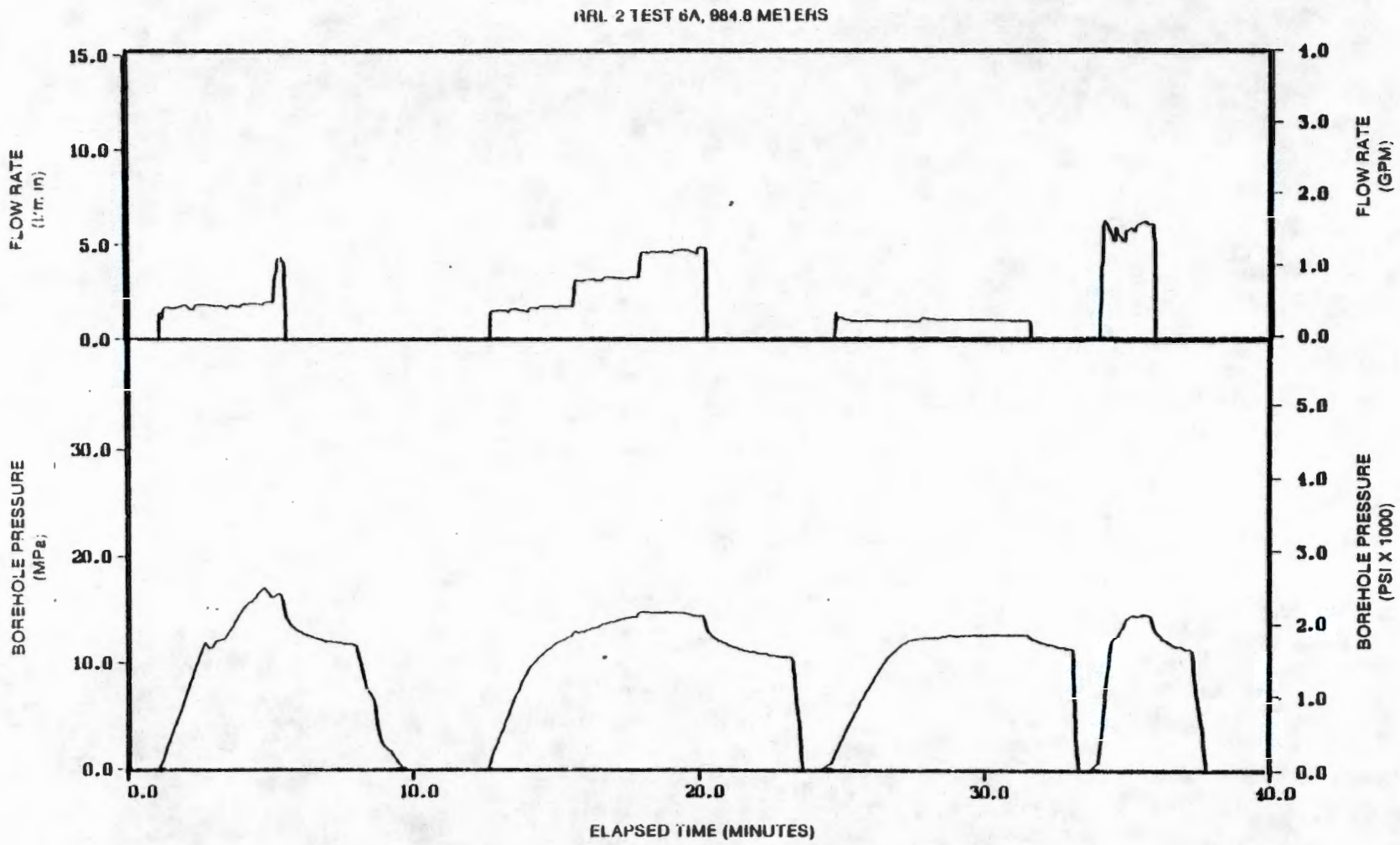
HRL 2 TEST 6A, 984.8 METERS
FLOW RATE (l/m. in)
FLOW RATE (GPM)
BOREHOLE PRESSURE (MPa)
BOREHOLE PRESSURE (PSI X 1000)
ELAPSED TIME (MINUTES)
15.0
10.0
5.0
0.0
4.0
3.0
2.0
1.0
0.0
30.0
20.0
10.0
0.0
5.0
4.0
3.0
2.0
1.0
0.0
0.0
10.0
20.0
30.0
40.0

No fracture impression taken for test interval 6A

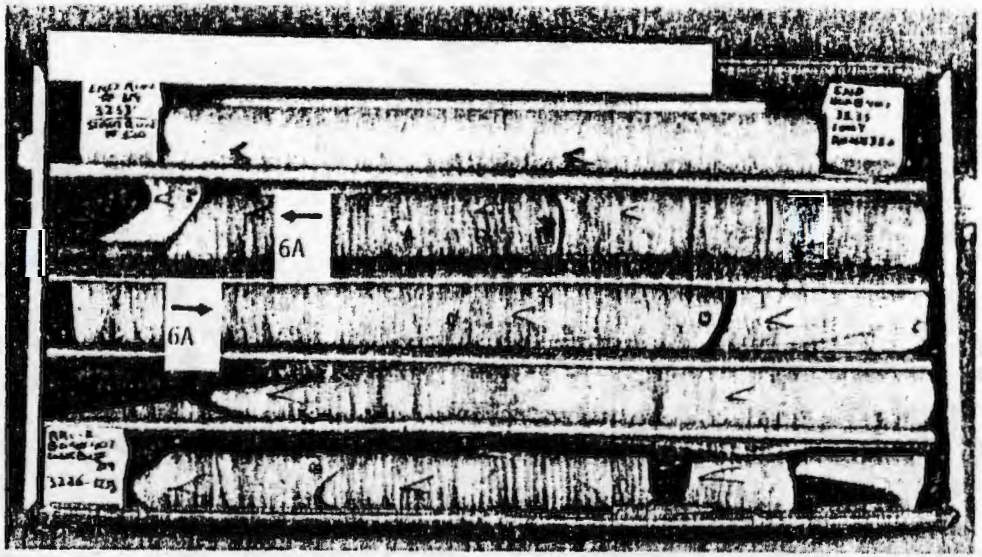

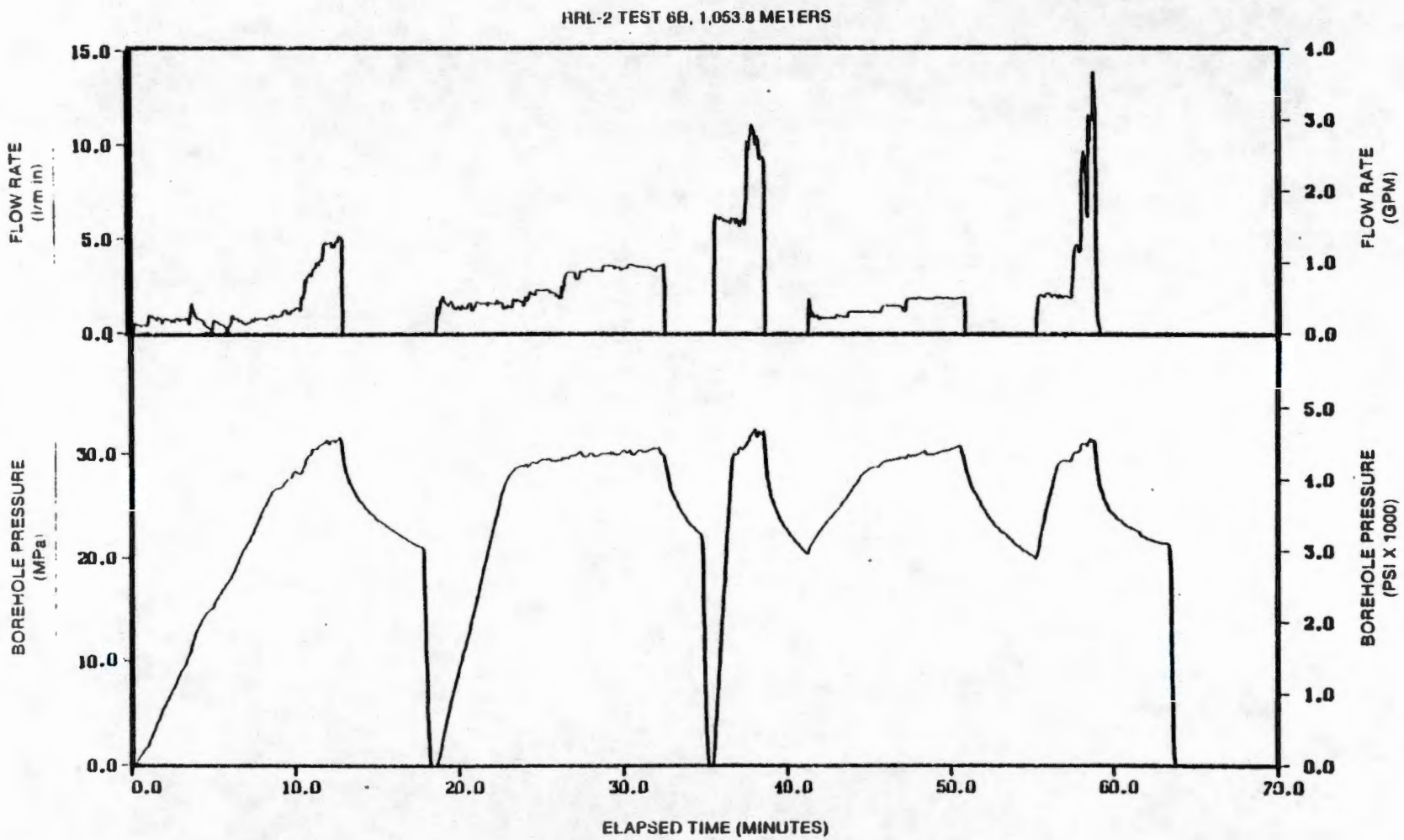
HRL-2 TEST 6B, 1,053.8 METERS
FLOW RATE (l/m in)
FLOW RATE (GPM)
BOREHOLE PRESSURE (MPa)
BOREHOLE PRESSURE (PSI X 1000)
ELAPSED TIME (MINUTES)
15.0
10.0
5.0
0.0
4.0
3.0
2.0
1.0
0.0
30.0
20.0
10.0
0.0
5.0
4.0
3.0
2.0
1.0
0.0
0.0
10.0
20.0
30.0
40.0
50.0
60.0
70.0

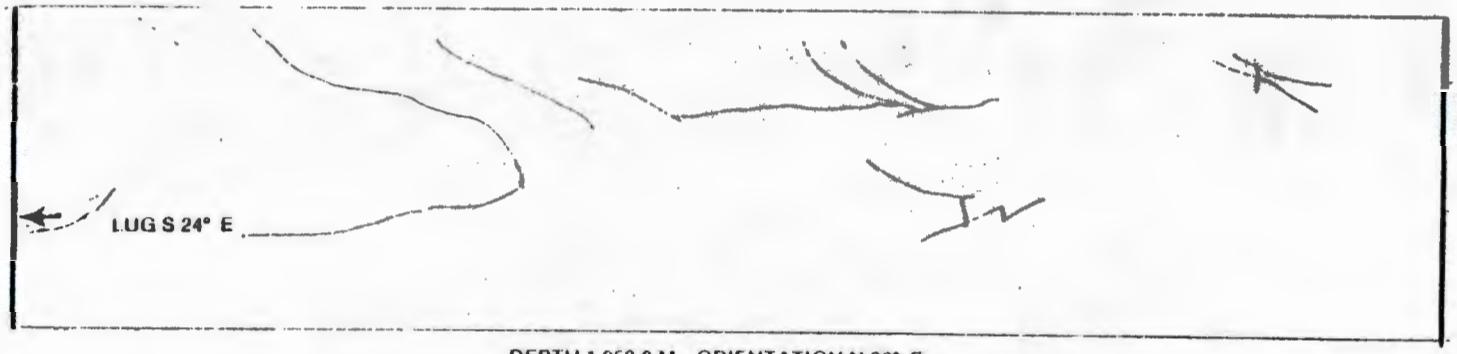

DEPTH 1,053.8 M ORIENTATION N 36° E

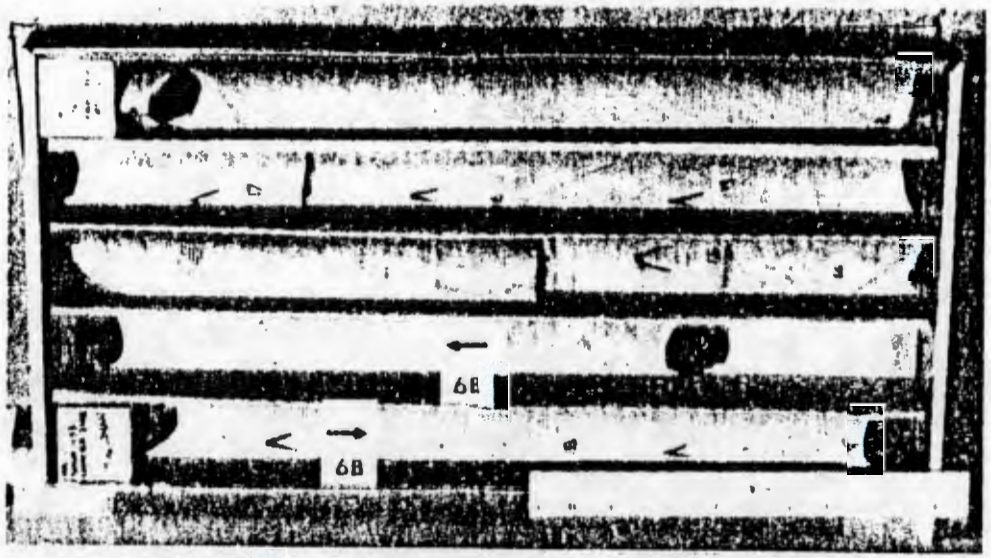

FRACTURE IMPRESSION AND CORE PHOTOGRAPH, RRL-2 TEST 6B

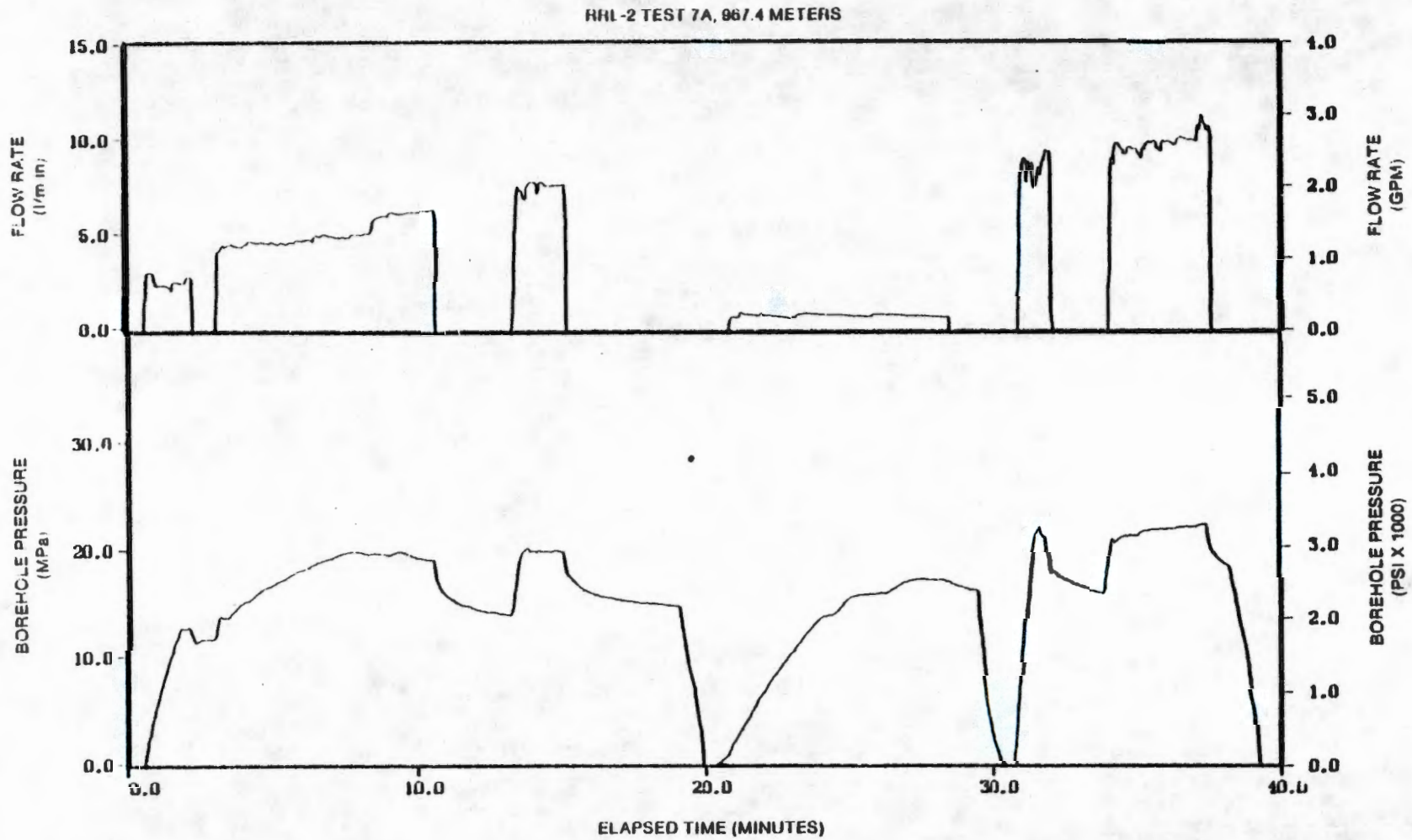
RRL-2 TEST 7A, 967.4 METERS
FLOW RATE (l/min)
FLOW RATE (GPM)
BOREHOLE PRESSURE (MPa)
BOREHOLE PRESSURE (PSI X 1000)
ELAPSED TIME (MINUTES)
15.0
10.0
5.0
0.0
4.0
3.0
2.0
1.0
0.0
30.0
20.0
10.0
0.0
5.0
4.0
3.0
2.0
1.0
0.0
0.0
10.0
20.0
30.0
40.0

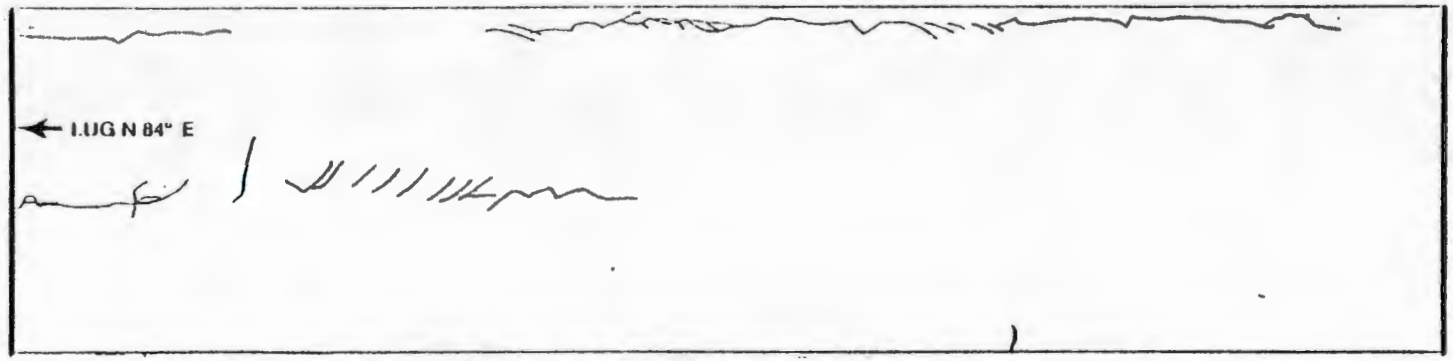

DEPTH 967.4 M ORIENTATION N 19° W S 18° E

FRACTURE IMPRESSION AND CORE PHOTOGRAPH, RRL-2 TEST 7A

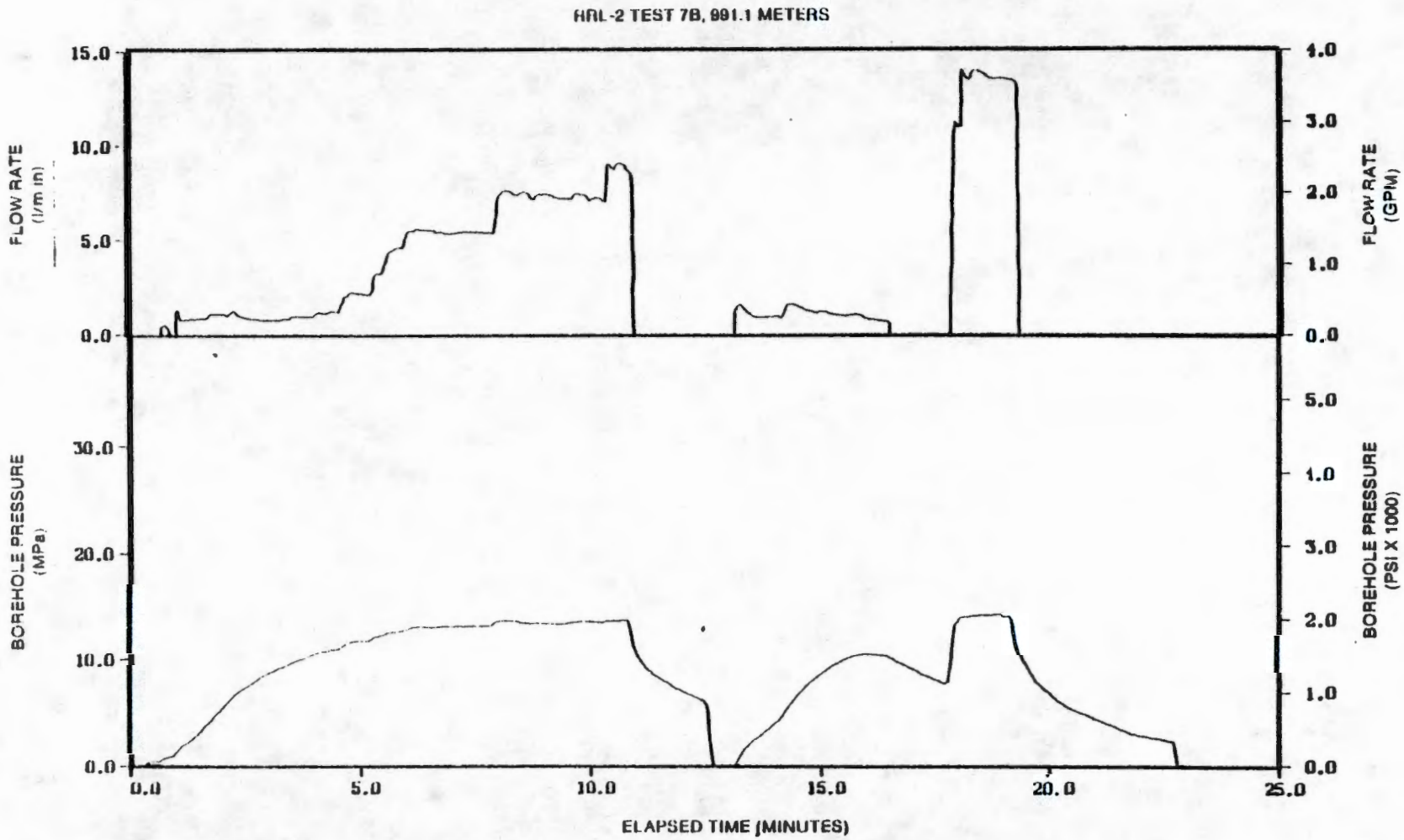
HRL-2 TEST 7B, 991.1 METERS
FLOW RATE (l/m in)
FLOW RATE (GPM)
BOREHOLE PRESSURE (MPa)
BOREHOLE PRESSURE (PSI X 1000)
ELAPSED TIME (MINUTES)
15.0
10.0
5.0
0.0
4.0
3.0
2.0
1.0
0.0
30.0
20.0
10.0
0.0
5.0
1.0
3.0
2.0
1.0
0.0
0.0
5.0
10.0
15.0
20.0
25.0

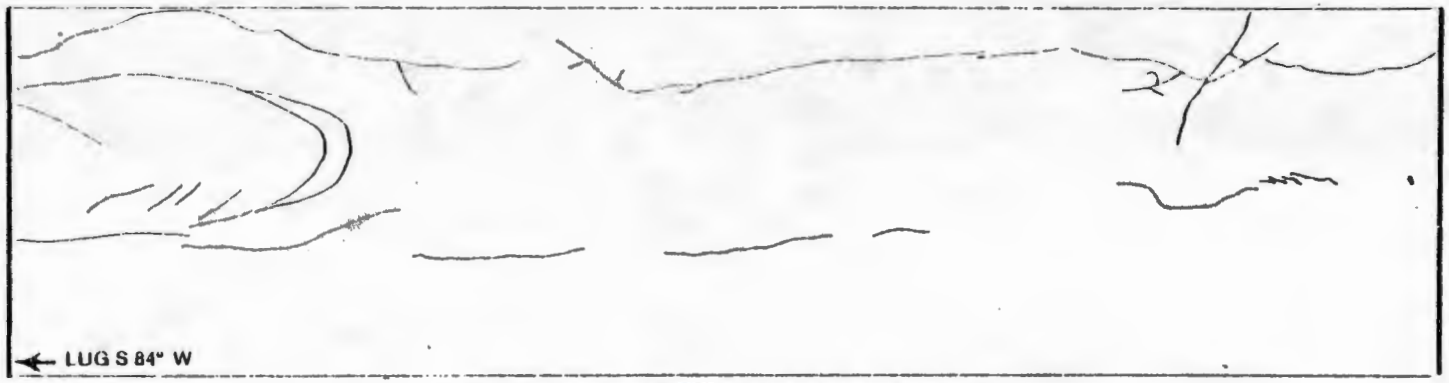

DEPTH 991.1 M ORIENTATION N 21° W S 24° E

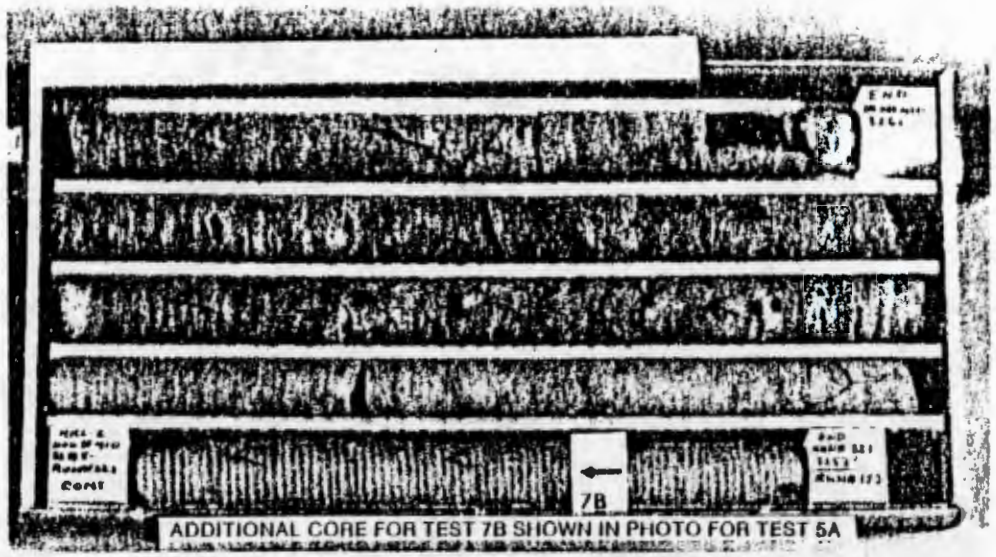

FRACTURE IMPRESSION AND CORE PHOTOGRAPH, RRL-2 TEST 7B

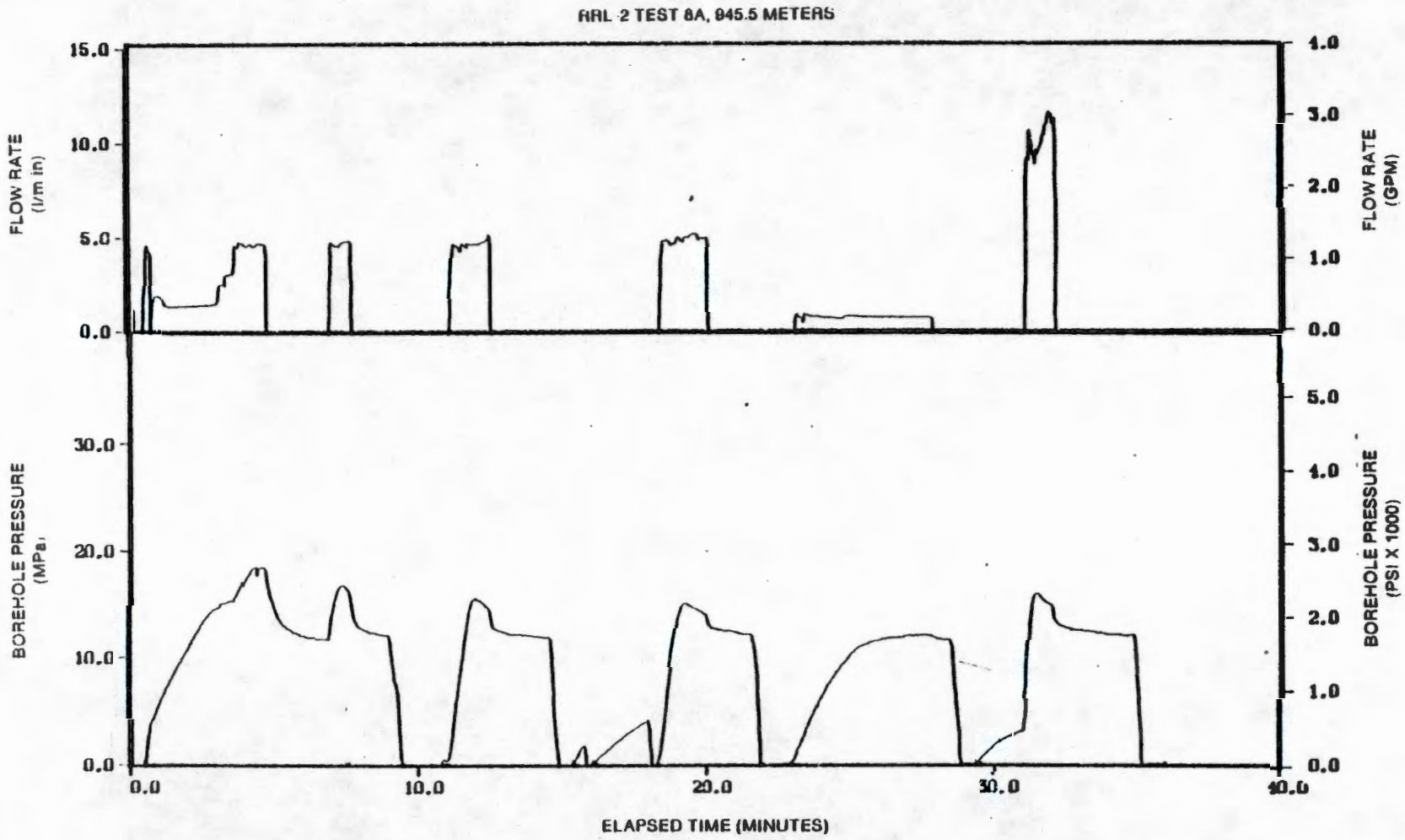
RRL 2 TEST 8A, 845.5 METERS
FLOW RATE (l/m in)
15.0
10.0
5.0
0.0
FLOW RATE (GPM)
4.0
3.0
2.0
1.0
0.0
BOREHOLE PRESSURE (MPa)
30.0
20.0
10.0
0.0
BOREHOLE PRESSURE (PSI X 1000)
5.0
4.0
3.0
2.0
1.0
0.0
0.0
10.0
20.0
30.0
40.0
ELAPSED TIME (MINUTES)

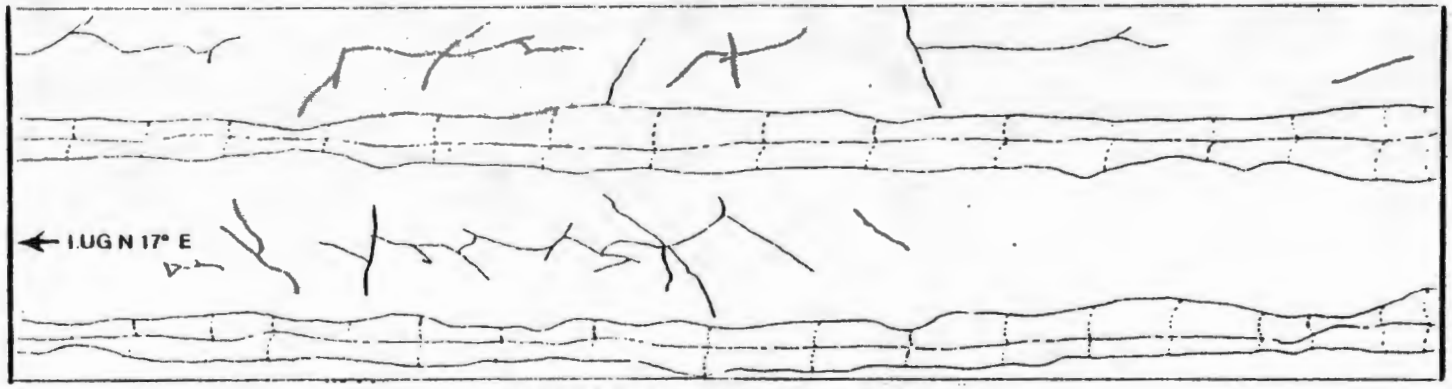

DEPTH 945.5 M ORIENTATION N 20° E S 13° W

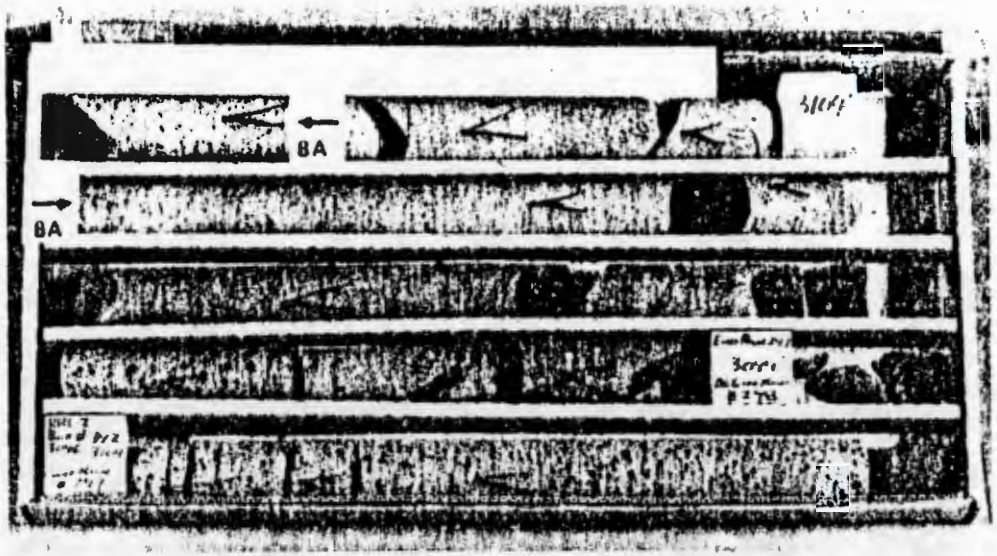

FRACTURE IMPRESSION AND CORE PHOTOGRAPH, RRL-2 TEST 8A

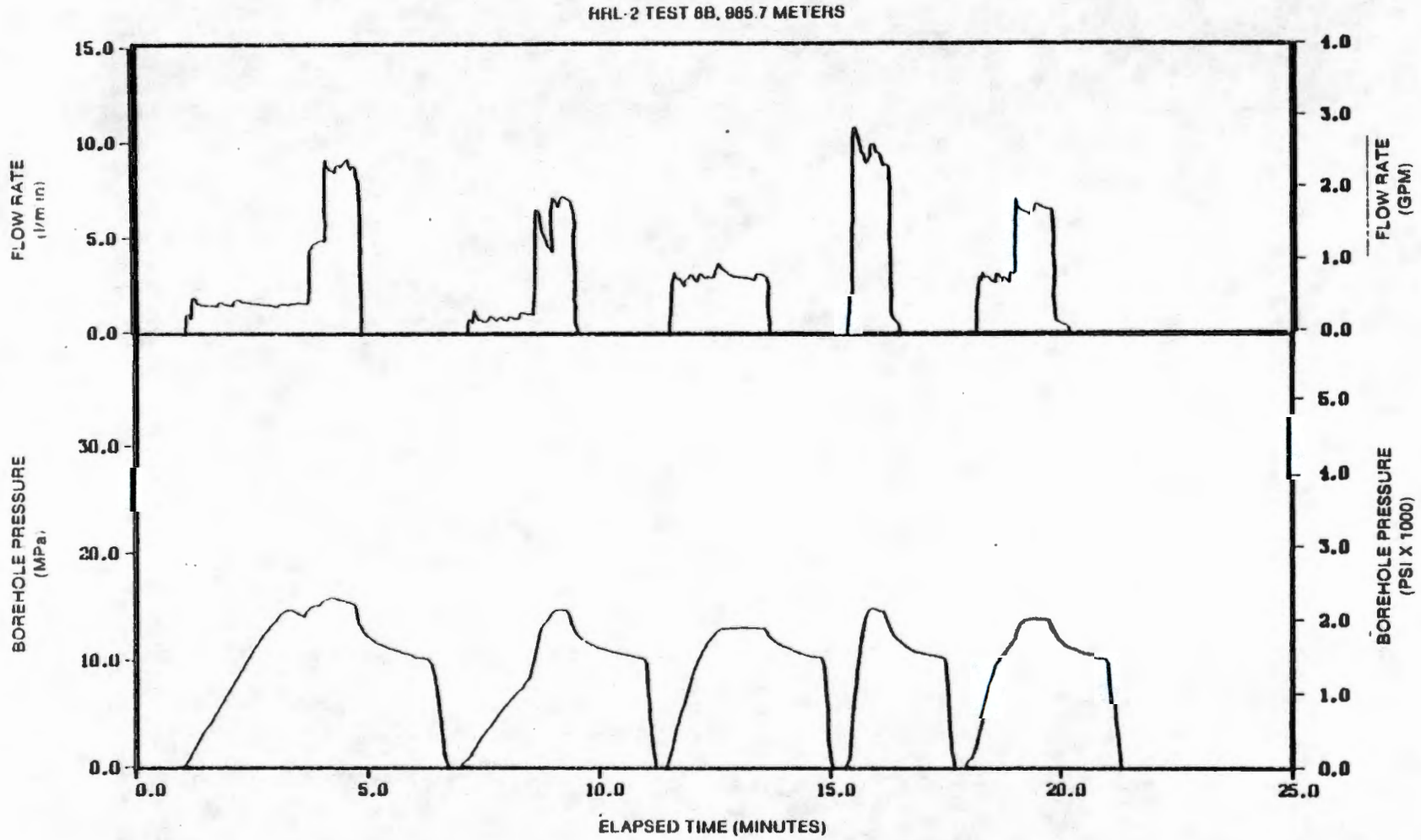
HRL-2 TEST 8B, 985.7 METERS
FLOW RATE (l/m in)
FLOW RATE (GPM)
BOREHOLE PRESSURE (MPa)
BOREHOLE PRESSURE (PSI X 1000)
ELAPSED TIME (MINUTES)
15.0
10.0
5.0
0.0
4.0
3.0
2.0
1.0
0.0
30.0
20.0
10.0
0.0
5.0
4.0
3.0
2.0
1.0
0.0
0.0
5.0
10.0
15.0
20.0
25.0

DEPTH 985.7 M ORIENTATION N 75° E S 43° E

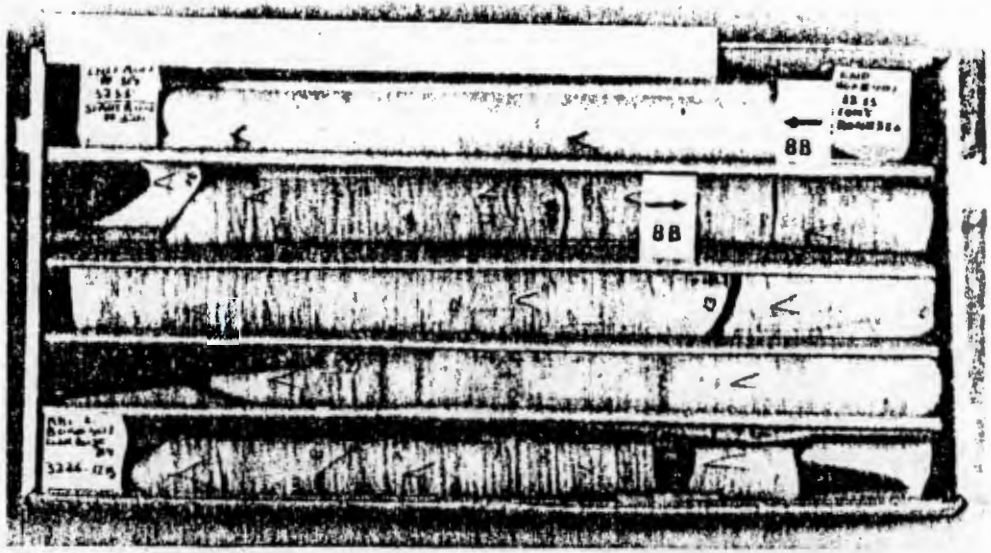

FRACTURE IMPRESSION AND CORE PHOTOGRAPH, RRL-2 TEST 8B

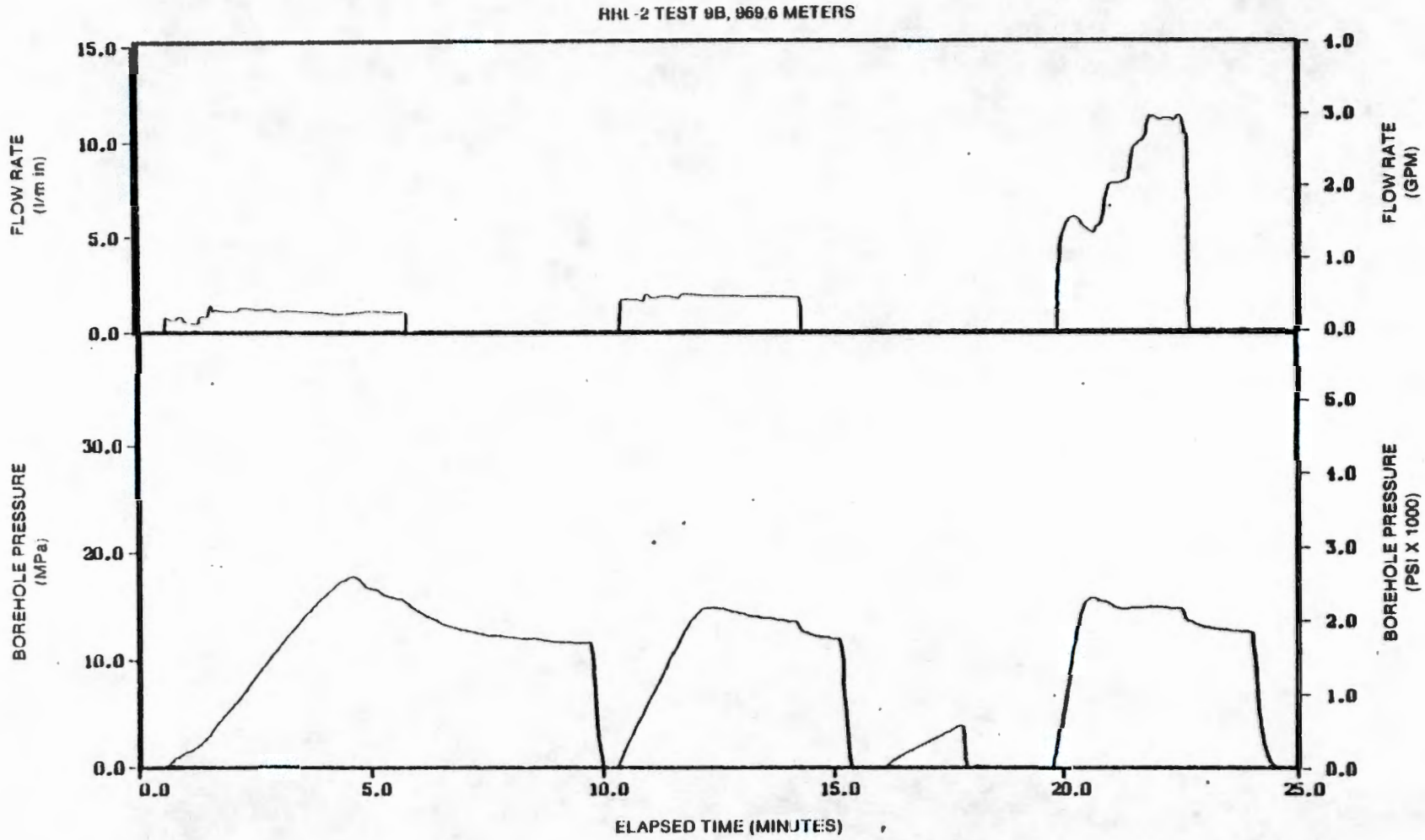
RRL-2 TEST 9B, 969.6 METERS
FLOW RATE (l/m in)
FLOW RATE (GPM)
BOREHOLE PRESSURE (MPa)
BOREHOLE PRESSURE (PSI X 1000)
ELAPSED TIME (MINUTES)
15.0
10.0
5.0
0.0
4.0
3.0
2.0
1.0
0.0
30.0
20.0
10.0
0.0
5.0
4.0
3.0
2.0
1.0
0.0
0.0
5.0
10.0
15.0
20.0
25.0

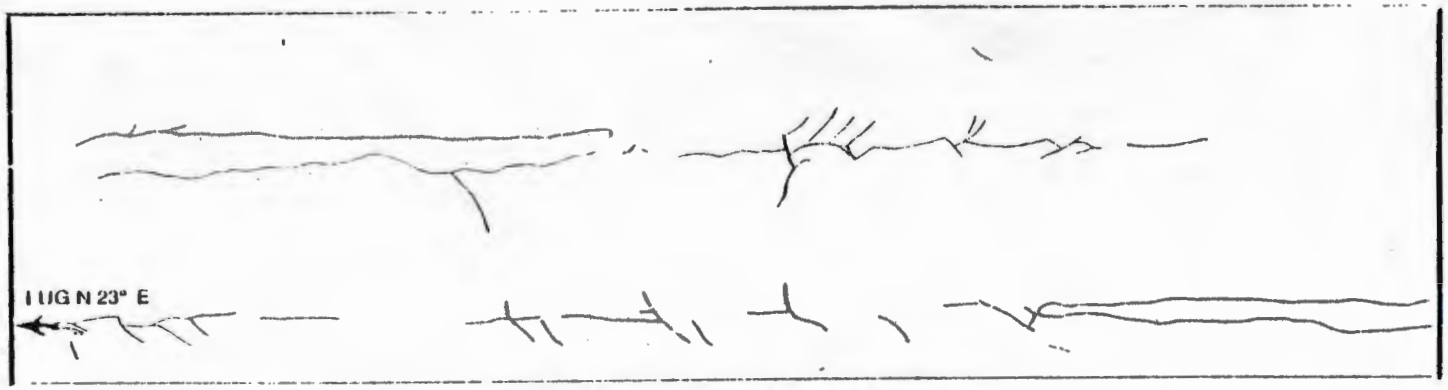

DEPTH 969.6 M ORIENTATION N 23° E S 08° W

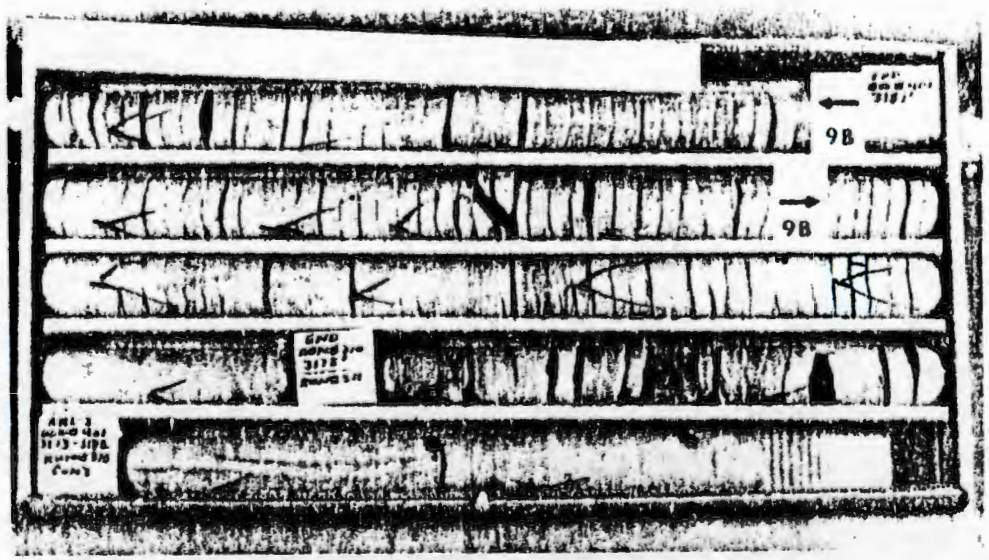

FRACTURE IMPRESSION AND CORE PHOTOGRAPH, RRL-2 TEST 9B

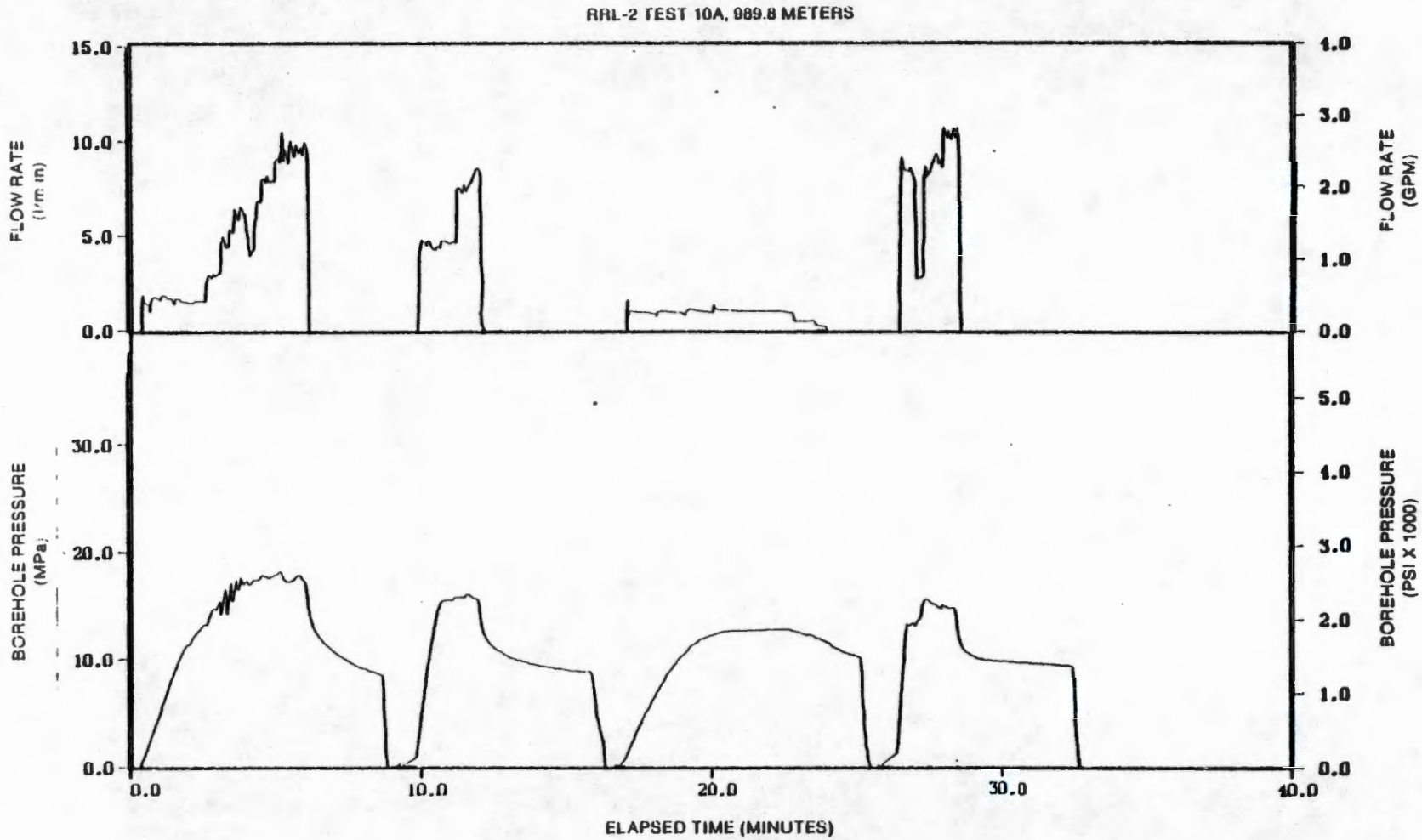
RRL-2 TEST 10A, 989.8 METERS
FLOW RATE (l/m in)
15.0
10.0
5.0
0.0
FLOW RATE (GPM)
4.0
3.0
2.0
1.0
0.0
BOREHOLE PRESSURE (MPa)
30.0
20.0
10.0
0.0
BOREHOLE PRESSURE (PSI X 1000)
5.0
4.0
3.0
2.0
1.0
0.0
0.0
10.0
20.0
30.0
40.0
ELAPSED TIME (MINUTES)

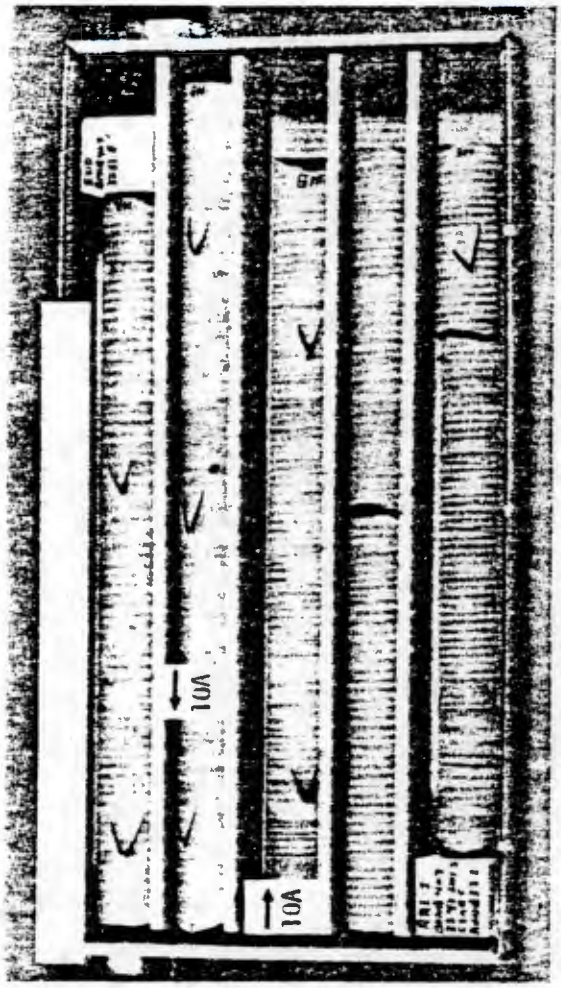

No fracture impression taken for test interval 10A

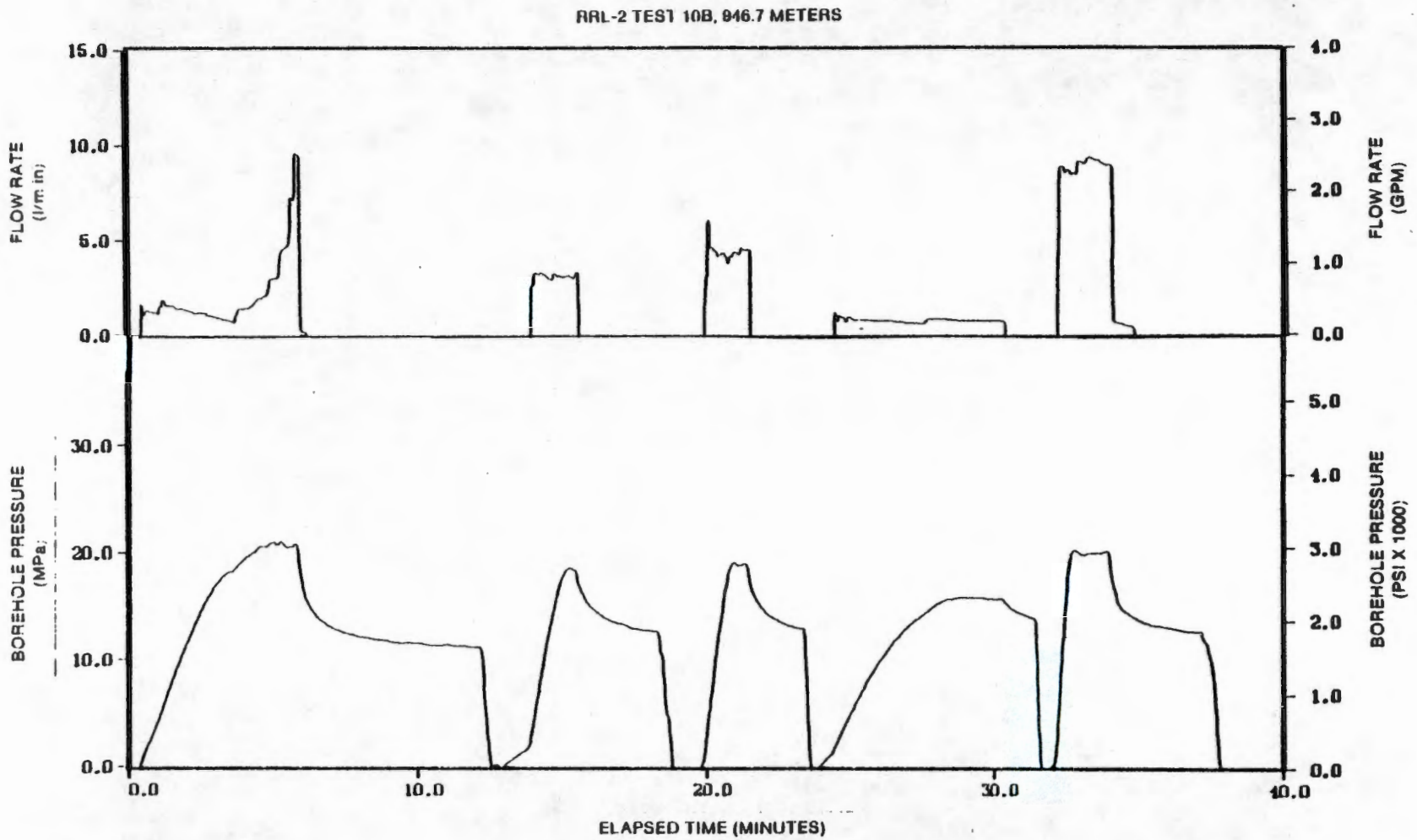
RRL-2 TEST 10B, 946.7 METERS
FLOW RATE (l/m; in)
FLOW RATE (GPM)
BOREHOLE PRESSURE (MPa)
BOREHOLE PRESSURE (PSI X 1000)
ELAPSED TIME (MINUTES)
15.0
10.0
5.0
0.0
4.0
3.0
2.0
1.0
0.0
30.0
20.0
10.0
0.0
5.0
4.0
3.0
2.0
1.0
0.0
0.0
10.0
20.0
30.0
40.0

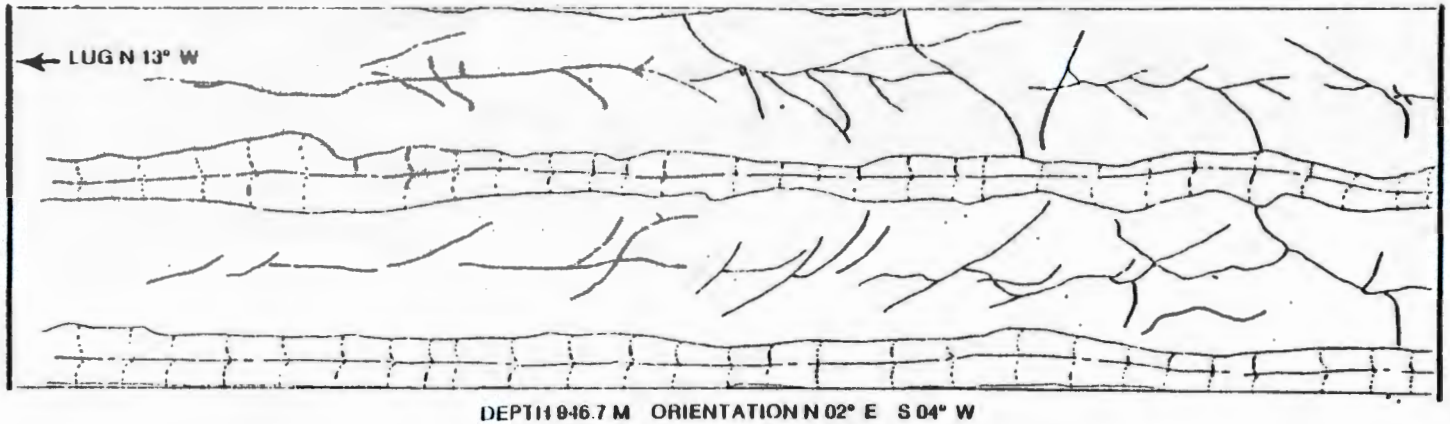

DEPTH 946.7 M ORIENTATION N 02° E S 04° W

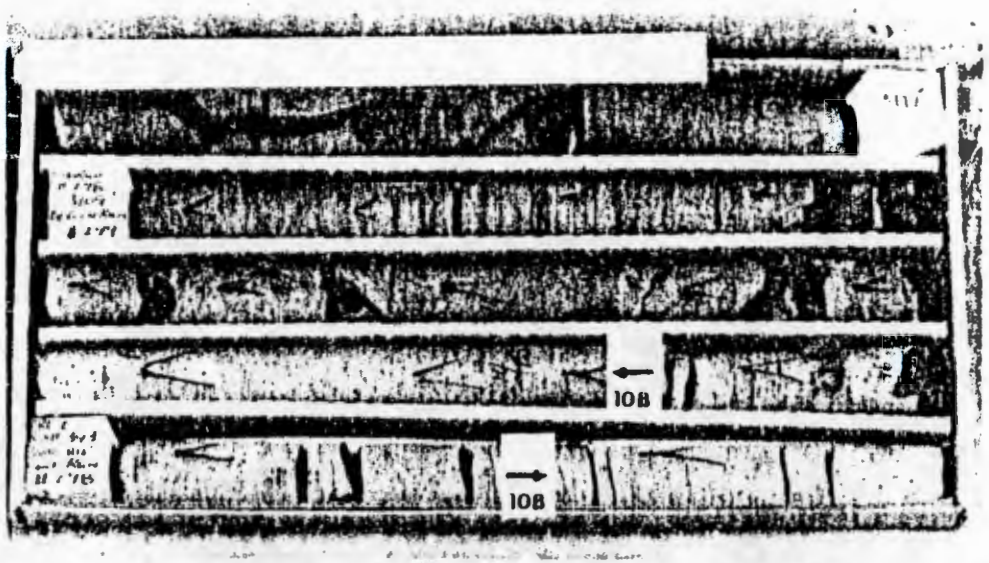

FRACTURE IMPRESSION AND CORE PHOTOGRAPH, RRL-2 TEST 10B

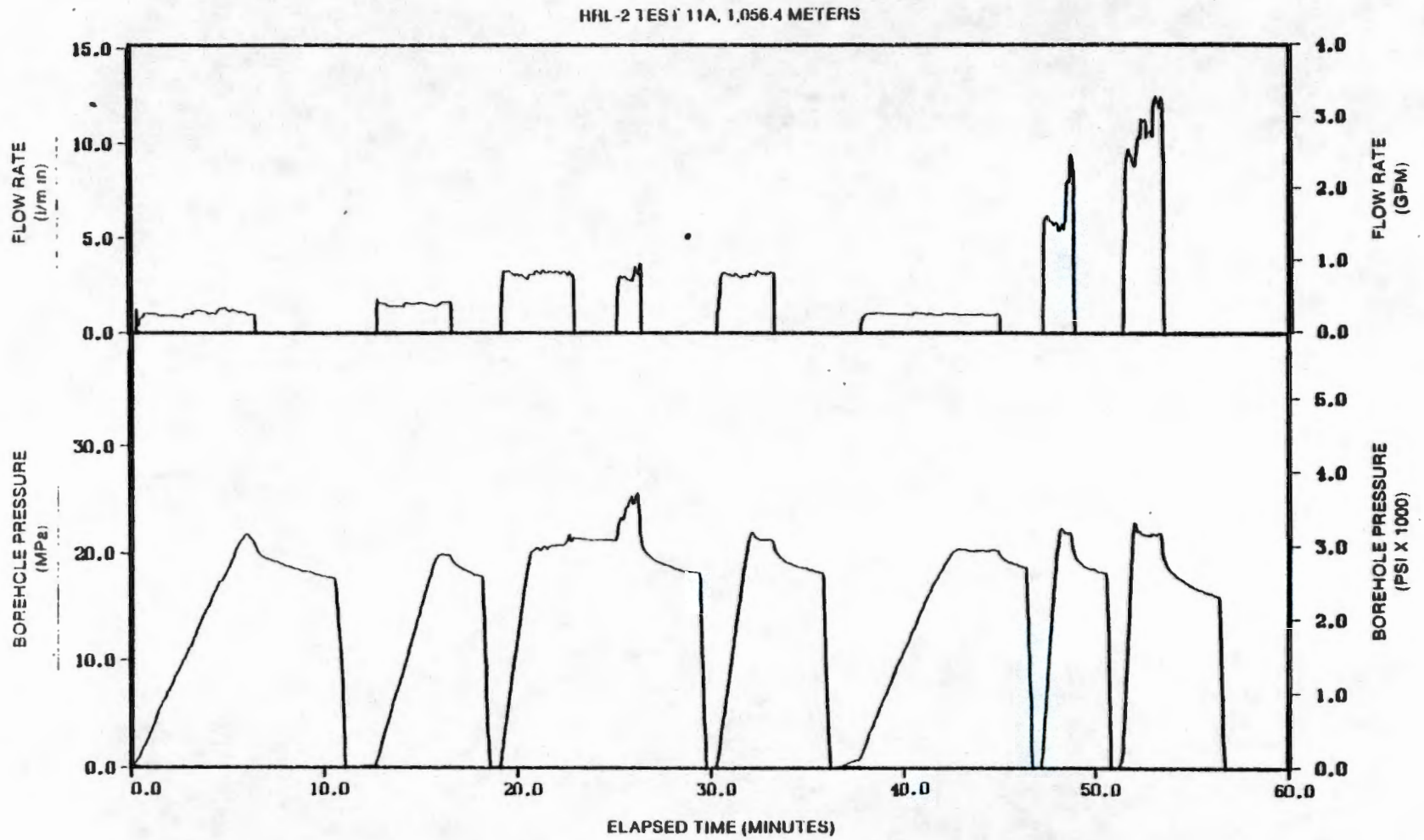
HRL-2 TEST 11A, 1,056.4 METERS
FLOW RATE (l/min)
FLOW RATE (GPM)
BOREHOLE PRESSURE (MPa)
BOREHOLE PRESSURE (PSI X 1000)
ELAPSED TIME (MINUTES)
15.0
10.0
5.0
0.0
4.0
3.0
2.0
1.0
0.0
30.0
20.0
10.0
0.0
5.0
4.0
3.0
2.0
1.0
0.0
0.0
10.0
20.0
30.0
40.0
50.0
60.0

DEPTH 1,056.4 ORIENTATION --

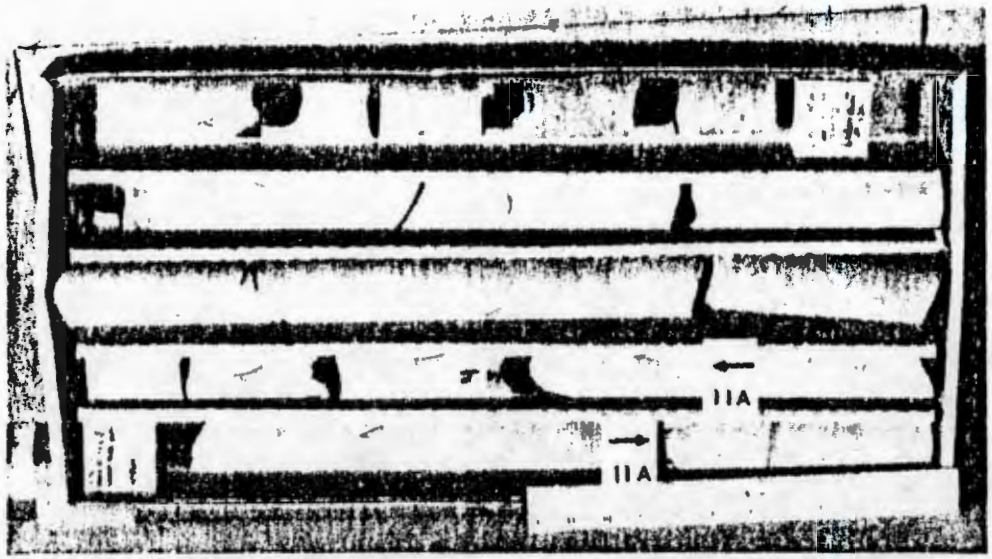

FRACTURE IMPRESSION AND CORE PHOTOGRAPH, RRL-2 TEST 11A

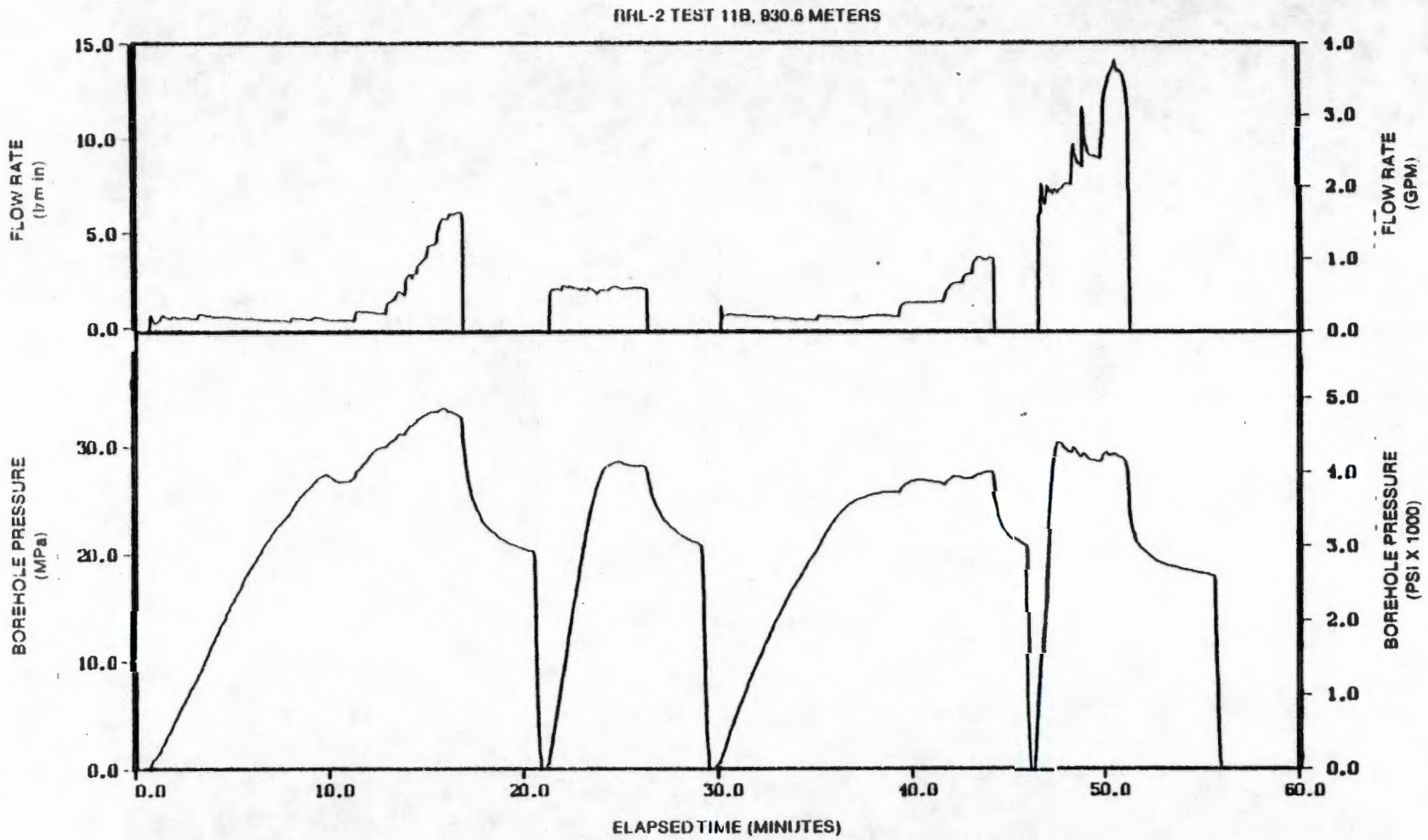
RRL-2 TEST 11B, 930.6 METERS
FLOW RATE (l/m in)
FLOW RATE (GPM)
BOREHOLE PRESSURE (MPa)
BOREHOLE PRESSURE (PSI X 1000)
ELAPSED TIME (MINUTES)
15.0
10.0
5.0
0.0
4.0
3.0
2.0
1.0
0.0
30.0
20.0
10.0
0.0
5.0
4.0
3.0
2.0
1.0
0.0
0.0
10.0
20.0
30.0
40.0
50.0
60.0

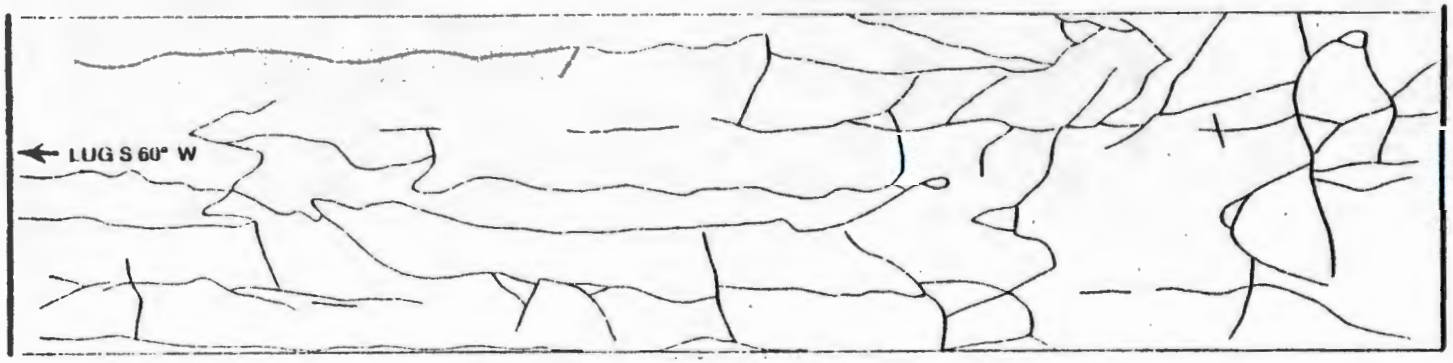

DEPTH 930.6 METERS

FRACTURE IMPRESSION AND CORE PHOTOGRAPH, RRL-2 TEST 11B

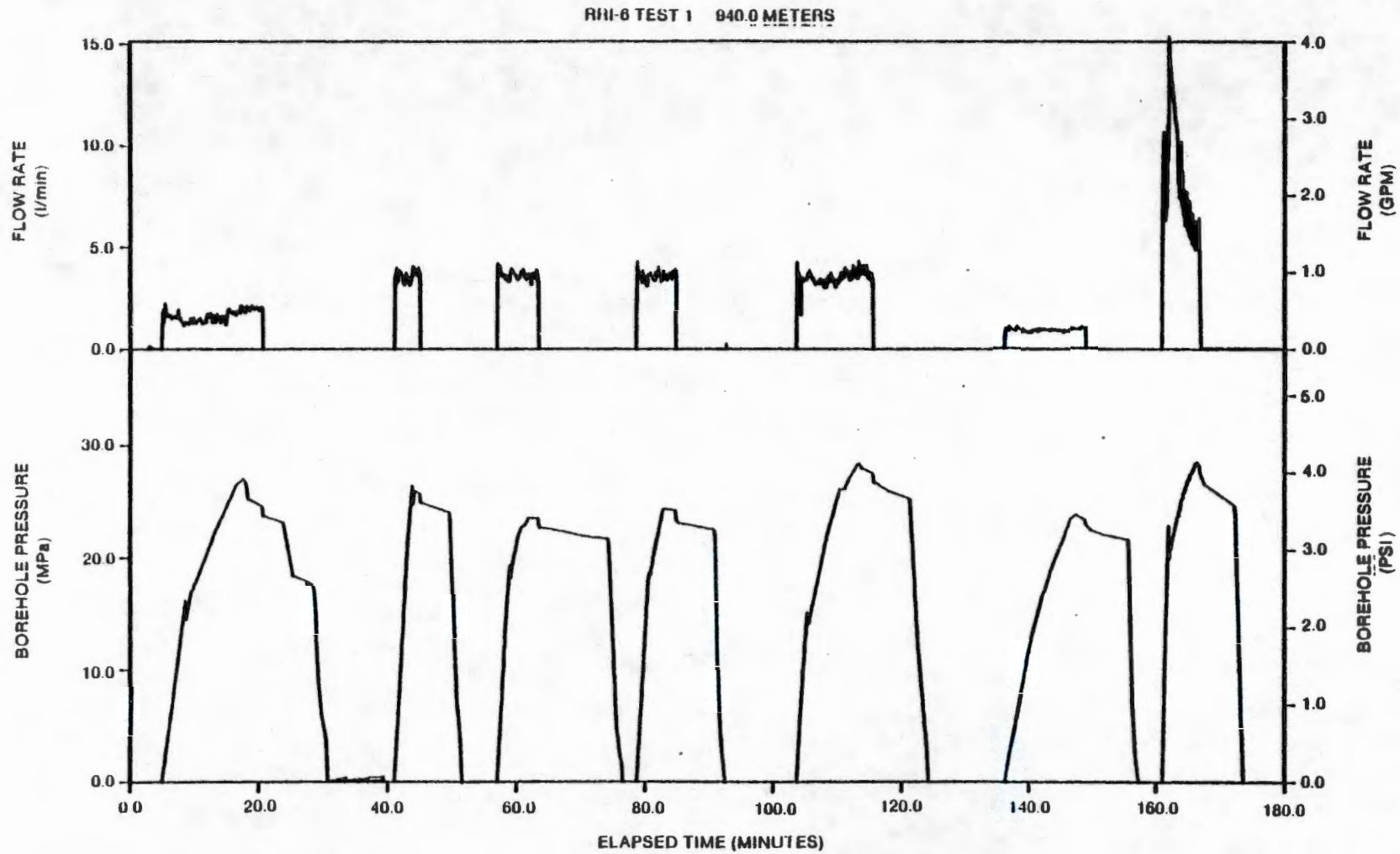
RRI-6 TEST 1 940.0 METERS
FLOW RATE (l/min)
FLOW RATE (GPM)
BOREHOLE PRESSURE (MPa)
BOREHOLE PRESSURE (PSI)
ELAPSED TIME (MINUTES)
15.0
10.0
5.0
0.0
4.0
3.0
2.0
1.0
0.0
30.0
20.0
10.0
0.0
5.0
4.0
3.0
2.0
1.0
0.0
0.0
20.0
40.0
60.0
80.0
100.0
120.0
140.0
160.0
180.0

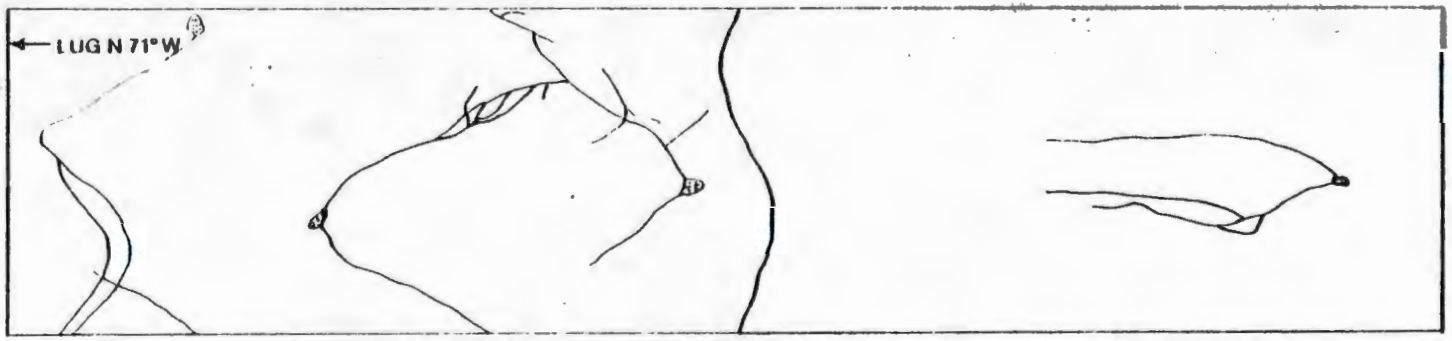

DEPTH 940.0 M NO FRACTURE ORIENTATION (940.6 M ON CORE)

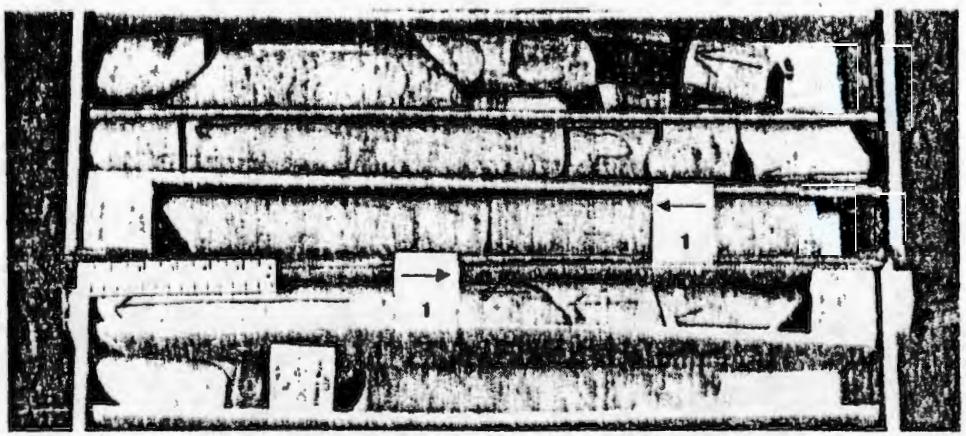

FRACTURE IMPRESSION AND CORE PHOTOGRAPH, RRL-6 TEST 1

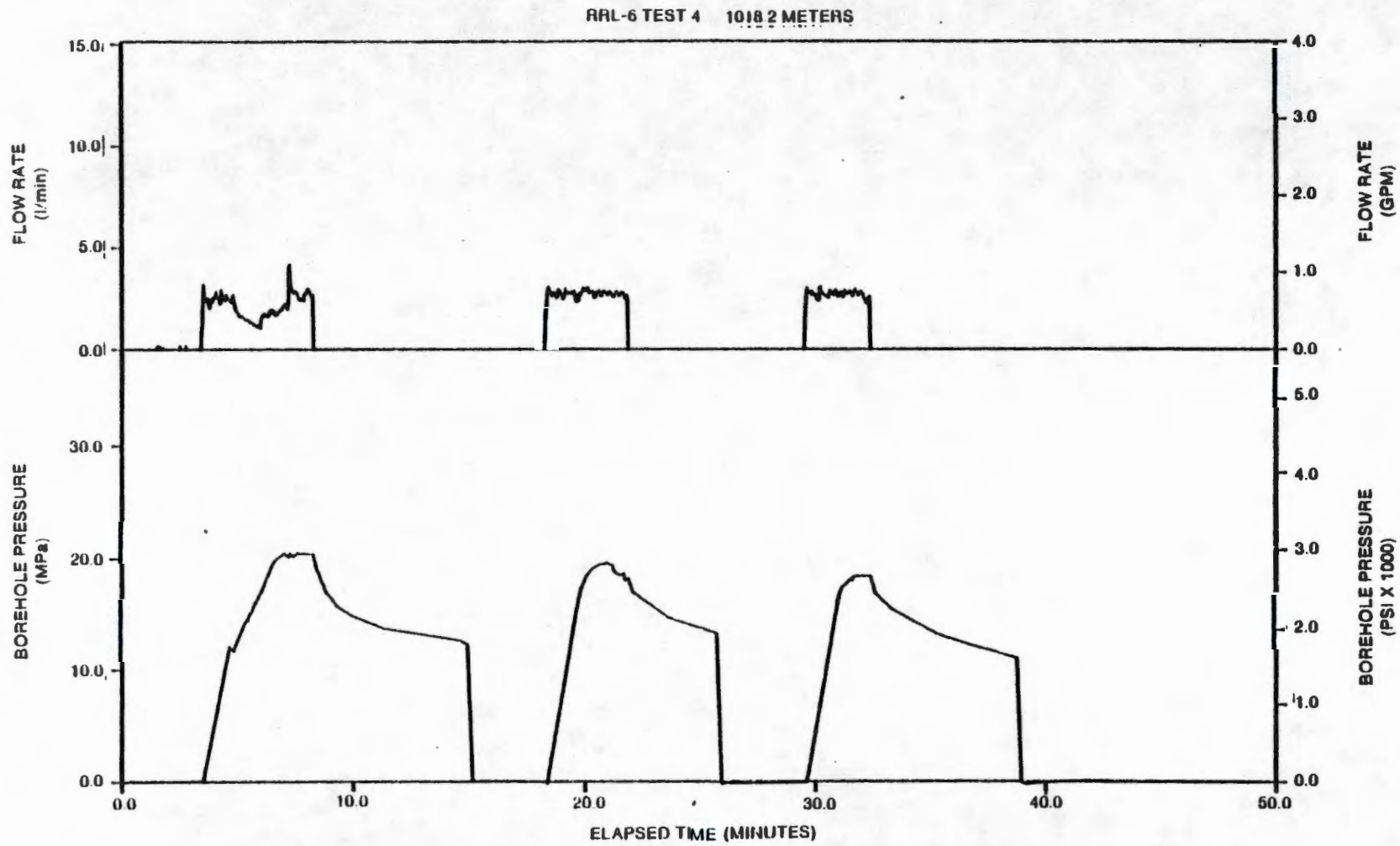

NOTE: TEST INTERVAL INFLUENCED BY TEST 3 AT 1016.8 METERS

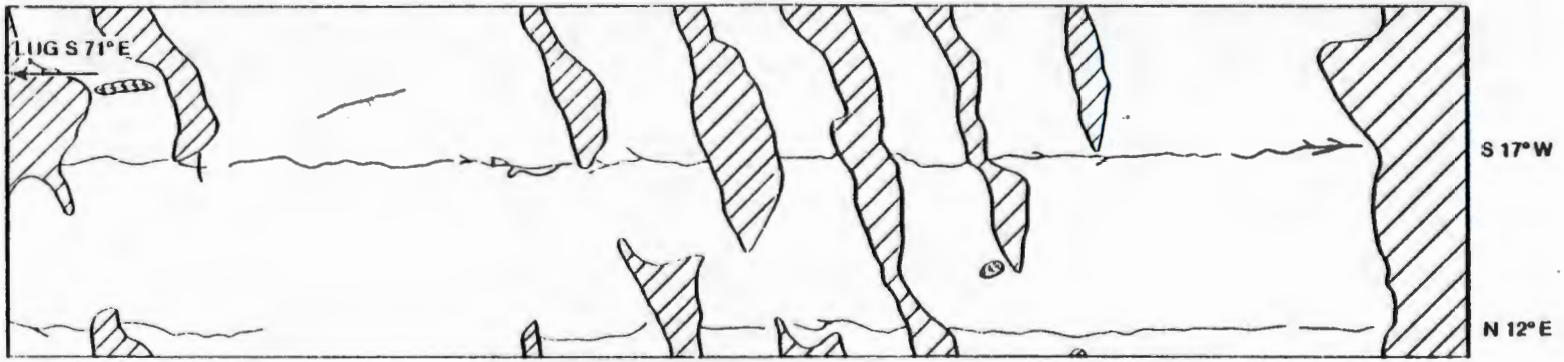

DEPTH 1018.2 M ORIENTATION S 17° W, N 12° E

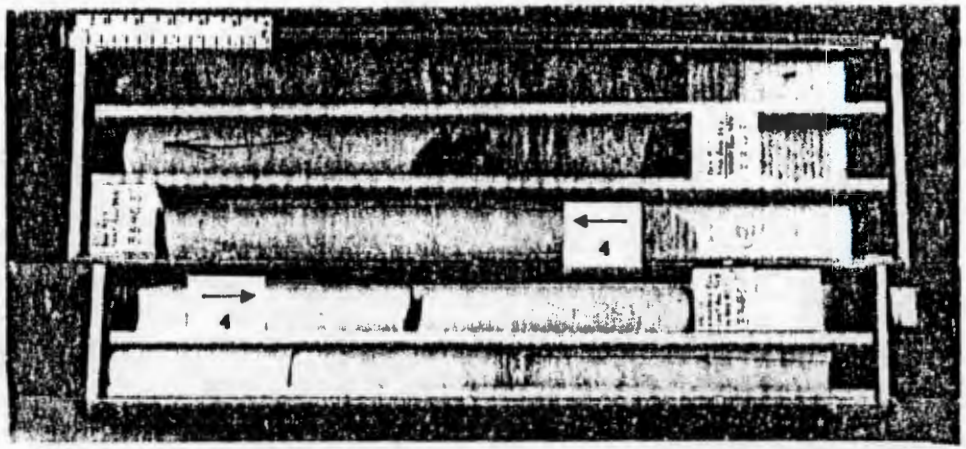

FRACTURE IMPRESSION AND CORE PHOTOGRAPH, RRL-6 TEST 4

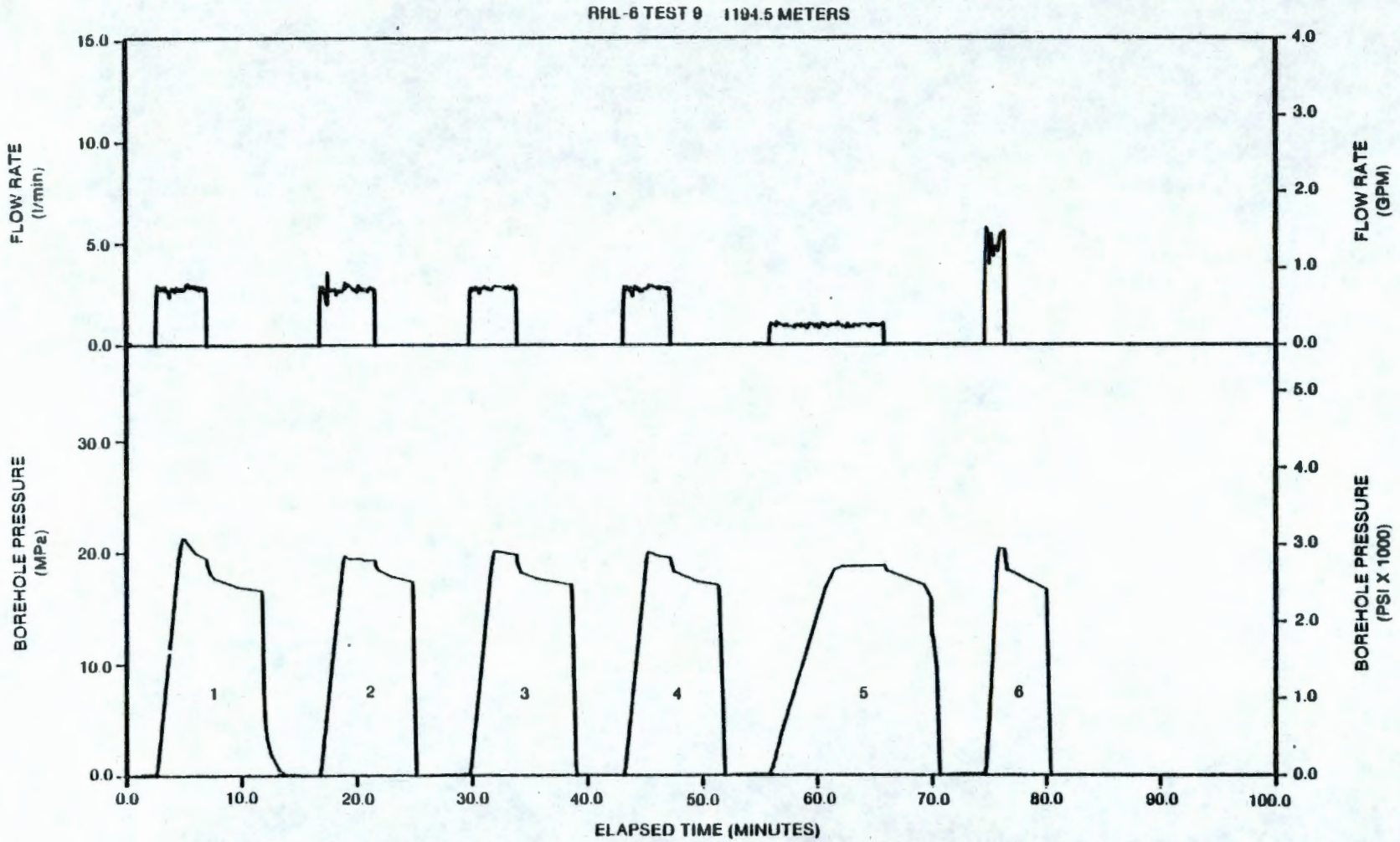

CYCLE	1	2	3	4	5	6	AVERAGE (STD DEV)
P_b	21.8	-	-	-	-	-	-
P_{isi}	19.3	19.3	19.3	19.3	-	-	19.3 (0.0)
P_{f_2}	-	18.3	18.3	13.8	-	-	16.8 (2.6)

DEPTH 1194 5 M NO FRACTURE IMPRESSION TAKEN

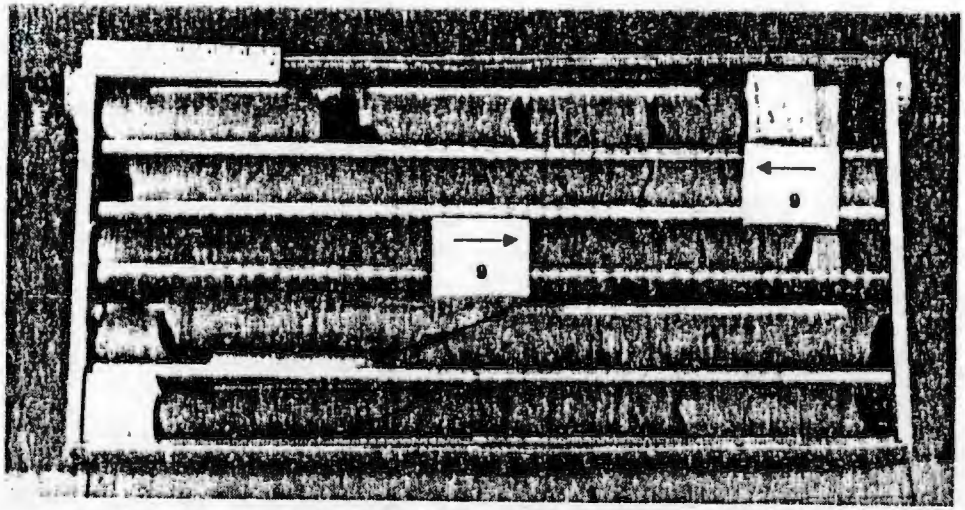

CORE PHOTOGRAPH, ARL-6 TEST 8

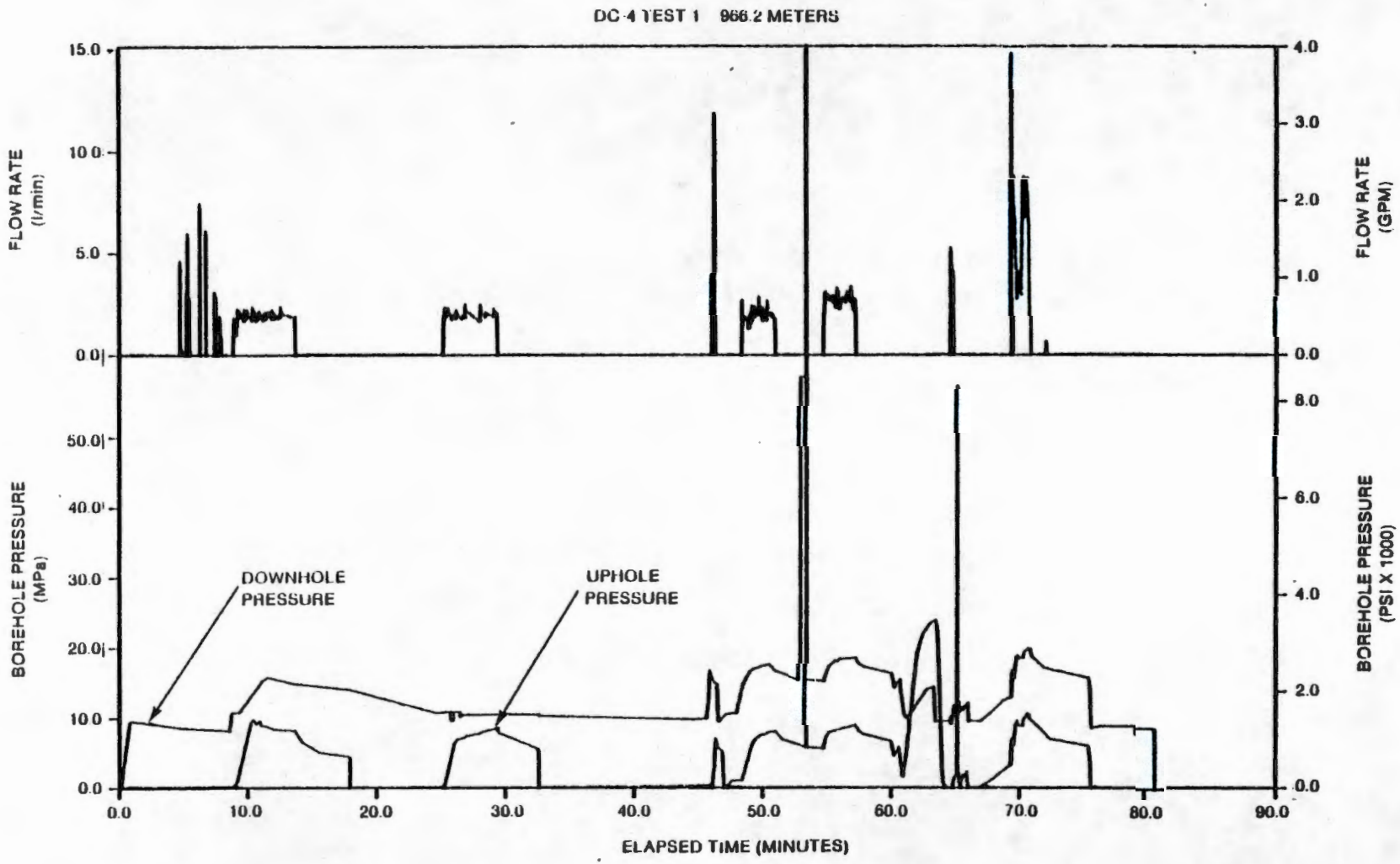
DC-4 TEST 1 966.2 METERS
FLOW RATE (l/min)
FLOW RATE (GPM)
BOREHOLE PRESSURE (MPa)
BOREHOLE PRESSURE (PSI X 1000)
DOWNHOLE PRESSURE
UPHOLE PRESSURE
ELAPSED TIME (MINUTES)
15.0
10.0
5.0
0.0
4.0
3.0
2.0
1.0
0.0
50.0
40.0
30.0
20.0
10.0
0.0
8.0
6.0
4.0
2.0
0.0
0.0
10.0
20.0
30.0
40.0
50.0
60.0
70.0
80.0
90.0

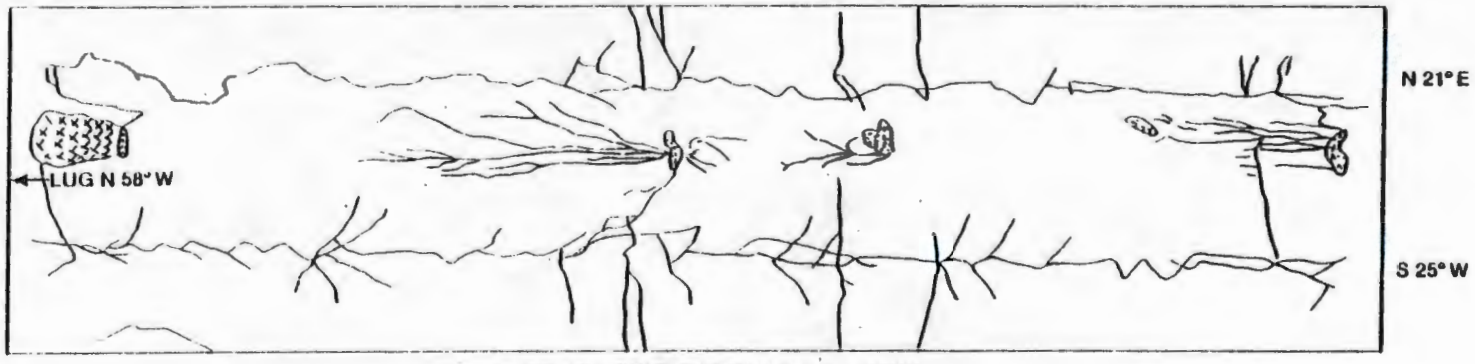

DEPTH 966.4 M ORIENTATION N 21° E, S 25° W

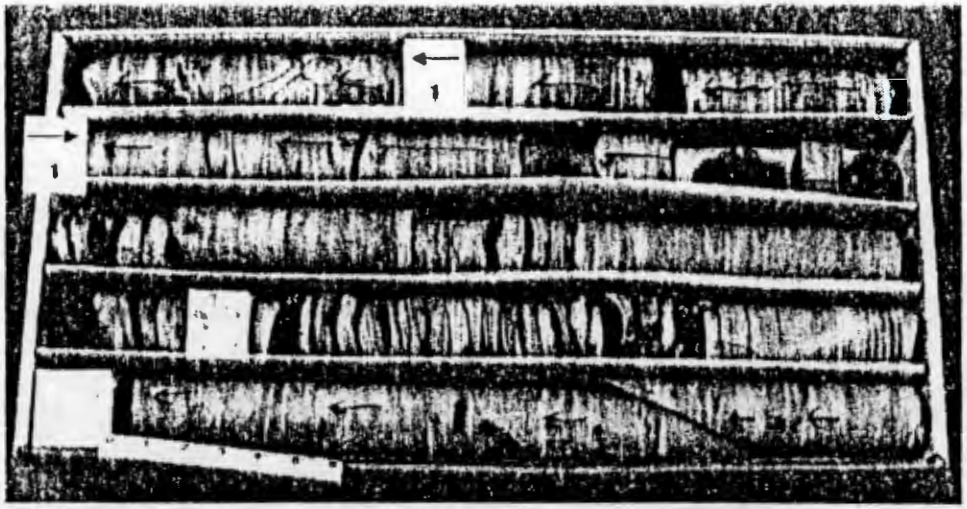

FRACTURE IMPRESSION AND CORE PHOTOGRAPH, DC-4 TEST 1

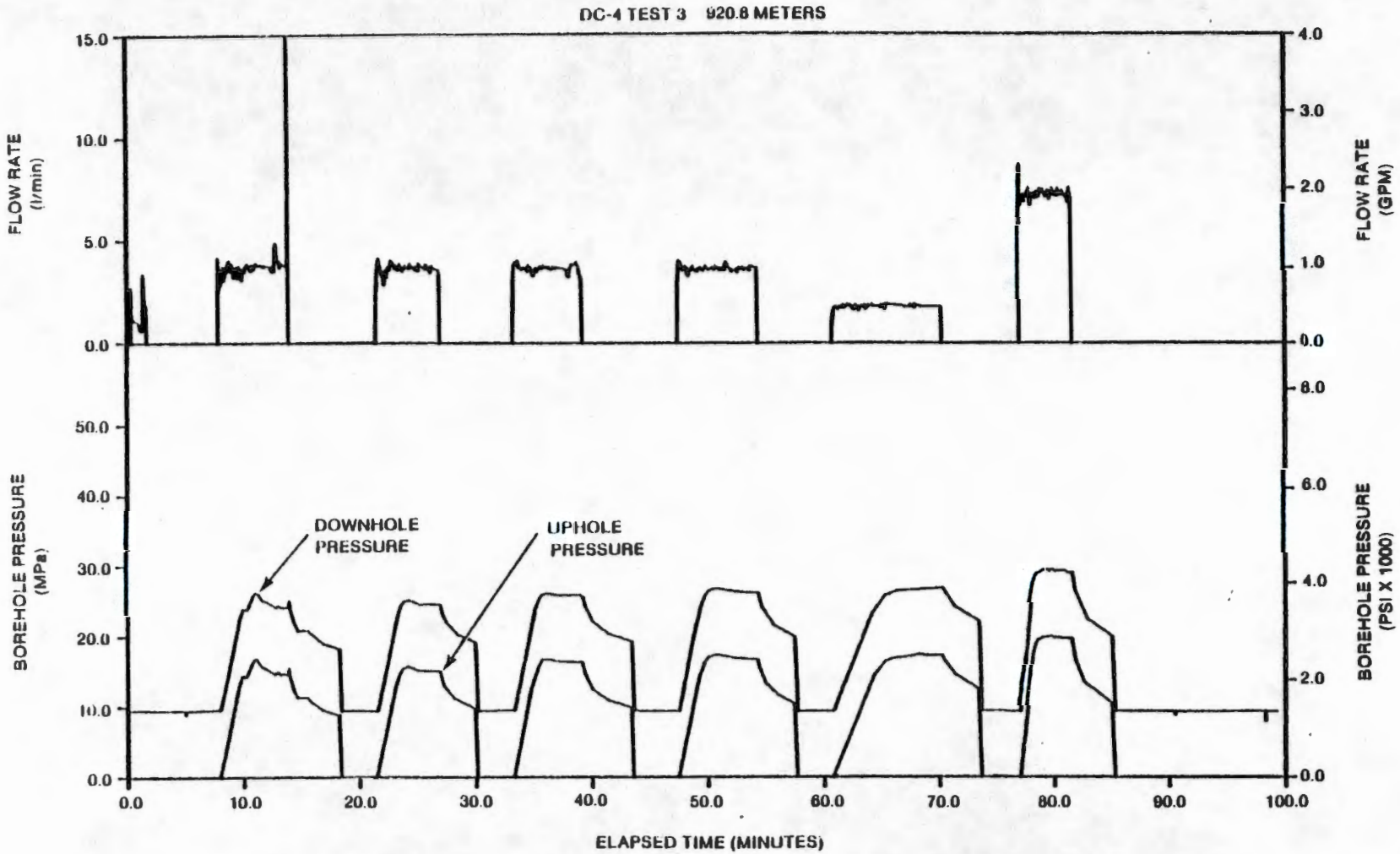
DC-4 TEST 3 920.8 METERS
FLOW RATE (l/min)
FLOW RATE (GPM)
BOREHOLE PRESSURE (MPa)
BOREHOLE PRESSURE (PSI X 1000)
DOWNHOLE PRESSURE
UPHOLE PRESSURE
ELAPSED TIME (MINUTES)
15.0
10.0
5.0
0.0
4.0
3.0
2.0
1.0
0.0
50.0
40.0
30.0
20.0
10.0
0.0
8.0
6.0
4.0
2.0
0.0
0.0
10.0
20.0
30.0
40.0
50.0
60.0
70.0
80.0
90.0
100.0

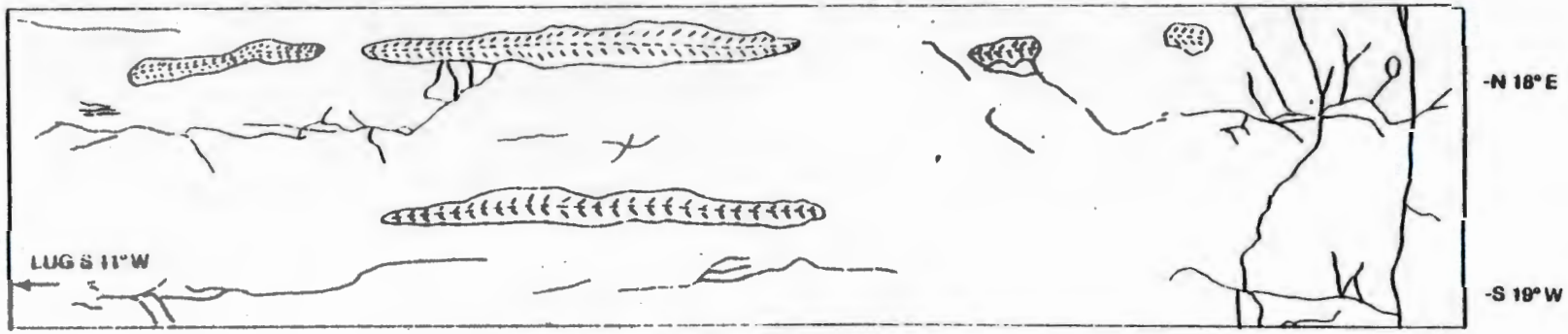

DEPTH 920.8M ORIENTATION N 18° E, S 19° W

FRACTURE IMPRESSION AND CORE PHOTOGRAPH, DC-4 TEST 3